THE WILD GOOSE ASSOCIATION

PROCEEDINGS OF THE

EIGHTH ANNUAL TECHNICAL SYMPOSIUM

17-19 OCTOBER 1979

WILLIAMSBURG, VIRGINIA

★ ★ ★ ★ ★

PUBLISHED BY

THE WILD GOOSE ASSOCIATION
4 TOWNSEND ROAD
ACTON, MASSACHUSETTS 01720

THE WILD GOOSE ASSOCIATION

The Wild Goose Association (WGA) is a professional organization of individuals and organizations having an interest in loran (long range navigation). It is named after the majestic birds that navigate thousands of miles with unerring accuracy. The WGA was organized in 1972 and its membership now includes hundreds of professional engineers, program managers, scientists and operational personnel from all segments of government, industry, and the user community throughout the world, working for the advancement of loran.

CONVENTION COMMITTEE

L. D. Higginbotham . . . . Chairman
W. F. Roland . . . . Co-Chairman
B. J. Uttam . . . . Guest Speakers
E. Roland . . . . Administration
R. S. Warren . . . . Technical Program
W. F. Rice . . . . Hospitality

BOARD OF DIRECTORS 1978-79

B. J. Uttam . . . . President
V. L. Johnson . . . . Vice President
R. Abraczinskas . . . . Secretary
C. S. Andren . . . . Treasurer

P. D. Abramson	W. H. Hilbun, III
J. M. Beukers	E. L. McGann
W. N. Dean	A. Pankopf
L. F. Fehlner	W. L. Polhemus
G. A. Gutman	J. P. VanEtten
L. D. Higginbotham	V. I. Weihe

BOARD OF DIRECTORS 1979-80

B. J. Uttam . . . . President
V. L. Johnson . . . . Vice President
B. Ambroseno . . . . Secretary
C. S. Andren . . . . Treasurer

R. Abraczinskas	W. H. Hilbun, III
P. D. Abramson	E. L. McGann
W. N. Dean	W. F. Rice
L. F. Fehlner	W. F. Roland
G. A. Gutman	J. P. VanEtten
G. Haroules	V. I. Weihe
L. D. Higginbotham	

TABLE OF CONTENTS

TABLE OF CONTENTS (Continued)

TECHNICAL SESSIONS OVERVIEW

ABSTRACTS AND BIOGRAPHIES

SESSION I - EQUIPMENT

W.N. Dean - Session Chairman

* * * * * * * * *

Biographical Sketch of Walter N. Dean

Walt Dean has been involved in the development of Loran-C, its predecessors and its offspring, for over 30 years. Although deeply involved in system concept and design, his major activity has been in test and evaluation of operating systems to understand better their peculiarities, and finding new ways to utilize the system.

He retired from Magnavox last spring and formed his own consulting company, Verdes Engineering Company. He has since done work for the U.S. Coast Guard, New York State, and several private firms, including Magnavox, on Loran and GPS studies.

Some of his earlier activities included non-paying jobs as Chief Engineer of Fort Wayne Public Television, and Chairman of the Fort Wayne Section of IEEE.

He has published some 15 papers and has 10 issued patents on Loran and radar.

SESSION I SPEAKERS

WALTER N. DEAN

JACK M. LIGON

CHARLES R. EDWARDS

STEPHEN C. BIGELOW

BRUCE CONWAY

AIRBORNE LORAN-C EVALUATION OF THE PRODUCTION AN/ARN-133 NAVIGATOR

by

Richard J. Adams

Systems Control, Inc. (Vt)
Champlain Technology Industries Division
2326 S. Congress Avenue, Suite 2-A
West Palm Beach, Florida 33406

An extensive flight test evaluation was performed on the production model of the AN/ARN-133 airborne Loran-C navigator. The evaluation was conducted from May 1978 through January 1979. Data was collected on the operational characteristics and system accuracy in three basic environments. Loran-C operation in the National Airspace System was evaluated primarily in the high density Northeast Corridor environment between Boston, Massachusetts and Washington, D.C. Loran-C system accuracy testing was performed primarily in the vicinity of the National Aviation Facilities Experimental Center (NAFEC). Loran-C overwater signal characteristics, absolute accuracy and repeatability were evaluated during tests in both the Gulf of Mexico and the coastal waters near Atlantic City, New Jersey. This report addresses the objectives, the data collection plans, the flight test procedures, the quantitative and qualitative results and the conclusions which evolved from this investigation.

The airborne Loran-C evaluation contained in this report was initially sponsored solely by the United States Coast Guard (USCG) as a part of the effort to establish Loran-C as the primary navigation system used to support their operational mission. Due to the need for the Coast Guard operations to integrate with conventional VOR/DME navigation in the National Airspace System (NAS), the USCG portion of the program included NAS compatibility demonstration flights. Upon successful completion of the initial demonstration by the USCG, the Federal Aviation Administration (FAA) examined the preliminary results and expressed an interest in supplementing the Coast Guard test program in order to gather additional data pertinent to the FAA interests. This report, therefore, presents the results of the USCG evaluation and the FAA addendum to the USCG program.

This report summarizes the significant results from all of the Loran-C tests performed to date. In order to organize the data and simplify the comprehension of the many results from these programs, this report categorizes the data into the three main categories of (1) Northeast Corridor Operational Testing, (2) NAFEC System Accuracy Testing and (3) Offshore Testing.

The discussion summarizes details for each of these categories including: Enroute, transition (spur) routes, and final approach results in the Northeast Corridor; prototype data, production data, and telemetry tracking data from NAFEC; deep probes (200 nm), coastline signal anomalies, ship/helo rendezvous, oil rig tests, search and rescue tests offshore.

* * * * * *

Biographical Sketch of Mr. Richard J. Adams

Mr. Adams has been a program manager in charge of systems design, flight testing and cockpit simulator testing of navigation/avionics hardware since 1972. He has performed contracts for the Federal Aviation Administration, the United States Coast Guard, the Department of Energy and the United States Air Force in the operational utilization of advanced navigation systems and concepts. In addition, Mr. Adams has consulted with private industry on projects ranging from the flight management system for the Boeing 767 to the design of a Digital Data Broadcast system suitable for General Aviation. Mr. Adams' Loran-C work for the USCG was initiated with the evaluation of the prototype TDL-424 system manufactured by Teledyne Systems Company in 1976.

Mr. Adams is a private pilot, a registered Professional Engineer, an active member in the American Society of Mechanical Engineers and the Institute of Navigation. Mr. Adams received his B.S. in Aeronautical and Astronautical Engineering from the University of Illinois in 1965 and his M.S. in Mechanical Engineering from the University of Florida in 1968.

PILOT: PRECISION INTRACOASTAL LORAN TRANSLOCATION--EXPLOITING LORAN-C IN THE HARBOR AND RIVER ENVIRONMENT

by

Jack M. Ligon
Office of Research and Development
U. S. Coast Guard Headquarters
Washington, D.C. 20590

Charles R. Edwards
The Johns Hopkins University
Applied Physics Laboratory
Laurel, MD 20810

The U. S. Coast Guard is engaged in a long-term program to evaluate the potential and develop the technology for precision navigation using Loran-C. The basic method is to use Loran-C in the repeatable mode for real time 2 or 3 line-of-position precision navigation, or piloting, in the vicinity of surveyed positions. This method can be augmented by offset or proportional differential corrections. PILOT user equipment which demonstrates application of this method is being developed for the Coast Guard by the Johns Hopkins University Applied Physics Laboratory. The PILOT combines time differences from a precision Loran-C receiver with survey information from a data tape cassette using simple algorithms to present the piloting situation on a CRT display. The PILOT is basically a modified Hewlett-Packard 2649A data terminal and demonstrates the practicality of precision user equipment in the $10K unit price range. The PILOT algorithms, hardware, and software are described, and the results of summer tests on the St. Marys River are given. It is concluded that PILOTing accuracies of better than 25 meters are achievable.

* * * * * * *

Biographical Sketch of Jack Ligon

Mr. Ligon is now the Radio Aids to Navigation Project Area Manager for the U. S. Coast Guard Office of Research and Development. He has divided his 18 years of Coast Guard service between communications and radio aids. His work with Loran covers the entire spectrum from precision simulation to treatment as a source of interference.

Mr. Ligon holds a MSE degree from the University of Pennsylvania and a BSEE degree from Virginia Polytechnic Institute. He is a member of the Institute of Navigation and the Wild Goose Association. His outside interests include church work, sailing, and camping.

Biographical Sketch of Charles Edwards

Mr. Edwards is the supervisor of the Systems Development Section and is the Program Scientist for the PILOT Program at the Johns Hopkins University Applied Physics Laboratory. He has been involved with the development of Loran guidance systems for 10 of his 16 years at APL.

Mr. Edwards received a BSEE from the University of Tennessee and is a member of Tau Beta Pi and Eta Kappa Nu. His hobbies include architecture, knife-making, sailing, and working on a cabin in the Appalachian Mountains.

A LORAN-C VESSEL LOCATION SYSTEM
FOR TRAFFIC CONTROL IN THE SUEZ CANAL

by

Stephen C. Bigelow

Megapulse, Incorporated
8 Preston Court
Bedford, MA 01730

The purpose of this system is to provide real-time vessel location data for the Suez Canal vessel traffic management system. The system consists of a three station Loran-C mini-chain, portable Loran-C receivers/VHF data transceivers for use aboard ships in the canal, data links from several sites along the canal and from the transmitter sites to the central control facility, several fixed Loran-C receivers/VHF transceivers to provide differential correction data and digital processing equipment to automatically poll both the fixed and the vessel borne receivers and to coordinate convert and smooth the vessel position data. This data is presented in real time on graphic map displays in the control facility (The display equipment is provided by the prime contractor, AILTECH.).

Some of the significant features of this system are:

- The Loran transmitters are monitored and remotely controlled from the central facility
- The Loran receivers are microprocessor based, fully automatic and have 10 nsec tracking resolution
- Multiple fixed monitor receivers are used to provide differential correction data
- With the exception of the vessel borne receivers the entire system is redundant to enhance its availability
- The system is capable of tracking 150 vessels simultaneously
- The position data accuracy specifications are on the order of 15 meters

This paper describes the design and implementation of this vessel location system in considerable detail.

* * * * * * *

Biographical Sketch of Stephen C. Bigelow

Stephen C. Bigelow is Vice-President, Operations of Megapulse, Incorporated. In addition to his administrative responsibilities, he has been involved in the design and development of solid-state Loran-C transmitting equipment. His speciality is system engineering including both hardware and software. He is presently leading the software design effort for the Suez Canal Vessel Traffic Management System.

Prior to joining Megapulse in 1970, he was a Senior Engineering Specialist at the Sylvania Applied Research Laboratory for six years and an Instructor in Electrical Engineering at Columbia University for seven years.

He received the B.S.E.E., M.S.E.E. and D.Eng.Sc. degrees all from Columbia University School of Engineering in 1955, 1956 and 1963 respectively.

ANALYSIS OF REAL WORLD LORAN RECORDINGS

by

Captain Bruce Conway

U.S. Air Force
Eglin Air Force Base, Florida 32542

The Air Force's AN/GRM-99 Dynamic Loran/Simulator Lab at Eglin AFB, Florida is involved in Loran receiver performance testing of the European environment using Loran RF tape recordings recorded in Germany. These tapes provide a powerful tool to evaluate and enhance receiver performance prior to the deployment of the AN/ARN-101 equipped F-4's to Germany. This paper discusses the simulator team's hardware system, taping procedures, and testing capabilities gained with these recordings.

The recording system is based around a Honeywell 5600C video tape recorder designed for in-the-field Loran recordings. With field experience, specific data requirements have been identified, calibration procedures developed, and system hardware problems solved. Special hardware was designed and built to record ECCM coded Loran for the Air Force's field tests.

These tapes are used in the lab to evaluate receiver's interference suppression capabilities, potential cross rate problems, search and settle performance, tracking accuracy, and dynamic receiver performance. The tapes provide a very powerful testing tool that makes sophisticated field performance evaluation possible in the comfort of a well-instrumented laboratory, and have added a new dimension to Loran simulation and testing capabilities.

* * * * * * * * * *

<u>Biographical Sketch of Captain Bruce Conway</u>

Captain Bruce Conway is an avionics simulation test engineer at Eglin AFB, Florida. He is responsible for simulator testing of the Loran/INS based digital avionics update for the Air Force's F/RF-4 aircraft. This testing includes Loran performance, aircraft system integration, and flight performance evaluation.

Prior to his work with the Air Force, Bruce was the project engineer responsible for the design of non-destructive quality control equipment for the plywood industry.

Bruce received the BSEE degree from the University of North Dakota, and the MSEE degree from Washington State University.

SESSION II - GRID CALIBRATION

J.D. Illgen - Session Chairman

* * * * * * * * *

Biographical Sketch of John Illgen

John Illgen is currently Director of Communication and Navigation Systems at Effects Technology, Inc. (Effects Technology, Inc. is a subsidiary of Flow General, Inc.). Mr. Illgen's current responsibilities include receiver development, field engineering, data processing, laboratory testing pertaining to communication and navigation system analyses. A communication/navigation software-hardware simulation (VLF through EHF) capability has been established at ETI for use in assessing satellite and terrestrial systems in normal and disturbed environments. Prior to joining ETI Mr. Illgen was a member of the professional staff at General Electric-TEMPO (Nov. 1973 to May 1979) and Computer Sciences Corporation (Jan. 1967 to Nov. 1973). He was program manager for a series of U.S. Coast Guard experiments aimed at investigating the potential use of Loran-C for Harbor and Harbor Entrance navigation. Mr. Illgen was a key participant in a project to determine conductivity and to observe Loran-C timing fluctuations in the Great Lakes region. Have conducted communication system analysis for a variety of communication systems including: Pilgrim, DSCS II and III, SMS to Buoy Links, FLTSATCOM, LES 8 and 9, various DCS communication command centers and interconnecting links (aircraft and satellite). John Illgen received the M. Sc. in Electrical Engineering upon completion of his studies from the Technical University of Denmark.

JOHN D. ILLGEN

JOSEPH L. HOWARD

RADHA R. GUPTA

ANDREW J. SEDLOCK

MORTIMER ROGOFF

PETER M. WINKLER

BRIAN TERRY

LORAN WARPAGE DATA BASE REQUIREMENTS

by

Joseph L. Howard

The MITRE Corporation
P.O. Box 208
Bedford, MA 01730

Differences between LORAN time differences (TDs) measured with a receiver and TDs calculated using secondary phase corrections from a homogeneous LORAN conductivity model, can be interpreted as irregularities in the actual hyperbolic lines of position (LOP). This condition is referred to as warpage. LORAN warpage occurs for two reasons. First, warpage occurs whenever the propagation medium is not uniform. Second, warpage occurs when LORAN signals travel over two or more different propagation mediums i.e. from land to sea and back to land. The presence of Loran warpage affects the normal coordinate conversion relationship between the regular LORAN hyperbolic grid and the corresponding geodetic (latitude, longitude) grid commonly used for navigation.

The effect of Loran warpage is corrected by the AN/ARN-101 LORAN system in a two part algorthm. The first part operates off-line and uses a paired data base of measured LORAN and geodetic coordinates to generate a set of 15 coefficients for each LORAN station. These coefficients are used in the second part of the algorithm each coordinate conversion cycle. The warpage is corrected during coordinate conversion by using the coefficients to estimate an effective wave impedance for the secondary phase correction of each LORAN time of arrival. This paper describes the considerations and methodology needed to obtain a useable data base that meets the requirements for coordinate conversion accuracy. The recent calibration of the Southeast U.S. LORAN-C chain at Eglin AFB, Florida is used as an example of the procedure.

* * * * * * *

<u>Biographical Sketch of Joseph L. Howard</u>

Joseph L. Howard is currently a member of the technical staff at the MITRE Corporation, Bedford, Massachusetts. His work includes planning for Navy Command Control and Communication projects plus technical support for the Air Force LORAN program. He joined MITRE in 1977 after more than eight years as an officer in the U.S. Air Force. From 1971 to 1977 he was assigned to the Tactical LORAN System Program Office. During that period, he was Program Manager for the AN/GRM-99 dynamic LORAN simulator and Engineering Test Director for the AN/ARN-101 LORAN navigation system.

He received his B.S. in Electrical Engineering in 1969 from the University of New Hampshire. He is a charter member of the Wild Goose Association and a member of I.E.E.E.

APPLICATION OF SEMI-EMPIRICAL TD GRID CALIBRATION TO THE WEST COAST LORAN-C CHAIN

by

R.R. Gupta
The Analytic Sciences Corporation
Six Jacob Way
Reading, Massachusetts 01867

E. Anderson
U.S. Coast Guard R&D Center
Avery Point
Groton, Connecticut 06430

This paper demonstrates the utility of semi-empirical Loran-C time difference (TD) grid calibration techniques. Theory is employed to determine the functional dependence of TDs on range and bearing from the Loran-C chain stations and TD measurement data are utilized to calibrate the (uncertain) coefficients incorporated in the semi-empirical TD model. A specific semi-empirical model is derived for the West Coast Loran-C chain where at-sea TD measurement data in Southern California have revealed large discrepancies between U.S. Coast Guard predictions and measurements. A significant reduction in the West Coast TD errors is achieved with the semi-empirically-calibrated model relative to the U.S. Coast Guard grid. The accuracy of the calibrated West Coast Loran-C grid is further evaluated by comparing the calibrated grid with measurements not used in model calibration. Results are also presented which show the sensitivity of the model accuracy to the quantity and distribution of measurement data used to calibrate the West Coast model. Data collection requirements guidelines are presented for future semi-empirical grid calibration efforts.

* * * * * * *

Biographical Sketch of Radha Raman Gupta

Radha Raman Gupta received his B.Sc.E.E. from India in 1956. After working for one year in India and three years for SERETE (Consulting Engineers) in France, he received the M.E.E. and Ph.D. degrees from Syracuse University in 1962 and 1965, respectively. During 1962 to 1965, he was also instructor at the Syracure University.

From 1966 to 1972, he was with Bendix Research Laboratories. Since 1972, Dr. Gupta has been with The Analytic Sciences Corporation. At present, he is involved in VLF and LF radio wave propagation studies. In 1978, he received the M.B.A. from Boston University.

Biographical Sketch of E. Anderson

Mr. Anderson is currently responsible for radio aids to navigation projects at the U.S. Coast Guard Research and Development Center in Groton, CT. Since joining the Center in 1973, he has directed design and development of remote monitor instrumentation systems, evaluation of microwave ranging systems, and directed testing, evaluation and analysis of Loran-C propagation characteristics for short baseline chains.

Prior to employment at the Research and Development Center in 1973, Mr. Anderson directed design and development of aircraft instrumentation systems at G.E. and Simonds Precision Products. His background also includes development of biomedical, nuclear, sound and vibration analysis and control systems. Mr. Anderson received a B.S. in Physics from Trinity College; B.E.E. in Electronic Engineering from Rensselaer Poly. Institute; and did graduate studies at the University of Connecticut.

LORAN-C GRID SURVEY IN HARBOR AREAS

by

LCDR Andrew J. Sedlock
Office of Research and Development
U. S. Coast Guard Headquarters
Washington, D.C. 20590

Three methods for surveying the Loran-C time difference coordinates of waypoints and prominent physical features of a harbor area for precision Loran-C navigation are described. Results are presented from field measurements on the St. Marys River Mini Loran-C Chain using a method which uses existing visual aids to navigation as a position reference. The survey methods described provide for accurate and timely Loran-C grid survey over a wide range of harbor areas. The general features of each method and details of the visual aids to navigation approach are presented. Analysis of field measurements show survey capability on the order of ten nanoseconds.

* * * * * * *

<u>Biographical Sketch of LCDR Sedlock</u>

LCDR Sedlock is a 1967 graduate of the U. S. Coast Guard Academy and received a Master of Science degree in electrical engineering from the University of Michigan in 1972. From 1972 to 1976 he was assigned to the Coast Guard Electronics Engineering Center (EECEN), Wildwood, New Jersey, where he was involved in the development of the Loran-C Receiver Test Complex II, Loran-C receiver testing, and Loran-C transmitter modifications. He is presently assigned to the Office of Research and Development at Coast Guard Headquarters where he is responsible for the development of Loran-C grid survey techniques in harbor areas.

LORAN COORDINATE CONVERSION

by

Mortimer Rogoff

4201 Cathedral Avenue, N.W. #914W
Washington, D.C. 20016

Peter M. Winkler

Emory University
Atlanta, Georgia 30322

Coordinate conversion of Loran time differences into accurate latitude and longitude positions is accomplished on hand-held calculators. Programs have been written for the HP-67/97, HP-41C, and TI-59 calculators, utilizing magnetic card memory to store the programs for repeated use. Accuracy of coordinate conversion is achieved by a process of local calibration which sharply reduces the effects of propagation and other errors; calibration points are established where latitude, longitude, and the time differences of two Loran slaves are known. Loran observations made in the vicinity of these calibration points result in latitude and longitude positions with errors kept to 200 yards, or less where greater accuracy is needed. The magnitude of error is controllable by adjusting the intervals between calibration points. The actual spacing between these points varies with location; in the open sea, or in some coastal areas, calibrations need be made at intervals of five to ten miles to keep errors down to the 200 yard level. Near many coasts, and within most harbors, calibration should be made at considerably narrower spacings -- say every mile or less -- to achieve the same level of performance. This method has been used to achieve reproducible, long-term position accuracies averaging 30 yards inside New York Harbor. The complete coordinate conversion program includes current calculation, display of estimated positions, and the calculation of course to steer to reach a desired destination or way point.

* * * * * * *

Biographical Sketch of Mortimer Rogoff

Mortimer Rogoff has been engaged in the development of long-range, low-frequency radio navigation systems, and in the application of programmable calculators and digital computers. He served in a number of engineering and executive positions at ITT Corp. from 1946 to 1968, and has been a consultant to government and industry from 1968 to the present; he is now a Principal in the firm of Booz, Allen & Hamilton Inc. Mr. Rogoff is the author of "Calculator Navigation" published by W. W. Norton & Co., New York, N.Y. He received a B.S.E.E. degree in Electrical Engineering from Rensselaer Polytechnic Institute in 1942 and a Master of Science in Electrical Engineering from Columbia University in 1949.

Biographical Sketch of Peter M. Winkler

Dr. Peter M. Winkler is Assistant Professor of Mathematics at Emory University, Atlanta, Georgia. Previously, he was Assistant Professor of Mathematics at Stanford University, Palo Alto, California, following service in the U.S. Navy from 1969 to 1971. Dr. Winkler received his Doctorate in Mathematics in 1975 from Yale University, following a BA degree from Harvard University in 1968. He collaborated with Mr. Rogoff in the book "Calculator Navigation," especially in the chapters on Loran and Celestial navigation. His fields of specialty in mathematics include Logic and Computability, and Combinatorics.

A COMPUTER PROGRAM TO CONVERT DECCA AND LORAN-A FIXES TO LORAN-C

by

Brian Terry

NORDCO Limited
P.O. Box 8833
St. John's, Newfoundland A1B 3T2

With the introduction of Loran-C as the principal radio navaid for Canadian waters, and the likely termination of Decca and Loran-A, it is desirable to have a speedy and accurate method of converting Decca and Loran-A fixes to the equivalent Loran-C fixes.

This paper describes a computer program which will convert any two-bearing hyperbolic fix composed of Decca, Loran-A or Loran-C bearings (in anticipation of reconfigured Loran-C chains), or any hybrid of these (e.g., a Decca/Loran-A cross-fix) to an equivalent pair of Loran-C bearings. The program uses a point-by-point method, with calculation of geographic position as an intermediate step. Loran-C Additional Secondary Factor is computed using a polynominal-type algorithm based on Bigelow's "modified Millington method".

The paper also discusses the results of field verification tests performed on the conversion program.

* * * * * * *

Biographical Sketch of Brian Terry

The author was born in Newfoundland in 1953 and has studied mathematics at Memorial University and at McGill University. In addition to mathematics and its applications his interests include music and film. He presently works for an oceanographic research and development company and is president of a film society.

SESSION III - SYSTEMS

J.M. Ligon - Session Chairman

* * * * * * * * *

Biographical Sketch of Jack Ligon

Mr. Ligon is now the Radio Aids to Navigation Project Area Manager for the U.S. Coast Guard Office of Research and Development. He has divided his 18 years of Coast Guard service between communications and radio aids. His work with Loran covers the entire spectrum from precision simulation to treatment as a source of interference.

Mr. Ligon holds a MSE degree from the University of Pennsylvania and a BSEE degree from Virginia Polytechnic Institute. He is a member of the Institute of Navigation and the Wild Goose Association. His outside interests include church work, sailing, and camping.

SESSION III SPEAKERS

JACK M. LIGON

JOHN E. BOYD

TOM W. JERARDI

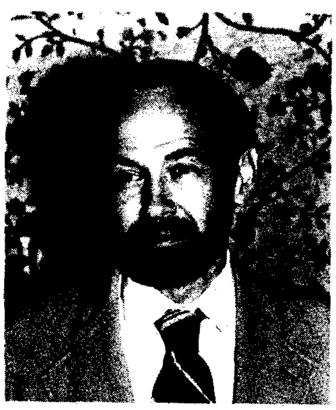

JAMES A. PERSCHY

JAMES P. VANETTEN

LONARS: Thirty Foot Geodetic Positioning from Loran-C

by

John E. Boyd

The Johns Hopkins University
Applied Physics Laboratory
Johns Hopkins Road
Laurel, Maryland 20810

The Loran Navigation Receiving System (LONARS) serves as the position reference for evaluation of submarine navigation equipment accuracy during submarine testing off the east coast of Florida. LONARS is a computer based receiving system developed for the U. S. Navy by The Johns Hopkins University, Applied Physics Laboratory. It incorporates several innovations to achieve very high accuracy including advanced statistical techniques in the data processing, a local monitor station, multiple GRI tracking and a calibration of the Loran-C net in the area of use.

Calibration of the local Loran-C grid was very successful. Using Cubic Corporation's DM-43 Autotape as reference, LONARS accuracy was demonstrated to be better than 15 feet each axis at sea. An apparent distortion in the Loran-C grid near the coast line resulted in a repeatable 35 foot error in port after the time difference to latitude/longitude coordinate conversion parameters were adjusted to cause the mean error at sea to be zero. This paper describes the development of the system, some of the accuracy related innovations, and the LONARS calibration.

* * * * * * *

<u>Biographical Sketch of John E. Boyd</u>

John E. Boyd is a mathematician for the Johns Hopkins University Applied Physics Laboratory. He joined the laboratory in 1974 after serving for four years as a naval officer. His experience is in inertial, sonar and radio navigation systems and in particular, Loran-C.

Mr. Boyd received a BA degree in mathematics from Humboldt State University (California) in 1968 and an MA in mathematics from The University of California in 1969.

LONARS, AN EXAMPLE OF ROBUST REAL TIME FILTERING

by

T. W. Jerardi

Johns Hopkins University
Applied Physics Laboratory
Johns Hopkins Road
Laurel, MD 20810

The concepts and philosphy of ROBUST ESTIMATION are reviewed. ROBUST is a technical statistical term. A procedure is ROBUST if it is not significantly affected by modest changes in the underlying assumptions.

In particular, the notion of sampling from contaminated distributions is addressed. It is shown that the Loran-C operating environment requires some type of ROBUST procedure.

As an example of ROBUST ESTIMATION, the LONARS tracking filter is described and simplified comparison to the more classic approaches is given. It is shown that ROBUST ESTIMATION is the basis for the superior performance demonstrated by LONARS.

* * * * * *

Biographical Sketch of T. W. Jerardi

Tom Jerardi is a member of the professional staff of the Johns Hopkins University Applied Physics Laboratory. He received his Bachelor's Degree in Electrical Engineering from Drexel University and Master's in Mathematical Sciences from the Johns Hopkins University. He has spent his entire professional career at APL on varied assignments in Space Systems, Navigation and related fields including extended temporary duty assignment to the Defense Communications Planning Group.

THE DESIGN OF THE LONARS SENSOR

by

James A. Perschy

The Johns Hopkins University Applied Physics Laboratory
Johns Hopkins Road
Laurel, Maryland 20810

The following paper gives a brief description of the design of the sensor portion of LONARS, a Loran navigation receiving system developed for the Strategic Systems project Office of the U.S. Navy. The LONARS hardware consists of an antenna, the sensor, a digital computer, a data recorder and a display. The sensor is the hardware designed specifically for LONARS. The sensor design allows the editing out of signals contaminated by burst noise, or cross rate interference between stations, before averaging in tracking loops.

To the maximum extent possible commercially available modules are utilized. The sensor contains an Austron tuned RF amplifier with APL-built digitally programmable attenuators. A single Datel sample-and-hold and 12 bit analog-to-digital converter module digitizes the RF data with sample intervals of 2.5 microseconds. Digitized data is temporarily stored in a digital control module before transferal to a Hewlett-Packard type 2109 computer for data processing. The digital control module provides the interface between the sensor and the computer, generates data measurement timing signals, and facilitates closed loop testing through the computer. A calibration unit, containing an Austron 5 mHz oscillator and a Hewlett-Packard digitally programmable wide band attenuator, provides a 100 kHz signal to the RF section for measuring signal delay versus gain through the RF section. A display unit, utilizing a miniature Tektronix oscilloscope and timing signals from the digital control module, provides convenient visual monitoring of Loran signals and the position of tracking points.

Four LONARS sensors have been fabricated at APL and are in operation. Three sensors are utilized with LONARS installations aboard ship. One sensor is configured for use as a land base transmitter monitor.

* * * * * *

James A. Perschy was born in Washington, D.C. He worked as a field engineer on the UNIVAC I computer at the Bureau of Census while attending The George Washington University School of Engineering. In 1958, after receiving a BSEE degree he joined The Johns Hopkins University Applied Physics Laboratory as Associate Engineer. He advanced to Senior Engineer while working on satellite data processing systems in 1962, and received an MS in Physics degree from The University of Maryland in 1965. He was appointed to the Principal Professional Staff of the Applied Physics Laboratory in 1976. Mr. Perschy holds six patents, and is a section supervisor. He presented a paper at the 1974 Wild Goose Convention titled "Progress Report on the USAF Group Phase Test."

REDUCTION OF INTERFERENCE TO LORAN-C

by

James P. Van Etten

ITT Avionics Division
390 Washington Avenue
Nutley, New Jersey 07110

ABSTRACT

The Loran-C multipulse transmissions have spectral lines at frequencies determined by the Group Repetition Interval (GRI) and the standard signal phase code pattern. Similarly, the receiver system receives all signals having spectral energy around spectral lines determined by the receiver strobe GRI and the strobe phase code pattern.

Whenever two loran chains with different GRI's have common spectral lines and the receiver strobe phase code pattern responds to these common spectral lines, there will be crossrate interference.

Previous studies have suggested (1) means to eliminate these interference effects by use of different transmitter phase code patterns and GRI selection and (2) methods to reduce the interference by selection of transmitter GRI's within a geographic area.

This paper suggests system means to "eliminate" crossrate interference through use of a unique family of GRI's and retention of the standard phase code pattern for the transmitted signals together with a different strobe phase code pattern in the receiver. Use of this proposal requires no system changes to the existing signal-in-space specification, but does require GRI assignment from a family of acceptable GRI's. This family of acceptable GRI's together with a defined receiver strobe phase code pattern insures that all Loran-C signals, as received, will be mutually orthogonal, thus "eliminating" crossrate interference on a worldwide basis.

This analysis also identifies the multiple frequencies throughout the 60-140 kilohertz band where stable carrier systems of relatively narrow bandwidth might be assigned or reassigned to "eliminate" synchronous CW interference.

* * * * * * *

Biographical Sketch of J. P. Van Etten

J.P. Van Etten was commissioned in the U.S. Coast Guard in 1943 after graduation from the Academy. He received the degree of EE from MIT in 1950. He served in the U.S. Coast Guard until 1958.

He joined ITT Laboratories in Nutley, New Jersey in 1958. He has served as Director of Engineering for Navigation Systems and for CNI Systems. Presently, he is Technical Advisor to the Vice President and Director of Engineering, ITT Avionics.

He is a Senior Member of the IEEE and a Member of the ION. He was a Member of the USCG Science Advisory Committee from 1970-1972. He is one of the Founding Directors of the Wild Goose Association and has served as a Director since its incorporation in 1972; he served as its President from 1974 to 1976.

SESSION IV - GRID STABILITY

R.S. Warren - Session Chairman

* * * * * * * * *

Biographical Sketch of Ronald S. Warren

Mr. Warren is currently Manager of the Navigation Systems Department for The Analytic Sciences Corporation (TASC). Areas of responsibility include inertial and radio navigation system studies which embody both Loran-C and Omega. Since joining TASC in 1969, he has directed studies of multisensor navigation systems with emphasis on system integration, error modeling, performance prediction and data analysis.

Prior to joining TASC, Mr. Warren had six years of experience as a system analysis engineer with the Raytheon Missile Systems Division of Raytheon Co. Mr. Warren received the B.S.E.E. degree from Michigan Technological University in 1963 and the M.S.E.E. degree from Northeastern University in 1970.

SESSION IV SPEAKERS

RONALD S. WARREN

JOHN D. ILLGEN

ROBERT H. DOHERTY

DAVID L. OLSEN

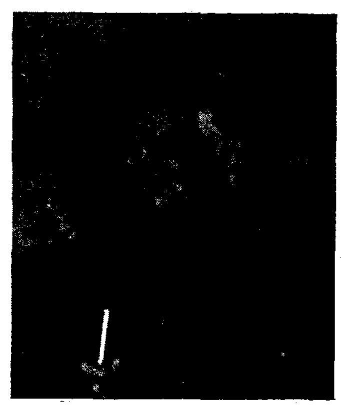

WALTER N. DEAN

LORAN-C PROPAGATION AND EQUIPMENT TIMING FLUCTUATIONS AND CONDUCTIVITY ESTIMATES OBSERVED IN THE GREAT LAKES REGION

John D. Illgen
Effects Technology, Incorporated
5383 Hollister Avenue
Santa Barbara, California 93111

Burt Gambill, Jr.
General Electric-TEMPO
816 State Street
Santa Barbara, California 93111

Tony Mason
Marinav Corporation
1140 Morrison Drive
Ottawa, Ontario, Canada

A series of measurements have been completed at sites along radials from Loran-C transmitters through three different areas in the Great Lakes region. Coverage is provided by the newly configured Northeast Coast Loran-C chain. An Accufix transmitter provided Loran-C signals in the Northwestern area near Lake Superior. This paper includes a description of Loran-C propagation and equipment fluctuations observed. Data is presented from approximately 15 measurement sites. The analysis of timing fluctuations will focus on the following:

1. Minor changes in TDs due to the passage of weather fronts over short and long propagation paths.
2. Magnification of timing fluctuations and local phase adjustments as distance increases from the control monitor.
3. Summary of RMS standard deviation and mean values (data represented for 24 hour period and 2 to 3 week periods).
4. Comparison with West Coast (USA) Loran-C and old East Coast (USA) timing fluctuations.

Additionally, the incremental time of arrival and time difference data obtained in the measurement program were used to obtain conductivity estimates. This portion of the analysis will focus on:

1. Comparison of conductivity values inferred from the data with original estimates from available conductivity maps.
2. Future data collection improvements.

John D. Illgen

John Illgen is currently Director of Communication and Navigation Systems at Effects Technology, Inc. (Effects Technology, Inc. is a subsidiary of Flow General, Inc.). Mr. Illgen's current responsibilities include receiver development, field engineering, data processing, laboratory testing pertaining to communication and navigation system analyses. A communication/navigation software-hardware simulation (VLF through EHF) capability has been established at ETI for use in assessing satellite and terrestrial systems in normal and disturbed environments. Prior to joining ETI Mr. Illgen was a member of the professional staff at General Electric-TEMPO (Nov. 1973 to May 1979) and Computer Sciences Corporation (Jan. 1967 to Nov. 1973). He was program manager for a series of U.S. Coast Guard experiments aimed at investigating the potential use of Loran-C for Harbor and Harbor Entrance navigation. Mr. Illgen was a key participant in a project to determine conductivity and to observe Loran-C timing fluctuations in the Great Lakes region. Have conducted communication system analysis for a variety of communication systems including: Pilgrim, DSCS II and III, SMS to Buoy Links, FLTSATCOM, LES 8 and 9, various DCS communication command centers and interconnecting links (aircraft and satellite). John Illgen received the M. Sc. in Electrical Engineering upon completion of his studies from the Technical University of Denmark.

Tony Mason

Qualified as a communications instructor in the Royal Marines and since 1969 has held management positions within the offshore industry with responsibility for international survey operations. Currently marketing manager for Marinav Corporation he was assigned as program manager for the Great Lakes Loran-C monitoring project.

Burt Gambill, Jr.

Manager, C^3 Program. Supervises and participates in studies of communication and navigation system performance. Terrestrial and satellite systems that operate at frequencies from ELF through SHF are modeled and analyzed. Mathematical models of the atmosphere and inosphere and propagation models are integrated into user-oriented system performance prediction computer codes. Burt Gambill received a B.S.E.E. from Oklahoma State University in 1954 and completed the Advanced Engineering Program, 1954-1957, General Electric Company and later participated in the Advanced Engineering Program as an instructor.

A METEOROLOGICAL PREDICTION TECHNIQUE FOR LORAN-C TEMPORAL VARIATIONS

by

Robert H. Doherty
Colorado Research and Prediction Laboratory, Inc.
1898 South Flatiron Court
Boulder, Colorado 80301

Lois W. Campbell
Analytical Systems Engineering Corp.
Old Concord Road
Burlington, Massachusetts 01803

Dr. Suren N. Samaddar
U. S. Coast Guard
Washington, D. C.

J. Ralph Johler
Colorado Research and Prediction Laboratory, Inc.
1898 South Flatiron Court
Boulder, Colorado 80301

ABSTRACT

Temporal variations in the propagation time of the Loran-C pulses due to changes in the electrical boundary condition at the surface of the earth, or due to the atmospheric refractive index variations resulting from weather systems, interact with the propagation mechanism for the groundwave and result in degradation of the navigation accuracy for the navigator. Temporal propagation effects vary with geographic locations, climate, seasons, and perhaps on the long term correlation with the sun spot cycle. The magnitude of these effects approach the order of microseconds in anomalous geographic regions, degrading the quality of the navigation service that the transmitting system provides.

Extensive measurements and analysis programs have shown that temporal variations are greater during cold conditions than during warm conditions. Also, when the variations are greatest there is apparently correlation with the surface temperature and refractive index dry term.

The results of this theoretical study demonstrate how the temporal variations are correlated with the refractive index lapse rate. In the winter this lapse rate is functionally related to the surface refractive index dry term. In the summer the effect of the dry term and the wet term tend to cancel reducing loran fluctuations and destroying the correlation with temperature variations. This theoretical study further demonstrates a technique where surface meterological measurements could be used to predict Loran-C temporal variations.

* * * * * *

Biographical Sketch of Robert H. Doherty

Since June, 1976, Robert H. Doherty has been Vice President of Colorado Research and Prediction Laboratory, Inc. ($CRPL_i$). He previously spent more than 25 years in radio propagation research work while employed by the various research laboratories of the U.S. Department of Commerce. His primary research studies have included low frequency propagation as it is related to navigation systems and the ionospheric D-region and interesting recorded geophysical phenomena. He has authored or co-authored more than 40 technical reports and papers with more than 20 open literature publications. Robert H. Doherty is one of the Founding Directors of the Wild Goose Association and has served as Director several times.

Biographical Sketch of Suren N. Samaddar

Suren N. Samaddar received a Ph.D. in Electrical Engineering from the University of Michigan, specializing in electromagnetic theory and wave propagation. He joined the Raytheon company in 1962 as a senior scientist and was responsible for conducting theoretical research in radiation from antennas, propagation in various media, and scattering from re-entry bodies. Dr. Samaddar joined the Calspan Corp. in 1970 and worked in soundwave propagation in oceanic waters, wave propagation in random media, and scattering from turbulent wakes behind re-entry bodies. In 1974 he joined GTE Sylvania, where he worked in the areas of EMP, ELF, VLF, and UHF propagation. Since 1976 he has been with the R&D Office of the U.S. Coast Guard specializing in Loran-C signal propagation studies.

Dr. Samaddar is a Senior Member of IEEE. He has published numerous papers.

Biographical Sketch of J. Ralph Johler

J. Ralph Johler is President of Colorado Research and Prediction Laboratory, Inc. (CRPLi). He holds degrees from the American University and George Washington University. From 1942 to 1976 his government career included working in various areas of physics for the U.S. Department of Commerce. He twice received the NBS Distinguished Authorship Medal (1/7/66 and 11/12/63) and has written 120 papers which have been published in various journals and as government documents.

Ralph Johler's professional work includes cosmic radio noise, atmospheric radio noise, design of noise measuring equipment; theory of radio propagation of LF, VLF, ELF, HF, and UHF; theory of magnetopolasmas, ground wave propagation, ionospheric wave propagation, pulse propagation, radio navigation pulses, sferics, nuclear pulses, mathematical and numerical techniques for special wave propagation problems such as propagation in a nuclear environment or in the presence of a disturbed ionosphere, LF radio navigation (Loran-C/D) and MF radio navigation (Loran-A). He has had extensive experience as a numerical analyst and in the applications of computers to the solution of mathematical problems.

Biographical Sketch of Lois W. Campbell

Mrs. Campbell has taken extensive courses in electrical engineering at Acadia University, Pembroke College and Northeastern University. She is a member of the Wild Goose Association, the IOA and URSI.

At ASEC, she has been involved in Loran-C propagation studies, the St. Lawrence Seaway navaid feasibility program and satellite communications analyses. Currently she is project engineer for the North Atlantic OMEGA Validation program.

Previously, Mrs. Campbell worked on HF OTH radar and communications system programs at Raytheon and VLF/LF propagation, communication and navigation programs at Pickard & Burns.

PRELIMINARY STABILITY ANALYSIS OF THE ST. MARYS RIVER MINI-CHAIN

by

LT David L. Olsen
CWO Charles E. Isgett

Office of Research and Development
U.S. Coast Guard Headquarters
Washington, D.C. 20590

Temporal instabilities on the order of several hundred nanoseconds were measured over the mini-chain's service area between Fall 1977 and Spring 1978. These instabilities, if true, could render the mini-chain unusable for precision navigation on the St. Marys River. A careful recollection effort was deemed necessary to verify the chain's performance and to definitively judge its navigation capabilities. In addition, a methodology is desired for establishing the stability of Loran-C signals in the general harbor and harbor entrance environment. This methodology is being investigated using the mini-chain.

A one year in-depth study of the mini-chain's stability has begun. The major preparations involved the creation of three fixed monitor sites plus the improvement of equipment and staffing at the monitor-control station. Time differences are recorded around the clock at the three new sites and at several transmitter stations. Data collected between February and April this year demonstrated a worst case variation of approximately 200 nanoseconds. This period included not only environmental changes but also various refinements in the equipment. These data cannot be considered to be the final measure of the mini-chain's performance, but are nonetheless informative.

The time difference data is being analyzed by a rather simple model which separates variations into uniform propagation effects, local errors and control errors The propagation component extracted from the preliminary data exhibits a high correlation with temperature, which can be attributed primarily to the vertical lapse rate of the index of refraction. The model bounds the physical effects which cannot be improved upon through equipment or procedural changes.

* * * * * * *

<u>Biographical Sketch of LT Olsen</u>

Lieutenant Olsen has been involved with the Loran-C navigation system since the start of his Coast Guard career in 1971. He spent his first tour of duty at the Coast Guard's Electronics Engineering Center in Wildwood, New Jersey, where he worked on the automation of Loran-C monitor and control equipment. Since 1975, Lt. Olsen has been assigned to the Office of Research and Development at Coast Guard Headquarters where he has been responsible for the development of Loran-C user equipment for precision navigation.

Lieutenant Olsen holds Bachelor and Master of Science degrees in Electrical Engineering from Iowa State University at Ames and the University of Illinois at Urbana. He is a member of the Wild Goose Association and the Institute of Navigation.

<u>Biographical Sketch of CWO Isgett</u>

Chief Warrant Officer Isgett is new in the field of Loran-C navigation systems. He has served as a project officer for the St. Marys River grid stability study since completing the Loran-C Engineering Course at the Coast Guard Academy in 1978. His project responsibilities have included site selection and equipment installation, plus writing programs to analyze the collected time difference measurements.

ECD VARIATIONS IN OVERLAND PROPAGATION

Walter N. Dean
26619 Shorewood Road
Rancho Palos Verdes CA 90274

Analysis of Loran-C data taken in 1977-78, along with recent measurements made by the Coast Guard in 1979 reveals some interesting variations of ECD over a variety of land propagation paths. These indicate that the nature of the terrain, especially its vertical profile, appears the major factor to change ECD. An extremely high correlation with signal strength is also observed. The significance of these data to marine, air and terrestrial users is discussed.

Biographical Sketch of Walter N. Dean

Walt Dean has been involved in the development of Loran-C, its predecessors and its offspring, for over 30 years. Although deeply involved in system concept and design, his major activity has been in test and evaluation of operating systems to understand better their peculiarities, and finding new ways to utilize the system.

He retired from Magnavox last spring and formed his own consulting company, Verdes Engineering Co. He has since done work for the U.S. Coast Guard, New York State, and several private firms, including Magnavox, on Loran and GPS studies.

Some of his earlier activities included non-paying jobs as Chief Engineer of Fort Wayne Public Television, and Chairman of the Fort Wayne Section of IEEE.

He has published some 15 papers and has 10 issued patents on Loran and radar.

SESSION V — WGA PANEL DISCUSSION

Subject: LORAN-C SIGNAL SPECIFICATION

Moderator: Jim VanEtten

Panel Members:

John Currie, Internav, Ltd.

Milt Dishal, ITT Avionics

Leo Fehlner, APL/JHU

Cdr Brent Mills, USCG (GWAN-2)

Cdr Steve Plusch, USCG (EEE-4)

"THE PANEL" LISTENS TO MILT DISHAL

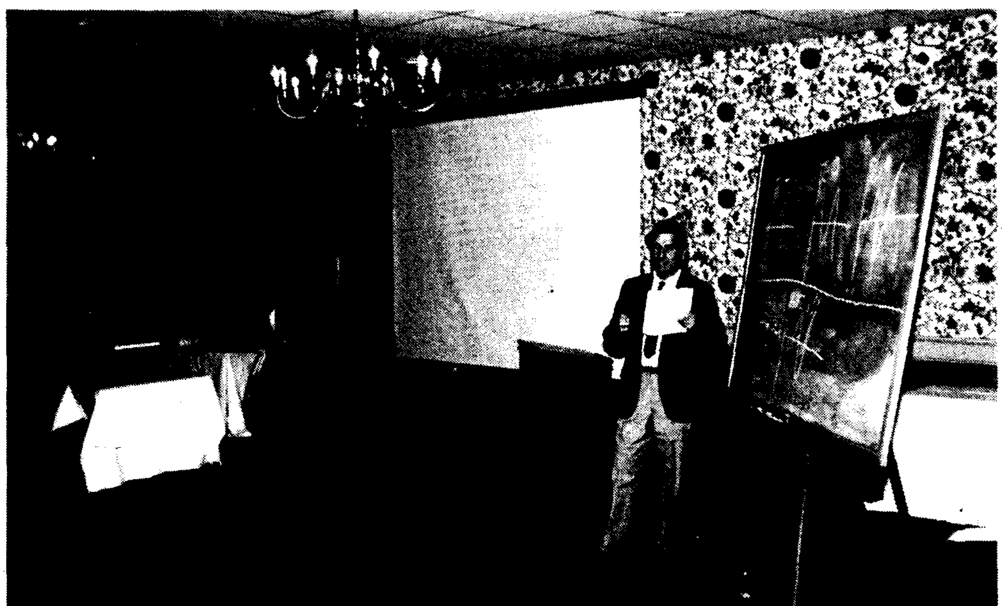

MILT DISHAL LEADS THE DISCUSSION

TECHNICAL PAPERS

AIRBORNE LORAN-C EVALUATION OF THE PRODUCTION AN/ARN-133 NAVIGATOR

Richard J. Adams
Systems Control, Inc. (Vt)
Champlain Technology Industries Division
2326 S. Congress Avenue, Suite 2-A
West Palm Beach, Florida 33406

INTRODUCTION

The implementation and acceptance of Loran-C as an airborne navigation system suitable for the missions of the United States Coast Guard, as well as for operations by the Coast Guard and other civil users within the National Airspace System (NAS), is addressed in this paper. This acceptance requires that several accuracy, repeatability, operational suitability and NAS compatibility questions be resolved. In order to answer these questions and to document the performance of the AN/ARN-133 navigator, a comprehensive evaluation program was developed. This paper summarizes the detailed results of the airborne Loran-C navigator tests performed by the Coast Guard to support the evaluation program.

BACKGROUND

The flight test program was performed from May 1978 through January 1979. The testing included verification of system accuracy, operational suitability testing in the Northeast Corridor, accumulation of data for IFR certification, long range overwater testing, and evaluation of Loran-C as a non-precision approach aid to both fixed and moving targets at sea.

The accuracy data was compiled during testing performed at the National Aviation Facilities Experimental Center (NAFEC) at Atlantic City, New Jersey and during the operational Northeast Corridor flights. These data were compared to and combined with the data previously collected (Reference 1) on the prototype TDL-424 airborne Loran-C navigator.

Operational data was obtained and procedural questions were addressed primarily using the Northeast Corridor test results. However, these results were complemented by results from the overwater/overland transition data, deep probes over the Atlantic Ocean and from operations in the Gulf of Mexico during the ship rendezvous and oil rig testing.

Both the accuracy data and the operational results were dependent on position information obtained from radar tracking and the airborne navigator lat/lon position information. These data were supplemented by detailed flight test observer logs as well as debriefing information obtained during the tests. The primary measure of performance was total system crosstrack error as measured with the tracking radar. This analysis was supported by examination of airborne flight technical error and airborne system errors in both the alongtrack and crosstrack directions. These four basic performance measures are defined as follows:

TSCT - Total System Crosstrack Error is defined as the actual aircraft deviation perpendicular to the desired course in the horizontal reference plane. TSCT was measured with precision tracking radar for the NAFEC tests and using ARTS III and IA radar for the operational testing.

FTE - Flight Technical Error is defined as the indicated amount of deviation from the desired course in the horizontal reference plane. The quantification of FTE was obtained by electronically measuring and recording deflections of the Crosstrack Deviation Indicator (CDI).

ASE - Airborne System Error is defined as the composite crosstrack error contributed by all airborne navigation equipment including sensors, receivers, computers, displays and any calibration, scaling or interconnecting errors peculiar to the system being evaluated.

ATE - Alongtrack Error is defined as the actual aircraft deviation from the desired position along the flight path. ATE results from the total error contributions of the airborne and ground equipment only. No FTE is used in determining the alongtrack error. ATE was measured using precision tracking radar for the NAFEC tests and using ARTS III and IA radar for the operational testing.

Both mean or bias errors (magnitude and direction) and two-sigma variability errors were calculated for TSCT, FTE, ASE and ATE where required.

SCOPE OF THE TESTS

Figure 1 summarizes the integrated

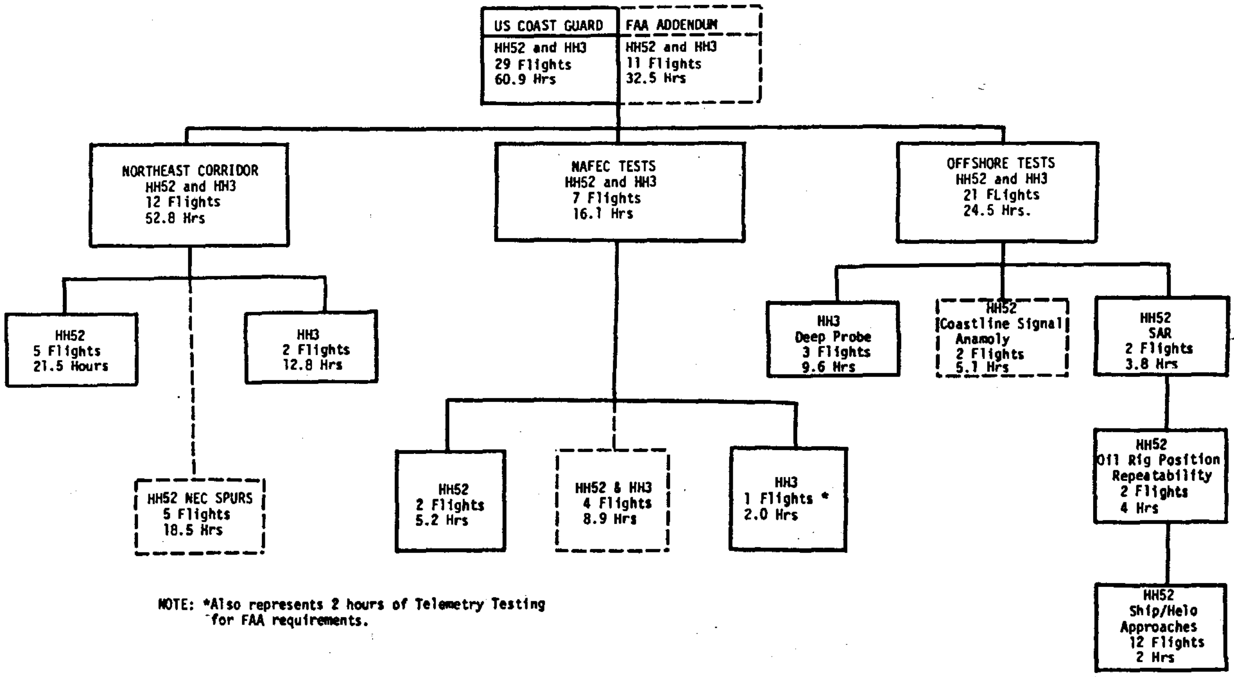

Figure 1 Integrated FAA and USCG Flight Test Program Summary

FAA and USCG flight test program. As shown in Figure 1, the scope of the integrated program was 93.4 hours. From this total flight time, over 6500 nautical miles of enroute data was obtained. The majority of this data (4133 nm) was collected flying the high density "Northeast Helicopter Corridor Routes from Washington, D.C. to New York City and from New York City to Boston." These routes have been approved by the FAA for area navigation at low altitudes (approximately 1500-4500 feet). The Jeppesen Company published a chart of these routes in December 1978. Alternate northbound and southbound routes were flown in both the non-updated and the preflight updated modes.

Included in this enroute data base was the Loran-C evaluation of the transition, or spur, routes currently flown to and from the Northeast Corridor by various users. These spur routes, in general, had even closer waypoint spacing and larger turn magnitudes (therefore higher pilot workload) than the published routes. The purpose of using Loran-C on all of these enroute segments was to demonstrate operational compatibility in today's ATC environment and to obtain data (using ARTS III and IA surveillance radar) on Loran-C accuracy. In addition, functional compatibility data on the production AN/ARN-133 Loran-C navigator was obtained as far as waypoint storage capability (the navigator stores nine waypoints) is concerned.

As shown in Figure 1, the NAFEC System Accuracy Tests were flown in the HH3 and HH52 aircraft with the production Loran-C navigator. This data was acquired to supplement the previous enroute, terminal and non-precision approach accuracy data collected with the prototype navigation in the HH52 aircraft (Reference 1). Figure 1 shows a total of 7.2 hours of NAFEC System Accuracy testing. The amount of data collected (sample sizes) was chosen to insure adequate statistical data reliability as described in Reference 2.

In addition to the accuracy testing performed at NAFEC, the FAA requested that a demonstration of the Loran-C navigator's telemetry function be performed. This data was of interest for possible applications to low altitude aircraft tracking for helicopter operations in general and for offshore oil rig operations in particular. A single flight was performed, entirely overland, to demonstrate this function. Real time aircraft telemetered position was recorded, as well as the EAIR indicated aircraft position.

The third major category of the integrated FAA and USCG Loran-C flight test program encompassed offshore operations. Figure 1 shows that these operations included both HH3 and HH52 test aircraft flying various profiles. In general, the HH3 was used for the longer duration flights due to its range capabilities. These included the deep probes overwater which ranged from 160 nautical miles to 200 nautical miles. The HH52 was used on a coastline signal anomaly test flown at dawn and dusk which zig-zagged across the coastline (five miles overwater and five miles overland) for a total along-track distance of 311 nautical miles covering 86 miles of coastline.

In addition to the coastline signal anomaly test, the HH52 flew two search and rescue patterns and two surveillance tests to substantiate prototype Loran-C navigator test results on these typical USCG operational scenarios. The search and rescue patterns covered a distance of 270 nautical miles. The surveillance tests required 280 nautical miles of enroute flying.

Finally, the HH52 was used for the Ship/Helo rendezvous procedures development performed in the Gulf of Mexico. The Loran-C navigator was utilized to simplify rendezvous procedures with both fixed and moving vessels. Preprogrammed waypoints, the navigator's ability to establish a new RHO/THETA waypoint from a preprogrammed fix, and the present position direct-to capability, were all used to develop a more accurate rendezvous with straightforward procedures requiring less pilot workload and reduced subjective judgement necessary on the part of the flight crew in order to perform the rendezvous.

DISCUSSION OF RESULTS AND ANALYSIS

The purpose of this section is to review the tabular and graphical data necessary to support the results and conclusions of this paper. The data discussed herein was collected during the operational flight test evaluation of the airborne AN/ARN-133 Loran-C navigator. The details presented in this section represent the results of a comprehensive review of the specific data collected on the ground, and in the air, regarding actual aircraft position, Loran-C indicated position, flight technical error, pilot workload, operational navigation problems and Loran-C equipment problems.

In order to establish the proper perspective regarding the numerous objectives of this evaluation, Table 1 delineates the flight test activity for each major test category in terms of the number of nautical miles flown for each type of testing. This quantification is interesting for two reasons. First, it is one method of presenting data for certification purposes when discussing enroute, terminal and final approach accuracy. Second, this subdivision allows an easy interpretation of how the production navigator data base integrates with the previously acquired prototype data (Reference 1). Table 1 summarizes the total number of nautical miles flown using the production AN/ARN-133 airborne Loran-C navigator. The data is categorized by the three major test areas which will be discussed subsequently. The enroute, terminal and offshore testing is shown by total nautical miles flown while the final approach data shows the number of each type of approach, which is more meaningful. It is significant to note that over 4100 miles of flying in the operational environment of the Northeast Corridor was successfully accomplished. This large amount of flight test activity, which was performed at altitudes from 500 feet to 4500 feet, did not reveal any significant operational problems from either the ATC or the flight crew's viewpoint. That is, no deviations from the planned route of flight occurred which caused either an ATC problem or an aircraft guidance problem.

Table 1 Production Loran-C Navigator Flight Test Program Summary

I. NORTHEAST CORRIDOR OPERATIONAL TESTING	
Enroute Distance Flown	4133 nm
Number of Approaches Flown	
Point-in-Space	43
Non-Precision	12
II. NAFEC SYSTEM ACCURACY TESTING	
Enroute Distance Flown	185 nm
Terminal Distance Flown (6 SIDs/6 STARs)	348 nm
Number of Approaches Flown	
Point-in-Space	0
Non-Precision	40
III. OFFSHORE TESTING	
Deep Probe Overwater (3 flights)	989 nm
Coastline Signal Anomaly	311 nm
Ship/Helo Rendezvous (12 approaches)	48 nm
Oil Rig Tests (9 approaches)	280 nm
Search and Rescue Test	270 nm
OFFSHORE TOTAL---------------	1898 nm

Figure 2 shows the composite aircraft tracks for both HH52 and HH3 helicopters. For ease of interpretation this figure is divided into two parts. Figure 2a shows the Washington, D.C. to New York, N.Y. data. Figure 2b shows the New York, N.Y. to Boston, Massachusetts data. The tracks were flown from November 5, 1978 to January 18, 1979. An inspection of Figure 2 shows that for all the flights performed, the test helicopters stayed well within the specified ±2 nm route width. A closer examination of the figure also shows that no significant track deviations occurred either at turns or due to data input workload. (The AN/ARN-133 stores only nine waypoints and the Southbound corridor route has 22 while the Northbound route has 20). These tracks, when viewed as a group (shaded areas), lead to the

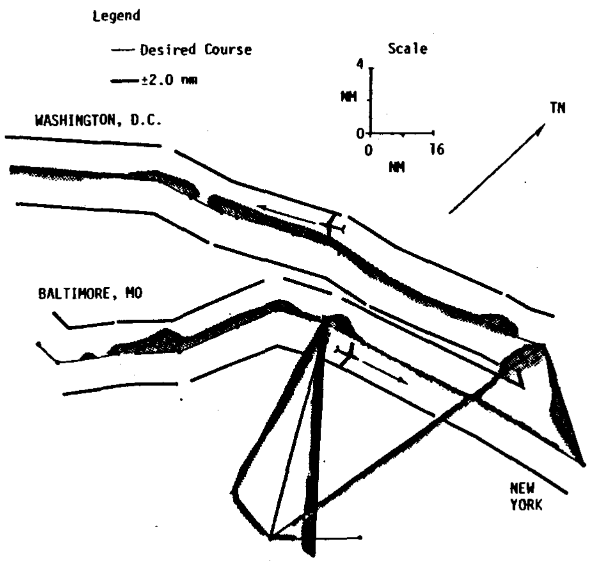

Figure 2a Composite Aircraft Flight Paths for the NEC Washington, D.C. to New York

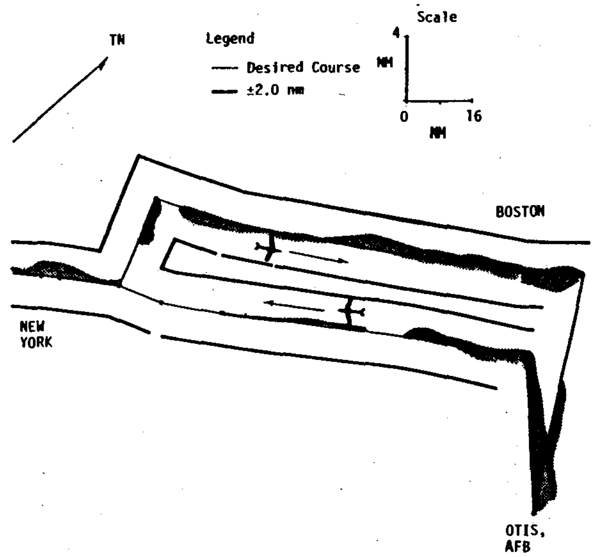

Figure 2b Composite Aircraft Flight Paths for the NEC New York, N.Y. to Boston, Mass.

conclusion that the test aircraft never strayed outside of ±1.0 nm from the desired track centerline.

In order to substantiate the qualitative interpretation of Loran-C accuracy based on Figure 2, statistics were generated as previously discussed. Table 2 presents a summary of those statistics to various levels of depth. The first row at the top of Table 2 presents an aggregation of all the NEC data collected on both helicopters in both updated and non-updated modes of operation. The net result of all these flights showed that TSCT errors fell with ±0.60 nm of the desired track on a two-sigma 95% probability basis. The mean error for this data was essentially zero (0.04 nm).

An examination of Table 2 can be made to investigate possible TSCT, FTE or ASE differences due to aircraft size, speed or maneuverability. Comparing the HH3 data (large, 140 knot aircraft) to the HH52 data (small, 80 knot aircraft) revealed no significant observable differences. Detailed segment by segment statistics for both test aircraft are presented in Reference 3. This data should be referred to for a more specific comparison of the two types of aircraft under identical Loran-C geometry conditions.

An overall assessment of the four performance measures shown in Table 2 results in the following set of error magnitudes:

Table 2 Overall Northeast Corridor Loran-C Data Summary
9960 Chain

TEST AIRCRAFT	DIR. OF FLT.	OPER. MODE	TSCT		FTE		ASE		ATE		REMARKS
			BIAS NM	±2σ NM	BIAS NM	±2σ NM	BIAS NM	±2σ NM	BIAS NM	±2σ NM	
HH52, HH3	N & S	NU & U	0.04	0.60	0.01	0.19	0.06	0.58	-0.09	0.69	All Data
HH52, HH3	N & S	NU	0.05	0.61	0.01	0.17	0.07	0.60	-0.19	0.64	Effect of
HH52	N & S	U	0.01	0.58	-0.01	0.21	0.04	0.51	0.11	0.61	Updating
HH52, HH3	N	NU	-0.11	0.39	0.02	0.19	-0.05	0.43	-0.29	0.34	NU
	S	NU	0.19	0.62	0.01	0.16	0.18	0.64	-0.11	0.77	N vs S
HH52	N	U	-0.06	0.54	0.00	0.30	0.00	0.40	0.39	0.47	U
	S	U	0.05	0.59	-0.01	0.14	0.06	0.56	-0.05	0.43	N vs S
HH52	S	NU	0.26	0.78	-0.01	0.14	0.26	0.79	0.16	0.32	Effect
HH3	S	NU	0.12	0.34	0.02	0.18	0.10	0.38	-0.37	0.73	of A/C
HH52	N	NU	-0.15	0.41	-0.00	0.23	0.03	0.48	-0.13	0.22	Type &
HH3	N	NU	-0.08	0.38	0.03	0.15	-0.11	0.36	-0.38	0.27	N vs S
HH52	S	U	0.05	0.59	-0.01	0.01	0.14	0.06	0.56	-0.05	N vs S & Effect of
HH52	N	U	-0.06	0.54	0.00	0.30	0.00	0.40	0.39	0.47	Updating

NOTE: NU - Non Updated
U - Updated
TSCT - Total System Crosstrack
FTE - Flight Technical Error
ASE - Airborne System Error
ATE - Alongtrack Error

	Maximum	Minimum	Aggregate
TSCT	0.78 nm	0.34 nm	0.60 nm
FTE	0.30 nm	0.14 nm	0.19 nm
ASE	0.79 nm	0.36 nm	0.58 nm
ATE	0.77 nm	0.22 nm	0.69 nm

This assessment reinforces the observation previously made regarding Loran-C accuracy. Specifically, the overall performance of Loran-C in the Northeast Corridor for a large number of flights showed that a ±1.0 nm two-sigma value was never exceeded. This certainly substantiates the ability of a Loran-C equipped aircraft to remain within the ±2.0 nm route width. However, this is not meant to imply that there are no potential operational problems associated with Loran-C navigation in this airspace environment. The following paragraphs present, discuss and analyze Loran-C utilization from an operational viewpoint.

A total of 58 events indicative of potential operational problems occurred during the Northeast Corridor evaluation of Loran-C. These problems were in the areas of Air Traffic Control, Pilot/Copilot procedures and Loran-C navigator hardware/software.

In order to develop a qualitative interpretation of the character of the three operational problem areas, each category was broken down further. ATC events were discovered in four general areas. These were: frequency congestion, airborne radio (transmitter and receiver) problems, route deviations for traffic and ATC coordination. Pilot/Copilot problems were found in seven general categories. These seven categories included: attention/fatigue, Loran-C training, turn overshoots, flight control/navigation, engine problems, route deviations for traffic and waypoint input errors. Finally, the Loran-C navigator problems occurred in five areas. These were: warn/advise lights, no automatic leg change, electrical system shutdown, display lock-up and loss of lock on Loran-C ground stations. Table 3 presents an analysis and categorization of the 58 operational problems experienced during the NEC testing.

Due to space constraints, the interested reader can refer to Reference 3 for a detailed analysis of all three major categories. The current discussion will highlight the Loran-C navigator problems listed in Table 3. For this category, 22 problems caused significant workload or navigation errors to warrant investigation. As shown in Table 3, the most frequent of these navigator events was the illumination of the warn or advise lights. This occurred 16 times during the NEC tests and five times during the transition or spur route tests. There are four basic causes which produce a warn light. These are: (1) not in track, (2) lat/lon runaway, (3) leg change calculation, and (4) checksum error. Of the sixteen NEC warn lights, seven were caused by the navigator going into "float" or "not-in-track" modes, six were caused by required secondary changes and the causes of the remaining three were undetermined. From an operational viewpoint it was even more significant to note that four of these 16 warn/advise indications occurred during either takeoff (2) or final approach (2). Although no serious operational problems occurred with three of the four, during the point-in-space approach to Boston, the warn/advise illuminated for nearly three minutes and the navigator was in float for this time. This type of occurrence is a serious operational problem in the approach phase of flight and could become an airspace problem in congested areas.

A more enlightening presentation of the individual warn/advise light occurrences is shown graphically in Figure 3. This illustration shows that discrete warn/advise lights occurred in the NAFEC, Baltimore, and Nantucket areas while repeated warn/advise indications were obtained in and around the New York City Metroplex, and in the Bridgeport, Connecticut area. Figure 3 also shows that the frequency of occurrence of secondary changes was concentrated on the baseline from Seneca to Nantucket.

In addition to the many Loran-C warn/advise occurrences, other navigator problems occurred. These other problems were due to the navigator's automatic leg change function not working properly (occurred twice), electrical system shutdowns (which also occurred twice), display lock-up and loss of ground station lock-on (each of which occurred only once). The cause of automatic leg change malfunction was not determined, but it did occur while the DTW and CTD readouts on the Loran-C navigator indicated that the aircraft was within the "arrive" circle. In one case, a 1.8 nm overshoot resulted and in the other a 0.5 nm overshoot resulted. It is operationally important to note that the warn/advise lights which were followed by electrical system shutdown did not cause any significant aircraft track deviations. In one case the warn was on for 2 minutes followed by a 12 second loss of electrical power. In the other case a 39 second warn was followed by a 10 second electrical shutdown. In the first case, the navigator reacquired and locked on to the ground station signals in 36 seconds and in the second case 45 seconds were required. These Loran-C navigator problems did not cause any large airspace deviations during the

Table 3 Operational Problems in the Northeast Corridor by Type and Frequency of Occurrences

PROBLEM CATEGORY	PROBLEM TYPE	NUMBER OF OCCURRENCES	TOTAL BY CATEGORY
Pilot/Copilot Problems	Turn Overshoots (Pilot)	8	
	Loran-C Training	6	
	Flight Control/Navigation	5	
	Attention/Fatigue	3	
	Waypoint Input Errors	3	
	Engine Problems	1	
	Route Deviation For Traffic	1	
Pilot/Copilot Total			27
Loran-C Navigator Problems	Warn/Advise Lights	16	
	No Automatic Leg Change	2	
	Electrical System Shutdown	2	
	Display Lock-up	1	
	Loss of Ground Station Lock	1	
Loran-C Navigator Total			22
ATC Problems	Frequency Congestion	4	
	Airborne Radio (Rec/Xmit)	[illegible]	
	ATC Coordination	2	
	Route Deviation for Traffic	1	
ATC Total			9

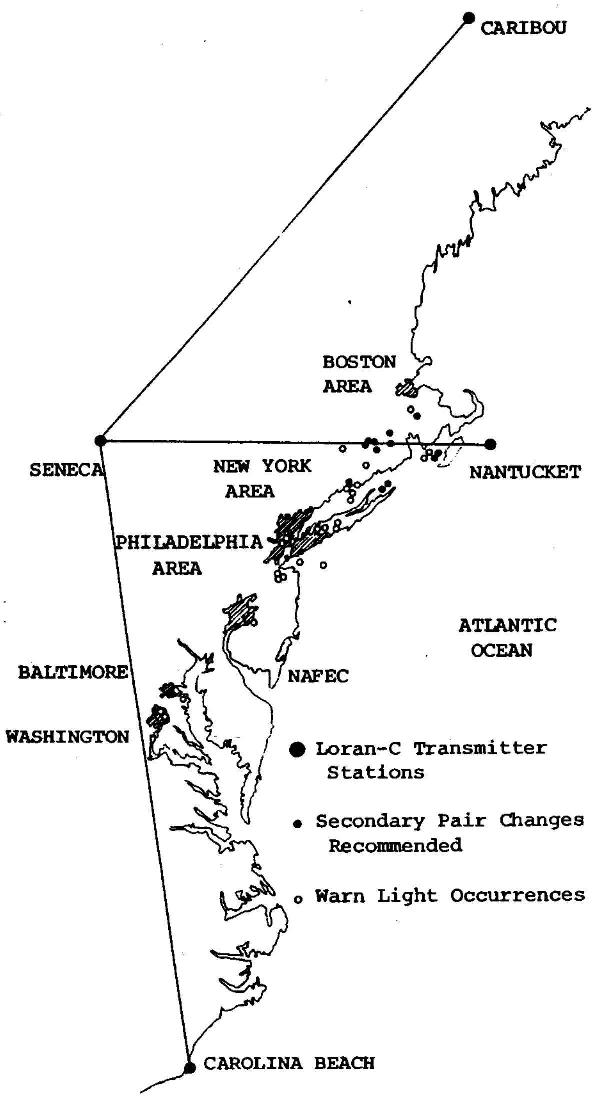

Figure 3 Locations of Warn Lights and Secondary Changes During the AN/ARN-133 NEC Testing

tests. However, they did tend to increase pilot/crew workload and they could become operationally significant under IMC, in high density operations or during critical flight phases.

Transition (Spur) Route Test Results

In addition to the enroute Northeast Corridor testing previously discussed, several flights were flown on routes which are currently in use, transitioning to and from the corridor. The specific routes tested were representative of operational routes used by Sikorsky Aircraft, Mack Truck, RCA and New York Airways. The data presented in this section assesses the performance of the Loran-C navigator on these routes.

Figure 4 illustrates the spur routes currently used, their geometry and their relationship to the entire Northeast Corridor route. Statistical data obtained on these routes is summarized in Table 4.

Table 4 Transition (Spur) Route Data Summary

ROUTE STRUCTURE	TSCT		FTE		ASE		DATA POINTS
	BIAS nm	$\pm 2\sigma$ nm	BIAS nm	$\pm 2\sigma$ nm	BIAS nm	$\pm 2\sigma$ nm	
SIKORSKY	0.06	0.69	0.05	0.21	0.06	0.66	1181
RCA	0.04	0.35	0.00	0.19	0.05	0.30	1007
MACK TRUCK	0.08	0.70	-0.03	0.24	0.11	0.66	1808

By comparing the spur route data to the summary results for the enroute Northeast Corridor data from Table 2, it can be seen that the Loran-C accuracy was essentially the same. Therefore, it was concluded that the shorter segment lengths and larger turn angles typical of the spurs did not cause any significant navigation problem when using Loran-C.

The New York Airways Spur routes were flown to heliports in the East River and

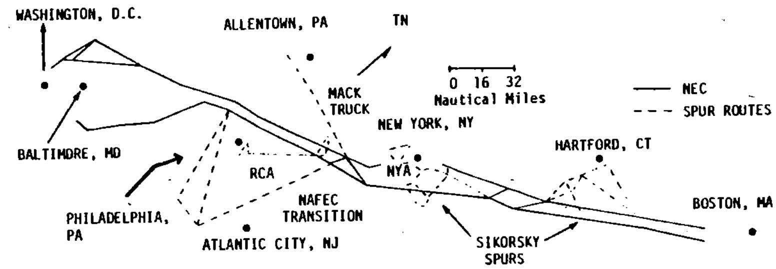

Figure 4 Overview of the NEC Test Routes

Hudson River areas of New York and New Jersey. The waypoints used in this test were the Pan Am helipad (Pan Am), LGA E. 34th Street helipad (LGA E. 34th), World Trade Center (WTC), Newark Dock or Ramp (EWR Dock) and Teterboro Airport (TEB). The planned route was designed to use prominent visual reference as navigation aids (Williamsburg Bridge, Manhattan Bridge, Brooklyn Bridge, Governor's Island, and Lincoln Tunnel). However, these aids were not programmed into the computer as waypoints for the test. These extra waypoints would have increased cockpit stress in programming because of their rapid use (about one every 40 seconds on the East River). The routes flown utilized these navigation reference points, as supplements to the programmed waypoints. This led to extensive use of the Hudson and East Rivers as desired flight paths since altitude obstructions, TCAs, arrival and departure traffic routes, as well as fuel considerations were hinderances to flying direct routes over Manhattan Island. As a result the routes were considerably simplified. As shown by the composite airborne Loran-C data in Figure 5, this test demonstrated the ability of the Loran-C navigator to provide accurate and repeatable navigation to waypoints in an operational environment which necessitates use of visual references. These visual reference and waypoint defined routes demonstrated minimum air traffic conflicts, normal controller communication workload, and a minimum of navigator programming time. Figure 5 shows that the repeatability of the desired routes were acceptable even though visual reference was used to supplement the Loran-C navigation information.

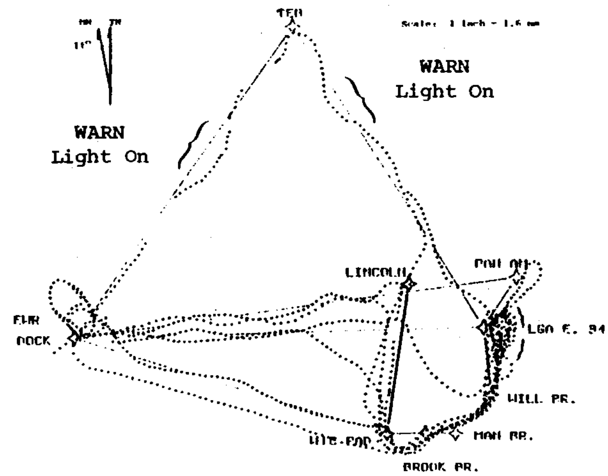

Figure 5 Airborne Loran-C Plot of the New York Airways Spur Route Flight Test

NAFEC System Accuracy Test Results

Table 5 summarizes the overall NAFEC System Accuracy test results for the AN/ARN-133 navigator. The data included in Table 5 allows several comparisons to be made. First of all, it is important to note that all the data in the table was flown using the Non Updated L/λ operating mode, that is, the area navigation waypoint information was prespecified on the charts, stored in the Loran-C navigator and flown in a manner compatible with the expected characteristics of an actual NAS user application. With this in mind, Table 5 shows a comparison of prototype and production Loran-C navigator data for two different helicopter types and two different Loran-C chains. As was the case for the prototype navigator, the production AN/ARN-133 navigator always remained well within the allotted two-sigma airspace for enroute, terminal and final approach. Aggregate TSCT errors for the navigator never exceeded ±2.0 nm in the terminal area. In the final approach area, TSCT bias errors to runway 04 at NAFEC approached ±0.4 nm, but did not exceed the ±0.6 nm allotted. More final approach accuracy data will be presented and analysed in detail subsequently. Table 5 does reflect the change of Loran-C chains (geometry). The production HH3 data taken on the new (9960) chain shows a smaller bias error (TSCT) than the corresponding prototype of production data taken with the old (9930) chain.

Flight Technical Error (FTE) data with the production navigator was not substantially different than the prototype unit. The FTE did not seem to increase significantly with the larger and faster HH3 aircraft. Using non-

Table 5 Summary of Non-Updated NAFEC System Accuracy Test Results

Navigator / Helicopter / Chain — Airspace	Prototype[1] HH52 9930 BIAS NM	Prototype[1] HH52 9930 ±2σ NM	Production HH52 9930 BIAS NM	Production HH52 9930 ±2σ NM	Production HH3 9960 BIAS NM	Production HH3 9960 ±2σ NM	AC 90-45A Requirement ±2σ NM
Enroute							
TSCT	0.39	0.12	0.42	0.08	.21	.54	2.50
FTE	-0.01	0.09	0.02	0.07	.01	.08	2.00
ASE	0.40	0.09	0.40	0.03	.21	.53	1.50
Terminal							
TSCT	0.03	0.51	0.08	0.46	.13	.32	1.50
FTE	0.01	0.15	0.03	0.10	.02	.12	1.00
ASE	0.02	0.49	0.06	0.46	.11	.32	1.12
Approach (Non-Updated L/λ)							
TSCT	-0.38	0.10	-0.36	0.11	-.26	.08	0.60
FTE	0.02	0.09	0.04	0.12	.05	.09	0.50
ASE	-0.39	0.04	-0.39	0.03	-.31	.03	0.33

[1] Prototype ASE sign convention was changed to satisfy the equation TSCT = FTE + ASE used in the production data reduction.

updated (raw) Loran-C signal accuracy did not affect FTE for either the old (9930) or the new (9960) Loran-C chains.

Examination of the Airborne System Error (ASE) substantiates the results obtained from the TSCT analysis. That is, Loran-C position errors never exceeded ±0.6 nm enroute or terminal and never exceed ±0.4 nm in the non-precison approach data in the crosstrack direction. However, a Loran-C accuracy problem did occur in the compliance with alongtrack accuracy requirements for non-precision approaches. This data will be discussed in the following paragraphs.

AC 90-45A Compliance Data

The acceptable means of compliance for demonstrating Loran-C capabilities as an area navigation system are thoroughly described in Reference 4. Table 6 compares the crosstrack and alongtrack Loran-C measured data to the specific AC 90-45A requirements. Measured and specified values are shown for enroute, terminal and approach airspace. The measured data shown in Table 6 was taken on both the HH3 and HH52 helicopters. The Loran-C navigator was flown in the non-updated mode for this entire data set.

Table 6 Overall Comparison of AN/ARN-133 Accuracy and AC 90-45A Requirements

	CROSSTRACK		ALONGTRACK	
	AC 90-45A	Measured	AC 90-45A	Measured
ENROUTE	2.5 nm	0.6 nm	1.5 nm	0.2 nm
TERMINAL	1.5 nm	0.5 nm	1.1 nm	0.6 nm
APPROACH	0.6 nm	0.5 nm	0.3 nm	0.5 nm

Examination of the crosstrack values in the table show that for both enroute and terminal operations, the navigator consistently performed well within the required limits. Both the AC 90-45A values and the measured values in Table 6 are two-sigma, 95 percent probability numbers. It can be concluded from these crosstrack statistics that Loran-C performed within the specified crosstrack limits for all three airspace regions.

In the alongtrack dimension, Loran-C showed similar positive results for enroute and terminal airspace. However, the approach accuracy did not meet the current AC 90-45A requirements. Table 6 shows that the specified AC 90-45A limit of 0.3 nm was exceeded by 0.2 nm for the statistical data base used. The impact of this degraded alongtrack accuracy during a non-precision approach, would be in properly determining when the aircraft had reached the Initial Approach Fix, the Final Approach Fix and the Missed Approach Point. Since each of these fixes are normally intercepted during the descent phase of flight, the alongtrack error propagates into an altitude error with respect to specified minimums at each of these fixes. The exact implication of the degraded Loran-C performance in the alongtrack dimension must be determined by the Federal Aviation Administration (FAA).

In order to provide the FAA with additional data for this decision, a detailed investigation into the final approach performance of Loran-C was undertaken. Specific final approach tests were performed with both the HH3 and the HH52 aircraft. Each aircraft executed several approaches to each runway at NAFEC (04, 22, 08, 26, 13, 31).

Figure 6 presents the EAIR tracking data for all of these approaches. This data shows the actual aircraft path vs the desired final approach course for each runway. Final approach TSCT errors were calculated from this data. However, Figure 6 shows qualitatively that the Loran-C bias error behaved consistently on reciprocal runway headings for all the data collected. Both HH3 and HH52 data is shown. All flights were flown using the new 9960 East Coast Chain.

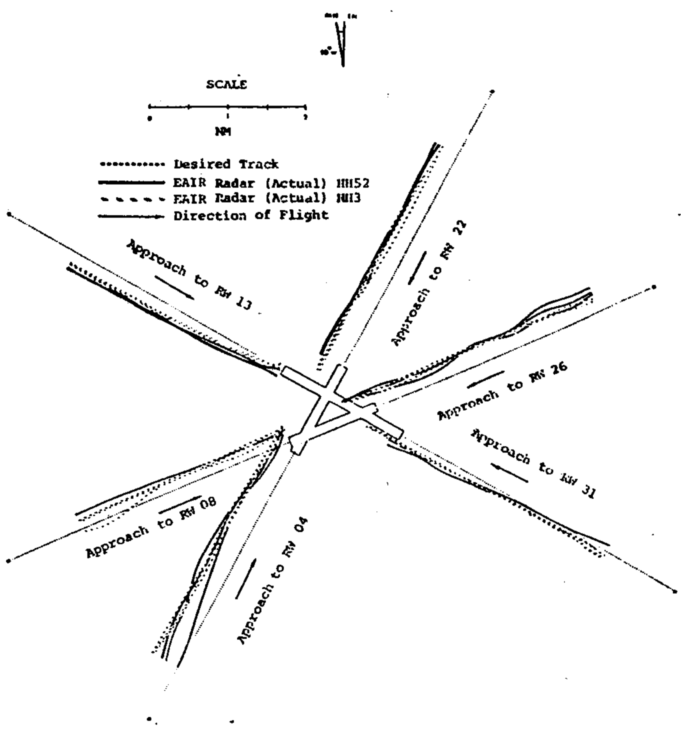

Figure 6 Multiple Runway Approach Data at NAFEC

Table 7 quantifies the TSCT data for each runway heading by aircraft type and for both aircraft aggregated. Detailed statistics for each route segment and for FTE and ASE as well as TSCT are presented in Reference 3. Table 7 shows that reciprocal heading runways had mean errors of comparable magnitudes and opposite signs as would be expected.

Telemetry Tracking Demonstration

In addition to the AC 90-45A Loran-C accuracy data base obtained at NAFEC, the production navigator was used to demonstrate a telemetry data link function. This test was flown at NAFEC to illustrate possible applications (or integration) with current ATC procedures for the offshore oil rig operators. The Loran-C telemetry provides a plot of aircraft present position below normal surveillance radar coverage which could be used both onshore and offshore. The objective of this demonstration was to qualitatively examine the Loran-C downlinked position data with respect to the precision EAIR radar track.

The telemetered position data is shown in Figure 7 compared to EAIR data and desired track. Figure 7 illustrates that downlink aircraft position data was obtained and that the accuracy of this data was not unreasonable relative to the actual aircraft track as measured by EAIR. The telemetry function demonstration was considered acceptable. However, the usability of this type of surveillance data for ATC purposes in such nonradar environments as the offshore oil rig areas must be determined by a significant amount of additional testing.

OFFSHORE TESTING

There were several test objectives to be satisfied which required flights overwater. The behavior of Loran-C signals and Loran-C accuracy out to the 200 nm limit of the Coastal Confluence Zone was of interest. This data was collected during a series of Deep Probes over the Atlantic Ocean off of Atlantic City, New Jersey. The existence of a Loran-C signal anomaly along the coastline had been hypothesized and was investigated both a dusk and at dawn. This data was collected during two creeping line patterns which criss-crossed the coastline along an 86 nm length. Other Loran-C data obtained offshore in the Atlantic included Search and Rescue tests to verify the performance of the production vs the prototype navigators.

Table 7 NAFEC Final Approach TSCT Summary (Production Navigator, 9960 Chain)

RUNWAY HEADING	HH3 (NON-UPDATED)		HH52 (NON-UPDATED)		AGGREGATE	
	Bias NM	±2σ NM	Bias NM	±2σ NM	Bias NM	±2σ NM
040°	-0.31	0.07	-0.26	0.24	-0.28	0.18
220°	0.29	0.07	0.32	0.07	0.31	0.08
080°	-0.08	0.12	-0.16	0.03	-0.10	0.13
260°	0.16	0.06	0.16	0.12	0.16	0.10
130°	0.15	0.04	0.16	0.06	0.16	0.05
310°	-0.11	0.04	-0.04	0.13	-0.08	0.12

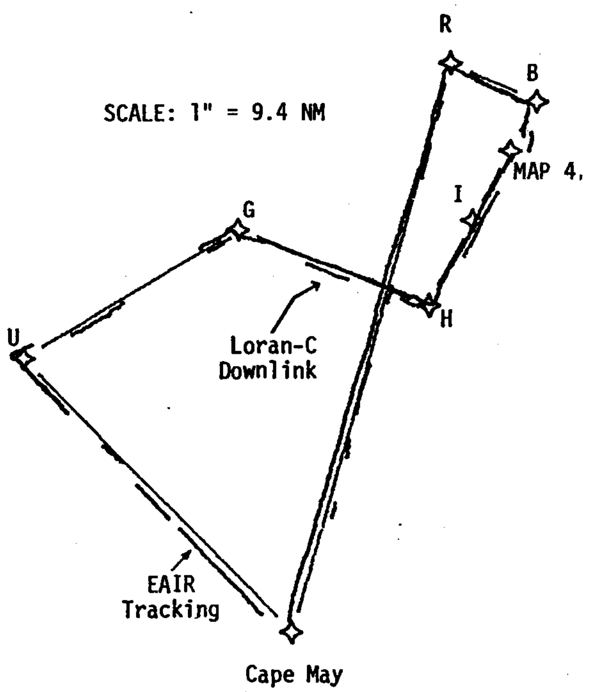

Figure 7 Loran-C Downlink Telemetry Tests

Additional flight testing of Loran-C accuracy and functional capabilities was conducted in the Gulf of Mexico. Ship/Helo rendezvous tests were performed to assess any improvement in rendezvous procedures attainable with Loran-C. Finally, oil rig tests were performed to verify the ability of Loran-C to accurately guide an aircraft to rigs in various cluster densities and to illustrate repeatability accuracy for USCG surveillance purposes.

The results of all five of these offshore experiments are presented and analyzed in the following paragraphs.

Deep Probe Overwater Testing

The deep probes offshore were performed to demonstrate operation of the Loran-C navigator during long range overwater missions and to document any signal propagation, functional or ATC operational problems in the execution of these flights.

Table 8 presents the statistical error analysis for the deep probe overwater testing. It is significant that none of the errors measured exceeded ±0.3 nm and that large numbers of data points were aggregated (52-460). It should also be noted that the 6-2 data was on the 9930 chain and the 11-7 data was on the 9960 chain (398 and 341 data points, respectively). If the Bravo to New Era segment statistics are compared for the effect of the new chain, the following results are obtained:

1) The 9960 data was more accurate based on both TSCT and ASE measures.

2) The ATE with the 9960 chain was approximately the same magnitude but of opposite sign compared to the 9930.

3) Both flights were flown accurately by the pilot based on measured FTE.

Since the orientation of the test pattern for the deep probe was basically East-West the behavior of the TSCT and ASE mean error magnitudes, as well as the ATE sign change, can be explained by examining the Loran-C northing and easting errors for the two different chains.

	6-2-78 9930	11-7-78 9960
Northing Error	-0.23	-0.07
Easting Error	-0.34	+0.38

Since the Northing error was greatly reduced with the 9960 chain, this was reflected in more accurate TSCT guidance along the basic easterly course (TSCT went from -0.25 nm to -0.07 nm on the Bravo to New Era segment.

Coastline Signal Anomaly Tests

These tests were structured to obtain data on the postulated overland/overwater transition anomaly which could impact Loran-C accuracy. The tests included two flights in the HH52 aircraft. A dawn creeping line pattern was flown back and forth along the coastline on 12-18-78 and a comparable pattern was flown at dusk on 1-19-79. The primary objective of these tests were to define and document the extent to which the land/water interface affects navigation accuracy using Loran-C. In order to accomplish these objectives it was necessary to examine both the actual aircraft track information obtained from EAIR and the Loran-C airborne indicated position data.

Figures 8 and 9 present the entire set of EAIR tracking data collected for the dusk and dawn coastline tests, respectively. The actual aircraft tracks are shown overlayed on the coastline. A cursory inspection of this data leads to the correct conclusion that no signal anomalies were observed. This conclusion was substantiated by the observer's logs and flight crew commentary. In addition, this was verified by the CDI deflection data recorded. However, due to the speed of the aircraft or the scale of these figures, it might be possible to miss an actual anomaly. Therefore, several coastline

Table 8 Deep Probe Overwater Statistics

WAYPOINTS	TSCT		FTE		ASE		ATE		ATO	NUMBER OF POINTS	CHAIN	DATE
	Bias NM	±2σ NM	Bias NM	±2σ NM	Bias NM	±2σ NM	Bias NM	±2σ NM	NM			
Bravo-New Era	-.2535	.0512	.0070	.0407	-.2605	.0334	.3223	.0241	74	398	9930	6-2-78
New Era-Charlie	-.0172	.0631	.0223	.0380	-.0395	.0595	.2999	.0394		65		
Bravo-New Era	-.0659	.0494	-.0325	.0471	-.0335	.0370	-.3790	.0236	74	341	9960	11-7-78
New Era-Charlie	.0957	.0648	.0012	.0261	.0946	.0679	-.4219	.0172		52		
Delta-Hotel	.0590	.0853	-.0028	.0351	.0618	.0792	.2688	.0254	200	460		

*ATO = ALongtrack Distance

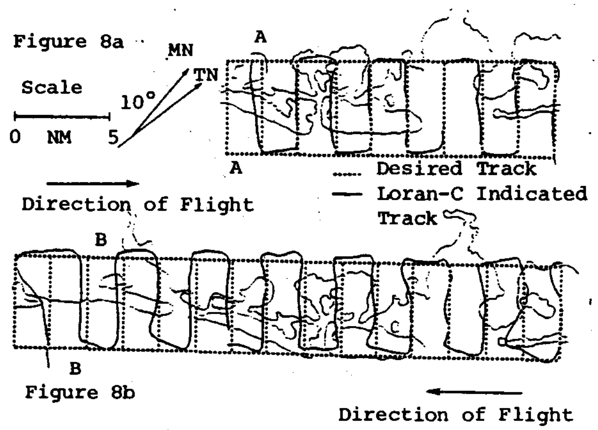

Figure 8 Dusk Coastline Signal Anomaly Test Profile of Loran-C Indicated Position

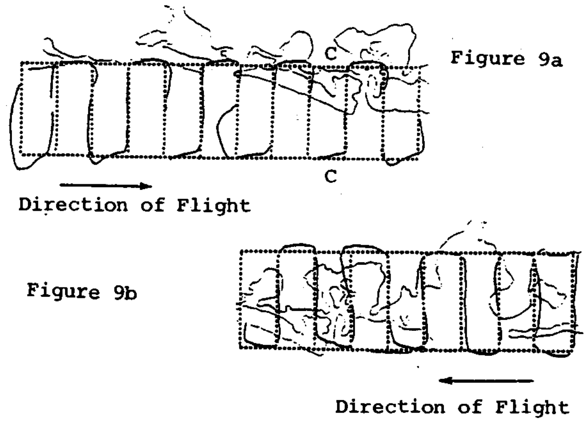

Figure 9 Dawn Coastline Signal Anomaly Test Profile of Loran-C Indicated Position

crossing points were examined carefully to try to discover the hypothesized anomaly. Based on this analysis of actual aircraft tracking data, lat/lon Loran-C data and CTD/ATD data, no significant coastline signal anomalies were discovered.

Ship/Helo Rendezvous Procedures Test Results

The ship/helo rendezvous test encompassed 17 flights for 2.0 hours. The results of this test were derived from airborne recorded data and the observer's logs only, since no tracking was available in the test area. The ship/helo rendezvous approaches were conducted to a stationary buoy although a ship had been secured for the test. Unfortunately, the ship was diverted for a priority surveillance activity during the testing period.

The test was divided into the three approach techniques illustrated in Figure 10. The specific flights for each technique will be discussed in chronological sequence. Technique 1 was evaluated during five approaches (four complete and one attempt) illustrated in Figure 11. Approaches 1 through 5 of Technique 1 were accomplished using the display hold function of the navigator to create a waypoint for the buoy's position, and the standard USCG ship/helo rendezvous and beep-to-hover procedures. After completing the tear-drop and stabilized on wind line (65° true), the aircraft was approximately 1.4 nm from the buoy for approaches 2-5, providing sufficient time for the pilot to complete each approach. The complete rendezvous required about 4 minutes per approach. The pilot and copilot confidence level was described as being "very high" and the workload as "low" for Technique 1 approaches. The headdown time for the pilot and copilot was about 5% and 10%, respectively.

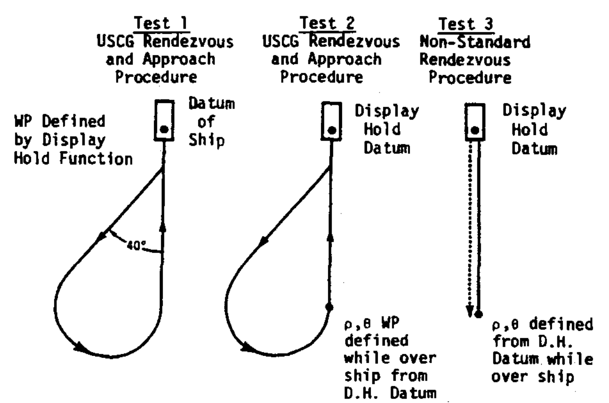

Figure 10 Ship/Helo Rendezvous Test Profiles

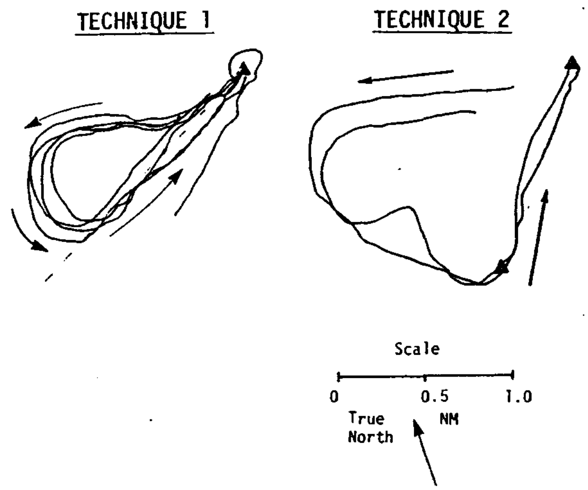

Figure 11 Ship/Helo Rendezvous Approach Profiles for Techniques 1 and 2

Technique 2, Figure 11, incorporated the USCG standard ship/helo rendezvous and beep-to-hover procedures with extensive Loran-C navigator utilization. The procedure was for the copilot to create the buoy position first with the display hold function, then create the FAF waypoint while the pilot proceeded downwind. The first attempt failed due to the inability of the copilot to provide navigation for the pilot to the FAF prior to coming to the first turn. The second attempt (Approach 1) was completed in approximately 7 minutes. The third and fifth attempts failed due to the copilot's inability to provide navigation prior to the pilot making the 40° turn from downwind. Attempts four and six failed because the copilot incorrectly calculated the FAF waypoint with the navigator's rho, theta function. The seventh attempt (Approach 2) required approximately 6 minutes to complete. During the tear-drop maneuver, the pilot misunderstood the copilot's instructions for the next turn as being an immediate maneuver, deviating from course by approximately 0.3 nm.

The pilot and copilot confidence level for Technique 2 was described as being "very low" and the workload level as "very high", requiring about 5% and 95% headdown time for the pilot and copilot respectively.

Technique 3, Figure 12, consisted of 5 complete approaches. This technique utilized the display hold function to create the buoy position and the rho, theta function to create the FAF as in Technique 2. However, straight departure and approach segments were used rather than the USCG tear-drop maneuver. It was determined that 1.7 nm was an adequate approach segment distance from the FAF to the buoy. Approaches 1, 2 and 3 were flown along the windline with a final approach leg heading 65° true. Approaches 4 and 5 were flown along a heading perpendicular to the windline, 155° and 335° true, respectively. There is a general indication of improvement through each successive approach. Except for the first approach, which required 7 minutes, all others were completed in approximately 5 minutes.

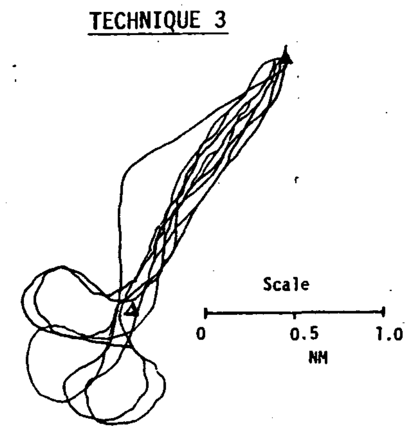

Figure 12 Ship/Helo Rendezvous Approach Profiles for Technique 3

The pilot and copilot confidence level for Technique 3 approaches were described as being "high" and the workload as "low", demanding about 5% and 15% headdown time, for the pilot and copilot, respectively.

For all approaches, regardless of workload, the Loran-C navigator provided navigation to the buoy with an average accuracy of 0.01 nm in CTD and 0.04 nm in ATD, relative to the FAF to buoy route segment.

Oil Rig Tests

This section presents the results of the accuracy and repeatability testing of the Loran-C navigator's applicability to the U.S. Coast Guard's surveillance/enforcement mission and the offshore oil industry. As previously described, accuracy and repeatability testing was performed on three oil rigs in the Gulf of Mexico near Mobile, Alabama. These rigs were located in areas of varying rig density. Approximately four minutes of data in lat, lon and TD's was acquired for each rig on two separate days. The Loran-C East Coast 9930 chain in the update mode was used for this test, as the Gulf of Mexico chain (7980) was not in scheduled service at that time.

Table 9 presents a summary of the

Table 9 Loran-C 2 d_{rms} Accuracy Of Test Oil Rigs In The Gulf of Mexico With Chain 9930

Oil Rig I.D.	Latitude (Degree, Min.)	Longitude (Degree, Min.)	Mean Position Error (Feet)	2 d_{rms} (Feet)	Data Points	Distance* Offshore (nm)
Chevron 107 A	29° 32.5333'	88° 43.6167'	1389.2	378.9'	23	73.6
Chevron MP 299 D	29° 15.1667'	88° 45.4500'	2478.3	507.0'	21	90.6
Chevron MP 41 C	29° 23.9000'	89° 00.7333'	598.4	114.4'	17	87.6
All Rigs	— —	— —	1505.9	1698.3'	61	—

*Distance from Bates Field, Mobile, Alabama

accuracy data in the form of 2 d_{rms}. Also defined in the table is the surveyed latitude and longitude of the oil rigs tested and their respective distances from Bates Field, Mobile, Alabama. 2 d_{rms} defines the radius of a circle where there is a 95.4% to 98.2% probability of locating a target within an associated 2 d_{rms} error in feet, for each rig or all combined. The 2 d_{rms} errors ranged from 114.4 feet to a maximum of 507.0 feet. For example, the 2 d_{rms} error 114.4 feet defines a circle whose radius is 114.4 feet in which there is a 95.4% to 98.2% probability of locating the Chevron MP 41C oil rig when the Loran-C navigator reads CTD and DTW equal to zero. The statistical combination of all rigs yields a 2 d_{rms} of 1698.3 feet.

The Mean Position Error in Table 9 represents the ability of the Loran-C navigator to provide guidance to a known position within an associated error in feet. The Mean Position Error ranged from 598.4 feet to a maximum of 2478.3 feet. The aggregate data of all rigs reveals a Mean Position Error of 1505.9 feet (0.248 nm), slightly smaller than the RNAV design tolerance (1519.0 feet).

SAR Operational Test

The flight test profile executed during the operational search and rescue testing is illustrated in Figure 13. This figure shows the test beginning at Cape May Air Station and proceeding enroute to the CSP (Commence Search Point) of a Creeping Line search pattern. Upon reaching the CSP, the HH52 helicopter immediately began a Creeping Line search of a fifty square mile area. A track spacing of two miles was used and a total of six legs, each 5.0 nm in length, were flown. Upon completion of the six legs of the Creeping Line search the aircraft immediately initiated a Sector Search. The Sector Search consisted of twelve sectors -- six legs and five cross legs -- with a central angle of thirty degrees.

After the last leg of the Sector Search had been flown, the aircraft

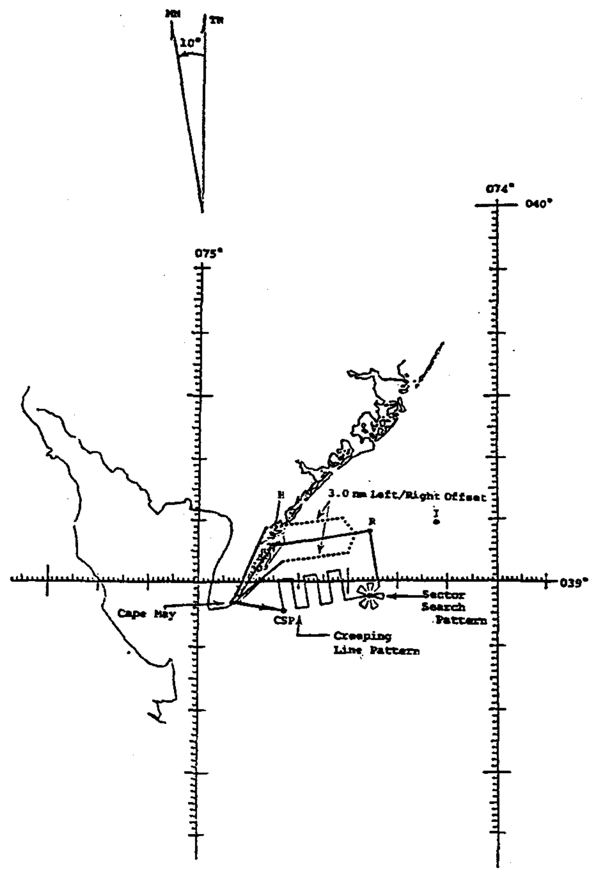

Figure 13 SAR Flight Test Profiles

proceeded direct to a rendezvous (R) waypoint defined as a range and bearing from a prestored intermediate (I) waypoint as shown in Figure 13. The purpose of this maneuver was to simulate a rendezvous with another helicopter or a ship prior to proceeding with the remaining mission requirements. After reaching the rendezvous waypoint, the aircraft transitioned to an enroute segment direct to "H" waypoint, which had been prestored. Once on this segment, either a 3.0 nm left or 3.0 nm right parallel offset maneuver was flown. Upon reaching the bisector angle or at a distance to waypoint (DTW) of 0.0 nm to the offset waypoint, the parallel offset was terminated and the aircraft proceeded direct to the Cape May waypoint (air station) at which time the test was terminated.

A. Creeping Line Patterns

Two identical SAR tests were performed and are shown in Figures 14 and 15. It should also be noted that although the crew was briefed prior to the testing, they had no inflight training for Loran-C creeping line and sector search execution. Discussion will consider each test separately due to particular circumstances involved in the latter test which greatly affected the results.

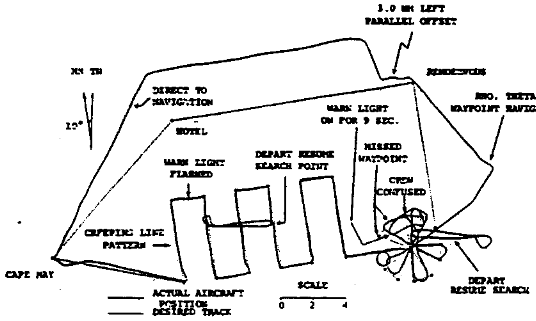

Figure 14 Search and Rescue Mission Test of 6-13-78

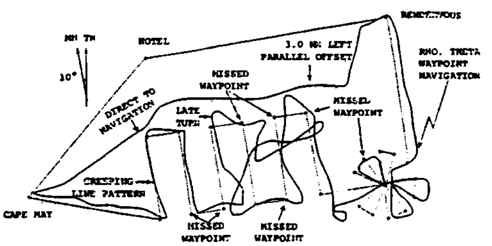

Figure 15 Search and Rescue Mission Test of 7-11-78

Accurate results were demonstrated by the Loran-C navigator's ability to provide guidance for the Creeping Line Pattern, Figure 14.

Only one Loran-C navigator problem occurred during the Creeping Line Pattern which involved a WARN light flash on pattern 1, segment 2, 3, but did not disturb navigation.

The second SAR test is illustrated in Figure 15. This test experienced apparent strong Loran-C signal interference throughout as indicated by the navigator's scalloped course guidance information. No WARN lights were encountered during this scalloping. Of the 25 waypoints used during the test, seven were missed due to large CTE and DTW fluctuations by as much as 0.25 nm. Six waypoints missed were in the creeping line pattern. This resulted in the workload becoming very high, with copilot head-down time about 80%, due to overflying waypoints, late turns, and having to execute manual leg changes. Investigation produced two possible interference sources. First, the frequent radio transmissions were observed from Annapolis. Second and more likely was confirmed by the Space Environment Laboratory, ERL, in Boulder, Colorado. On the date of this test at 1700Z a solar flare level was recorded in excess of X15, one of the largest ever recorded. The SAR test occurred between 1500Z and 1703Z.

Sector Search Patterns

The Sector Search Patterns were also illustrated in Figure 14 and 15. Figure 14 displays a significant amount of workload for the copilot, (about 95%) after the WARN light came on. The occurrence of the WARN light on pattern 1, segment 3, 4 was the only Loran-C navigator operational problem during the sector search. This WARN occurred approximately 0.26 nm prior to the waypoint change and lasted about nine seconds.

The sector search pattern shown in Figure 15 experienced one missed waypoint due to the signal interference, which caused the pilot to overshoot pattern 2, segment 1, 2 by about 0.5 nm. The last two patterns of the sector search were not flown due to low fuel.

Depart and Resume Search

The depart and resume search function of the Loran-C navigator was executed without any operational problems, demonstrating the ability of the navigator to provide precise navigation to a point which had been previously departed and resume search. This function operated equally well for both the creeping line and sector search patterns as indicated in Figure 14.

Figure 15 shows a situation where the depart, resume search function failed to operate properly on the creeping line pattern. The navigator provided guidance back to the leg where the aircraft departed from, but not to the same point. Upon arriving back at the proper leg, the navigator automatically sequenced a leg change as it was supposed to, however, it indicated that the aircraft was 3.0 nm left of the desired track when in reality it was not. A manual leg change by the copilot guided the aircraft to the next leg. Whether this malfuction was due to strong signal interference or a software problem has not been determined. Later attempts to depart and resume search were successful.

Rho, Theta Waypoint Navigation

Figures 14 and 15 also illustrated the use of the Loran-C navigator to create and provide guidance to a rho, theta defined waypoint. In Figure 14, the copilot required approximately two minutes to create the rho, theta waypoint from waypoint intermediate, which he was navigating to. Figure 15 shows a programming time that was much shorter. The same copilot as in Figure 14 created the rho, theta waypoint rendezvous and provide guidance from present position in approximately 40 seconds.

Parallel Offset Guidance

The parallel offset function provided guidance 3.0 nm right of track, Figure 14, and 3.0 nm left of track, Figure 15, with only one operational problem encountered. However, the test shown on Figure 15 was affected by apparent signal interference, in that the CTD on the Loran-C navigator and the CDI fluctuated, describing a wavy course. On each parallel offset test, guidance was provided to the bisector angle of the next leg in the auto waypoint sequence mode.

Direct-To Waypoint Navigation

No operational problems were encountered during the use of direct-to navigation from the parallel offset to Cape May. To execute this maneuver the copilot had to execute a manual leg change from present position to Cape May and then clear the parallel offset function or vise versa.

CONCLUSIONS

The major conclusions from the operational flight test evaluation of the production Loran-C navigator are summarized in this section. These conclusions are organized in the order of the general program objectives for the three major test categories. Following the statement of a conclusion regarding each general objective are summary conclusions for the more detailed objectives evaluated.

- Northeast Corridor Operational Testing

  The production Loran-C navigator was determined to be acceptable in the operational environment of the Northeast Corridor for both enroute and point-in-space approaches.

  1) The navigation accuracy and functional performance of the production navigator was acceptable from both the pilot's viewpoint and an ATC viewpoint.

  2) Operation of the Loran-C navigator in a primarily VOR/DME ATC environment in the NEC did not cause any significant operational problems.

  3) Pilot workload and ATC interfaces were acceptable on the transition routes to and from the Northeast Corridor utilizing the Sikorsky, Mack Truck, RCA and New York Airways routes.

  4) Additional non-precision Loran-C approach data was acceptable in the Boston, Massachusetts and Frederick, Maryland areas.

  5) Loran-C performed acceptably as an approach aid to point-in-space approaches flown at Boston, Massachusetts and Washington, D.C. as well as during the spur route PISA testing. This acceptable performance included approaches to unaided helipads.

  6) No significant VOR/DME signal dropouts were observed during the low altitude Northeast Corridor testing.

- NAFEC System Accuracy Testing

  The production Loran-C navigator satisfied AC 90-45A accuracy requirements for enroute and terminal area in both alongtrack and crosstrack directions. For non-precision approaches, the navigator satisfied the crosstrack accuracy requirements but did not satisfy the alongtrack accuracy requirement.

  1) Additional Loran-C navigator accuracy data was compiled for AC 90-45A compliance using the HH3 and HH52 helicopters.

  2) The production Loran-C navigator's telemetry position down link function worked acceptably as an aircraft surveillance aid.

- Offshore Testing

  The production Loran-C navigator performed acceptably during all phases of offshore testing.

  1) Operation of the Loran-C navigator was successfully demonstrated during long range (100-200 nm) overwater missions.

  2) No Loran-C signal anomaly was measured or observed during the

overland/overwater transition testing.

3) The Loran-C navigator reduced workload and improved accuracy during ship/helo rendezvous tests and offshore oil rig tests.

4) The production Loran-C navigator verified the prototype navigator's accuracy and repeatability during SAR and surveillance testing.

REFERENCES

1. Hughes, M. and Adams, R.J., "An Operational Flight Test Evaluation of a Loran-C Navigator", Systems Control, Inc. (Vt.), Champlain Technology Industries Division, for the United States Coast Guard Office of Research and Development, CG-D-9-77, March 1977.

2. Adams, R.J., "An Operational Evaluation of Flight Technical Error", Systems Control, Inc. (Vt.), Champlain Technology Industries Division for the Federal Aviation Administration Systems Research and Development Service, FAA-RD-76-33, November 1976.

3. Adams, R.J. and McKinley, J.B., "Airborne Evaluation of the Production AN/ARN-133 Loran-C Navigator", Systems Control, Inc. (Vt.), Champlain Technology Industries Division, for the United States Coast Guard Office of Research and Development, CG-D-32-79, July 1979.

4. Anonymous, "Approval of Area Navigator Systems for Use in the U.S. National Airspace System", Department of Transportation, Federal Aviation Administration, FAA Advisory Circular 90-45A, Appendix A, Section 2, 21 February 1975.

PILOT: PRECISION INTRACOASTAL LORAN TRANSLOCATION--EXPLOITING LORAN-C IN THE HARBOR AND RIVER ENVIRONMENT

by

Jack M. Ligon
Office of Research and Development
U. S. Coast Guard Headquarters
Washington, D.C. 20590

Charles R. Edwards
The Johns Hopkins University
Applied Physics Laboratory
Laurel, MD 20810

The U. S. Coast Guard is engaged in a long-term program to evaluate the potential and develop the technology for precision navigation using Loran-C. The basic method is to use Loran-C in the repeatable mode for real time 2 or 3 line-of-position precision navigation, or piloting, in the vicinity of surveyed positions. This method can be augmented by offset or proportional differential corrections. PILOT user equipment which demonstrates application of this method is being developed for the Coast Guard by the Johns Hopkins University Applied Physics Laboratory. The PILOT combines time differences from a precision Loran-C receiver with survey information from a data tape cassette using simple algorithms to present the piloting situation on a CRT display. The PILOT is basically a modified Hewlett-Packard 2649A data terminal and demonstrates the practicality of precision user equipment in the $10K unit price range. The PILOT algorithms, hardware, and software are described, and the results of summer tests on the St. Marys River are given. It is concluded that PILOTing accuracies of better than 25 meters are achievable.

* * * * * * *

Biographical Sketch of Jack Ligon

Mr. Ligon is now the Radio Aids to Navigation Project Area Manager for the U. S. Coast Guard Office of Research and Development. He has divided his 18 years of Coast Guard service between communications and radio aids. His work with Loran covers the entire spectrum from precision simulation to treatment as a source of interference.

Mr. Ligon holds a MSE degree from the University of Pennsylvania and a BSEE degree from Virginia Polytechnic Institute. He is a member of the Institute of Navigation and the Wild Goose Association. His outside interests include church work, sailing, and camping.

Biographical Sketch of Charles Edwards

Mr. Edwards is the supervisor of the Systems Development Section and is the Program Scientist for the PILOT Program at the Johns Hopkins University Applied Physics Laboratory. He has been involved with the development of Loran guidance systems for 10 of his 16 years at APL.

Mr. Edwards received a BSEE from the University of Tennessee and is a member of Tau Beta Pi and Eta Kappa Nu. His hobbies include architecture, knife-making, sailing, and working on a cabin in the Appalachian Mountains.

LORAN-C PILOTING

Introduction

As a navigator procedes from the Coastal Confluence Zone into harbor entrances, harbors and rivers, his requirements for both positioning accuracy and timeliness increase on the order of 500 times. The number of information sources also increases and the navigator must integrate the data from all of these sources. He has crossed the boundary separating piloting from navigation.

Large areas of the U.S. Coastal Confluence Zone are presently, or will shortly be, covered by Loran-C signals which are charted to an accuracy of 0.4 km. It is known that these signals are repeatable to within a few tens of meters. These signals are also present in harbors and harbor entrances and potentially form the basis for a precision navigation system. This paper discusses a method for exploiting these Loran-C signals and describes the PILOTing hardware which is the keystone for this exploitation. The name PILOT--Precision Intracoastal Loran Translocator--is not meant to imply automatic piloting, but rather to highlight the significantly different frame of reference which exists in the piloting domain.

Loran-C PILOTing

The first two words forming the acronym "PILOT" refer to the environment; the last two refer to the method.

Intracoastal waters are typically characterized by visible or physical features: channel boundaries, visual aids-to-navigation, coastlines. They are also characterized by significant over-land Loran-C propagation paths and warped time difference grids. In these waters, positioning in an absolute, geodetic sense (latitude/longitude) is of little value. Also, the orientation of the vessel is as important as its position. Precision must be relative to these intracoastal realities--"precise" enough for safe, speedy vessel operation.

The method is basically Loran-C translocation. Given a reference site and its corresponding Loran-C time differences, estimate the location of a Loran-C receiver at another site in the vicinity of the reference site, based upon the time difference measurements taken there. This is essentially the same as the method used in conventional satellite position translocation and in many Loran waypoint navigation systems.

ENVIRONMENTAL REQUIREMENTS

Calibration

If the latitude and longitude of all the essential navigation features in a particular river or harbor were known and, if there were a perfect propagation prediction model, calibration would be unnecessary. There are over 100,000 visual navigation aids installed in the U.S. intracoastal waters, and the latitude and longitude are known for very few of them; yet, they serve their purpose. In the past, attempts have been made to utilize the most accurate Loran-C prediction methods in the piloting environment, but unfortunately these require a larger geological data base than the corresponding Loran data base for river and harbor "calibration" by measurement, and still do not provide sufficient accuracy.[1]

When calibration is by measurement coding delays or System Area Monitor reference time differences are held constant and the time difference field is measured as it is. No attempt is made to adjust the coding delays to cover the service area in some sort of "least squares" error sense to fit the imperfect propagation model. Calibration by measurement brings up five questions: the questions of density of survey, of coordinate conversion algorithm, of positioning, of survey time difference measurement, and of temporal stability. The questions of density of survey and coordinate conversion algorithm are very tightly coupled. On the St. Marys River, a survey interval of approximately 3 kilometers coupled with navigational aid relative position taken from the river charts and processed using the PILOT coordinate conversion algorithm provided "sufficient" navigational accuracy. That is, the PILOT showed the vessel to be in the center of the channel and passing the proper navigational aids when it appeared to the observer that this was the case. The remaining three questions have been addressed and are discussed in greater detail in the papers by Sedlock,[2] Olsen,[3] and Johler[4]. In summary, there is a very effective method for surveying the Loran-C time differences relative to the visual aids and features used by the pilot himself, and that the stability question is vital and is ultimately solved by a form of differential corrections.

Reliability and Speed

The piloting environment places constraints upon navigational equipment that do not exist in the more open waters. The pilot needs much higher accuracy and reliability. The safety of his vessel cannot tolerate the loss of a fix caused by failure of one of the navigational transmitting stations. In Loran-C this translates to 3-LOP fixes, with drop-back 2-LOP fixes, including those when the Master station has a casualty.

The pilot does not have time to convert numbers to a position on a chart. His navigational display should provide him with an immediate picture of his situation so that he can rapidly respond to it. This translates to a visual plan display with navigational aids, channel boundaries and some shoreline features indicated.

Other Issues

It is possible, and PILOT is the demonstration case, to meet the requirements of the piloting environment with a compact user equipment for approximately $20,000, including the cost of a "better grade" Loran-C receiver. The pilot will probably not be able to obtain satisfactory operations using a low-cost CCZ Loran-C receiver.

PILOT

Description

The PILOT, developed for the U. S. Coast Guard by the Applied Physics Laboratory of Johns Hopkins University, is an electronic aid for piloting vessels in harbors and rivers. Prerecorded tape cartridges, containing a sequence of chartlets and other navigation information, provide the PILOT with a degree of "local knowledge." The vessel's present position and heading, continuously determined from a loran receiver and the vessel's gyro, are displayed on the current area chartlets. Chartlets of two different scales (master and detail) are always available for operator selection. Position information relative to waypoints (intermediate destinations) is displayed to the left of the chartlet. A horizontal bar graph, representing the vessel's relative cross track position, can be displayed along the bottom of the display.

There have been many systems constructed for similar purposes in the past. The earliest was probably the Decca track plotter in the early 1960s. Modern track plotters are

TYPE	REPRESENTATIVE EQUIPMENT	TD-XY CONVERSION METHOD	AREA OF USE	DISPLAY	NAVIGATIONAL FEATURES DISPLAYED	COMMENTS
Area TD	DECCA Plotter (Cir 1962)	None, TD of land boundary predicted	CCZ	Strip Chart	As desired.	Distorted chart X-Y
Track-line TD	Several receivers and devices	None	CCZ	Alpha-numeric or analog	None	Distances given in micro-seconds. Could be used in HHE with waypoint survey.
Track-line X-Y	C-LAD, User I, LONA, several receivers	Inverse Prediction	CCZ	Alpha-numeric or analog	None	Use Latitude & Longitude In HHE could be used used with TD waypoint survey, but cannot be used Lat-Long or X-Y.
Area X-Y	COGLAD, several track plotters	Inverse Prediction	CCZ HHE	X-Y plotter	None	Use Latitude and Longi-tude or X-Y.
	User II	Inverse Prediction	HHE	Video Graphics & Alpha-numerics	As desired.	Shows vessel position and orientation. Ultimately required intensive survey. Primarily an R/D device. Very long chartlet change time.
	Modified User II	Inverse Prediction	HHE	Color Graphics & Alpha-numerics	As desired. Data on disc memory.	Color graphics and RAYDIST and Miniranger sensors added.
	PILOT	G-Matrix with flat earth hyper-bolic grid	HHE	Video graphics chartlets analog, & alpha-numerics	As desired. Display and conversion data on tape cassette.	Shows vessel position and orientation. Uses way-point and limited navaid survey information. Rapid chartlet change and display update. Built to demonstrate technology.

TABLE 1
COMPARISON OF VARIOUS TYPES OF USER EQUIPMENT

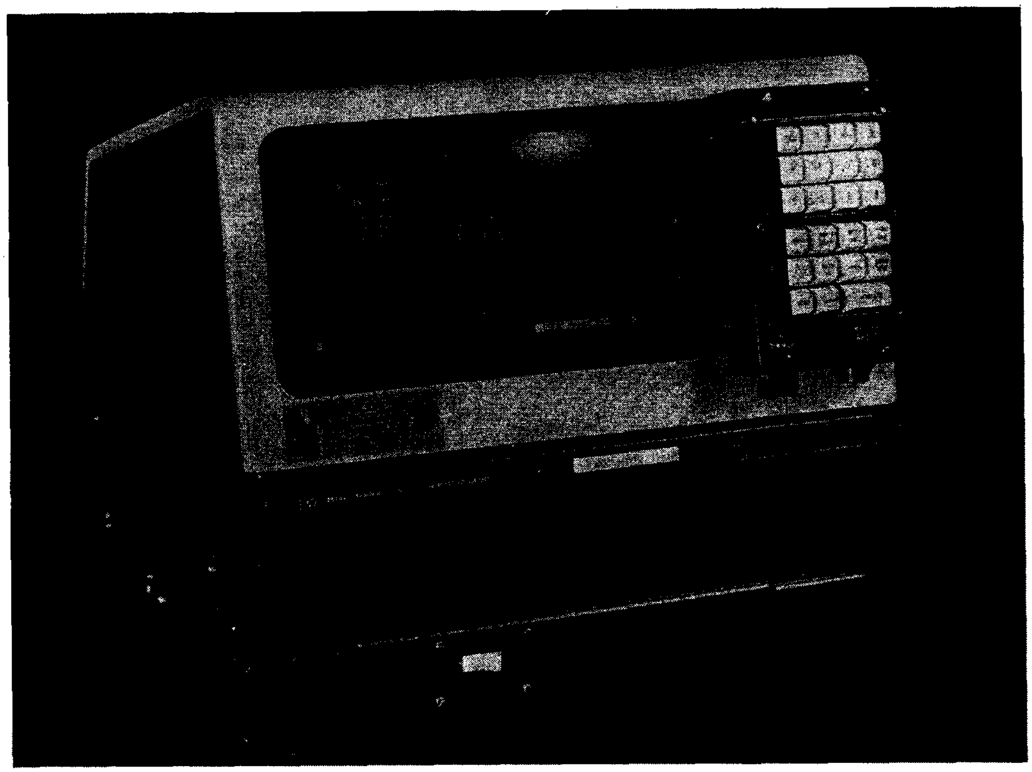

Figure 1 PILOT

found on many fishing vessels. Table 1 lists some of these coordinate conversion/display devices and comments upon their features as they relate to the harbor and river environment. As can be seen, the PILOT is a logical progression from these devices. It solves the coordinate conversion problem which had in the past been the major obstacle to HHE implementation, and it demonstrates the feasibility of reliable PILOTing using a single, compact video display terminal.

Navigational Charts

The PILOT is basically a data processor. All coordinate conversion constants and navigational background information is provided on a cassette which is, in effect, a Loran-C navigational chart on a magnetic tape medium. A single cassette can contain as many as 100 of these chartlets, more than enough to permit a complete transit of the St. Marys River, which is approximately 100 kilometers long. Sedlock[2] contains a deeper discussion of the chartlet calibration. In summary, the method involves the creation of a linked mosaic of ideal flat-earth hyperbolic Loran-C grids fixed at the calibration points with aids and geographic features charted onto these grids. This implies a slight distortion of the physical world if the real Loran-C grid is distorted. On the St. Marys River, this distortion was small enough to be unnoticeable, even with calibration point separations as great as 10 kilometers. Had the distortion become too great, additional survey points would have been necessary. Since the identical model is used within the PILOT for coordinate conversion, the charting accuracy is as good as the repeatable accuracy.

HARDWARE DESCRIPTION

Graphics Terminal

The PILOT is shown in Figure 1.

The nucleus of the PILOT system is a Hewlett Packard 2649A microprogrammable graphics terminal. This OEM device was selected because it has a separate graphics processor with memory, dual tape cartridge units, and an 8080 microprocessor that could be modified and programmed as required. Modifications to the HP 2649A terminal included: converting the 8080 microprocessor from software math to hardware math by adding an Advanced Micro Devices (AMD) 9511 arithmetic processing unit, developing a two-receiver interface board to mount inside the terminal, developing an interface board to connect to the ship's gyro and to a time difference bias (differential correction) box, replacing the large general purpose keyboard with a small predefined keypad, and building a short base for the terminal to serve as a cable junction box. The system block diagram is shown in Figure 2.

Receiver Interface Board

The dual receiver interface board is designed around an 8085 microprocessor and a second 9511 math unit. This microprocessor performs the following functions: input, convert, identify, edit, filter and dead reckon (DR). The use of two Loran receivers permits cross chain position fixes. The data format of most receivers can be accommodated (up to 50 parallel lines per receiver) by changing the input software module.

Heading and TD Bias Board

The heading and TD bias board includes a 10-bit synchro-to-digital converter and can accept heading information from either a gyro or a magnetic compass with a shaft encoder. Storage registers on this board can store three sets of TD bias numbers (± 7999 nanoseconds). These registers can be loaded either by the operator from the keypad or from a remote box or modem via an interface cable.

Keypad

Operation of the PILOT terminal was simplified by replacing the HP keyboard (105 keys) with a small keypad (23 keys) having eleven function keys, plus twelve numerical and cursor control keys.

SOFTWARE DESCRIPTION

Figure 2 is the PILOT functional Data Flow Diagram.

Memory. Approximately 17,000 bytes of machine language code were developed at APL for the PILOT terminal and an additional 40,000 bytes of the original HP code was retained. Structured programming and assembly language was used for maximum efficiency.

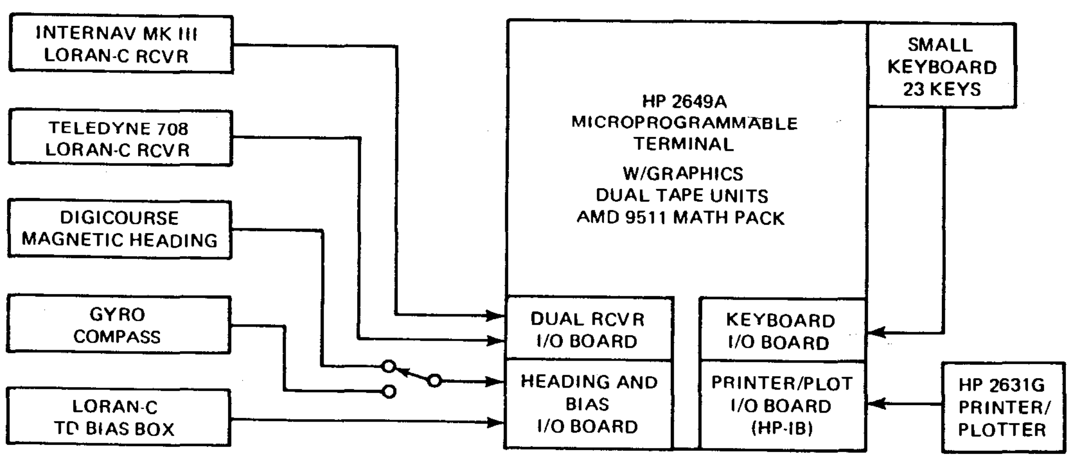

System block diagram.

Figure 2

TD Filtering. Digital filtering is used on each TD as part of the pre-processing performed on the receiver interface board. An alpha/beta filter was modified to induct turning acceleration feedback. For receivers with relatively slow data rates (i.e., less than two sets of TDs per second), the TDs are dead-reckoned every 100 miliseconds using the last known velocity and turning acceleration. Three different filter time constants may be selected by the operator from the keyboard.

Coordinate Conversion. The 8080 microprocessor performs a full order, iterative transformation approximately twice per second. When three good TDs are available, a 2 X 3 minimum variance "G" matrix is used. Each term of the matrix is preweighted to produce a best fit with the expected relative signal strength. When only two TDs are available, one of three 2 X 2 unweighted matrices is used.

Chartlet Cassettes

Chartlet cassettes contain an index file, master files and detail files. The index file contains a title block and a list of all master chartlets on the cassette. Each master file contains the graphics for 8-16 miles of track, the area matrix coefficients, transmitter coordinates and supplemental data such as display origin, scale and rotation. Each detail file contains the graphics for 1-2 miles of track, the TD's and X, Y coordinates of the current waypoint, bearing angles to and from the WP and supplemental data.

Master chartlets provide "look ahead" by showing the next several waypoints; detail chartlets provide a closer view of the vessel's current situation. Each master file is followed by one or more detail files. North-up or track-up chartlets may be used.

Chartlets can be developed using a digitizer, minicomputer or calculator, and the PILOT terminal reconfigured as a 2649A terminal. The original chartlet cassettes for the St. Marys River were produced at APL, and the Coast Guard Research and Development Center is currently setting up a system for producing them for other locations.

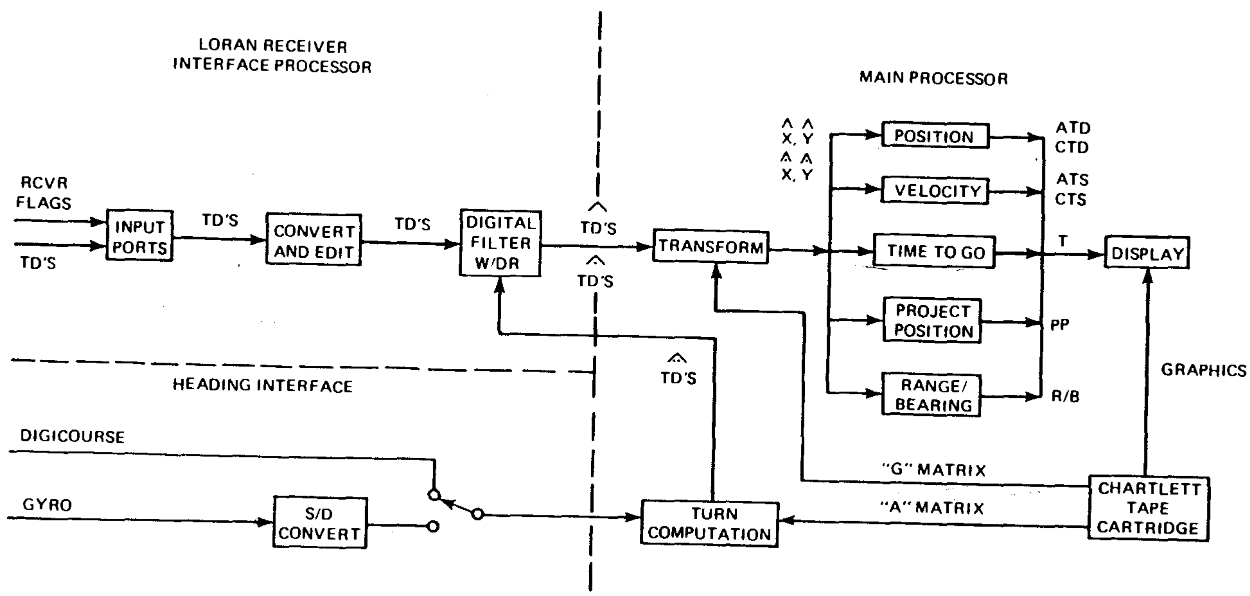

Functional data flow diagram.

Figure 3

TEST RESULTS

The PILOT development project is still in progress and new software features are being added daily. The PILOT system was tested on the St. Marys River during the first week in October 1979.

The Receiver

The Loran-C receiver used was an INTERNAV MK III Survey Receiver. The receiver had been previously tested in the laboratory and could typically be expected to provide an accuracy of 30 nanoseconds under a variety of signal conditions. The St. Marys River signal environment was so benign that performance in the 10 nanosecond range (relative to a reference Austron-5000) was observed.

The PILOT

Overall performance was excellent. The PILOT successfully combined the receiver TDs with survey data taken during August and September and chartlets prepared from the NOAA navigational charts to provide accurate position and situation information. The references in most areas were visual ranges and buoys, and were quite good. The navigational solutions were based upon waypoint surveys, and the chartlets were calibrated by using the surveyed location of a single aid on each one. Quantifiable accuracy tests will be completed next year, but visual accuracy was excellent. The PILOT indicated the boat to be on track when it was in fact on the visual range and showed the boat to be passing along between the buoys when this was the case. There was no noticeable grid warp--possibly the result of the low-conductivity of both the fresh water and the Laurentian Shield upon which the area is located. A repeatable mode error budget is given in reference 3.

The Future

Future plans include deployment aboard an ice breaker this winter and other vessels next summer. These deployments will be followed by quantitative and human factor tests.

Conclusion

The PILOT opens an entirely new area for precision Loran-C navigation.

REFERENCES

1. Illgen, J.D. and Feldman, D.A., LORAN-C SIGNAL ANALYSIS EXPERIMENTS "AN OVERVIEW," Proceedings of Conference on Navigation in Transportation, September 19-21, 1978.

2. Sedlock, A.J., SURVEYING IN THE TIME-DIFFERENCE DOMAIN, Wild Goose Association Eighth Annual Symposium, October 17-19, 1979.

3. Olsen, D.L., and Isgett, C.E., PRELIMINARY STABILITY ANALYSIS OF THE ST. MARYS RIVER MINI-CHAIN, Wild Goose Association Eighth Annual Symposium, October 17-19, 1979.

4. Johler, R., Doherty, R.H., Samaddar, S.N., and Campbell, L.W., A METEOROLOGICAL PREDICTION TECHNIQUE FOR LORAN-C TEMPORAL VARIATIONS, Wild Goose Association Eighth Annual Symposium, October 17-19, 1979.

A LORAN-C VESSEL LOCATION SYSTEM FOR TRAFFIC CONTROL IN THE SUEZ CANAL

Dr. Stephen C. Bigelow
Megapulse, Incorporated
8 Preston Court
Bedford, Massachusetts 01730

ABSTRACT

The purpose of this system is to provide real-time vessel location data for the Suez Canal Vessel Traffic Management System. The system consists of a three station Loran-C mini-chain, portable Loran-C receivers/VHF data transceivers for use aboard ships in the canal, data links from several sites along the canal and from the transmitter sites to the central control facility, several fixed Loran-C receivers/VHF transceivers to provide differential correction data and digital processing equipment to automatically poll both the fixed and the vessel-borne receivers and to coordinate convert and smooth the vessel position data. This data is presented in real-time on graphic map displays in the control facility (the display equipment is provided by the prime contractor, AILTECH).

Some of the significant features of this system are:

- The Loran transmitters are monitored and remotely controlled from the central facility.
- The Loran receivers are microprocessor based, fully automatic and have 10 nsec tracking resolution.
- Multiple fixed monitor receivers are used to provide differential correction data.
- With the exception of the vessel-borne receivers the entire system is redundant to enhance its availability.
- The system is capable of tracking 150 vessels simultaneously.
- The position data accuracy specifications are on the order of 15 meters.

This paper describes the design and implementation of this vessel location system in considerable detail.

INTRODUCTION

The operation and maintenance of the Suez Canal is the responsibility of the Suez Canal Authority (SCA). The SCA is presently embarked on a multi-year program to widen and deepen the canal and to improve canal operations. One part of this program involves the installation of a modern Vessel Traffic Management System (VTMS). The purpose of this VTMS is to provide real-time vessel traffic information to operational personnel. This information will be presented at three operations centers at the northern and southern ends of the canal and the central canal operations center in Ismailia which is near the canal midpoint.

The Suez Canal VTMS consists of four major subsystems. These are referred to as the radar, Loran, data management and display (DM&D) and communications subsystems. The prime contract for the VTMS program is between the SCA and Eaton Corporation, AILTECH Division. Funding is being provided by the U.S. Agency for International Development and by the SCA. Major subcontractors for this program are the AIL Division of Eaton Corporation, Megapulse and the Mobile Radio Department of General Electric. The radar and DM&D subsystems are the responsibility of AIL. Megapulse is providing the Loran subsystem. An extensive radio communications network for use in traffic management will be implemented using G.E. equipment.

The radar subsystem consists of three tracking radar installations, one covering each port and its approaches and the third covering the Great Bitter Lake. Vessel position data obtained using these radars is converted to Suez Canal map coordinates and presented visually by the DM&D subsystem at the operations centers in the form of video map displays.

The DM&D subsystem also presents on these same map displays vessel position data obtained from the Loran subsystem. Loran derived data is used to track vessels as they transit the canal. In addition to providing real-time vessel traffic information, the DM&D subsystem maintains multiple files of traffic related data which may be accessed by operational personnel to aid them in organizing and expediting safe vessel traffic flow through the canal.

The communications subsystem consists of several fixed base and relay stations and a large number of portable transceivers. This subsystem will provide voice communications between traffic control personnel at the operations centers and several categories of operational and administrative personnel. These include harbor pilots, canal pilots, maritime agents, dredger captains, etc.

This introductory description is intended to give an overview of the Suez Canal VTMS. The topic of this paper is the Loran subsystem of the VTMS.

LORAN SUBSYSTEM DESCRIPTION

The Loran-C vessel location subsystem of the Suez Canal VTMS consists of the following equipment:

- 3 Loran-C transmitters
- 150 Carry-On Receiver/Transmitters (CORTs)
- 5 VHF CORT relay transceivers
- 5 fixed CORT monitors
- Loran chain monitor
- Loran transmitter remote control equipment
- 3 UHF remote control links
- Loran data processor
- Special test and maintenance equipment
- Spares.

The geographic deployment of the major elements of the Loran-C vessel location equipment is shown in Figure 1. The Loran subsystem block diagram is presented in Figure 2. The three Loran-C transmitters are sited to provide excellent Loran signal coverage of the entire length of the canal. Each transmitter radiates 6 kW.

The CORTs are portable battery powered Loran-C receivers combined with data modems and VHF transceivers. Every vessel which transits the canal is piloted by a Suez Canal Authority pilot. A CORT will be put aboard each vessel with the SCA canal pilot prior to its transit and temporarily installed. The CORT will then be removed and taken ashore with the pilot at the end of the transit. During the transit of a vessel the CORT receives Loran-C signals and processes these signals to obtain time difference (TD) measurements. Periodically the CORT is polled by the Loran data processor and responds with TD information.

The CORT relay transceivers are located along the canal at Port Said, Kantara, Ismailia, Kabrit and Port Taufik. These transceivers are connected to the Loran data processor at the central control facility at Ismailia by dedicated telephone circuits. CORT polling messages are transmitted by telephone from Ismailia to the CORT relay nearest a vessel and then by VHF to the vessel-borne CORT. The CORT reply message follows the same route back to Ismailia.

The fixed CORT monitors are identical to the vessel-borne CORTs except that they have their power supplied from the mains. These CORTs are permanently installed at the same five sites as the CORT relay transceivers. Their function is to monitor the Loran-C signals for temporal variations. These CORTs are polled in the same fashion as CORTs on vessels. The TD data obtained from fixed CORT monitors, however, is used by the Loran data processor to differentially correct the TD data from vessels.

The Loran chain monitor equipment is located at the central control facility in Ismailia. The function of the Loran chain monitor is to provide information to operational personnel on Loran transmitter operation. This information is used to control the Loran transmitters.

Loran transmitter remote control equipment is provided at each of the Loran transmitter sites and at Ismailia. This equipment permits the status of each Loran transmitter to be determined and changed by remote control from the central operations facility in Ismailia.

The three UHF remote control links in conjunction with dedicated telephone circuits provide the communication links between Ismailia and the three Loran transmitter sites. These links are used both for remote control and for voice communication.

The Loran data processor equipment is located at the central control facility. The major interface between the Loran subsystem and the DM&D subsystem is a 9600 baud full duplex data channel between the Loran processor and the DM&D processor. The Loran processor receives start and stop tracking messages from the DM&D processor and sends it track data messages for each active vessel. The main functions of the Loran data processor are to control the polling of active vessels, to differentially correct vessel TD data, to convert TD data to the canal coordinate system, to estimate the position and velocity of each vessel, to provide vessel position and velocity data to the DM&D processor periodically and to process and log chain monitor data.

The special test and maintenance equipment and the spares are used to support the operation and maintenance of the Loran subsystem. A Loran transmitter test set, two CORT test sets and three CORT battery charger racks are provided for this purpose together with a year's supply of maintenance spares.

A more detailed description of the major elements of this subsystem is given in the following subsections.

Loran Transmitter

Each of the three Loran transmitter sites are essentially identical. The Loran transmitting antennas are 300 foot top-loaded monopoles. The transmitter site equipment is housed in three transportable shelters. These are grouped together at the edge of the Loran antenna ground plane which is approximately 300 feet in diameter. The shelter arrangement is shown in Figure 3.

The diesel shelter houses the triply redundant diesel electric generators and their associated control equipment. Any one generator can supply all site prime power requirements.

The support shelter contains site maintenance equipment, spares and limited personnel support equipment and supplies.

The block in Figure 3 labelled Radio Link indicates the location of a 50 foot tower which supports the UHF communications antennas.

The transmitter shelter houses both the Loran transmitter equipment and the UHF communications transceivers. The UHF equipment consists of two redundant G.E. base stations transceivers each connected to its own antenna. Audio input/output switching is provided to permit this equipment to be used for voice communications. Normally it is used for data communications with the remote control units.

The Loran transmitter equipment comprises two completely redundant transmitters with RF output switching between the Loran antenna and a dummy antenna. A sketch of the front of the transmitter equipment is shown in Figure 4. The seven cabinets housing the transmitter equipment have a total length of just under 16 feet. They are mounted in the middle of the shelter to permit access to both the front and the rear of the cabinets.

Each transmitter is housed in three cabinets. The control cabinet contains a cesium beam frequency standard, a pulse amplitude and timing controller (PATCO), a Loran timing unit (LTU), a remote control unit (RCU) and a battery pack.

The cesium standard provides the timing reference for the transmitter. The timing unit uses the 5 MHz output from the cesium standard to derive all of the timing signals needed to generate Loran-C pulse groups at the chain group repetition interval. It also can make local phase adjustments (LPA) to the transmitter timing in steps as small as 10 nsec.

The PATCO uses timing signals from the LTU and feedback measurements of the transmitter output to implement closed loop control of the amplitude, timing and carrier frequency of the transmitter output pulses. Transmitter timing is maintained through prime power outages by means of the control unit battery pack.

Each of the four half-cycle generators (HCG) converts prime power into a high power pulse which is 5 usec wide, and, therefore, is a half-cycle of the Loran-C 100 kHz carrier frequency. Two HCGs are connected to produce positive pulses and the other two are connected to produce negative pulses. When a positive phase coded Loran-C pulse is generated, the two positive output HCGs are triggered and then 15 usec later the two negative output HCGs are triggered. To generate a negative phase coded pulse this triggering sequence is reversed.

The combined output of all four HCGs goes to the coupling network which uses an LC tank circuit to shape this output to match the standard Loran-C envelope on the rise of the pulse and a switched RLC network (tailbiter) to control the shape of the pulse tail.

The output network consists of an antenna matching transformer and a motor driven variable inductor which is part of the automatic frequency control loop.

The antenna simulator is an RLC network with the same impedance characteristics as the real Loran antenna. The switch connects the output of one transmitter to the antenna and the other to the antenna simulator.

The Loran transmitter sites are designed for unattended operation. Equipment status is automatically monitored and reported to the central control facility via the remote control units. Transmitter and prime power generator switchover takes place automatically under certain fault conditions and transmitter switchover can also be controlled remotely. The standby Loran timer is periodically synchronized with the online timer to preserve chain timing when transmitters are switched.

All of the transmitter site equipment is redundant except for the Loran antenna. Redundant remote control data links are provided between all transmitter sites and the central control facility.

<u>Carry-On Receiver/Transmitters</u>

The Carry-On Receiver/Transmitter (CORT) is a portable battery powered, fully automatic Loran-C receiver combined with a modem and a VHF transceiver. A sketch of a CORT is shown in Figure 5. It is approximately 16 inches high, 15 inches wide and 8 inches deep. It weighs about 37 pounds. The only operating control is the power switch. A separate antenna and antenna coupler (not shown in the figure) are provided with the CORT. For transport the antenna coupler is secured in the recess in the upper left corner of the CORT case. The antenna and other accessories are stored in a pouch attached to the side of the case.

The CORT electronics are housed in the upper portion of the case. The major electronic subassemblies are the Loran-C receiver, the modem, the VHF transceiver and a DC-to-DC converter. The lower part of the case houses a 12 volt Ni-Cad battery pack with sufficient capacity to operate the CORT for a minimum of 20 hours. The two parts of the case are separable to facilitate maintenance and battery recharging.

The Loran-C receiver was designed by the International Navigation Co (Internav). The tracking loop resolution is 10 nsec. A microprocessor is used to control automatic search and acquisition and to process the TD data. Average TDs are computed with zero steady-state velocity error to a precision of 1 nsec. The microprocessor also handles bidirectional data communications via a universal asynchronous receiver/transmitter (UART).

The modem provides full duplex interfaces with the UART and the VHF transceiver. The data rate is 1200 baud and FSK modulation is used in the audio portion of the data channel.

Each CORT is assigned a unique ID. Polling messages containing CORT ID data are broadcast from the CORT relay stations along the canal. Each CORT decodes all messages received. Whenever a CORT receives a polling message containing its own ID, it responds by transmitting its TD data back to the relay station.

All CORTs transmit at one fixed VHF frequency and must receive at a different fixed VHF frequency. Therefore, CORTs must be polled one at a time in sequence. The maximum CORT polling rate, as determined by the 1200 baud data rate and the number of data bits in the CORT reply message, is ten CORTs per second. The polling message for the next CORT in sequence is transmitted during the same interval that a CORT reply message is being received.

The CORT is designed for easy installation on a wide variety of vessels. The CORT case will be placed on the bridge wing deck and secured with a strap. The antenna coupler, which is connected to the CORT by a cable, will be clamped to the rail or other convenient surface. The antenna will then be be assembled and attached to the coupler.

<u>VHF CORT Relay Transceivers</u>

The length of the canal is subdivided into five CORT polling zones. Two way CORT data communications coverage of each of these zones is provided from a VHF CORT relay transceiver site located near the canal. Redundant G.E. transceivers are installed at each relay site. Each transceiver site is connected to the central control facility by a dedicated full duplex telephone circuit with E an M signalling. The E and M lines are used to key the relay transmitters to poll the five zones sequentially. Zone switching is under control of the Loran data processor. Switching between the redundant relay transceivers at each relay site may be done by remote control from the central control facility.

Fixed CORT Monitors

A CORT is permanently installed at each of the five CORT relay sites. These CORTs are polled along with those installed on vessels in the canal. Since these CORTs are at fixed locations, their TDs should ideally be invariant. Any variation of the fixed CORT monitor TD's is a measure both of Loran transmitter timing drift and of time-varying propagation anomalies. On the assumption that such temporal effects are nearly uniform over the relatively small extent of a CORT polling zone, the TD variation in each zone as measured by a fixed CORT monitor may be used to differentially correct the TD measurements obtained from all vessel-borne CORTs in the same zone.

The improvement in the accuracy of Loran-C position determination by means of this differential Loran-C mode of operation is well known. In the usual navigational applications of Loran-C it is not practical to provide differential correction data to all vessels using the system. However, in the Suez Canal VTMS application, since vessel position information is required only at the central control facility, implementation of differential Loran-C is quite straightforward.

Loran Chain Monitor

The Loran chain monitor equipment, which is located at the central control facility, consists of two redundant CORTs. These are permanently installed in the same manner as the fixed CORT monitors along the canal. They are polled, however, by an accessory device which is interfaced directly to the CORT by means of a connector. The modem and VHF transceiver portions are not used in this mode of CORT operation.

The accessory device presents a digital display of the measured TDs and also transmits TD and receiver status data to the Loran processor.

The Loran processor calculates means and standard deviations of the TD data from both Loran monitors. These calculated values are printed and stored. Also, if the mean TDs drift out of tolerance or if the Loran monitor status information indicates an abnormal condition, operational personnel are automatically alerted.

Thus the function of the Loran chain monitor equipment is to provide information necessary to maintain proper Loran-C chain operation.

Loran Transmitter Remote Control Equipment

The Loran transmitter remote control equipment located at the central control facility consists of two redundant remote control units (RCU) and the switchgear needed to permit connecting them to any of the communications links between the central control facility and the three Loran transmitter sites.

The centrally located RCUs are identical with those which are part of each transmitter. They may be used to request transmitter site status information and to control transmitter site operations.

UHF Remote Control Links

The remote control communication links between the central control facility and the three Loran transmitter sites are implemented using G.E. UHF transceivers. Each UHF link is doubly redundant. The link between Ismailia and the master Loran transmitter site uses a direct UHF path. The links to the Loran secondary sites use dedicated telephone circuits from Ismailia to the canal ports and UHF paths from there to the Loran transmitter sites.

Loran Data Processor

The Loran data processor equipment is located at the central control facility. It consists of two redundant Digital Equipment Corporation PDP-11/60 processors each having dual disk drives and dual keyboard/printers. Associated with each processor is a special purpose device referred to as the CORT off-line polling equipment (COPE). Manual switches are provided to change processor status from operational to redundant backup.

CORT Off-Line Polling Equipment. The COPE is a microprocessor based device. One of its main functions is to poll CORTs by encoding polling messages and sending them sequentially to the

CORT relay transceivers. Its other main function is to receive and decode CORT reply messages. The COPE has a 2400 baud full duplex interface with the 11/60 main processor. It also has an interface with the dedicated telephone circuits from Ismailia to each of the five CORT relay transceiver sites.

The COPE receives the following information from the main processor. It is given the CORT ID of each vessel when Loran tracking of the vessel is to start and again when it is to stop. It is given the number of the CORT relay transceiver within whose coverage zone each vessel is located when tracking of the vessel is to start and whenever a vessel moves from one zone to another. It is given a polling priority number in the range one to four for each vessel being tracked whenever the main processor program determines that the polling interval for that vessel should be changed.

With this information the COPE creates and maintains an active CORT polling table organized first by polling zone and second within each zone by polling priority. In generating CORT polling messages the COPE scans this table. In each complete scan the COPE performs the following functions. It controls the keying of CORT relay transmitters one zone at a time. It selects the appropriate telephone circuits for polling CORTs in the given zone. Within each zone it polls all CORTs assigned polling priority 1 (PP1), one half the CORTs with PP2, one third the CORTS with PP3 and one fourth the CORTs with PP4. On the next scan of the table the COPE polls all the PP1 CORTs, the other half of the PP2 CORTs, the second third of the PP3 CORTs, etc. When there are only a few active CORTs in the system the COPE maintains a minimum scan interval of five seconds.

As each CORT reply message is received by the COPE it is decoded and checked for errors. If none are detected, the received TDs are encoded together with the time interval since the last polling of the CORT and this data is sent to the main processor.

<u>Main Processor</u>. The two redundant PDP-11/60 Loran processors each have 64K words of memory and use the DEC RSX-11M operating system. The two main processor functions are providing vessel position and velocity data to the DM&D subsystem and providing Loran chain monitor information to operational personnel. The implementation of this latter function has already been discussed.

Vessel position and velocity are calculated every second using a six-state Kalman estimator. Since the Suez Canal channel is composed of straight segments and curved segments of constant radius, the dynamic model of vessel motion assumes uniform vessel linear acceleration and/or uniform angular velocity. When the length, beam and gross weight of a vessel are known, these parameters are used in modelling vessel dynamics.

Each time vessel position and velocity are updated a check is made to see if new CORT measurement data is available. If no new data is available, position and velocity are updated based on the model and vessel past history. This provides a coast mode of operation. If new data is available, it is used to correct errors in the estimated vessel position and velocity and to update estimated vessel linear acceleration and angular velocity.

If there are less than 100 active CORTs in the system, position and velocity data messages are sent to the DM&D subsystem for each vessel being tracked at three second intervals. When there are between 100 and 150 active CORTs, vessel track data messages are sent to the DM&D subsystem every four seconds. This change in message rate is necessitated by the limited channel capacity (9600 baud) between the Loran and DM&D processors.

Each time vessel linear acceleration and angular velocity estimates are updated, an estimate of the rates of change of these two parameters is also made. These estimates of the rate of change of linear acceleration and the rate of change of angular velocity are used together with the estimated vessel velocity to set the polling priority of the vessel.

If a vessel has just entered the system, or if it has a large rate of change of linear acceleration, or if it has a large rate of change of angular velocity, then it is assigned polling priority 1 (PP1). If the rate of change of linear acceleration and the rate of change of angular velocity are both low, then the vessel is assigned PP3 unless its velocity is above a threshold in which case it is assigned PP2. Vessels with a moderate rate of change of linear acceleration or angular velocity are assigned PP2. Vessels at anchor, i.e. with near zero velocity are assigned PP4.

Whenever new vessel measurement data is received from a CORT it is processed as follows. First the time the data is received from the COPE is calculated. Then the TDs are differentially corrected using data from the appropriate fixed CORT monitor. The corrected TDs, the time interval between the TD measurements and the time they were received are stored in the vessel track file. A flag is set indicating to the Kalman estimation program that new measurement data is available.

Whenever the estimation program finds this flag set, it first checks the rate of change between the new and the previous TDs for reasonableness. If an excessive rate of change is detected, the new TDs are discarded. Otherwise the new TDs are extrapolated to the next vessel update time using the interval between TD samples, the time the new TDs were received and the time of the next update. The extrapolated TDs are then converted into the Suez Canal coordinate system. The resulting measurement of vessel position is used to correct the Kalman estimator.

SYSTEM PERFORMANCE

Since the Loran subsystem of the Suez Canal VTMS has not yet been installed, no measured performance data is available at this time. The Loran subsystem has, however, been designed to meet the followign performance specification:

- Vessel tracking capacity:
  Up to 150 vessels.
- Position measurement error:
  Less than 15 meters.
- Velocity measurement error:
  Less than 0.5 km/hr.

SUMMARY

The purpose of the Suez Canal Vessel Traffic Management System (VTMS) has been described. The function of the Loran subsystem as a source of real-time vessel position and velocity data for the VTMS has also been discussed. Detailed descriptions of the equipment provided to implement the Loran subsystem function have been presented. In addition, to the extent possible within a limited space, the techniques used to provide the required Loran subsystem performance have been explained.

The applications of Loran-C to automatic vessel position monitoring for purposes of traffic control and management is relatively new. The Suez Canal VTMS represents the first use of Loran-C in a large scale marine vessel traffic system. It is expected that much useful information about the operational performance of this type of Loran-C application will be obtained from the Suez Canal system.

While almost all of the hardware needed to implement the Loran subsystem of the Suez Canal VTMS has been "off-the-shelf", much effort has been expended to reconfigure, repackage and integrate this hardware for this system. The availability of this hardware together with the operational experience obtained from this system is expected to increase interest in the use of Loran-C for the control of river and harbor traffic and for the monitoring of fleets of land vehicles.

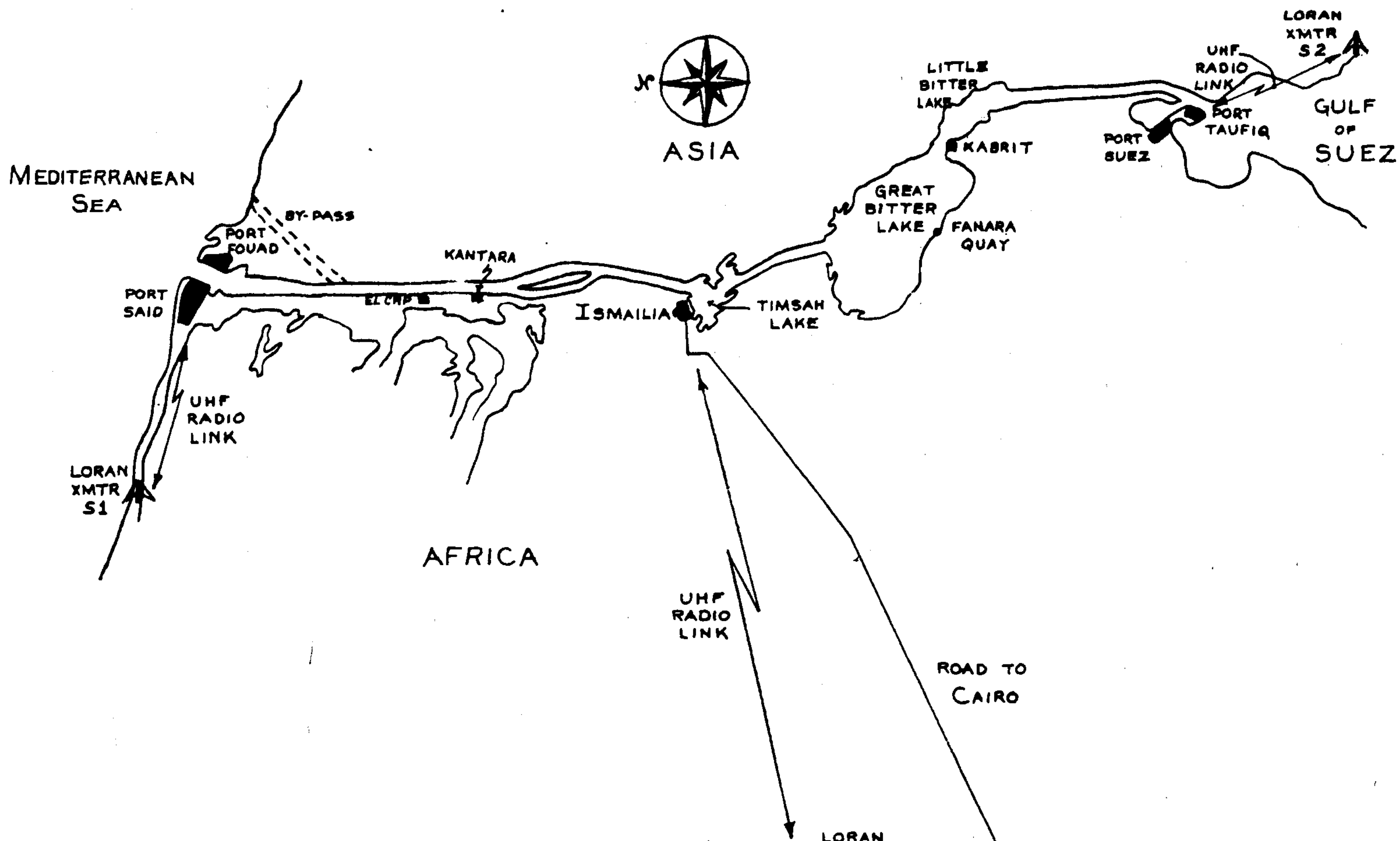

FIGURE 1. GEOGRAPHIC LAYOUT OF
SUEZ CANAL LORAN SYSTEM.

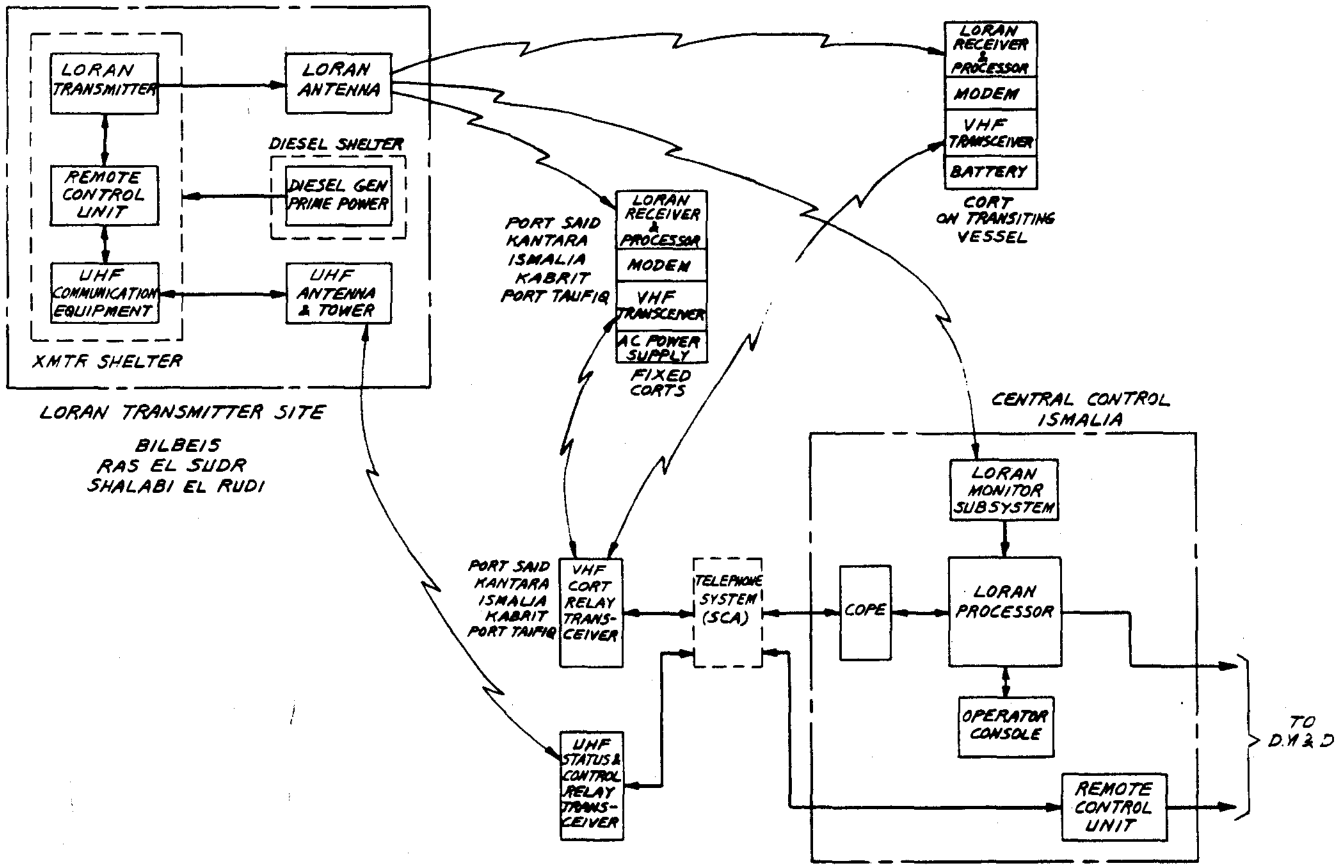

FIGURE 2. LORAN SUBSYSTEM BLOCK DIAGRAM

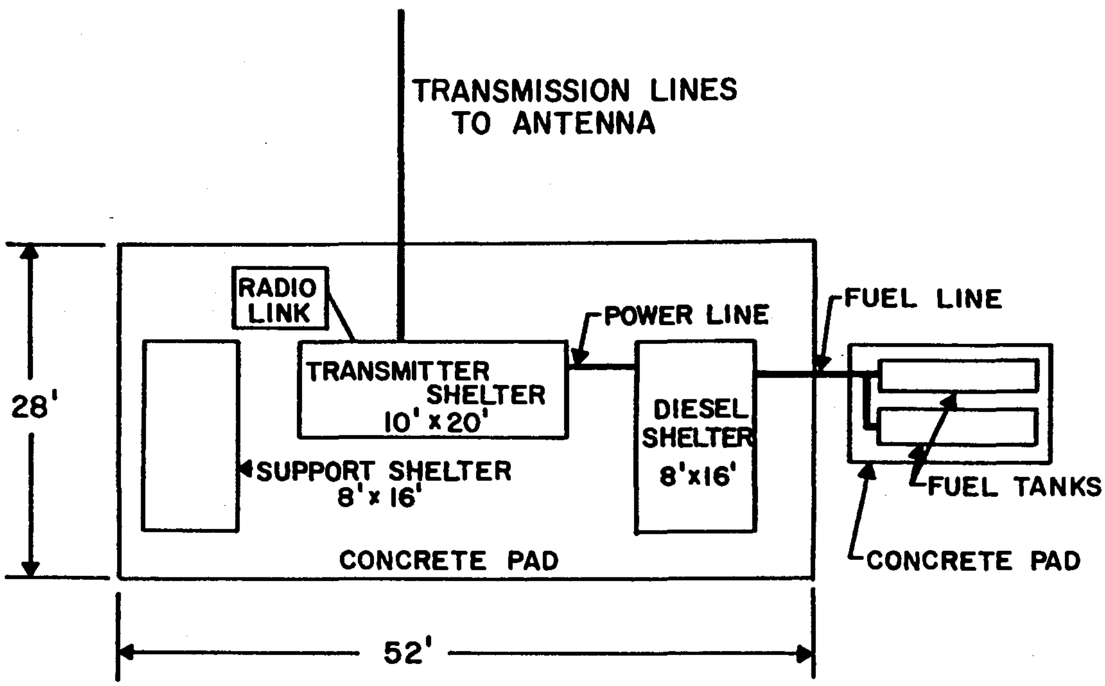

FIGURE 3. LORAN TRANSMITTER SITE LAYOUT.

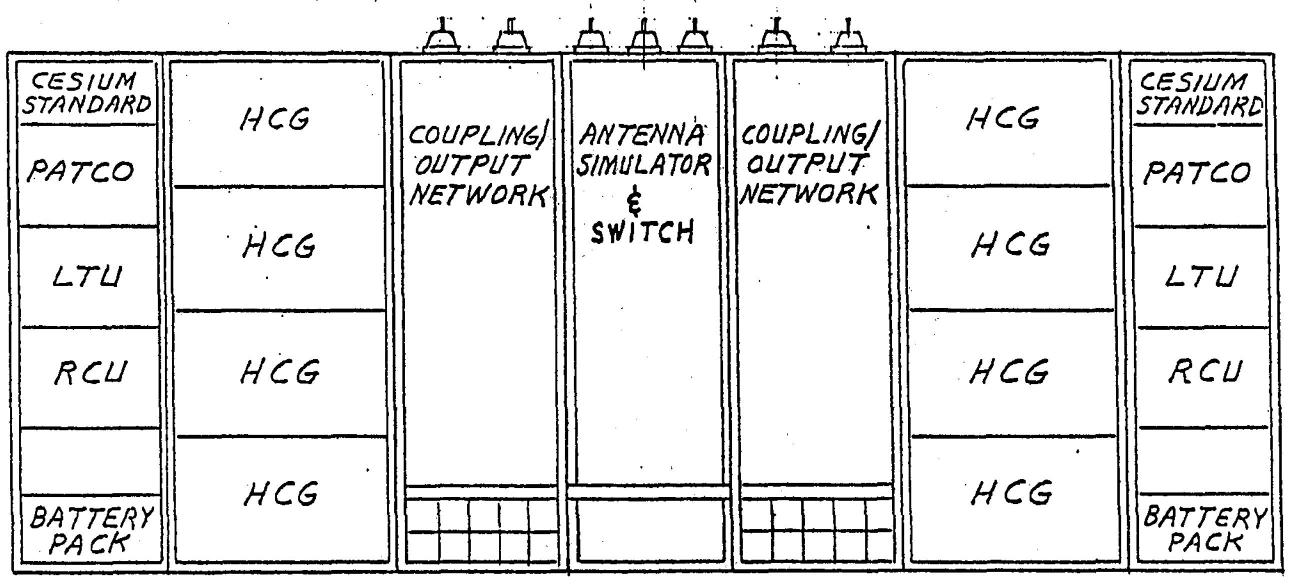

FIGURE 4. REDUNDANT LORAN TRANSMITTER.

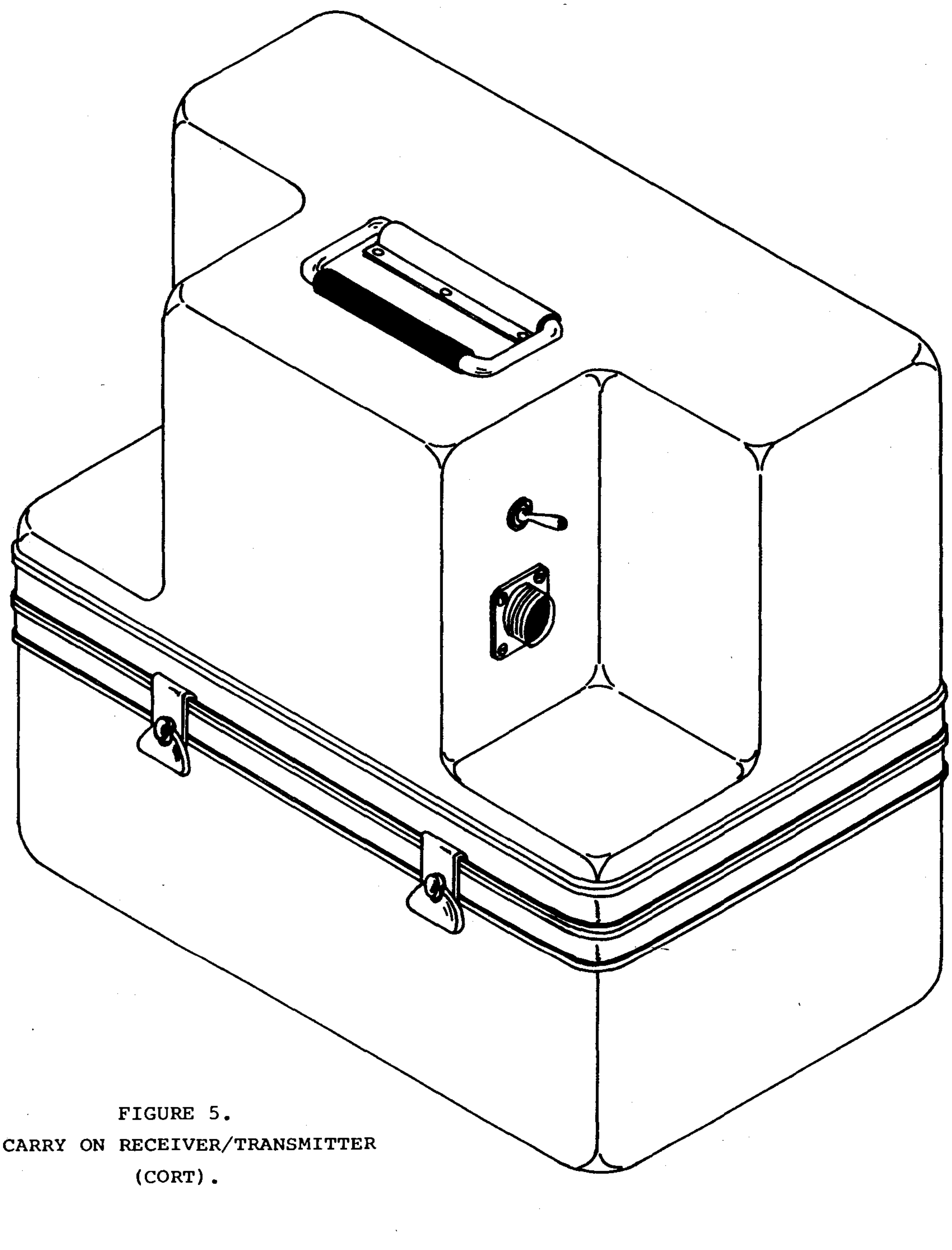

FIGURE 5.
CARRY ON RECEIVER/TRANSMITTER
(CORT).

ANALYSIS OF REAL WORLD LORAN RECORDINGS

Captain Bruce A. Conway
United States Air Force
ESD/OL-AF (Detachment AFOO)
Eglin AFB, Florida 32548

Magnetic tape recordings of the loran band have been used to supplement and enhance loran receiver evaluation at the United States Air Force (USAF) AN/GRM-99 Dynamic Loran/Inertial Simulator laboratory at Eglin AFB, Florida. The paper addresses the use of these recordings with the AN/GRM-99 simulator to provide laboratory testing and analysis of real world loran receiver performance. Loran band recordings have been used in the laboratory to evaluate receiver interference suppression capabilities, potential cross rate problems, in-field search and settle performance, tracking accuracy, and dynamic receiver performance. Many of these evaluations would have been impossible without the recordings complementing the simulator capabilities. In particular, this paper discusses the AN/GRM-99 simulator, the testing capabilities gained using the loran band signals reproduced from magnetic tape, the magnetic tape recording system requirements, tape recording procedures, problems encountered, and limitations of the system.

BACKGROUND

This loran recording/simulation effort has evolved to meet a need that cannot be met with loran recordings, simulation, or live flight test alone. This section describes the AN/GRM-99 simulator laboratory, previous loran recording efforts, and the requirements for recordings to supplement simulation.

AN/GRM-99 Simulator Laboratory

Requirements. The AN/GRM-99 Simulator laboratory was designed to support the testing of the AN/ARN-101 digital modular avionics system update to the F-4E and RF-4C aircraft. The prime navigation information for this system is derived from integrated loran/inertial navigation system (INS) measurements. The loran receiver in this system must function given the high dynamics of jet fighter aircraft, adverse radio frequency interference (RFI) conditions, low power loran transmitters, and spoofing and meaconing. The AN/GRM-99 provides loran/INS signals under computer controlled conditions to provide the required test conditions in the laboratory. As shown in figure 1, the AN/GRM-99 also provides real time data collection, reduction and display; aircraft flight profile generation; and aircraft, loran, and inertial modeling.

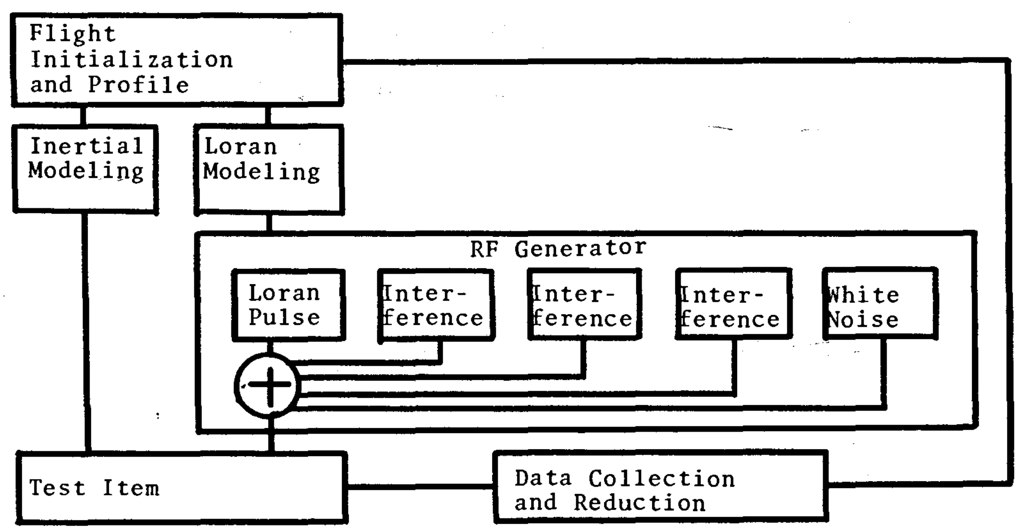

Figure 1. AN/GRM-99 Simulator Block Diagram

Simulation Capabilities. The AN/GRM-99 simulator can model any Loran-C or Loran-D chain, skywave effects, envelope-to-cycle discrepancy (ECD) effects, dynamic loran signal strengths, secondary phase effects, and noise level. The simulator also supports three interference sources, two of which are capable of frequency shift keying (FSK) or synchronous interference with doppler shifts, and one which is capable of on and off continuous wave (CW) keying. Rate aiding outputs and inertial outputs synchronized to the simulated composite loran rf signal are provided by the simulator to the system under test.

Receiver Evaluations. The receiver evaluations performed on the AN/GRM-99 simulator include Loran-C and Loran-D performance and tracking accuracies under specified sets of environmental, noise, interferance, and vehicle dynamic conditions; receiver dynamic range and sensitivity; search and settle as well as tracking accuracies with various Loran-C skywave delays and amplitudes, ECD conditions, and dynamic imbalance; and receiver dynamic response to jamming and meaconing.

Previous Loran Recording Efforts

The USAF Tactical Loran System Program Office, ESD/DCL, tasked the 1839 Electronics Installation Group, Field Measurements Branch to provide an electromagnetic compatibility survey for two proposed loran chains. In connection with these surveys, a number of tape recordings of the rf environment around 100 kHz were made, with support provided by ITT Avionics, Nutley, New Jersey. These tapes proved to be useful as a noise source during loran receiver testing; however, their usefulness was limited by the narrow bandwidth of the antenna coupling unit (ACU). The tapes were recorded specifically to test the predecessor to the AN/ARN-101, the AN/ARN-92 against the proposed chains. Evaluation of the AN/ARN-92 receiver was accurate, but evaluation of any other system was limited by the narrow signal bandwidth. The follow on tapes provided with the support of Air Force Communications Service (AFCS) 1974 Communications Group, Det 4 were recorded with a wide band ACU, to enable evaluation of any loran receiver.

Requirement for Recordings to Supplement Simulation

Simulator Limitations. The loran rf recordings complement the simulator capability to evaluate simulated in-field system performance. Simulator testing alone provides the capability to measure limits of receiver performance against a single signal parameter, but is limited when measuring limits of performance against the many combinations of signal parameters encountered. This knowledge of receiver performance enables only a limited prediction in-field receiver performance. Additionally the limits of simulation are reached when insufficient data exists to predict ground conductivities and absolute loran signal strengths, sky wave effects, atmospheric noise levels, loran cross rate interference effects, and the local rf environment.

Recording Limitations. The use of the tape recorded loran in the laboratory provides a good evaluation of static in-field receiver performance, signal levels, and rf environment. Dynamic receiver performance evaluation and signal level limits evaluation are impossible against recorded loran.

Flight Testing Limitations. Most of the receiver evaluation performed in the laboratory with the simulator and magnetic tape recordings would have been impossible, expensive, and/or less extensive if performed in live flight tests. The simulator can provide loran signals from a proposed loran chain to mix with recorded rf, can provide dynamic loran rf to mix with recorded rf, and can provide loran signal conditions and repeatability not possible with live flight. Additionally, the quality and quantity of instrumentation and signal measurement tools in the laboratory are not available in the field.

TESTING CAPABILITIES WITH LORAN RECORDINGS/SIMULATION

The requirement to bring the real world to the simulation laboratory can be met with recordings of the loran rf. This section discusses the testing capabilities gained with the loran recording/simulation testing, with recorded loran alone, and the unique capabilities gained with recordings of the USAF electronic countermeasure (ECM)/electronic counter-countermeasure (ECCM) loran field tests at Fort Hood, Texas.

Receiver Evaluation with Recorded Loran Band RF Signals/Simulator Generated Loran Signals

Laboratory Tools Available. The first benefit of bringing the real world loran band rf signal into the laboratory via the tape recordings is the availability of testing tools in the laboratory. A spectrum analyzer, oscilloscope, and simulator generated scope trigger signal enable frequency and time domain measurements. The AN/ARN-101 receiver is interfaced to the AN/GRM-99 simulator, allowing transfer of the loran receiver signal measurements to the AN/GRM-99 to be listed at a line printer, recorded on a strip chart recorder, and reduced via the simulator statistical routines.

Test Repeatability. The second benefit of using tape recordings to supplement AN/GRM-99 simulation is the repeatability of tests. Improvements to receiver performance, and receiver performance comparison between two receivers can be tested against a "standard" simulated real world loran environment.

Increased Flexibility. The limits of receiver performance can be evaluated in the simulated real world environment, enabling accurate predictions of the receiver coverage area. With simulator generated loran signals, the signal attenuation, pulse risetime, ECD, skywave effects, and receiver dynamics can be controlled. With this control, the simulator can test and evaluate functional performance of receivers while subjected to a range of real world conditions not practical in actual flight tests.

Conditions Unavailable to the Receiver. Requirements that have been met only in the simulator lab using magnetic tape recordings include receiver evaluation against proposed chains; receiver evaluations in areas where an AN/ARN-101 equippped F-4E fighter aircraft would be unwelcome; and system performance evaluation prior to deployment. This testing has provided valuable insight into Air Force tactical loran system deployment, and enabled timely definition of system problems prior to deploying the first operational production AN/ARN-101 system.

Receiver Testing with Recorded Loran Only

"Prove" Simulation. Bringing the real world to the laboratory via the magnetic tape recordings allows in-depth analysis of the loran environment and receiver performance. The recorded loran signal fidelity, bandwidth, timing integrity, and signal level are sufficient for the receiver to acquire lock against the loran signal playback. This enables receiver signal measurements and the laboratory equipment measurements to define the loran signal strength to enable accurate simulations. Though insufficient data exists to accurately predict absolute loran signal strength values, these values can be duplicated if known, and any deviations from these values can be accurately predicted.

Envelope Calibration. The AN/ARN-101 loran receiver is a linear receiver which employs an internally generated envelope calibrate pulse. Accurate cycle selection during signal acquisition requires an envelope calibration that will allow use of envelope calibrate pulse measurements to predict the actual loran pulse measurements. The tape recording system can be used as a pre-deployment tool to enable these envelope calibrations.

Tape Recorded ECM/ECCM Environment

USAF ECCM Field Tests at Ft Hood, Texas. The USAF modified an AN/ARN-101 equipped RF-4C and the Ft Hood Loran-D chain to support ECCM airborne and ground field testing. This included the construction of a transmitter to provide ECM signal formats to include:

1. Synchronous CW transmissions
2. Nonsynchronous CW transmissions
3. Normal Loran-D signals
4. Intentional loran type interference
5. Cross rate interference
6. Coherent Repeater

These signals were used in ways to produce the greatest disruption of desirable loran transmissions. The field tests were conducted with Loran-D transmissions both with and without ECCM coding.

ECCM Field Test Loran Signal Recording. The magnetic tape recording system was deployed to the field tests to record the ECM/ECCM signals. Special hardware was constructed to record the ECCM coded loran signals to enable useful playback. ECCM coded loran can be used only by a receiver equipped with an ECCM code initializer and generator, and knowledge of the Group Repetition Interval (GRI) count of the ECCM transmitters. The hardware designed for these recordings enabled the appropriate marking of GRI count to allow an ECCM receiver to use these recordings. These recordings allow simulator laboratory evaluation of ECCM modified receivers.

RECORDING SYSTEM HARDWARE

Given that bringing the real world into the simulation laboratory meets testing requirements and provides a valuable tool for receiver evaluation, the next requirement is for the hardware to do this in an accurate, timely manner. The section describes the recording system both in overview and by individual component.

System Overview

System Capabilities. The loran band magnetic tape recording system is based around a Honeywell 5600C Magnetic Tape Recorder/Reproducer. The recorder is used in the direct record/reproduce mode, servoed against a rubidium or cesium timing standard to accurately maintain frequency spectral properties. The bandwidth of the system is 60 kHz to 150 kHz, which accurately maintains the loran pulse shape and interference signal strengths. The recorder direct record/reproduce electronics support a 39 dB dynamic signal range. This combined with the 20 dB of gain in the ACU, and the selectable 0-40 dB of gain in the signal path provide a system capable of recording loran signals from approximately +30 dB above 1 uv/m to +100 dB above 1 uv/m.

Overall System. The recording system including electronic calibration and measurement equipment is shown in figure 2. This is the equipment required in the field to record accurately and confidently, and support laboratory evaluation requirements.

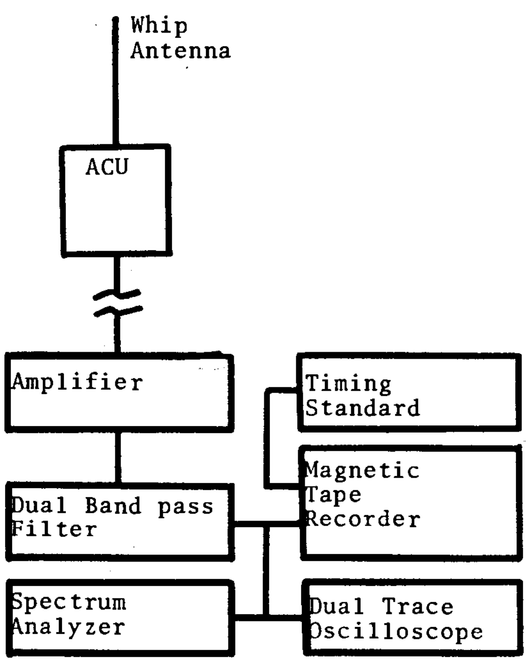

Figure 2. Recording System

System Components

Magnetic Tape Recording System. The Honeywell 5600C with direct record/reproduce amplifiers and servo track ran at 30 inches per second (ips) provides accurate signal fidelity and timing integrity to record and reproduce loran band rf signals for receiver evaluation.

Reference Oscillator. The reference oscillator provides the 100.000 kHz signal to record the servo track required to maintain accurate timing and frequency spectral properties. This should be a rubidium or cesium frequency standard.

Antenna System. For accurate recording the antenna system used must first be tested with a receiver to demonstrate no pulse distortion. This requires an adequate ground plane, broad band ACU, and whip antenna. For an accurate measure of gain through the system, an injection capacitor and signal generator are required to generate a known signal at the input, and an oscilloscope to measure the signal at the input of the tape recorder.

Amplification and Filtering. The amplifier used in the loran signal path provides high pass filtering with an adjustable corner frequency set at 6.00 kHz, and 0-40 dB of selectable in 10 dB steps. This provides the required gain with minimal phase shift distortion. A dual adjustable band pass filter can be used in some circumstances to gain signal-to-noise ratio (SNR) to meet specific testing requirements.

Instrumentation. A voltmeter, dual trace oscilloscope, and spectrum analyzer will meet the instrumentation requirements. These aid in calibration and loran band signal definition to enable accurate laboratory use of the tapes.

Magnetic Recording Tape. The correct choice of magnetic recording tape is important. The Honeywell 5600C will support the 4600 ft, 1 mil thickness, 10 1/2 inch aluminum reels of 1/2 inch recording tape; or the 7800 ft, 1/2 mil thickness recording tape. The tape parameters which are important are the tape bandwidth, the signal dropout specification, the length, and the cost. The tape should be a medium bandwidth tape to support recording frequencies near 100 kHz at 30 ips. The signal dropout specification affects the timing integrity maintained by the servo track.

Any dropouts on this track effectively shift the timing reference back by 20 us steps, which makes accurate receiver tracking impossible. The tape length determines the maximum length of a single laboratory receiver trial. The 4600 ft tape runs for 28 minutes, and the 7800 ft tape runs for about 45 minutes. The 7800 ft tape is most expensive, has the best dropout specification, and has given the best performance.

RECORDING IN THE FIELD

With the requirement for recordings and the recording system defined, the task remaining is to record the real world loran rf band signals. This section discusses the guidelines followed for recording in the field, the problems encountered, and the solutions to these problems.

What to Record

Proposed Chain Evaluation. The decision of what to record was driven by the specific testing requirements and the freedom of control over the loran environment available. For the case of recording background loran rf to simulate a proposed chain against, the only control available over the loran environment was that of choosing recording time and location. The actual recording times included both day and night, and the locations were chosen as close to the operational theater as possible. These general guidelines were followed in all recordings.

European Loran Recording. The recording system was deployed to Germany in the Spring of 1978 to support evaluation of the AN/ARN-101 receiver performance against the USAF AN/TRN-21 Loran-D chain. The major concern was the performance of the AN/ARN-101 in the adverse RFI/weak signal strength condition of Germany. In addition to control of recording time and location, the operators controlled the Loran-D chain. This enabled recording of pairs of tapes, one with the Loran-D chain on and one with the Loran-D chain off. The first tape was used to establish loran signals for the second tape where the AN/GRM-99 supplied the loran. Loran signals were also recorded at location within twenty miles of each transmitter for loran pulse envelope calibration for the AN/ARN-101.

ECCM Recordings. The tape recording system was deployed to Ft Hood, Texas in November 1978 to record the ECM/ECCM loran environment to create a standard library of recordings to evaluate ECCM modified receivers against. The operators had control of the ECM jammer and the ECCM modified transmitters, and were able to perform tests solely for the purpose of 'spoofing' the tape recorder. Special hardware was designed and built to support marking a specific GRI count to enable accurate ECCM mode playback.

Recording System Problems Encountered

Servo Track Signal Dropouts. The loss of timing integrity due to a signal dropout on the servo track was the problem encountered most often. The remedies to this were to maintain clean record heads on the tape recorder, use a tape with a good rating for signal dropouts, use a medium bandwidth tape, and record a dual servo track to use the 'or' of these two signals to drive the servo phase lock loop circuitry.

Inadequate bandwidth. The rf bandwidth should be larger than the bandwidth of the receiver under test to maintain accurate pulse shape and interference signal levels.

Limited Dynamic Range. The 39 dB dynamic range of the tape recorder can be less than the imbalance in loran signal strength when recording very close to a transmitter. The solution is to pick recording sites to avoid this large loran signal level imbalance.

CONCLUSION

This report discussed the requirements, capabilities, and limitations of this loran recording/simulation system. These magnetic tape recordings of loran rf signals have brought the real real world into the laboratory and have enabled accurate loran receiver evaluations. These evaluations have enabled timely decisions in support of proposed loran chains and modifications to the AN/ARN-101 for system deployment.

LORAN WARPAGE DATA BASE REQUIREMENTS

by

Joseph L. Howard
The MITRE Corporation
P. O. Box 208
Bedford, MA 01730

ABSTRACT

Differences between LORAN time differences (TDs) measured with a receiver and TDs calculated using secondary phase corrections from a homogeneous LORAN conductivity model, can be interpreted as irregularities in the actual hyperbolic lines of position (LOP). This condition is referred to as warpage. LORAN warpage occurs for two reasons. First, warpage occurs whenever the propagation medium is not uniform. Second, warpage occurs when LORAN signals travel over two or more different propagation mediums i.e. from land to sea and back to land. The presence of LORAN warpage affects the normal coordinate conversion relationship between the regular LORAN hyperbolic grid and the corresponding geodetic (latitude, longitude) grid commonly used for navigation.

The effect of LORAN warpage is corrected by the AN/ARN-101 LORAN system in a two part algorithm. The first part operates off-line and uses a paired data base of measured LORAN and geodetic coordinates to generate a set of 15 coefficients for each LORAN station. These coefficients are used in the second part of the algorithm each coordinate conversion cycle. The warpage is corrected during coordinate conversion by using the coefficients to estimate an effective wave impedance for the secondary phase correction of each LORAN time of arrival. This paper describes the considerations and methodology needed to obtain a useable data base that meets the requirements for coordinate conversion accuracy. The recent calibration of the Southeast U.S. LORAN-C chain at Eglin AFB, Florida is used as an example of the procedure.

INTRODUCTION

For many applications, the usefulness of LORAN depends on conversion from hyperbolic navigation to geodetic navigation. The process of coordinate converting LORAN time differences to latitude longitude can introduce a significant amount of positional error. This error is caused by the simple fact that the LORAN grid is <u>not</u> directly related to the geodetic grid. Non-cancelling signal propagation errors cause a shift or bend in the smooth regular hyperbolic lines of position. This is called LORAN warpage and is a function of the propagation path or medium the LORAN signal crosses.

LORAN warpage can be corrected during coordinate conversion by using an appropriate model for the secondary phase correction term. Most coordinate conversion algorithms assume a regular homogeneous LORAN grid and model a single type of propagation medium for the entire coverage area. This assumption is not valid for accurate navigation over land where more than one type of propagation medium is involved with a LORAN signal path. For very accurate coordinate conversion over land areas, the influence of each propagation medium must be considered. In areas of severe warpage, such as mountanous, this requires a detailed piecewise addition of all contributing factors to arrive at an effective delay or impedance value. This process must be repeated for all three LORAN stations (M, A, B) in the triad. For regions where less coordinate conversion accuracy is required, average impedance values can be selected for each LORAN station. These values are selected based on the average propagation medium for that signal path.

The U. S. Air Force has demonstrated very accurate coordinate conversion over areas of severe LORAN warpage. This procedure uses a two part algorithm for determining the secondary phase correction*. This algorithm is implemented in the AN/ARN-101 Digital Avionics System. The first part of the algorithm uses a paired data base of measured LORAN time differences and geodetic latitude longitude coordinates to generate a set of coefficients.

*Reference 1

The coefficients are then used in the second part of the algorithm each coordinate conversion cycle to compute the secondary phase correction term. Thus, the accuracy of the final coordinate conversion depends on the selection and corresponding accuracy of the measured data base. This paper presents the general procedure for obtaining an accurate data base for the AN/ARN-101 coordinate conversion algorithm.

GENERAL DATA REQUIREMENTS

The LORAN coordinate conversion data base consists of LORAN time differences (TDs) and corresponding geodetic positions (Latitude/Longitude). Measured (observed) data is desired but interpolated, derived, or calculated data can be used if it meets the accuracy requirements of the system.

The warpage coefficient generation program requires that five geographic areas be defined as shown in Figure 1. The prime coverage area is centered over the desired operational region. The size of the prime area is variable but it is normally limited to 100 nautical miles by 100 nautical miles or smaller. Within the central prime area, the warpage coefficient generation program uses the LORAN data base in a regression model to calculate coefficients. These coefficients are then used in an interpolation equation which calculates the effective wave impedances as a function of position in the prime area.

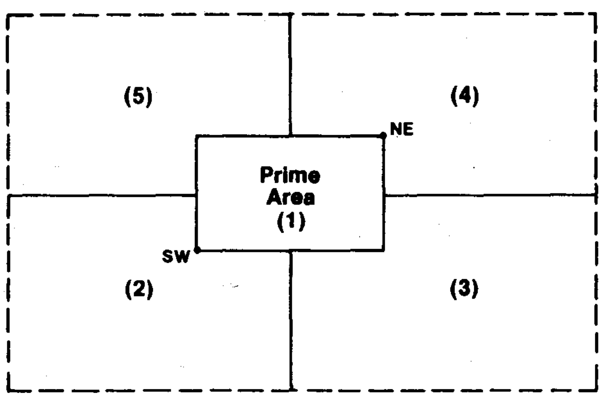

Figure 1.
AN/ARN-101 Warpage Correction Areas

The uniform distribution of data points within the prime area is very important. Ideally, when the prime area is divided into square cells which are 5 nautical miles by 5 nautical miles in size, each cell should contain at least one data point. This distribution insures that the prime area will be accurately modeled. This is a minimum density requirement. More data points per cell in the prime area will generally result in a more accurate model. Locations outside the designated prime area are used to calculate an average wave impedance for the four areas outside the prime area. Usually data points at a distance of 10 to 20 nautical miles from the edges of the prime area are sufficient for a good effective impedance model for the outlying areas. More data points may be required if severe warpage is encountered.

The AN/ARN-101 LORAN warpage model was designed for aircraft and requires LORAN warpage coefficients at four altitude levels in the prime area. Each altitude level must have a separate data base according to the following table:

Level	Altitude Range for Data Point
Ground	0 to 2500 feet
5000 feet	2500 to 7500 feet
10000 feet	7500 to 12500 feet
15000 feet	12500 to 17500 feet

Data points for geodetic locations at other than ground level, are not required to be the same geodetic locations as the ground level point. However, the requirement for a minimum of one data point per cell does apply. For other applications such as vehicle monitoring, only ground level data is required.

DATA BASE REQUIREMENTS

This section presents specific requirements to develop a LORAN warpage data base. The Southeast U. S. LORAN-C chain at Eglin AFB Florida is used as an example, and the following procedures will be covered.

- Selection of the Prime Area
- Selection of Secondary Stations
- Estimate of LORAN Warpage
- Data Collection Requirements
- Generation of Warpage Coefficients

Selection of the Prime Area

The Eglin AFB prime coverage area used with the old East Coast LORAN-C chain was a 42 by 72 nautical mile rectangle. The size of this prime area requires a minimum of 126 data points evenly distributed over the entire area. The previous data base provided 126 data points, but they were not evenly distributed. These data points were concentrated over the west and east land ranges of Eglin AFB with a scattering of points in other areas. This uneven distribution of data points caused problems with coordinate conversion at some edges of the prime area. From this, it is concluded that it is better to reduce the prime area to a manageable size and collect data points that are evenly distributed. Figure 2 is a map of the Eglin AFB land ranges showing approximately a 35 by 52 nautical mile rectangle located by the Northeast and Southwest corners shown below.

NE 30° 50.00'N
   85° 55.00'W

SW 30° 15.00'N
   86° 55.00'W

This represents a reasonable sized prime area for the Southeast U.S. LORAN-C chain at Eglin AFB, Florida. The map is delineated by a grid every 5 minutes of angle. Thus, if each square of grid contains at least 1 calibration point the minimum distribution requirements have been satisfied.

Selection of Secondary Stations

The Southeast U. S. LORAN-C chain offers different combinations of slave stations which can provide coverage for Eglin AFB. The complete data for this chain is contained in Table I.

Table I

Southeast U.S. LORAN-C Chain – Rate 7980 (SL2)

Station	Latitude and Longitude	Station Function	Coding Delay and Baseline Length	Radiated Peak Power
Malone, Florida	30-59-38.74 N 85-10-09.30 W	Master	–	1.0 MW
Grangeville, Louisiana	30-43-33.02 N 90-49-43.60 W	W Secondary	11,000 μs 1809.54 μs	1.0 MW
Raymondville, Texas	26-31-55.01 N 95-50-00.09 W	X Secondary	23,000 μs 4443.38 μs	400 kW
Jupiter, Florida	27-01-58.49 N 80-06-53.52 W	Y Secondary	43,000 μs 2201.88 μs	300 kW
Caroline Beach, N. Carolina	34-03-46.04 N 77-54-46.76 W	Z Secondary	59,000 μs 2542.74 μs	700 kW

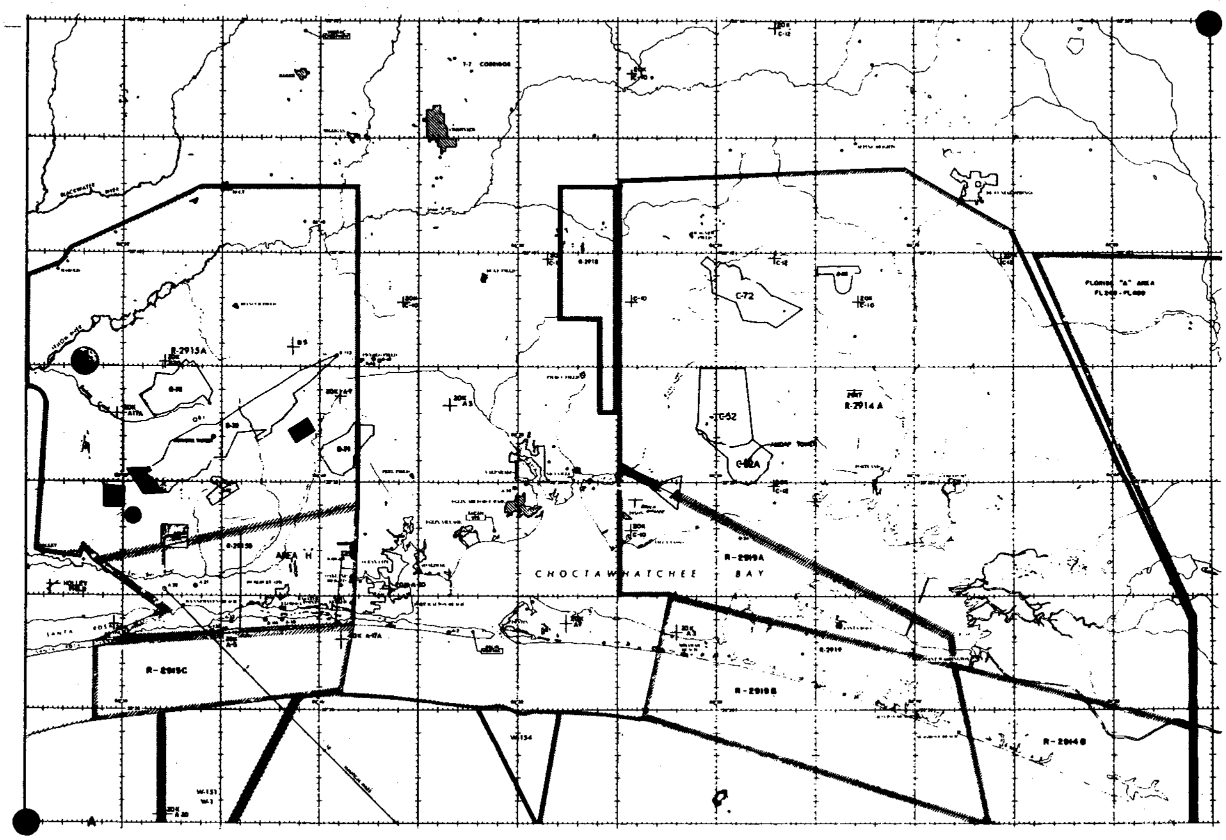

Figure 2. Eglin AFB Land Ranges

Computer generated maps showing the Geometric Dilution of Precision (GDOP) for all master-slave combinations of the Southeast LORAN-C chain were computed to help select the best secondary stations. Analysis of this data indicates that the Raymondville slave (X) generally provides a lower GDOP over Eglin AFB. But its baseline goes directly through the selected prime area. This will result in rapid changes in GDOP over the Northeast corner of the Eglin prime area. For this reason the Malone-Grangeville-Jupiter triad (M-W-Y) is selected to provide the best overall coverage for Eglin AFB. Figure 3 shows the location of Eglin AFB in relationship to the Southeast U. S. LORAN-C chain (7980) and the old East Coast LORAN-C chain (9930).

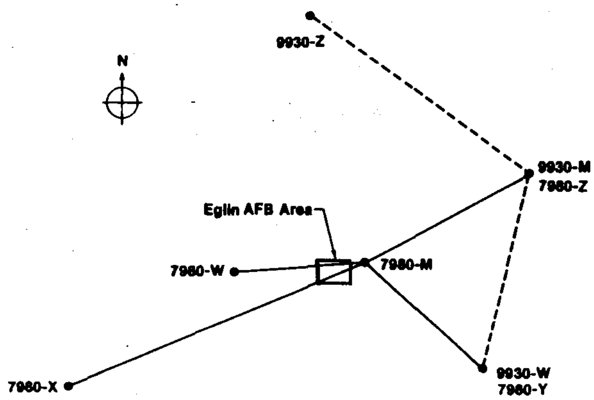

Figure 3.
Southeast U.S. LORAN-C Chain Configuration

Estimate of LORAN Warpage

Rough estimates of the effective impedance for each station are needed to determine if warpage in the prime area is mild or severe. These estimates are also initially used in the AN/ARN-101 for all areas and at all altitudes until a sufficient data base is available and warpage coefficients are computed.

Estimation Proceedure

These initial estimates of effective impedance can be made using the following procedures:

(1) Using a map that covers the prime area and the three transmitters (Master, Slave A, Slave B), select a point approximately in the center of the prime area.

(2) Draw the line from the selected point to the Master station and estimate the fraction (x_{sea}) of this path that is seawater, the fraction ($x_{normal\ land}$) of this path that is normal land, and the fraction ($x_{rough/dry\ land}$) of this path that is rough/dry land. Note that $x_{sea} + x_{normal\ land} + x_{rough/dry\ land} = 1$. The estimated impedance (Δ estimate) is then calculated by evaluating:

$$\Delta_E = (0.001055)\ (x_{sea}) + (0.03)\ (x_{normal\ land}) + (.05)\ (x_{rough/dry\ land})$$

(3) Repeat step 2 for Slave A.

(4) Repeat step 2 for Slave B.

The three estimates can be used in the AN/ARN-101. This is accomplished for the prime area by setting the constant term α_0 to the estimate of effective impedance and setting the other 14 warpage coefficients for each transmitter to zero (α_1 through α_{14}). This must be done at each of the four altitude levels. This procedure provided the following estimates of effective impedance:

Master - Malone, Florida
100% normal land
$\Delta_{E_m} = (0.03 * 1) = 0.03$

Secondary W - Grangeville, Louisiana
5% sea
95% normal land
$\Delta_{E_W} = (0.001055 * .05) + (0.03 * .95) = 0.0285$

Secondary Y - Jupiter, Florida
55% sea
45% normal land
$\Delta_{E_y} = (0.001055 * .55) + (0.03 * .45) = 0.01441$

The effective impedance estimate for Jupiter (Slave Y) has the greatest uncertainty. Severe warpage is expected due to the changing ratio of land and sea interfaces as the straight line path to Jupiter is swept across the Eglin AFB area. This changing land and sea interface for the Jupiter path is exactly the same as when Jupiter was used with the East Coast LORAN-C chain. Within the East Coast chain, the Jupiter slave was determined to be responsible for the majority of all LORAN warpage. Since the transmission path for the Southeast U. S. chain is identical for the Jupiter slave, the same severe warpage is expected for the Southeast U. S. LORAN-C chain.

This assumption is substantiated by comparing the differences between measured and calculated values of Jupiter's TD in both the East Coast and Southeast LORAN-C chains. This comparison was done for the points shown in Table II and the resulting error was the same direction and nearly the same magnitude in each case.

The data in Table II was calculated to estimate the expected positional accuracy of the AN/ARN-101 coordinate converter (Q factor)*, the path of the time difference line of position (LOP direction), and relative range and bearing to each station. This data shows excellent geometric coverage for the Eglin AFB area. The instantaneous (planer) path of a TD LOP was calculated from the azimuths to the LORAN stations by the following equation:

$$LOP_S = \mathrm{Tan}^{-1} \frac{\cos\psi_S - \cos\psi_M}{\sin\psi_M - \sin\psi_S}$$

where: ψ_M = Bearing to master station

ψ_S = Bearing to secondary station

Figure 4 shows the TD Lines of Position from Table II overlaid on a map of Eglin AFB. Based on these calculations it is concluded that the LORAN coverage from the Southeast U.S. LORAN-C chain will be uniform with TD crossing angles of approximately 72 to 77 degrees.

Data Collection Requirements

The prime area is usually sufficiently large that the data base will be collected over a long period of time. TD measurements taken for the data base must be compensated for weather, diurnal, and seasonal effects in order to be consistent and accurate. Ground monitors are needed to accumulate a history of TD data and establish standard TDs associated with the monitor. TDs collected in the field are then corrected by an amount determined from the following equation:

$$TD = TD_{meas} + TD\ inst - TD_{std}$$

where: TD_{meas} = Raw measured TD from the field

TD_{inst} = Instantaneous TD of the Monitor

TD_{std} = Standard TD of the Monitor.

The data base may be collected by ground mobile receivers at known benchmaks, geodetic survey points, or by an aircraft equipped with LORAN

Table II

LORAN Warpage Data

Southeast U.S. LORAN-C Chain Eglin AFB, FL

Location	AN/ARN-101 Q – Factor		Station LOP and TD Data				TD	
	TD	Q	ID	LOP Direction	Range (nm)	Bearing (Deg)	Observed	Calculated
N 30.47483334°			M	–	75.94	65.83		
W 86.51061667°	W-X	-0.85	W	169.84	223.88	273.85	13728.119	13728.118
Bldg 100	W-Y	1.76	X	157.13	642.69	248.44	30950.435	30950.462
Simulator Lab	X-Y	1.67	Y	93.65	394.97	121.47	47176.907	47176.908
N 30.53706389°								
W 86.74996389°	W-X	0.86	M	–	86.08	71.46		
B-70 Target	W-Y	1.60	W	172.27	211.23	273.07		13587.039
New Cowbell	X-Y	1.50	X	159.58	632.20	247.69		30822.771
			Y	96.23	407.59	121.00		47192.215
N 30.63666°								
W 86.30888334°	W-X	-0.79	M	–	62.58	70.00		
C-72 Target	W-Y	1.70	W	170.66	233.68	271.31	13871.442	13871.355
C-5	X-Y	1.59	X	158.99	655.72	247.97		31113.619
			Y	96.76	390.99	123.51	47233.543	47234.860

*Q factor is the absolute value of the determinate of the coordinate conversion gradient matrix. Values greater than 0.1 are required for conversion.

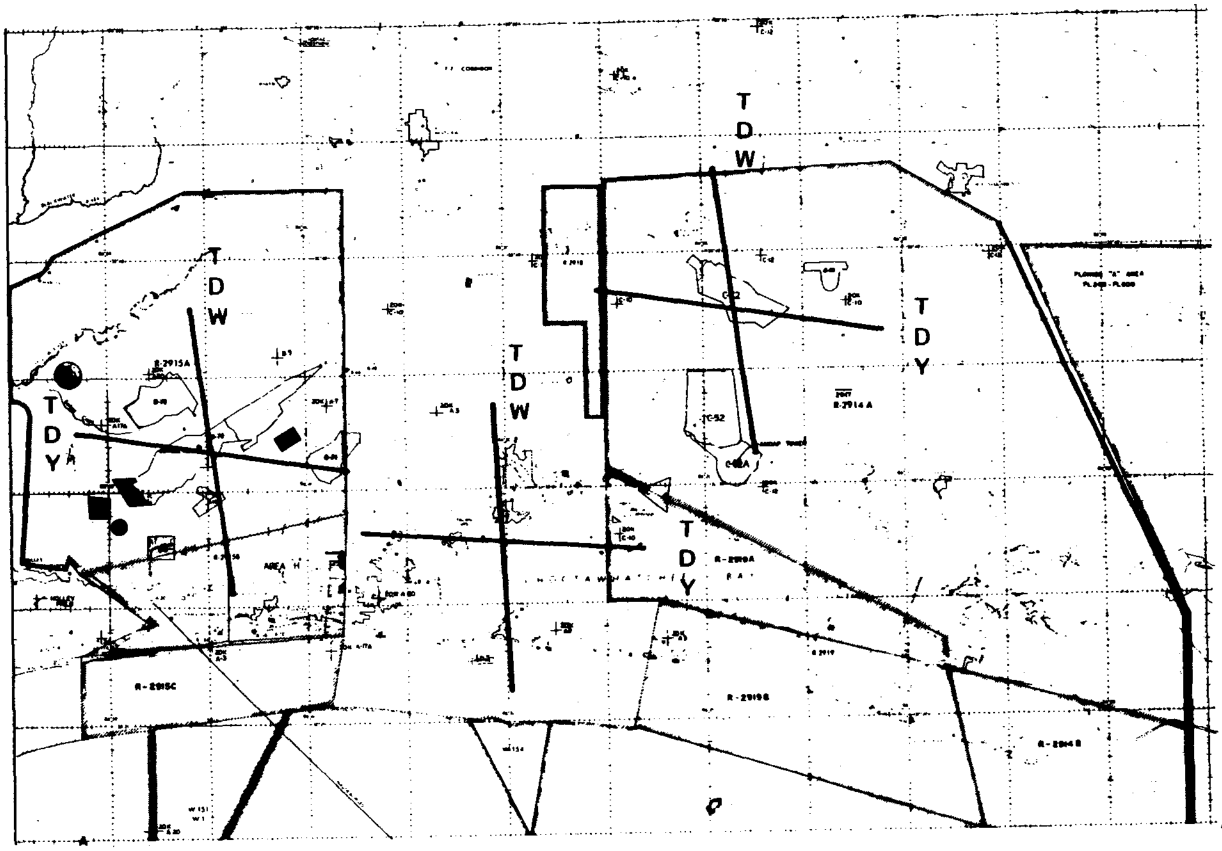

Figure 4. TD Lines of Position

and other equipment for independent ground position location. When aircraft are used to collect the data base, the instantaneous aircraft locations should be accurate to 150 feet (1σ) or better. Measurements with position uncertainties of up to 300 feet (1σ) may be used, but only if more accurate measurements cannot be obtained. When positional measurements cannot be made to accuracies better than 300 feet(1σ), then the data point should not be used. If this condition is prevalent over the prime area, then the prime area cannot be adequately modeled and "average" values of effective impedance will usually provide the same statistical accuracy.

Generation of Warpage Coefficients

Collection of the data base is only the first step in the procedure to correct for the effects of LORAN warpage. The data base must be processed by the warpage coefficient generation program to calculate a set of fifteen coefficients for each LORAN secondary station. This program requires the following data as an input:

- The Northeast and Southwest corners of all 5 correction areas
- LORAN station locations
- Slave emission delays
- Spheriod Model
- Transmission ranges
- Program constants
  - Effective impedance of master station (estimated average)
  - Atmospheric vertical lapse factor (0.85)
  - Atmospheric index of refraction (1.000338)
- Data base for the area of interest.

Currently the warpage coefficient generation program is in IBM card format and the above data is entered on IBM punch cards. The format for this data is specified in the program users manual*.

The input data base is used by the warpage coefficient generation program to model the warpage and estimate the effective impedance for coordinate conversion of each data point. Once the effective impedances are determined to the accuracy of the data base, warpage coefficients are generated. The current version of the program uses only one coefficient to model the master station. The estimated value of master impedance used for input is also the coefficient for the master station. For each secondary station, one of the 15 coefficients is the average effective impedance for that station while the remaining 14 coefficients are constants for a 4th order polynomial. This polynomial is used to adjust the average effective impedance as a function of position within the prime area. With this method, the coefficients can effectively model the warpage and provide the wide range of impedances needed for correction. This process is implemented in the second part of the AN/ARN-101 coordinate conversion algorithm.

SUMMARY

For many applications LORAN must be coordinate converted to latitude and longitude. Changes in the propagation medium over land signal paths warps the smooth hyperbolic lines of position and affects the accuracy of LORAN coordinate conversion. The effects of warpage can be corrected by proper selection of the secondary phase correction term but the selection is complicated by the severity of the warpage. Mild warpage can be approximated by a regular smooth LORAN grid and a single effective impedance correction model. Correction for severe warpage depends on location and requires an individual correction for each station and each location. Precision coordinate conversion in areas of mild and severe warpage requires an accurate data base of known geodetic positions and measured TDs. This data base is then used to model the LORAN warpage. In the AN/ARN-101 algorithm, warpage coefficients are developed in a warpage coefficient generation program. These coefficients transfer the warpage model to the second part of the algorithm which selects the proper secondary phase correction for coordinate conversion. This algorithm has demonstrated the ability to accurately model both mild and severe warpage as well as the rapidly changing warpage encountered with multiple land-sea-land interfaces.

*Reference 2

REFERENCES

1. "AN/ARN-101 Computer Program Development Specification, RF-4C", CB1001-004, Lear Siegler, Inc., Contract F19628-76-C-0024.

2. "Warpage Coefficient Generation Program Users Manual", YV1007, Lear Siegler, Inc., 18 May 1976, Contract F19628-76-C-0024.

3. "Wild Goose Association Radionavigation Journal", 1978.

APPLICATION OF SEMI-EMPIRICAL TD GRID CALIBRATION TO THE WEST COAST LORAN-C CHAIN

by

R.R. Gupta
The Analytic Sciences Corporation
Six Jacob Way
Reading, Massachusetts 01867

E. Anderson
U.S. Coast Guard R&D Center
Avery Point
Groton, Connecticut 06430

ABSTRACT

This paper demonstrates the utility of semi-empirical Loran-C time difference (TD) grid calibration techniques. Theory is employed to determine the functional dependence of TDs on range and bearing from the Loran-C chain stations and TD measurement data are utilized to calibrate the (uncertain) coefficients incorporated in the semi-empirical TD model. A specific semi-empirical model is derived for the West Coast Loran-C chain where at-sea TD measurement data in Southern California have revealed large discrepancies between U.S. Coast Guard predictions and measurements. A significant reduction in the West Coast TD errors is achieved with the semi-empirically-calibrated model relative to the U.S. Coast Guard grid. The accuracy of the calibrated West Coast Loran-C grid is further evaluated by comparing the calibrated grid with measurements not used in model calibration. Results are also presented which show the sensitivity of the model accuracy to the quantity and distribution of measurement data used to calibrate the West Coast model. Data collection requirements guidelines are presented for future semi-empirical grid calibration efforts.

INTRODUCTION

Semi-empirical Loran-C time difference (TD) grid calibration techniques have been successfully employed to develop an accurate (approximately 100 nsec, rms) calibrated grid for the St. Marys River Loran-C chain where groundwave signal paths exhibited "nearly homogeneous" signal propagation properties (Ref. 1). This paper extends the utility of semi-empirical techniques to the development of a calibrated Loran-C grid for the Coastal Confluence Zone (CCZ) where signal paths must be considered as mixed, i.e., part land and part sea water. Also, the operational practicality of adopting semi-empirical techniques as a grid calibration tool for Loran-C CCZ regions is assessed in terms of quantity and distribution of calibration data required to achieve a desired grid accuracy. In particular, semi-empirical TD grid calibration techniques are applied to the West Coast Loran-C chain where the U.S. Coast Guard predictions are reported to result in large charting errors, especially in the CCZ between Los Angeles and San Diego.

THEORETICAL BASIS

Groundwave Phase Delay Models

Loran-C groundwave phase delay* is generally expressed as

$$\phi = T + SF$$
$$= \frac{n}{c} R + SF \qquad (1)$$

where n is the surface refractive index, c is the speed of light in a vacuum, R is the range to the transmitting station, and SF† is the Secondary Phase delay (also known as Secondary Phase factor) caused by the finite conductivity and vertical lapse rate (of refractive index) along earth's surface. The first term in Eq. 1 is called the primary phase delay (T) and is the dominant term in this equation. Computation of T involves well-known parameters. Although the second term of Eq. 1 is more than an order of magnitude smaller than the primary phase delay, it is by far the most complex to compute due to irregularities as well as inhomogeneous electrical properties (conductivity) of the earth's surface.

A number of analytical and empirical SF computation techniques (or models) have been reported in the literature (Refs. 2 through 5). The most commonly-used models are:

*Phase, phase delay, propagation delay and time delay are used interchangeably throughout this paper, and they are expressed in units of time.

†Throughout this paper, SF denotes the total secondary phase factor of the groundwave signal propagating over any land/water path and not the SF associated with an equivalent sea water path.

- Homogeneous/smooth path model
- Mixed Path -- Millington's empirical method
- Inhomogeneous Path -- Integral Equation approach.

The homogeneous/smooth path model (Ref. 2) is useful for SF computations over a homogeneous (i.e., uniform electrical properties) signal propagation path along a smooth earth, such as an all-sea water path. On the other hand, Millington's empirical approach (Ref. 3) is useful for computing the SF over a mixed (multiple-homogeneous segment) path. This approach empirically combines SFs of various homogeneous segments (derived from homogeneous/smooth path model) of a mixed path. The accuracy of Millington's approach is reported to be good (Ref. 6) provided reasonably accurate estimates of the homogeneous segment SFs are available.

When the propagation path is inhomogeneous and the terrain is irregular, such that it cannot be modeled satisfactorily by either the homogeneous path or Millington's mixed path model, a more sophisticated and complicated integral equation model (Ref. 5) can be used. However, the numerical solution of the integral equation is generally expensive and cumbersome except for simple terrain irregularities and requires a relatively large computer storage capability to process all of the physiographic data characterizing the path.

In summary, analytical prediction models are useful if the modeled propagation path scenario closely approximates the "real-world" scenario and if the propagation path parameters are known. Usually, the real-world signal propagation medium of interest is far too inhomogeneous and irregular to be easily idealized. Additionally, the required propagation path parameter values are rarely known with the required precision.

The approach taken herein is <u>to employ semi-empirical grid calibration techniques, similar to those used for calibrating the St. Marys River Loran-C chain (Ref. 1). The "physics" of the propagation medium are used to establish a functional form of the signal phase delay model and measurement data are used to calibrate the (uncertain) coefficients of the model</u>. The semi-empirical model can be made as complex as desired and will approach the theoretical model in the limit. However, increased complexity requires estimating an increased number of uncertain coefficients in the model, which in turn increases the amount of measurement data required. Since the primary purpose for developing a grid calibration model is to reduce the amount of measurement data required to establish a Loran-C grid, a <u>compromise</u> must be made between model complexity and measurement data requirements.

<u>TD Grid Calibration Equation</u>

The <u>true</u> time difference (TD_i) between the time-of-arrival of a groundwave signal from the i^{th} (= w, x or y) secondary station and the time-of-arrival from the master station (m) is given by

$$TD_i = (T_i - T_m) + (SF_i - SF_m) + ED_i \quad (2)$$

where ED_i is the true emission delay. (For the West Coast chain, emission delay is the coding delay plus the true baseline length of the i^{th} secondary station.)

The semi-empirical model to be developed herein will utilize land and sea TD measurement data to calibrate the model. These measurements are corrupted by measurement noise including position reference errors, and are related to the true TD by

$$\underbrace{\text{Measured } TD_i}_{z_i^*} = \underbrace{\text{True } TD_i}_{TD_i} + \underbrace{\text{Measurement Noise}}_{v_i'} \quad (3)$$

In subsequent discussions of the TD data quality and model calibration procedure, it is convenient to transform the measured TD_i into an "Adjusted TD_i" which is defined as

$$ATD_i \equiv z_i = z_i^* - (T_i - T_m) - \overline{ED}_i \quad (4)$$

where $\overline{ED}_i$ is the published (constant) emission delay implemented at the secondary station (Ref. 8). Substituting Eqs. 2 and 3 into Eq. 4 gives

$$z_i = (SF_i - SF_m) + v_i \quad (5)$$

where v_i (= $\Delta ED_i + v_i'$) is the total measurement error, and ΔED_i is the difference between the true and published emission delay for the i^{th} secondary station.

CALIBRATION DATA ANALYSIS

The U.S. Coast Guard-measured data provided for model calibration include TD data collected at land (all-land path) sites and at sea (part land and part sea water path) sites (see Table 1). The land data set includes three TDs/ site: TD_w (TDW), TD_x(TDX) and TD_y (TDY), collected at 27 coastal sites distributed along the U.S. West Coast as shown (by triangles) in Fig. 1. The sea data set consists of two TDs/ site (TDX and TDY) collected at 23 sea sites located in the Southern California [between Lompoc (near Santa Barbara) and San Diego] CCZ as shown (by circles) in Fig. 1. Based on information from discussions with various sources and engineering judgement, the receiver measurement error was assumed to be between 0.1 - 0.2 μsec.

TABLE 1

WEST COAST MODEL CALIBRATION DATA BASE SUMMARY

TYPE OF DATA	NUMBER OF DATA SITES	NUMBER OF MEASUREMENTS			TOTAL NUMBER OF TD DATA POINTS
		TDW	TDX	TDY	
Land	27	25	27	24	76
Sea	23	*	23	23	46
Combined Land and Sea	50	25	50	47	122

*No data available.

The calibration data are then nonparametrically analyzed to identify

- Potential outliers that do not fit the data set
- Significant functional dependence(s) in the data on geophysical propagation parameters
- Correlated trends between land and sea data
- Likely cause/effect relationships between data and geophysical characteristics.

For each TD component (i.e., TDW, TDX and TDY), the land and sea subsets were analyzed as a function of

- Range to secondary station
- Range to master station
- Differential range between secondary and master station
- Path bearing angle at master station

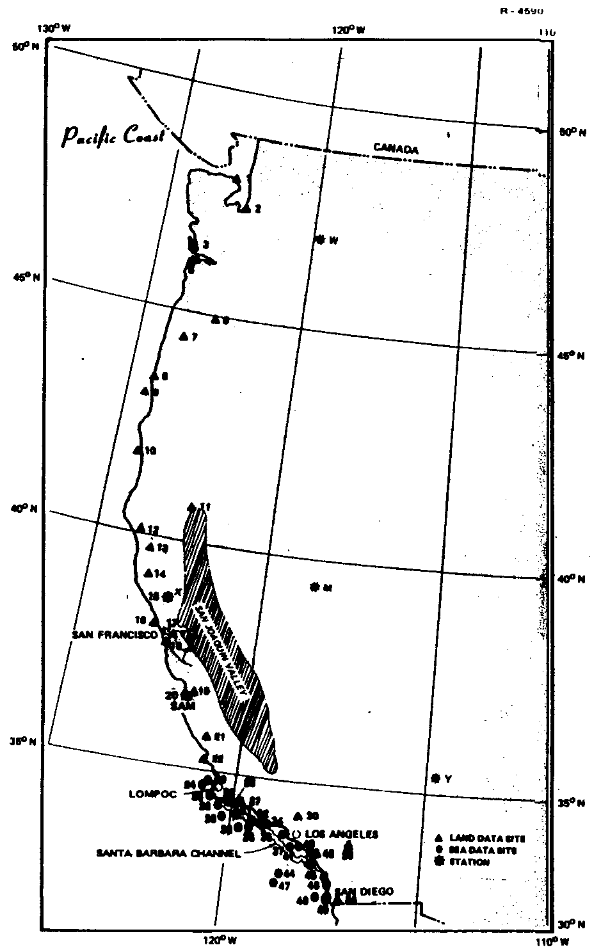

Figure 1 West Coast Loran-C Chain TD Measurement Data Site Locations

- Path bearing angle at secondary station.

Figures 2 through 4 present functional dependence plots of TDW, TDX and TDY components, respectively. Each figure shows adjusted TD measurements as a function of (a) site path bearing angle (from north) at the secondary station, and (b) site differential range (differential primary phase delay) between secondary and master station. In addition to functional dependence trends, examination of these figures reveals that there is a rather strong correlation between land and sea data subsets of each TD component. Figure 5 presents a composite plot of all three TD components for the ensemble of land and sea data as a function of differential range to identify any common range-dependent trend (or trends) embodied in all of the three TD components.

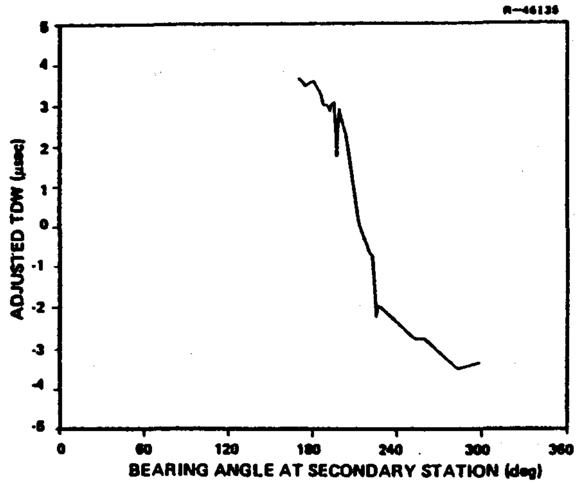

(a)

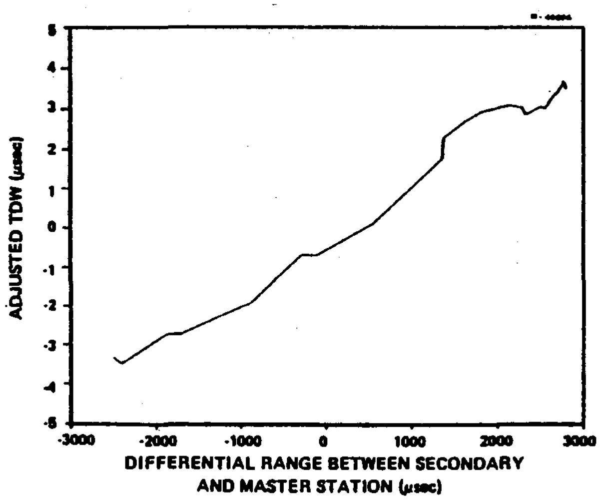

(b)

Figure 2 Adjusted TDW (Land Data) as a Function of (a) Path Bearing Angle at W Secondary Station and (b) Site Differential Range Between W Secondary and Master Station

Analysis of measurement data based on plots shown in Figs. 2 through 5 reveals the following:

- Dominant and very similar linear range-dependent trends in TDW and TDY but no identifiable trend in TDX

- Highly correlated trend between land and sea data as a function of both range and bearing angle

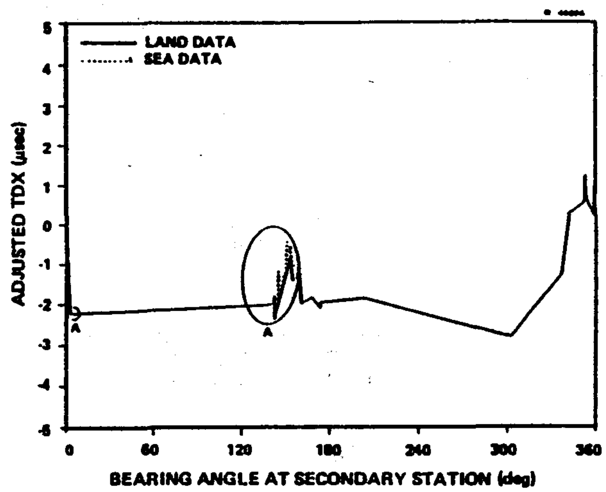

(a)

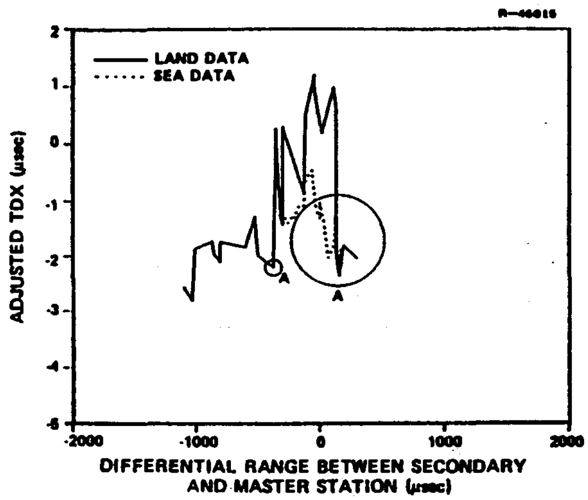

(b)

Figure 3 Adjusted TDX (Land and Sea Data) as a Function of (a) Path Bearing Angle at X Secondary Station and (b) Site Differential Range Between X Secondary and Master Station

- TDX data behavior is significantly different than that of TDW or TDY; however, no obvious outliers in either TDW, TDX or TDY data

- TDX data identified as "A" are significantly different than the remainder of TDX data.

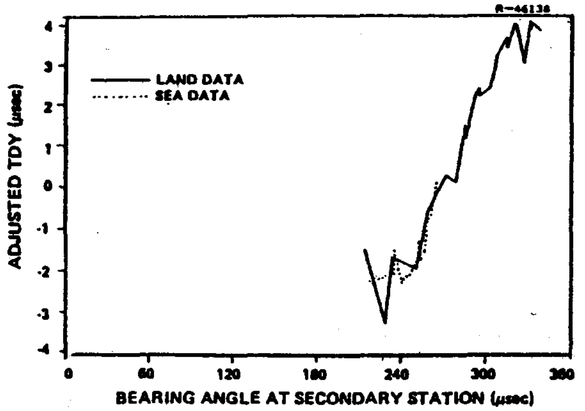

(a)

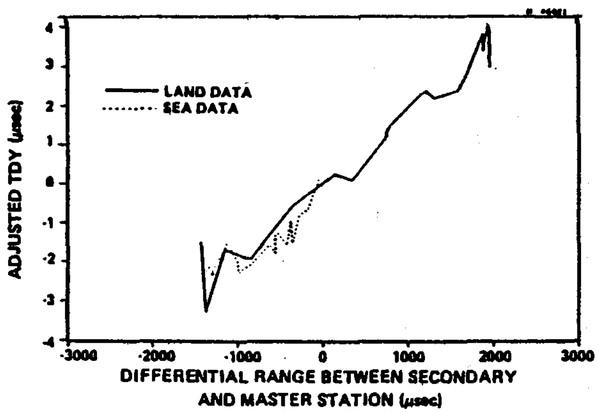

(b)

Figure 4 Adjusted TDY as a Function of (a) Path Bearing Angle at Y Secondary Station and (b) Site Differential Range Between Y Secondary and Master Station

Further examination of TDX data (although not essential for the semi-empirical model development) indicated that all X station radial paths in the TDX data between bearing angles of approximately 3 and 150 deg from north (identified as "A" in Figs. 3 and 5) exhibited behavior as a function of differential range grossly different than the remainder of TDX data. This suggested the possibility that a terrain with propagation propagation properties different from those of the remaining chain coverage area may exist in the region within these bearing angles. Indeed, the location of the San Joaquin Valley (see Fig. 1) whose conductivity is higher than that of the surrounding area by an order of magnitude (Ref. 7), is roughly defined by this region. Because of the San Joaquin Valley's orientation relative to the X station and the shoreline, all X station radial paths leading to the CCZ between Los Angeles and San Diego are expected to be affected by the presense of the valley and will exhibit signal propagation behavior drastically different than the rest of the X station signal coverage area.

In summary, the data are considered to be consistent with the expected theoretical behavior. The "apparent anomalous" behavior of some TDX data seems to have been caused by the San Joaquin valley region whose conductivity is an order of magnitude higher than the surrounding region. There is a strong correlation between the behavior of land and sea data suggesting that land data alone may be sufficient to calibrate a mixed path model. The data support the use of both range and bearing angle dependences in the TD model structure.

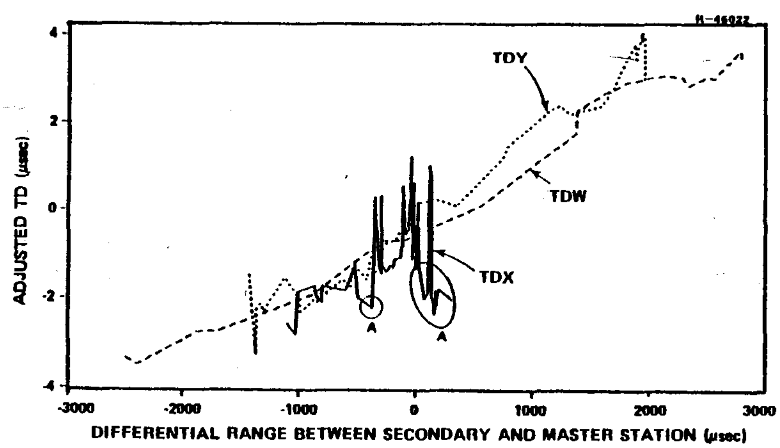

Figure 5 Adjusted TDW, TDX and TDY Components as a Function of Site Differential Range Between Secondary and Master Station

CALIBRATED TD MODEL

Two alternative model calibration approaches, shown as A and B in Fig. 6, were considered. Approach A is designed to assess the utility of using only land based data for CCZ model calibration as compared to using both land and sea based data in approach B. In approach A, the land model is calibrated while the sea model is based on theory (i.e., with *a priori* known coefficients); in approach B, the composite land and sea model is calibrated with the combined land and sea data.

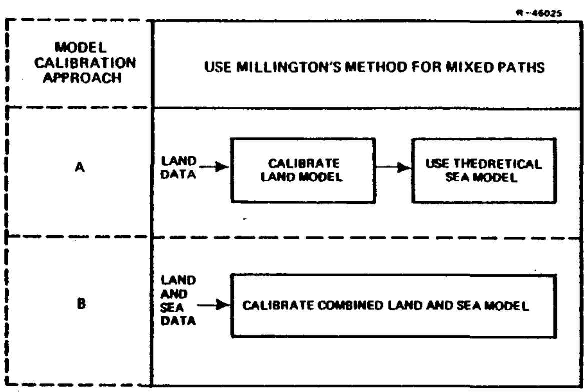

Figure 6 Alternative Model Calibration Approaches

Model Calibration Methodology

It is convenient to model the transformed form of the TD measurements, i.e., adjusted TD measurements given by Eq. 5, which is simply the difference between the measured TD and the sum of differential primary phase delay between secondary and master station (a function of well-known parameters) plus the published constant emission delay implemented by the secondary station. Thus, in the adjusted TD measurement equation, the unknown quantities are the SF_i and SF_m associated with all-land path and mixed (part land and part sea) path. The candidate semi-empirical model structures considered for the land and sea SFs are as follows.

Land SF Model

Based on the West Coast chain topography and incorporating the results of calibration data analysis, the following two candidate forms for the land SF model were considered:

- "Localized" Range/Bearing (LRB) Model

$$SF_j = A_o + [A_1 + B_1 f_x(\beta_x)]\, T_j \tag{6}$$

- "Generalized" Range/Bearing (GRB) Model

$$SF_j = A_o + A_1 T_j + \left[\sum_{\ell=1}^{L} \left(C_{j\ell} \sin \ell\beta_j + D_{j\ell} \cos \ell\beta_j\right)\right] \tag{7}$$

where L is a positive integer; A_o, A_1, B_1, $C_{j\ell}$ and $D_{j\ell}$ are uncertain model coefficients; β_j is the path bearing angle at the j^{th} (= w, x, y or m) station; T_j is the path range to the j^{th} station; and function $f_x(\beta_x)$ is zero for all chain stations except for the X station. For the X station, f_x is zero unless the X station radial (signal path) passes through the San Joaquin Valley, then it is unity.

The LRB model is purposely kept as simple (fewest uncertain model coefficients) as possible yet designed to embody distortions (warpages) to the X station SF caused by the San Joaquin valley. The GRB model, on the other hand, includes bearing angle dependences for all four chain stations instead of the X station alone, as is the case in the LRB model. Consequently, the GRB model is relatively more complex and is expected to exhibit performance superior to the LRB model. Note that a calibrated model is expected to be accurate and applicable only over the extent of ranges and bearing angles embodied in the calibration data. Hence, outside the region covered by the calibration data, the model may not be as accurate as within the data coverage region.

Sea SF Model

The structure considered for the sea SF model is

$$SF = \begin{cases} \dfrac{a_{-1}}{T} + a_o + a_1 T \ \mu\text{sec}, & \text{if } 10 \le T < 540\ \mu\text{sec} \\[2ex] \dfrac{a'_{-1}}{T} + a'_o + a'_1 T \ \mu\text{sec}, & \text{if } T > 540\ \mu\text{sec} \end{cases} \tag{8}$$

where T is the range; a_k and a'_k (k = -1, 0 and 1) are sea coefficients considered evaluates the fit of the 3- (or 2-) dimensional TD site residual (i.e., all TD components together at a site) to the data.

Calibrated Models

Of the candidate GRB land SF models considered, the TD model incorporating the following GRB functional form yielded the best performance:

$$SF_j = A_o + A_1 T_j + \sum_{\ell=1}^{2} [C_{j\ell} \sin \ell\beta_j + D_{j\ell} \cos \ell\beta_j] \tag{9}$$

where

j = w, x, y or m Transmitting Station

$C_{w1} = C_{x1} = C_{y1} = 0$

$D_{w1} = D_{x1} = D_{y1} = 0$

$C_{x2} = 0$

$D_{y2} = 0$

Table 2 describes the number of uncertain coefficients included in the "best" GRB model and the LRB model under each of the two calibration approaches considered.

Note, in approach A where only land data are used to calibrate the land model, one bias state (coefficient) per land TD component is required in the TD model (see Table 2) to account for a possible constant bias (shift) in the secondary station emission delay and the unobservable biases in the land SF models. However, in approach B where both land and sea data are used to calibrate the composite land and sea model, an additional bias state per sea TD component was included (as shown in Table 2) to result in zero-mean residuals. If sea TD bias states are not included in the model, the mean TD residual is non-zero, and furthermore the rms TD residual is significantly larger than that obtained with sea TD bias states. Thus, a total of three land TD bias states (for TDW, TDX and TDY) were included in the TD model calibrated in approach A, while three land, and two sea TD bias states (for TDX and TDY) were used in the TD model calibrated in approach B. As expected, the magnitude of the sea bias states in the model calibrated in approach B are approximately the same as the corresponding means in the sea TD residuals obtained in approach A where sea TDs were computed using a calibrated land model, and the theoretically-derived sea model. There were not sufficient data to identify the likely sources of the observed sea TD biases. The land/sea water interface "phase recovery" effect (Ref. 5) may be responsible for part of the observed sea TD biases.

Calibrated Model Performance

Over Calibration Data Base

Table 3 summarizes the rms TD residuals for the LRB and GRB TD models calibrated with: (1) land data alone (approach A) and (2) combined land and sea data (approach B). In this table, the rms value of the residuals at the 46 sea calibration TD data points (and also for over the entire set of 122 land and sea calibration TD data points) are presented.

TABLE 2

NUMBER OF COEFFICIENTS IN LRB AND GRB TD MODELS

T-3593

APPROACH	LOCALIZED RANGE/BEARING (LRB) MODEL					TOTAL NUMBER OF COEFFICIENTS	GENERALIZED RANGE/BEARING (GRB) MODEL					TOTAL NUMBER OF COEFFICIENTS
	RANGE (T)		BEARING β	BIAS			RANGE (T)		BEARING β	BIAS		
	LAND	SEA	LAND	LAND*	SEA†		LAND	SEA	LAND	LAND*	SEA†	
A CALIBRATED LAND MODEL (THEORETICAL SEA MODEL)	1	–	1	3	–	5	1	–	8	3	–	12
B CALIBRATED COMPOSITE LAND AND SEA MODEL	1	4	1	3	2	11	1	4	8	3	2	18

*TDW, TDX AND TDY
†TDX AND TDY

as known* (no uncertainty) for approach A and unknown (uncertain) for approach B.

Model Calibration Procedure

The West Coast TD grid calibration procedure is illustrated in Fig. 7. The first step in the model calibration procedure is to hypothesize candidate model structures for the land and sea SF models. In approach A, the sea model is known (theoretical) and therefore only the land model is hypothesized as opposed to approach B where both land and sea models are postulated.

Next, Millington's method (which empirically combines the SFs of the land and sea segments of a mixed path) is employed to determine the SF for mixed paths included in the sea data. Both land and mixed path SFs obtained with candidate SF models (Eqs. 6 through 8) are then substituted in the adjusted TD measurement equation (Eq. 5) which is then ready to be calibrated with the measurement data.

The next step in the calibration procedure is to provide a priori information to the coefficient estimation algorithm about the initial estimates and uncertainties of model coefficients, and TD measurement error statistics. The Kalman filter (Ref. 8) provides a convenient method to estimate the model coefficients. The a priori information on the coefficients was developed by a combination of data analysis results and expected theoretical behavior of Loran-C signals over land and sea water paths. In particular, the sea water SF model coefficients were constrained to lie within the expected range of the theoretical coefficient values. This was done to extend the utility of the calibrated CCZ model beyond the CCZ region (where no measurement data were available for model calibration).

The TD component (i.e., TDW, TDX or TDY), and hence adjusted TD component measurement errors were assumed to be random with zero mean. Since, initial attempts to calibrate candidate West Coast TD models consistently yielded TD residuals with an rms level of about 0.4 μsec, TD component measurement error in the calibration procedure was assumed to be 0.4 μsec. Note, 0.4 μsec error includes receiver measurement error of 0.1 - 0.2 μsec, data site position location reference errors, unmodeled TD warpage conditions and emission delay variations from site-to-site.

More than 20 candidate GRB model structures (Eq. 7) with varying numbers of harmonic terms as well as the single LRB model structure (Eq. 6) were considered for the land SF model. The sea SF model was always chosen to be a 3-term, range-dependent model given by Eq. 8. Each candidate land SF model in combination with the theoretical sea SF model (approach A), or semi-empirical sea SF model (approach B), was calibrated with land data (approach A) or combined land and sea data (approach B).

Performance of each calibrated candidate combined land and sea model was evaluated in terms of the statistical reasonableness of the calibrated model fit to the data. Statistical reasonableness was quantified as indicated in Fig. 7 in terms of the standard deviation of individual TD component site residuals and the chi-square test which

*The known sea coefficients are obtained by fitting Eq. 8 to the homogeneous/smooth earth theoretical predictions (Ref. 2).

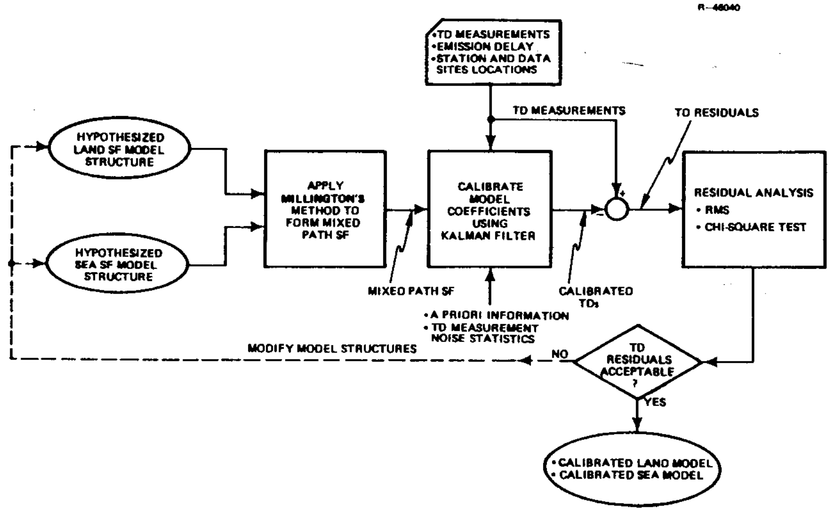

Figure 7 TD Grid Calibration Procedure

TABLE 3

PERFORMANCE COMPARISON OF LRB AND GRB MODELS

T-3566

CALIBRATION APPROACH	MODEL	NUMBER OF DATA POINTS		RMS TD RESIDUAL - μSEC	
		LAND	SEA	SEA DATA POINTS (46)	LAND AND SEA DATA POINTS (122)
Calibrated Land Model (Theoretical Sea Model)	LRB	76	-	0.703	0.636
	GRB	76	-	0.769	0.570
Calibrated Composite Land and Sea Model	LRB	76	46	0.343	0.521
	GRB	76	46	0.350	0.390

TABLE 4

TD RESIDUAL STATISTICS OF GRB MODEL OVER CALIBRATION DATA BASE (APPROACH B)

CALIBRATION DATA BASE	RMS TD RESIDUAL - μsec			
	TDW	TDX	TDY	COMBINED TD COMPONENTS
Land	0.308	0.501	0.382	0.408
Sea	*	0.388	0.306	0.350
Combined Land and Sea	0.308	0.457	0.347	0.390

*No sea calibration data available.

Comparison of sea rms TD residual statistics (Table 3) obtained with the LRB and GRB models shows similar performance for the two models, using either approach. However, calibration approach B yields a factor of two improvement in the sea rms residual over those obtained in approach A. Thus, from considerations of sea residuals alone, approach B is preferred over approach A. Further comparison of rms residuals obtained with the LRB and GRB models (Table 3) over the entire set of land and sea calibration data points indicates that the GRB model yields superior performance. Therefore the GRB model calibrated with both land and sea data was selected as the "best" performance TD model for calibrating the West Coast Loran-C chain. The residual statistics obtained with the GRB model for the indicated TD components and data sets are summarized in Table 4.

Figure 8 presents the TD residuals (solid curve) at each land and sea data site obtained with the calibrated West Coast GRB model. The data collection sites are arranged in order from north to south (see Fig. 1). For comparison, Fig. 8 also shows the calibration data (i.e., the adjusted TD measurements as dotted line). Both data and residuals have breaks (or gaps) at sites where no measurement data are available. (Note, there are no sea data for the TDW component.)

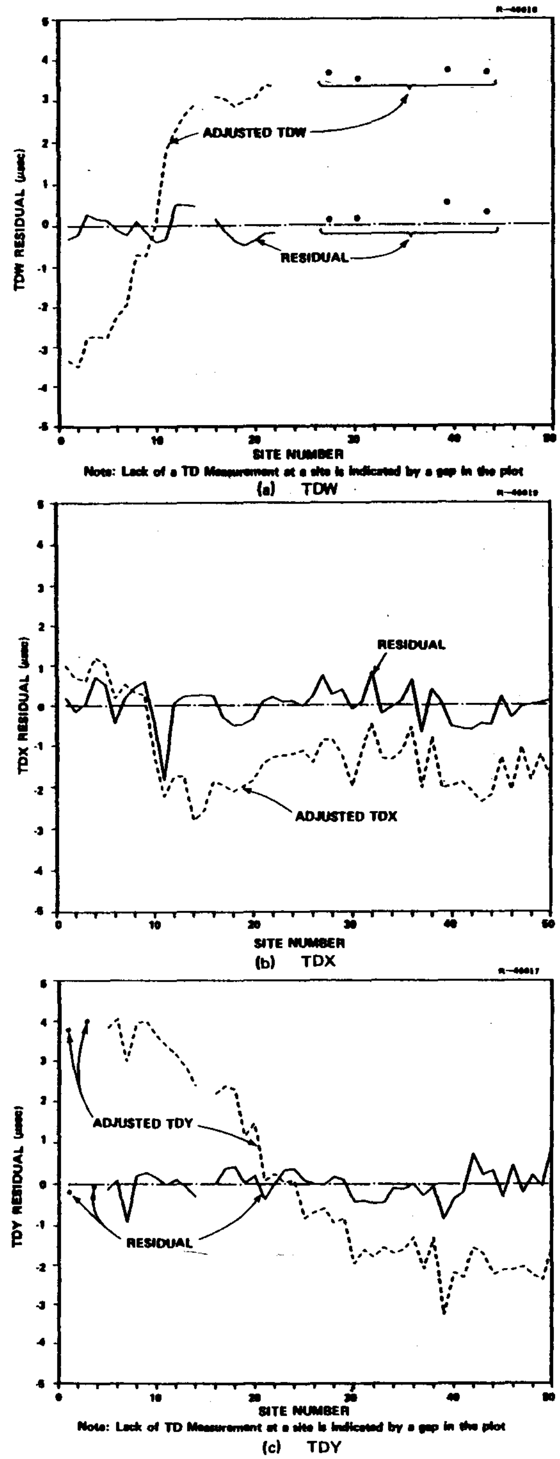

Figure 8 TD Residuals for GRB Model Calibrated With Combined Land and Sea Data (Approach B)

Over Validation Data Base

The calibrated model was also evaluated at the 25 sea sites not used for calibrating the West Coast model. The rms TD residual of the calibrated model over the ensemble of all 50 validation TD data points (i.e., 25-TDX and 25-TDY) is 0.42 μsec, a factor of four improvement over the current U.S. Coast Guard TD grid charting procedures (Ref. 2).

MODEL ACCURACY SENSITIVITY ANALYSIS

Approach

Two mutually exclusive data bases (Table 5) were formed, for the sensitivity analysis studies, out of the available TD measurement data to calibrate the West Coast TD grid model. The two data bases are referred to as the sensitivity data base and the evaluation data base. The sensitivity data base consists of both land and sea data sites (distributed from Canada to San Diego), subsets of which are used to calibrate the sensitivity analysis model. The accuracy of each calibrated model was assessed with the evaluation data base which includes only sea sites distributed in the Southern California CCZ (between Lompoc and San Diego).

TABLE 5

SENSITIVITY AND EVALUATION DATA BASES SUMMARY

DATA BASE	NUMBER OF DATA SITES			NUMBER OF TD DATA POINTS		
	LAND	SEA	TOTAL	LAND	SEA	TOTAL
Sensitivity	27	12	39	76	24	100
Evaluation	-	11	11	-	22	22
Combined	27	23	50	76	46	122

A number of subsets of the sensitivity data base were used to calibrate the sensitivity model. These subsets included:

- Uniform distributions of combined land and sea calibration data sites as shown in Fig. 9
- Clusters of land calibration sites (located either north or south of San Francisco) with uniform distribution of sea sites located in Southern California, as shown in Fig. 10.

Each of the calibration data sets (subsets of the sensitivity data base)

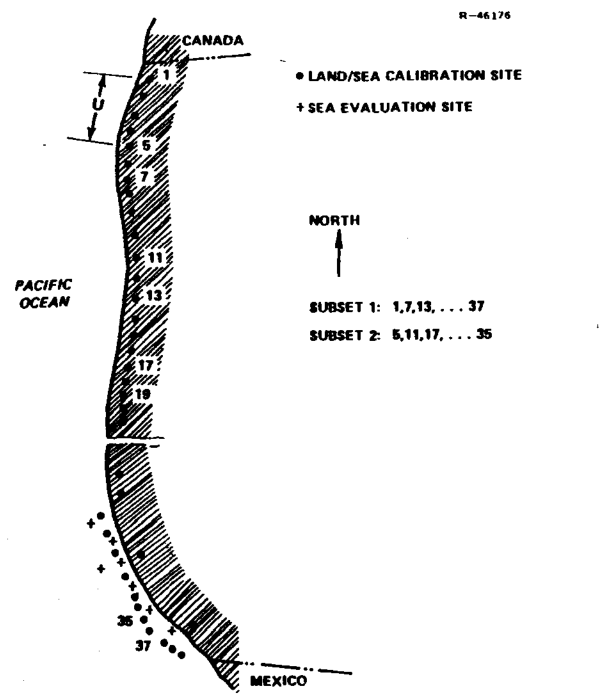

Figure 9 Illustration of Uniformly Distributed Combined Land and Sea Calibration Data Sites

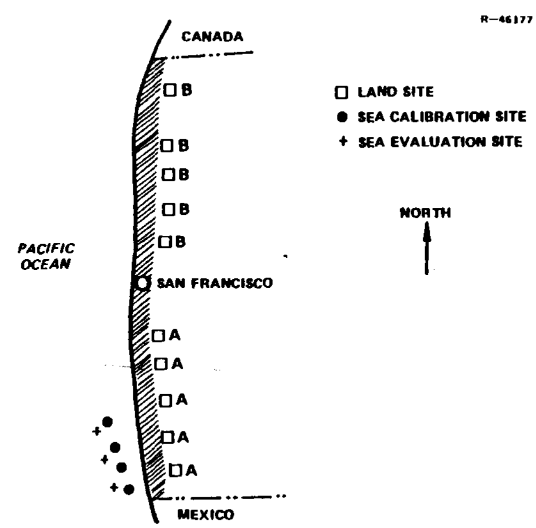

Figure 10 Illustration of Clustered Land Calibration Sites and Uniformly Spaced Sea Calibration Sites

was used (one at a time) to calibrate the sensitivity model by the calibration procedure described in the preceding section. The calibrated model was then used to compute the TDs and

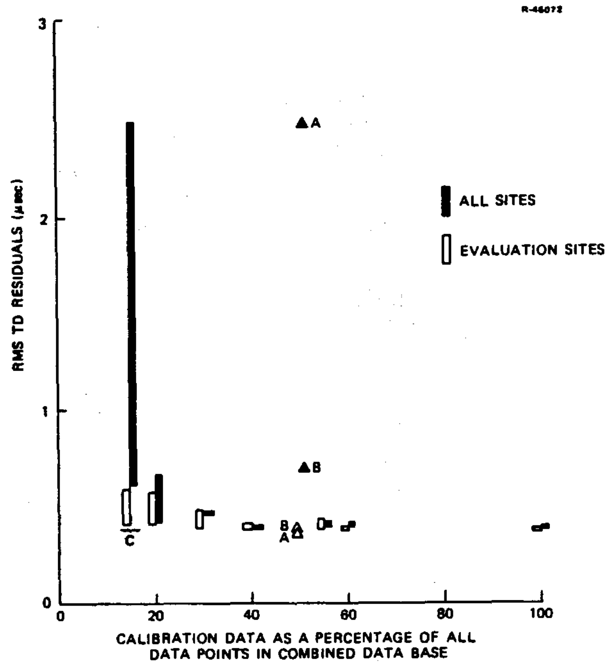

Figure 11 Model Accuracy Sensitivity to Quantity and Distribution of Calibration Data

resulting TD residuals at all sites in the combined data base. The rms of the TD residuals of each calibrated model was then computed over: (1) the "evaluation sites" (i.e., ensemble of all TD components at all sites in the evaluation data base) and (2) "all sites" (i.e., ensemble of all TD components at all sites in the combined data base).

The rms TD residuals obtained with the GRB model calibrated with subsets of the sensitivity data base are shown in Fig. 11 as a function of quantity and distribution of the calibration data, where

- The quantity of calibration data is expressed as a percentage of TD data points in the combined data base (which includes data points in both sensitivity and evaluation data bases)
- The data distribution is keyed as a bar (representing uniform data site distribution) or a triangle (denoting clusters of calibration data sites)
- The length of a bar shows the spread of the computed rms TD residuals obtained for models calibrated with several uniformly distributed subsets of the sensitivity data base, each containing approximately the same number of data points
- Adjacent solid and open areas, bars or triangles, are the corresponding rms TD residuals over all sites and evaluation sites, respectively.

The rms residuals shown for 100 percent of the data are the residuals of the model calibrated with all the available data (i.e., including evaluation data) and are shown for comparison purposes. Brief explanations of the observed calibrated model accuracy behavior for both clustered and uniformly distributed calibration data conditions are presented in the following sections.

Clustered Sets of Calibration Data

Two specific examples of clustered data sets are shown in Fig. 10. Calibration data set A (see Fig. 10) includes all land data south of San Francisco and all sea data available in the sensitivity data base (also south of San Francisco). No calibration data north of San Francisco is contained in data set A. Consequently, the model calibrated with data set A performs poorly over data sites north of San Francisco as manifested by the high rms residual computed over all sites. On the other hand, the calibrated model is expected to exhibit excellent performance in the region south of San Francisco where all of the calibration and evaluation sites are located. This performance is manifested by the low residual value computed over the evaluation sites.

Calibration data set B includes land data north of San Francisco and all sea data (south of San Francisco) -- thus, the sensitivity data base includes data distributed--(although not uniformly) over the entire West Coast. Consequently, the model calibrated with data set B is expected to have a relatively better residual performance, especially over the data sites located north of San Francisco, than the model calibrated with A. This is manifested in Fig. 11 by a smaller rms residual over all sites for case B. Note, evaluation site residuals for both cases are comparable, since both subsets A and B include calibration data over the region covered by the evaluation sites. From the comparison of calibrated model performance for the two sets, it is concluded that the calibration data set must be representative of the region to be calibrated.

Uniformly Distributed Calibration Data Sets

A number of uniformly distributed calibration data sets with varying data density were analyzed. As an example, consider the computed spread of residuals, labeled as "C" in Fig. 11. Adjoining residual bars labeled all sites and evaluation sites correspond to the use of 18 calibration data points, roughly 13 percent of the combined data. These bars depict the spread of computed rms residuals ("C") for four different uniformly distributed calibration data subsets formed from the sensitivity data base by retaining every sixth data site. For this case, two of the four subsets of the sensitivity data base considered are labeled 1 and 2 in Fig. 9. Subsets 1 and 2 are similar except subset 2 does not span the northern tip of the U.S. West Coast area (identified as "U" in Fig. 9) and covered by sites 1 through 5. Thus, the model calibrated with subset 2 extrapolates over "U" while the model calibrated with subset 1 interpolates over "U". Therefore, the all site residual performance of the model calibrated with subset 2 is inferior to the performance using subset 1, as manifested by the highest all site residual value. There is very little spread, as expected, in the evaluation site residuals because all four calibration data subsets cover the region of evaluation sites.

As expected, the spread in rms residual values (Fig. 11) associated with both all sites and with the evaluation sites decreases with increasing density of the data in a uniformly distributed calibration data set. No significant improvement in the West Coast calibrated grid rms residual performance is observed with the use of more than 40 percent of the available data for model calibration data.

Sensitivity Analysis Conclusions

Based on the West Coast model accuracy sensitivity analysis results, it is concluded that

- A uniform distribution of 50 percent of the available measurement data provides a CCZ TD grid with an rms accuracy of 0.40 μsec as compared to 0.35 μsec with 100 percent of data
- Data collection sites should be selected to provide a relatively uniform distribution along the coast with an average spacing of 100-200 km over the region of interest (as compared to 50-100 km for land sites and ~20 km for sea sites in the available measurement data)
- Additional data sites should be concentrated in regions receiving signal paths through known or suspected anomalous propagation region(s) (e.g., San Joaquin Valley)
- Combination of land and sea data yields a higher accuracy calibrated grid than possible with land data alone.

Although the issue of utilizing land vs sea data was not fully investigated due to limited quantity and spatial (coastal) coverage provided by the available sea calibration data, preliminary results indicate the following:

- Either land or sea data may be used to calibrate a CCZ grid
- Some sea data are always desired to identify land/sea interface effects
- Sea data collected over a wider coastal region will help to identify potential source(s) of the sea TD biases seen in the West Coast sea data
- Both near and far from shore sea data will provide greater observability to sea model parameters (coefficients)
- Inclusion of land data greatly reduces the required density of sea calibration data as the dominant bearing dependence effects are easily observable in the land data.

CONCLUSIONS

The utility of semi-empirical techniques to accurately calibrate Loran-C grids in the CCZ has been demonstrated by applying these techniques to the West Coast Loran-C CCZ. In this CCZ region, current U.S. Coast Guard prediction procedures have been reported to result in significant charting errors (Ref. 7). The TASC-developed algorithm exhibits the following characteristics:

- RMS TD error of 0.42 μsec over the sea TD measurement data points not used in model calibration and 0.35 μsec over the data points used in model calibration

- RMS position error of less than 400 m in the Southern California CCZ -- a factor of four improvement over the current charting procedures (Ref. 7)

- Reasonably accurate TDs beyond the CCZ (where measurement data were not available for model calibration)

- Computationally simple (can be implemented on a hand-held electronic calculator similar to the HP-67)

- Cost effective since much less calibration data are required than for other known calibration procedures

- Can be easily extended to include data from other coverage regions as it becomes available.

In addition the results of this study show:

- Land data alone can be used to calibrate the West Coast CCZ grid with an rms TD error of approximately 0.8 μsec

- Inclusion of sea calibration data produces a factor of two improvement in the calibrated grid accuracy

- A uniform distribution of 50 percent of the available data (average spacing of 100-200 km) provides an rms CCZ grid accuracy of 0.40 μsec as compared to 0.35 μsec acheived with 100% of the available data.

In summary, semi-empirical TD grid calibration techniques are both effective and efficient for developing an accurate Loran-C CCZ grid.

REFERENCES

1. Warren, R.S., Gupta, R.R., and Shubbuck, T.J., "Design and Calibration of a Grid Prediction Algorithm for the St. Marys River Loran-C Chain," Proc. of Seventh Annual Technical Symposium of the Wild Goose Association (New Orleans, LA), October 1978.

2. Johler, J.R., Keller, W.J., and Walters, L.C., "Phase of the Low Radio Frequency Ground Wave," National Bureau of Standards, Cicular 573, June 1956.

3. Millington, G., "Ground Wave Propagation over an Inhomogeneous Smooth Earth," Proceedings of the Institute of Electrical Engineers, Vol. 96, Pt. III, January 1949.

4. Hufford, G.A., "An Integral Equation Approach to the Problem of Wave Propagation over an Irregular Surface," Quarterly Journal of Applied Math., Vol. 9, No. 4, 1952.

5. Wait, J.R. and Walters, L.C., "Curves for Ground Wave Propagation Over Mixed Land and Sea Paths," IEEE Transactions on Antennas and Propagation, Vol. AP-11, January 1963.

6. Illegen, J.D., and Feldman, D.A., "Loran-C Signal Analysis Experiments, 'An Overview'," Proc. of the Seventh Annual Technical Symposium of the Wild Goose Association (New Orleans, LA), October 1978.

7. Doherty, R.H., and Johler, J.H., "Interpretation of West Coast Loran-C Spatial Errors Using Programmable Calculator Analysis Techniques," Proc. of the Seventh Annual Technical Symposium of the Wild Goose Association (New Orleans, LA), October 1978.

8. Gelb, A. (Editor), Applied Optimal Estimation, M.I.T. Press, Cambridge, MA, 1974.

LORAN-C GRID SURVEY IN HARBOR AREAS

by

LCDR Andrew J. Sedlock
Office of Research and Development
U. S. Coast Guard Headquarters
Washington, D.C. 20590

Three methods for surveying the Loran-C time difference coordinates of way-points and prominent physical features of a harbor area for precision Loran-C navigation are described. Results are presented from field measurements on the St. Marys River Mini Loran-C Chain using a method which uses existing visual aids to navigation as a position reference. The survey methods described provide for accurate and timely Loran-C grid survey over a wide range of harbor areas. The general features of each method and details of the visual aids to navigation approach are presented. Analysis of field measurements show survey capability on the order of ten nanoseconds.

* * * * * * *

Biographical Sketch of LCDR Sedlock

LCDR Sedlock is a 1967 graduate of the U. S. Coast Guard Academy and received a Master of Science degree in electrical engineering from the University of Michigan in 1972. From 1972 to 1976 he was assigned to the Coast Guard Electronics Engineering Center (EECEN), Wildwood, New Jersey, where he was involved in the development of the Loran-C Receiver Test Complex II, Loran-C receiver testing, and Loran-C transmitter modifications. He is presently assigned to the Office of Research and Development at Coast Guard Headquarters where he is responsible for the development of Loran-C grid survey techniques in harbor areas.

INTRODUCTION

The Coast Guard is currently engaged in a development program for precision Loran-C navigation in harbor areas. The key element in this program is the PILOT user equipment which provides position estimates based upon Loran-C time difference (TD) measurements, a flat-earth hyperbolic grid (FEHG) coordinate conversion algorithm, and chartlets stored on a magnetic tape cartridge.[1] The chartlets contain position and TD coordinates for waypoints, description of channel boundaries and aids to navigation, and computational constants for the FEHG algorithm. If harbor areas were accurately surveyed (in the geodetic sense) and Loran-C propagation models were highly accurate, the data necessary to produce chartlets could be directly calculated. Since neither is true, a technique has been developed to survey the TD coordinates for waypoints and to test for TD grid warp which could affect the accuracy of the navigation solution. This survey technique applies to a wide range of navigation scenarios including relatively wide open areas such as San Francisco Bay and severely restricted channels such as the St. Marys River. In addition, the survey technique is cost effective, and data reduction and analysis can be accomplished in the field as the survey progresses.

CLASSIC APPROACH

The classic approach to the survey problem is to use a high accuracy reference system to position a survey vessel at a point and simultaneously record position and TD coordinates. This is the basic approach that was used in initial attempts to survey waypoints on the St. Marys River. Several difficulties arise with this approach. An accurate geodetic description of channel boundaries and aids to navigation does not exist, and where accurate coordinates do exist, they are not always consistent with geodetic control points ashore. Often existing geodetic control points ashore are not recoverable or are in locations unsuitable for locating the reference system transponders, and additional control points must be surveyed. The cost of establishing the necessary geodetic control ashore, operating the position reference system, and performing the TD survey are substantial. As the navigation channel becomes more restrictive the inconsistency between survey coordinates and coordinates for channel boundaries and aids to navigation becomes intolerable. The costs both in time and dollars for a geodetic survey of channel boundaries and aids to navigation for an entire harbor are totally prohibitive.

A NEW APPROACH

The basic problem producing chartlets for precision Loran-C navigation is relating the Loran-C TD grid to the navigation situation of channel boundaries, shoals, aids-to-navigation, etc. This paper describes an approach which has been developed for determining TD coordinates of the physical features of a harbor by surveying. In addition analysis tools are used to obtain position coordinates which describe the spatial orientation of the physical features consistent with the TD grid. Although these position coordinates are accurate enough in a local sense that deviations from geodetic coordinates are imperceptible, no attempt is made to tie the position coordinates to a geodetic reference.

Since visual aids-to-navigation form the basic position reference, the approach has been termed the Visual Grid Survey. A TD measurement set has been developed by the Coast Guard Research & Development Center to accurately and efficiently measure, record and process TD information. Analysis tools include the techniques for determining waypoint TDs and X-Y coordinates using the FEHG algorithm developed for the PILOT user equipment. The FEHG algorithm calculates position relative to a reference waypoint based upon the difference between observed TDs and the TDs for the reference point.

General Procedure

The general procedures for a Visual Grid Survey are:

a. choose waypoints from harbor charts and estimate the waypoint coordinates (e.g. latitude, longitude)

b. compute the FEHG parameters for these positions

c. estimate the positions of surrounding features needed for PILOT chartlets relative to the waypoint, i.e. construct first cut chartlets

d. survey the TDs of ranges, shoals, channel edges, aids-to-navigation, etc. in the area of each waypoint

e. define the TDs of each waypoint

f. refine the actual position offsets of charted features with respect to each waypoint using the FEHG algorithm and channel edge TD data.

g. link the chartlets from a central or major waypoint by calculating the position of adjacent waypoints from the surveyed waypoint TDs and the FEHG algorithm.

This procedure results in chartlets that are locally exact models of reality. Charting and chart-pickoff errors are removed but local grid warp and TD survey errors remain.

Waypoints. As outlined above, the first step in the survey chartlet preparation process is the selection of waypoints. The waypoints are defined based upon navigation charts and the knowledge of traffic patterns. The intersection of two ranges, intersection of two channel centerlines, intersection of right half channel centerlines, or the intersection of two commonly used tracklines all define possible waypoints. There are two general approaches to determining waypoint TDs. The first approach is used where the waypoint is defined by the intersection of two visual ranges. The visual ranges provide very precise crosstrack information. In a small region near the waypoint the Loran-C TD grid can be approximated by the linear model below:

$$TDX-TDX_o = a_{11}\ (x-x_o) + a_{12}(y-y_o) + n_x \qquad (1)$$
$$TDY-TDY_o = a_{21}\ (x-x_o) + a_{22}(y-y_o) + n_y \qquad (2)$$
$$TDZ-TDZ_o = a_{31}\ (x-x_o) + a_{32}(y-y_o) + n_z \qquad (3)$$

where

TDX, TDY, TDZ are observed TDs

TDX_o, TDY_o, TDZ_o are waypoint TDs

x, y are position coordinates of the observation

x_o, y_o, are waypoint position coordinates of the waypoint

$a_{i,j}$ are coefficients of the gradient matrix (directional derivatives of the TD grid)

n_x, n_y, n_z are error terms due to noise and nonlinearity

Along the centerline of a visual range

$$(y-y_o) = m\ (x-x_o) \qquad (4)$$

where m = arctan (Theta)
Theta = course line

Substituting equation (4) into equations (1), (2), and (3) results in a set of equations for the trackline in TD space.

$$(TDY-TDY_o)=C_1(TDX-TDX_o)+n_1 \qquad (5)$$
$$(TDZ-TDZ_o)=C_2(TDY-TDY_o)+n_2 \qquad (6)$$
$$(TDX-TDX_o)=C_3(TDZ-TDZ_o)+n_3 \qquad (7)$$

where

$$C_1 = (a_{21}+a_{22}m)/(a_{11}+a_{12}m)$$
$$C_2 = (a_{31}+a_{32}m)/(a_{21}+a_{12}m)$$
$$C_3 = (a_{11}+a_{12}m)/(a_{31}+a_{32}m)$$

$$n_1 = n_y-n_xC_1$$
$$n_2 = n_3-n_yC_2$$
$$n_3 = n_x-n_3C_3$$

Linear regression can be used to fit a straight line to TD data collected along each of the tracklines using a visual range as a position reference. The resultant regression lines of TDs are in the form:

$$(TDY-TDY_i)=a_i(TDX-TDX_i) \qquad (8)$$
$$(TDZ-TDZ_i)=b_i(TDY-TDY_i) \qquad (9)$$
$$(TDX-TDX_i)=c_i(TDZ-TDZ_i) \qquad (10)$$

where

TDX_i; TDY_i; TDZ_i are averages

i=1,2 (i.e. trackline 1 and trackline 2)

Each of the above pairs of simultaneous equations can be solved to estimate the waypoint time differences. Two estimates for each of the waypoint TDs are obtained. The agreement of these estimates is one measure of quality of the survey.

The quality of the resultant waypoint survey is a function of several factors. The location of the ranges is an important consideration. In the ideal case, both sets of range markers are near the waypoint. The ability of the operator to determine when the survey vessel is on the range decreases as a function of distance from the range markers. The confidence bounds on the regressive lines are minimum at the mean values; therefore the ideal survey pattern is an X centered (approximately) at the waypoint. This pattern is not always realizable since there may be insufficient water beyond the waypoint or range markers may become obscured shortly after the waypoint is passed. The survey tracklines should be kept short to insure linearity of the TD grid over the survey area. Several runs are made on each trackline to randomize errors in positioning the survey vessel on the trackline.

The crossing angles of the survey lines also affect the accuracy of the solution. In general, when the tracklines cross at a shallow angle on the navigation chart, the TD tracklines will also cross at shallow angles.

Figures 1, 2, and 3 illustrate the determination of waypoint TDs based on TDs measured on two intersecting ranges on the St. Marys River. This is almost an ideal case. Both sets of range markers were near the waypoint and it was possible to bracket the waypoint in an X survey pattern. The crossing angles are near ideal (50-88 degrees). The resultant solutions display excellent agreement as shown in Table 1.

Unfortunately not all channels are marked by ranges. The approach in this case is an interactive one which utilizes the FEHG algorithm and judgement. The first step is to survey the TDs of the channel features (channel edges, aids-to-navigation, shoals, etc.) in the area around the waypoint. A fathometer can be used to detect channel edges and shoals. Buoys and fixed aids are marked by circling or stationing near them. An initial estimate is made of the waypoint TD from a simple prediction program and the FEHG algorithm can be used to plot the channel features surveyed. If the estimate of the waypoint is incorrect, the location of the waypoint with respect to the channel features will appear offset. The correction which should be applied to correct this offset in x-y coordinates translates into a TD correction for the waypoint. The procedure can be repeated until the survey officer is satisfied that the waypoint is positioned correctly. This procedure works particularly well when one of the channels is marked by a range.

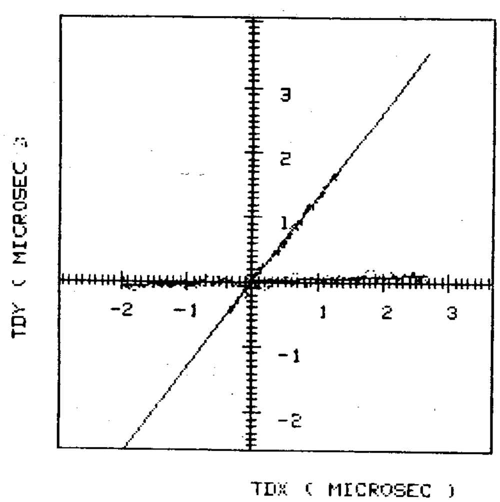

TDY VS TDX MEASURED ON TWO INTERSECTING VISUAL RANGES WITH RESULTANT REGRESSION LINES

FIGURE 1

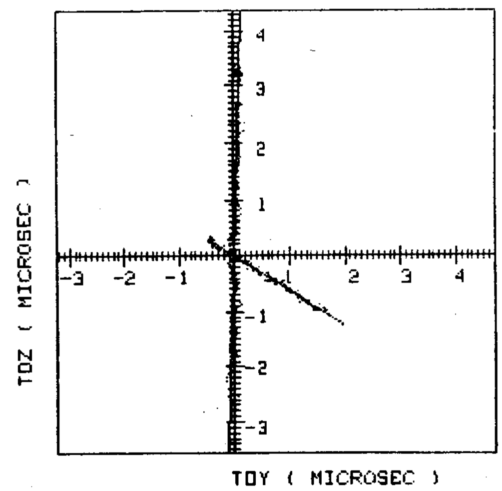

TDZ VS TDY MEASURED ON TWO INTERSECTING VISUAL RANGES WITH RESULTANT REGRESSION LINES

FIGURE 2

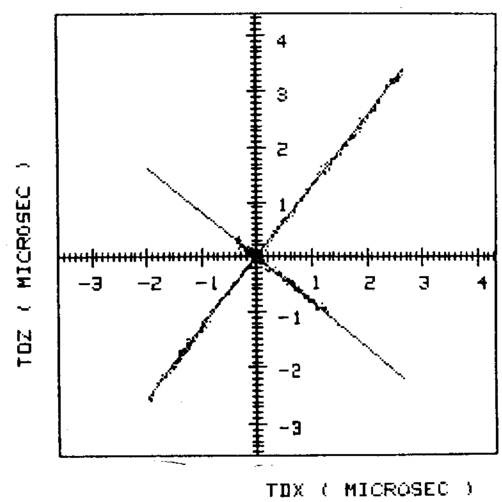

TDZ VS TDX MEASURED ON TWO INTERSECTING VISUAL RANGES WITH RESULTANT REGRESSION LINES

FIGURE 3

DATA SET	TDX	TDY	TDZ
TDX/TDY	11260.256	22332.410	-
TDY/TDZ	-	22332.410	33299.094
TDX/TDZ	11260.257	-	33299.092

COMPARISON OF WAYPOINT CALCULATIONS FOR EACH PAIR OF REGRESSION LINES SHOWN IN FIGURES 1, 2 & 3

TABLE 1

Figures 4 and 5 illustrate the above approach applied to a waypoint on the St. Marys River where neither channel was marked by a range. The waypoint in this example was defined as the intersection of the centerlines of two adjacent channels. In Figure 4 the buoys on the east side of the channel for the southern trackline plot appear to lie almost on what should be the centerline. On the northern trackline, the channel centerline and western edge coincide. Figure 5 shows the result of moving the waypoint such that the tracklines are properly centered in both of the channels.

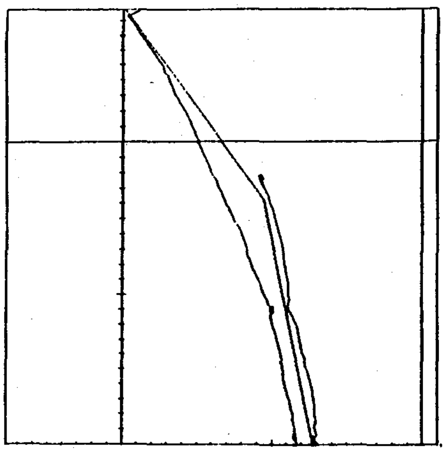

PLOT OF CHANNEL EDGE FEATURES REFERENCED TO INCORRECT WAYPOINT TDS

FIGURE 4

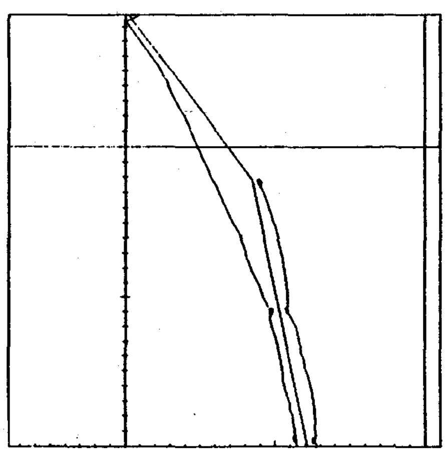

PLOT OF CHANNEL EDGE FEATURES REFERENCED TO CORRECTED WAYPOINT TDS

FIGURE 5

Channel Features. Once the TD coordinates of a waypoint have been determined, the next step in the survey is to determine the position offsets of channel features with respect to the surveyed waypoint. A plot is made using the TD data for the channel features near a waypoint transformed by the FEHG into planar coordinates. The survey officer then digitizes and stores the relative x-y locations of channel edges, shoals, aids-to-navigation, etc.

Figure 6 illustrates a typical plot of channel edge features in x-y coordinates in the area around one of the waypoints on the St. Marys River. Figure 7 is a portion of the navigation chart covering the same area.

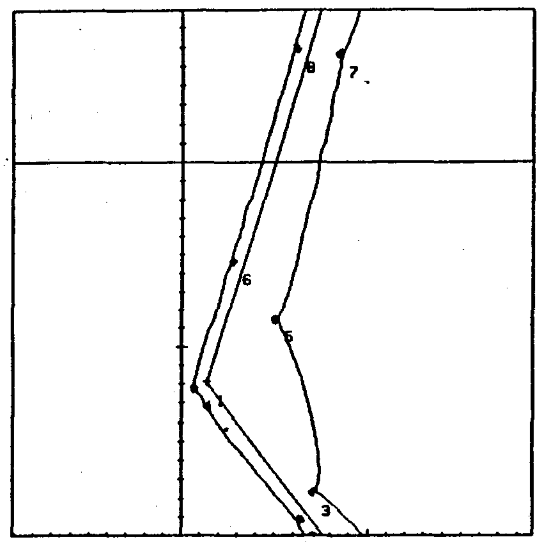

TYPICAL PLOT OF CHANNEL EDGE FEATURES DERIVED FROM TD MEASUREMENTS

FIGURE 6

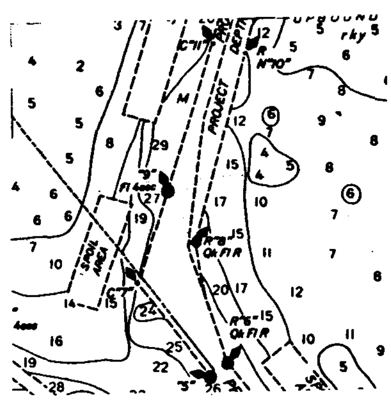

PORTION OF NAVIGATION CHART FOR AREA SHOWN IN FIGURE 6

FIGURE 7

Daisy-chaining Chartlets. The next step in the survey process is to calculate the position of each of the waypoints based upon the survey data. A central, well established waypoint is defined as the reference point for the overall survey area. The positions of the waypoints adjacent to the reference waypoint are calculated based on the reference waypoint position and TDs and the surveyed TDs of the adjacent waypoints. Successive waypoint positions are calculated in the same manner from each adjacent waypoint. The differences between projected waypoint positions and the original positions estimated from nautical charts are due to original charting errors, chart pickoff errors, cumulative Loran-C grid warp waypoint-to-waypoint, and TD survey errors.

Short-distance Grid Warps. The procedure of daisy-chaining waypoints absorbs the effects of long-distance grid warps. There may exist short-distance grid warps along tracklines. This error can be minimized by introducing trackpoints at appropriate points between the waypoints. Trackpoints are reference points located between two waypoints. Both the position and TDs for a trackpoint can be estimated from the channel feature data.

SURVEY EQUIPMENT. A Time-Difference Survey Set (TDSS) was fabricated at the U.S. Coast Guard Research and Development Center to permit collection and analsis of Loran-C TD data. The TDSS consists of an Austron-5000 monitor receiver interfaced to a Hewlett Packard 9845 calculator. The TDSS provides real time data display, processing, and storage during the data collection phase and data reduction and analysis during post mission analysis. During data collection, three sets of TDs are processed and stored. The TDSS provides a real time display of the data in the form of a TD-TD plot on the calculator's CRT display. Cumulative statistics are calculated as the data is collected and are displayed in two forms. A bar graph on the CRT display indicates the confidence bound on the regression lines calculated. The survey officer may also obtain a printout of the cumulative statistics on command. At the end of a data run the calculator outputs a hard copy of the plot and a printout of the statistical data. If a waypoint is being surveyed using two ranges, the survey officer may calculate the mean waypoint TDs on location. Depending on the results of the calculation, he may choose to resurvey one of more of the tracklines or to move on to the next task. TD data collected along channel edges may be translated to x-y coordinates and plotted on the CRT on location for an on-scene check of the data collected.

A fathometer and highly maneuverable shallow draft vessel complete the equipment necessary for a "visual survey." With the fathometer and suitable vessel, it is a relatively simple task to find the dredged channel boundaries and maneuver along them. The shallow draft and maneuverability features of the vessel simplify the task of marking aids to navigation and collecting data on ranges outside channel boundaries. A typical survey crew is comprised of a survey officer, equipment operator/technician, and vessel operator.

AUGMENTATION TECHNIQUES

The line where a harbor area begins and the Coastal Confluence Zone ends is a fuzzy one. Areas such as the approach to New York Harbor, areas of Puget Sound, Chesapeake Bay, Delaware Bay, etc., may not be suitable for using Visual Grid Survey. In general such areas are relatively wide open and there are a minimum of aids marking channels. The problem is more to survey channel separation zones rather than well marked restricted navigation channels. Inconsistencies as large as several hundred feet between positions estimated from navigation charts and a position reference are undetectable by the mariner in such situations. In these areas it may be more efficient to use a survey system which incorporates a position reference. Two such systems have been conceptualized and are discussed in the following sections.

Inertial Survey System

As its name implies, the Inertial Survey System uses a survey grade inertial survey system (ISS) incorporating special operating procedures and post mission data analysis as a position reference and a helicopter as the survey vessel. Loran-C TD data is collected as the helicopter hovers over the waypoint. The helicopter pilot receives guidance information from a navigation display driven by the INS. Waypoint positions are input to the INS which are estimated from the navigation charts for the area being surveyed. Position corrections to account for inertial draft between updates are calculated at the end of the data collection period. The Loran-C TDSS used for visual survey is too heavy and bulky for helicopter deployment and a helicopter TD measurement package will have to be developed to fill this need.

The ISS using a helicopter as the survey platform has the advantage of being able to cover a large area in a short time. The biggest disadvantage is cost to lease and the availability of inertial survey services. Geodetic control points must also be established as update points for the ISS. This adds to the total survey costs and time to implement.

Microwave Survey Reference

The microwave survey system conceptually consists of the Loran-C TD measurement system used for the visual survey system with a position reference system sensor input. As in the ISS approach, waypoint positions are estimated from navigation charts. Instead of hovering over the waypoint, the survey vessel records TD and position data while maneuvering in a cloverleaf pattern about the waypoint. The position of the waypoint and the location of the vessel are displayed on the calculator CRT. Waypoint TDs are calculated by reflecting the measured TDs to the waypoint using a linear transformation.

$$\underline{TD}p = \underline{TD} + \underline{A}\ (\underline{Z}p - \underline{Z}) \qquad (11)$$

where

$\underline{TD}p$ is the estimated waypoint TD vector

$\underline{TD}$ is the measured TD vector

$\underline{Z}p$ is the waypoint position vector

$\underline{Z}$ is the position vector at measurement point

$\underline{A}$ is a gradient matrix which is a function of the positions of the Loran-C transmitting stations and the waypoint.

Individual samples are averaged until the confidence bound of the mean is within some preset tolerance level.

Data is also collected along tracklines between waypoint and perpendicular to the tracklines using the positioning system as a reference. This data is used to determine the presence of grid warp and to bound the navigation errors.

SUMMARY

The Visual Survey Method is the ultimate approach for Loran-C TD grid survey in restricted waterways. This approach ties together the Loran-C TD grid and the world of the mariner. The result is a set of waypoint position and TD coordinates and relative position coordinates for harbor features such as channel edges and aids-to-navigation which are incorporated into chartlets for Loran-C user equipment. The position coordinates for these channel features are calculated from TD measurements based on waypoint TD and position coordinates. The waypoint positions are calculated in a daisy-chain fashion from a central waypoint based on the difference in TD between adjacent waypoints. This procedure eliminates charting and chart pick-off error and absorbs long range grid warp. The remaining error sources are due to errors in the TDs for the waypoints and channel features and local grid warp. The effects of local grid warp are minimized by establishing trackpoint(s) as necessary between waypoints.

In some areas it may not be feasible to apply the visual technique. Two approaches have been conceptualized to survey these areas. At this time it is not clear whether these approaches will be required. The accuracy of relatively simple propagation models may be more than adequate to calculate waypoint TD coordinates in these cases.

REFERENCES

1. Ligon, J.M. and Edwards, C.R., PILOT: Precision Intracoastal Loran Translocation--Exploiting Loran-C in the Harbor and River Environment.

LORAN COORDINATE CONVERSION

by
Mortimer Rogoff, Booz·Allen & Hamilton Inc.
and
Peter M. Winkler, Emory University

1. INTRODUCTION

The presentation of this paper is the first public discussion of a project that was begun approximately 5 years earlier when the authors undertook the programming of an HP-67 calculator to convert LORAN hyperbolic coordinates into latitude and longitude. This was part of a larger project involving the programming of this calculator, the SR-52, and later, the TI-59 and HP-41C for use in many applications of coastwise, sailboat racing, celestial, and loran navigation. The results of most of these efforts are now available in book form.[1] The program listings for making loran coordinate conversions from either time-difference to latitude and longitude, or vice-versa, are given in the appendix of this book. This paper (does not contain the algorithms; the reader desiring them is referred to the program listings) will describe the need for correcting the loran lattice, the results obtained after compensation, and what appears to lie ahead in the field of coordinate conversion.

2. THE NEED FOR CORRECTING THE LORAN LATTICE

The existence of distortions in the loran lattice is well-known and needs no elaboration here. Loran C at 100 Kilohertz is primarily a groundwave system; as a result, it is affected by secondary-phase factors that produce a hyperbolic lattice that is not the one predicted by an earth model that is both salt-water and sperical.

The conversion process needs to take into consideration these distorting effects; if not, the displaced latitude and longitude positions will be erroneous. This is not a casual or trivial statement, since the development of Loran C is reaching the point where many marine interests are beginning to rely on its navigational accuracy. Many factors are simultaneously pressing this art into greater acceptance: lowered prices for more capable, automatic receivers; growth in the size of the yachting fleet; reequiping of many vessels — e.g., the commerical fishing fleet — with Loran C equipment as a result of the termination of Loran A operations; the continued expansion of capability, reduction in size and price of microelectronics. In addition, many manufacturers are developing and marketing coordinate converters and plotters that are integrated with their receivers, so that the user has the opportunity to navigate in the familiar coordinates of latitude and longitude or distance and bearing. This convenience is seductive; it creates the impression that the displayed positions are authoritative (because they are understandable) and therefore correct.

The problem with this convenience is that it is based on the premise that the coordinate converter incorporates the necessary offsets as part of the conversion process. Some do not, and others do so only imperfectly; still others rely on the user to introduce offsets into the converter to bring the display to a correct position. A very few actually incorporate a comprehensive model of behavior from which corrections can be deduced.

A further complication arises from the fact that the data from which these corrections can be made are not fully available; although this is a situation that is improving. Coordinate converters rely on error-reducing means based on either predictions or surveys of errors. Government charts today represent the best standard of accuracy in Loran C. They are in the process of being improved, to reach an accuracy level of 0.25 nm throughout the Coastal Confluence Zone. These charts, which are in fact manual coordinate converters, employ offsets predicted by knowledge of variations in ground conductivity available to the chartmakers.

The hand-held, programmable calculator fills a need in this coordinate conversion situation at this time, occupying a role midway between the fully manual loran chart and the fully automatic coordinate converter. It is automatic in the sense that it operates with an internal algorithm and displays either latitude/longitude or distance/bearing from pre-selected way points. It is manual in the sense that its input (time-differences) are manually

[1] Calculator Navigation, Mortimer Rogoff, W.W. Norton & Co., New York, 1980.

inserted at its keyboard, and provision is made for manually changing the data used to accommodate the offsets needed for accurate conversion.

The particular method that we have employed to achieve accurate coordinate conversion relies on measuring the actual time delays observed at a position, as well as knowing the latitude and longitude of the position. By knowing that data, it then becomes possible to achieve a "shift" (along the baseline) of the two slaves relative to the master that accounts for the observed time-differences at that place. This compensation also serves to eliminate, at least in the locality of the observation, other distortions inherent in the nonspherical earth, or those due to local anomalies in the received signals.

By using this method, corrections are precomputed for the areas in which the loran is to be employed (it works equally well for Loran A or Loran C) with the caveat that the user change the correction data as he moves from place to place with a frequency that is appropriate to his need for precision.

The user is not restrained to the areas for which there is loran chart coverage; he is free to observe loran readings in any place in which he operates, and to prepare calibration data for these places. On the other hand, they can be made by obtaining the data from loran charts. In the latter case, corrections can be made only when there is chart coverage, and with accuracies no better than is inherent on the charted lattice.

The authors are continuing to expand the methods of using calculators for this purpose. The TI-59 and the new Hewlett-Packard Model 41C calculator have now been programmed to contain area coverage of the corrected lattice; this is an improvement over the "point-calibration" inherent in the previously published volume.

3. THE RESULTS OBTAINED AFTER CALIBRATION

The method of coordinate conversion has been applied successfully in a number of different situations, some of which are illustrated in this paper.

The first, shown in the figure entitled "Area Calibration", involves calibration data taken from a scale of 1:80,000 chart. Four points, marked A, B, C, D were employed: latitude, longitude, and the time differences at these points for the X and Y slaves were read from the chart. Each of these data points was input to the calculator program that computes actual time delays along the baseline, and these time delays are then used as the basis for calculating position when running the loran locator program. The HP41-C and the TI-59 calculators have been programmed to accept these four data points as input to a process of area calibration. In this mode, any unknown place within the area marked by A, B, C, D is located once the two X and Y time differences are keyed into the calculator. The calculator routine employs a linear interpolation process for producing a pair of emission delays that it obtains by interpolation from the values previously computed at the corners A, B, C, D. These two delays are then used in the conversion process.

The illustration shows the errors produced at four points within the area, measured by comparing the computed latitude and longitude to those obtained by chart measurement at each of the selected intersections; these range from 74 down to 36 yards.

This technique has been extended to larger sections of charts by producing sets of polynomials that describe the contours of emission delays that are appropriate for use within the area of the chart.

These polynomials are also useful in defining the behavior of the lattice when a small area is surveyed with greater precision. The figure entitled "Polynomial Calibration" is based on a calibrating function (emission delays) for each of the two slaves stored in the calculator's memory. The higher-order terms, up to the fourth order, used in these polynomials permit more accurate generation of the emission delays than is available from linear interpolation from just four corners of the covered area. The results in the illustration show reproducible error performance of 30 yards (average). These data were taken from actual observations in the Staten Island anchorage area of New York Harbor, using the now-discontinued 9930 chain. It should be noted that the 30-yard error performance was obtained after removing offsets of 0.2 microseconds in the Y and Z slaves that were observed at a reference poistion in the anchorage. In effect, this converted the later measurements into a form of differential loran; such usage may become necessary if high-precision results are to be obtained. Instrument, system, or propagation anomalies may exist from time to time whose error-producing results may exceed permissible values. In such cases, it will be desirable to measure these lattice shifts, and to make their values known to users in the area. These changes can then be used as offsets applied to all observed values.

Lattice shifts can be observed by an individual user at a known location, e.g., at a pier, or can be broadcast to all users in the area over a communications channel from a monitoring location. This loran calibration broadcast, or "LORCAST", sent on a radiobeacon, or any other harbor-control channel, would restore accuracy to the lattice in the event that there are unexpected shifts.

Finally, the figure labeled, "Loran Fixes, Ambrose Channel" illustrates the result of using a single calibration point in the Ambrose Channel in New York Harbor. Each cross is a measured position fix calculated from data taken while stationary at a channel buoy. Results of better than 50 yards of position accuracy were obtained over a length of approximately five miles of the channel. Where a prior survey shows that a single calibration is adequate for any particular operational area, this is clearly the simplest method of coordinate conversion that can be used.

3. THE FUTURE OF CALCULATOR COORDINATE CONVERSION

It is fairly easy to predict a bright future for hand-held calculators used as loran coordinate converters. What was impossible on an HP-65 was barely achievable on a HP-67. The newer HP-41C, with over 2K bytes of memory can make accurate conversions over an extended area of hundreds of square miles. The future HP-XX will surely outdo this performance, as will those available from Texas Instruments, and other makers.

What is actually possible is real-time input from a loran receiver combined with other variables of vessel movement, permitting rapid calculation of fixes, currents, and courses to steer to reach desired way-points or destinations. This is just the result of following the trend of more and more logic and memory density.

The existence of more memory implies storage of more and more secondary-phase factor data which gives the conversion process its accuracy. Probably, in the final analysis, it will not be the limitations of calculator memory that determine performance, but the availability of the secondary-phase factor data to fill that memory that will be the pacing element.

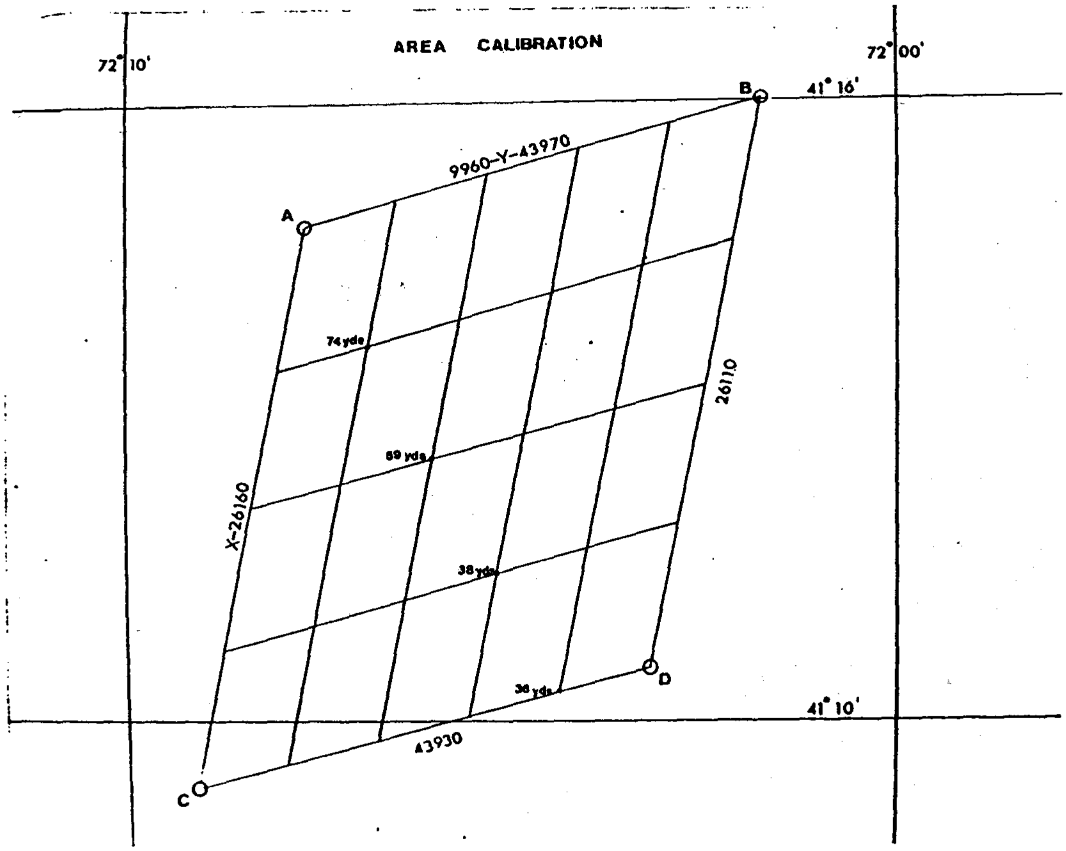
AREA CALIBRATION
72° 10'
72° 00'
41° 16'
41° 10'
A
B
C
D
9960-Y-43970
X-26160
26110
43930
74 yds
59 yds
38 yds
36 yds

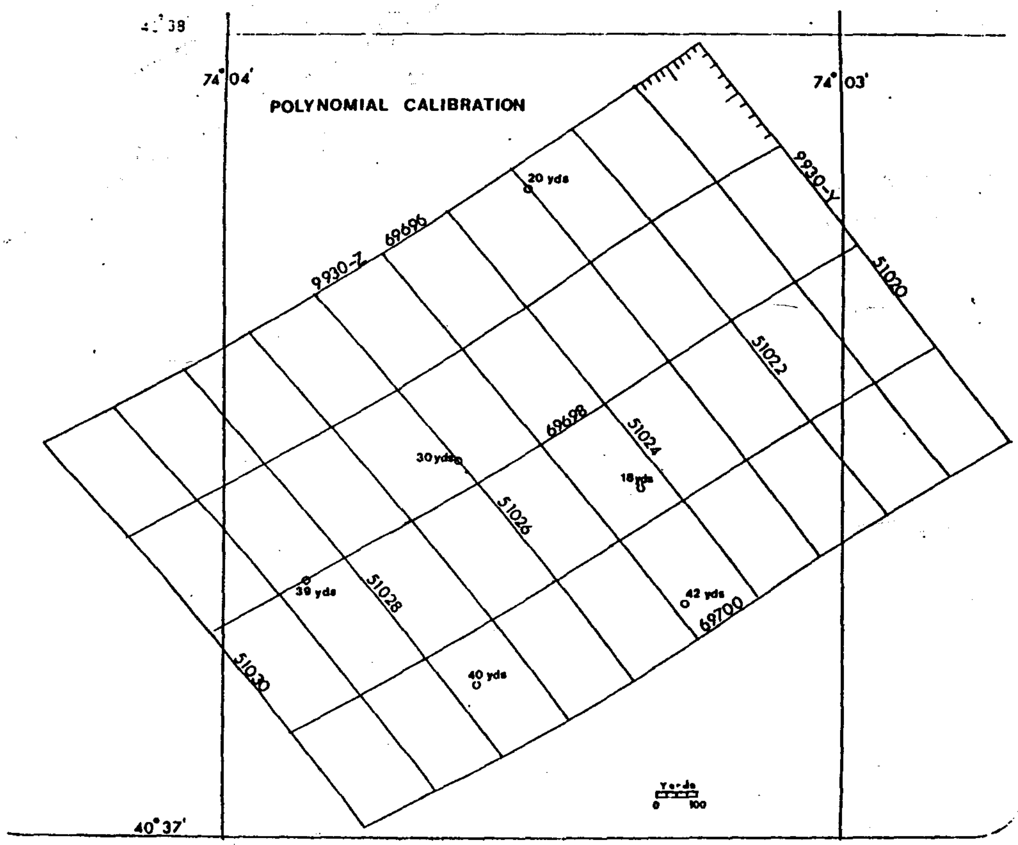
POLYNOMIAL CALIBRATION
74° 04'
74° 03'
40° 37'
9930-Z 69696
9930-Y
51020
51022
51024
51026
51028
51030
69698
69700
20 yds
30 yds
18 yds
39 yds
42 yds
40 yds
Yards
0 100

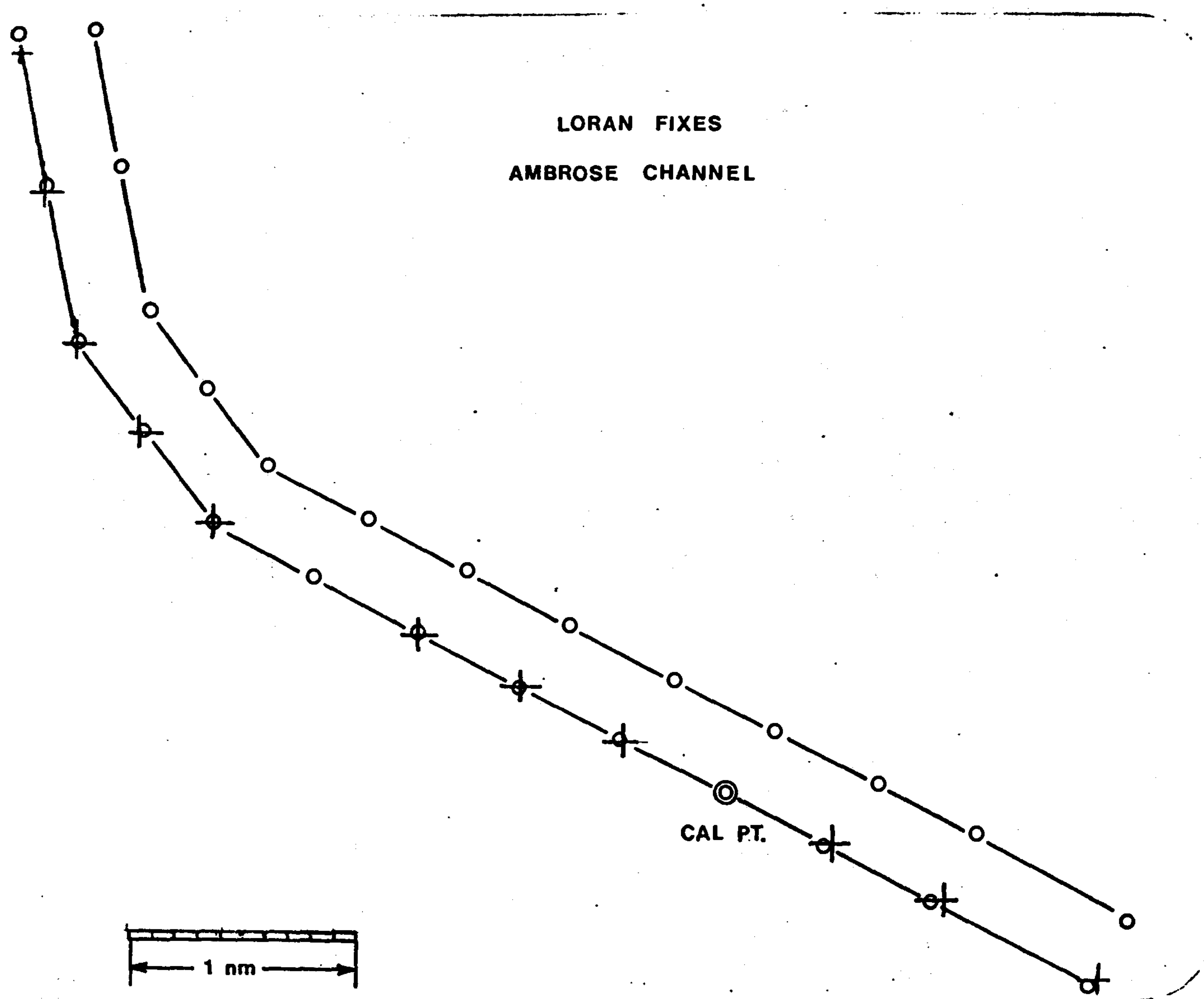
LORAN FIXES
AMBROSE CHANNEL
CAL PT.
1 nm

A COMPUTER PROGRAM TO CONVERT DECCA AND LORAN-A FIXES TO LORAN-C

Brian F. Terry
NORDCO Limited
P.O. Box 8833
St. John's, Newfoundland A1B 3T2

ABSTRACT

This paper describes a computer program which will convert any two-bearing hyperbolic fix composed of Decca, Loran-A or Loran-C bearings (in anticipation of reconfigured Loran-C chains), or any hybrid of these (e.g., a Decca/Loran-A cross-fix) to an equivalent pair of Loran-C bearings. The program uses a point-by-point method, with calculation of geographic position as an intermediate step. Loran-C Additional Secondary Factor is computed using a polynominal-type algorithm based on Bigelow's "modified Millington method". The paper also discusses the results of field verification tests performed on the conversion program.

INTRODUCTION

As new radio navigation systems are developed to replace existing ones, users who have recorded positional information in terms of the older systems will be faced with the task of converting this information to co-ordinates in the new system. This situation presently exists in the U.S. where Loran-C has replaced Loran-A as the principal public radio navaid, and it is likely to occur in Canada with Loran-C being used to replace Decca and Loran-A. Among those most affected by these developments are fishermen who have recorded over the years Decca/Loran-A fixes denoting good tows, hangups, wrecks, etc. and who will need the equivalent Loran-C fixes in order to return to the positions after Decca/Loran-A have been removed from service. In areas where there will be an overlap between the termination of Decca/Loran-A and the implementation of Loran-C, the conversion could be accomplished by using receivers for both old and new systems and recording the different bearings simultaneously. As this would entail maintaining at least two receivers and visiting the points for which conversion is needed, it could be expensive or impractical. Another possible way to perform the conversion would be via charts, though this would be time-consuming and inaccurate. The computer program described herein represents the basis of a possible third method of performing the needed conversions, namely to use computers (either portable or accessed by telephone) and have the program operated by navaid users themselves or by trained persons.

The current version of the program is designed for use in Atlantic Canada, and recognizes all stations on the following navaid chains:

- Decca 7 (Nova Scotia), 6 (Cabot Strait), 9 (Anticosti), 2 (Newfoundland)
- Loran-A 1H1, 1H2, 1H3, 1H7, 3H4, 3H5, 1L2, 1L3
- Loran-C 9930, 9960, 7930, 7970, 5930 (in anticipation of a new chain)

It can be modified for use in other areas by incorporating the appropriate station data. In fact, it would not be difficult to include other navaid systems.

DESCRIPTION OF THE CONVERSION PROGRAM

The program was developed on a PDP 11/34 minicomputer using ANSI standard FORTRAN IV. All arithmetic is performed in double precision.

The algorithm chosen to perform the conversion is a point-by-point method via geographic position, i.e., each pair of Decca/Loran-A/Loran-C cross-bearings determines a latitude/longitude (lat/long, position, fix), for which the new Loran-C bearings (TD's) are computed. In choosing this algorithm, it was possible to include two additional features in the program, namely: (i) to compute the lat/long determined by any given pair of cross-bearings, (ii) to compute Loran-C bearings at a given lat/long. Descriptions of these features are implicit in the description of the main feature of the program.

Preliminary tests of the algorithm showed that to be reasonably accurate it must include computation of the so-called Additional Secondary Factor (ASF, also known as propagation delay, phase lag) in Loran-C. The inclusion of this computation increased both the storage requirements and the execution time of the program. The algorithm chosen to compute ASF is based on Bigelow's (1) "modified Millington method" for computing ASF over a signal path consisting of segments of varying conductivity. A digitized coastline is used in determining these signal path segments, and the computation of ASF over each (homogeneous) path segment is accomplished using formulas developed by P. Brunavs (2).

To increase operational efficiency the current version of the program was divided into two separate computer jobs: an interactive job to accept and check input data in preparation for conversion, and a batch job to perform the conversions. This enables program operators to enter a list of data for conversion, submit the batch job to process this data, and while the batch job is in progress enter the next list. For the purpose of this paper, however, the process will be treated as continuous.

Input

In designing the program so as to be easily operated by persons with little or no knowledge of computer methods, care was taken to make the input section "foolproof", i.e., capable of detecting any erroneous input data, and also to have efficient and easily recognizable codes for the various input items.

The items of input required for each conversion are: (i) a pair of cross-bearings which may be any combination of Decca, Loran-A and Loran-C; (ii) an approximate lat/long determined by the cross-bearings; (iii) the desired Loran-C output. (The approximate lat/long is needed as a starting point for the fix computation and also for the computation of Decca sector numbers.) This information is entered as one line of data, which is processed as a character string and decoded into the required items based on set format rules. A typical input line is of the form:

```
                                desired
bearing1#bearing2#lat/long#Loran-C
```

(The symbol # represents any delimiter, usually a comma or blank space.) The items in this input line must be in the following formats:

```
bearings:
 Decca DCLRR.RR  e.g., D7C01.50
  where D denotes a Decca bearing
        C is the chain number (e.g.,
          7,6,9,2)
        L is the zone letter (i.e., A,
          B,C...J)
        RR.RR is the lane value
 Loran-A LLLRRRR e.g., 1H21100
  where LLL is the rate (i.e., 1H1,
          1H2, etc.)
        RRRR is the bearing in micro-
          seconds (μsec.)
 Loran-C CCCCLRRRRR.RR e.g.9930X35794.58
  where CCCC is the chain number
          (e.g., 9930, 9960, etc.)
        L is the slave letter
        RRRRR.RR is the bearing in
          μsec.
lat/long DT,MT#DDN,MN e.g. 50,05,054,45
  where DT is between 00 and 90 degrees
          north lat.
        MT is between 00 and 60 minutes
          north lat.
        DDN is between 000 and 180
          degrees west long.
        MN is between 00 and 60 minutes
          west long.
desired CCCCLM (e.g., 9960WX)
Loran-C
  where CCCC is the chain number
        L and M are station letters
          valid on CCCC
```

The program receives an input line as a character string, and the line is decoded into the items described in the format rules. If an error occurs in decoding (usually because of an illegal character) the line is rejected and the operator notified of the error. If the line is successfully decoded, each item is checked for validity: chains and slaves must be recognizable (the Decca lane value is used to determine whether the slave is Red, Green or Purple), bearings must be within bounds, degrees and minutes of lat/long must be within bounds. The detection of an invalid item results in rejection of the input and an error message to the operator. If all items are valid conversion begins.

Conversion to lat/long

For each input bearing, the master and slave station data (coordinates, emission delay, baseline length, etc.) are retrieved using subroutine DCINF, LAINF or LCINF, which contain respectively all Decca, Loran-A and Loran-C data. Since Decca zone letters repeat in groups of 10 (A, B ...J) called sectors, each input Decca bearing requires computation of the sector number. This is determined by first computing the total lane value at the approximate lat/long and using the given bearing and the possible sector numbers 1, 2 and 3 to compute three total lane values, then choosing that sector number which gives the value closest to the total lane value at the approximate lat/long.

Next each input bearing is checked against baseline extension values. Because a bearing too near a baseline extension could result in an erroneous fix (e.g., on the wrong side of the extension), any bearing within 1 lane in Decca or 5 μsec. in Loran-A and Loran-C results in termination of the conversion. Otherwise processing continues with preparation of the variables required by the fix routine FIX.

The algorithm which forms the basis of FIX is fully described in S. Grant (3). It uses the method of least squares to compute corrections to the estimated position, applies these corrections to obtain a new position closer to the true position, and iterates this procedure until the correction terms are negligible. Also, it uses the inverses of the variances expected in the observations to obtain the "co-variance matrix" of lat/long, which yields the semi-major axis of the fix error ellipse. The crucial step which permits the handling of hybrid fixes (e.g., Decca 7 Red with Loran-A 1H7) is that rather than using the input bearings themselves as the observations the routine uses the slave-master range differences determined by the bearings. A spherical distance routine SPHRD based on the Andoyer-Lambert formula is used, together with the approximate lat/longs and the lat/longs of masters and slaves, to obtain the elements of the least squares matrices. The input parameters for FIX are:

- OBS - a pair of slave-master range differences
- WT - the inverses of the standard deviations expected in the range differences
- SLAT, SLON - vectors of slave and master lats and longs
- ALAT, ALON - approximate lat/long

For i = 1, 2, bearing (i) determines parameters as follows:

SLAT (2i-1) = lat of master* (1)
SLON (2i-1) = long of master (2)
SLAT (2i) = lat of slave (3)
SLON (2i) = long of slave (4)

Decca OBS(i)=(2xTL-BL)xLW (5)

where TL is the total lane value
BL is the baseline length in lanes
LW is the lane width on the baseline in metres

$$WT(i) = \frac{1}{(0.1xLW)^2} \quad (6)$$

Loran-A OBS(i)=(B(i)-BL-CD)xAVEL (7)

where B(i) is the bearing in μsec.
BL is the baseline length in μsec.
CD is the emission delay in μsec.
AVEL is the propogation veloc ity for the rate in m/μsec.

$$WT(i) = \frac{1}{AVEL^2} \quad (8)$$

Loran-C OBS(i)=(B(i)-BL-CD)xVEL (9)

where B(i) is the bearing
BL is the baseline length in μsec.
CD is the emission delay in μsec.
VEL is vacuum velocity in m/μsec (229.7925 is used)

$$WT(i) = \frac{1}{(0.15 \times VEL)^2}\ ^{**} \quad (10)$$

These parameters are passed to FIX, which computes and returns the following:

- ALAT, ALON - lat/long determined by the cross-bearings
- ATPA - the "covariance matrix" of lat/long
- SMJAX - the semi-major axis of the fix error ellipse in metres
- IER - an error flag

If the error flag is set, it indicates that one of three errors has occurred, namely: (i) no solution is possible e.g., if the lines of position are parallel; (ii) the computation diverged, possibly due to a poor approximate position; (iii) no solution was obtained after fifteen iterations, again possibly due to a poor approximate position; and the conversion is terminated and a message output. If either or both of the input bearings is Loran-C, the master and slave ASF at the computed lat/long are determined as described below, the appropriate range difference is decreased by the difference of slave and master ASF in metres, then FIX is again invoked and the revised range differences used to determine a new position.

Computation of Loran-C TD's

The computed lat/long, the co-variance matrix of lat/long and the desired Loran-C pair are passed to subroutine LORNC which computes the TD's by the formula

$$TD=\frac{DISTS-DISTM}{VEL}+CD+BL+PLS-PLM \quad (11)$$

where DISTS is the distance to the slave in metres
DISTM is the distance to the master in metres
VEL is the vacuum velocity in m/μsec
CD is the emission delay in μsec

*Since Decca lane values increase from master to salve, while Loran-A and Loran-C bearings decrease from master to slave, the positions of Decca master and slave are reversed in equations (1) - (4).

**Equations 6, 8 and 10 reflect expected deviations of 0.1 lane, 2 μsec. and 0.3 μsec. in Decca, Loran-A and Loran-C bearings respectively.

BL is the baseline length in μsec
PLS is the slave ASF in μsec (see below)
PLM is the master ASF in μsec (see below)

The routine also uses the "covariance matrix" of lat/long to determine an error estimate for each TD. The TD's and error estimates are returned to the main program segment.

Computation of Loran-C ASF. This computation is achieved using several routines. PHASE determines the signal path segments from the transmitter to the given position by checking whether the great circle segment between transmitter and position intersects the great circle segment joining consecutive points of the digitized coastline (resident in a common block). When the coastline has been exhausted, the range from transmitter to each segment end- point is computed and these ranges are sorted in ascending order. Then each segment is assigned a conductivity (4. mho/m for water, 0.002 mho/m for land produce the best results) by assuming that the first segment is land and then alternating land-water. These ranges and conductivities are passed to subroutine PHLAG which uses Bigelow's (1) "modified Millington method" as follows: Each range, the previous range (or zero), and the conductivity of the segment between them together determine a value PLG obtained from subroutine LNPLG described below. These values are summed to obtain ASF1. Then the roles of transmitter and receiver are reversed by replacing each range with its complement with respect to the total range, and the above process is repeated to obtain ASF2. The total ASF is the mean of ASF1 and ASF2.

The subroutine LNPLG receives two ranges RNG1 and RNG2 and a conductivity. Following Brunavs (2), it retrieves the coefficients (dependent on conductivity) for Brunavs' eight-term polynomial (a function of range) which gives the ASF in metres for each range at the given conductivity. The value returned to PHLAG is the difference of these ASF values, i.e., it is (ASF for RNG2) minus (ASF for RNG1).

Output

The output from each conversion includes the semi-major axis of the fix error ellipse which indicates the quality of the fix, a warning if the fix is within 20 km of the coastline which may cause anomalies in the Loran-C ASF computation, and the desired Loran-C TD's as well as error estimates for them.

TESTS OF THE CONVERSION PROGRAM

The primary test of the program was a comparison of the conversion to Loran-C of observed Decca/Loran-A/Loran-C bearings against simultaneously observed Loran-C. The data for this test was collected at sea during three cruises:

C.C.G.S. "Narwhal" November 1978 in the areas off southern Newfoundland, Cabot Strait, Gulf of St. Lawrence, off eastern Nova Scotia, Georges Bank and Bay of Fundy.

C.C.G.S. "Hudson" February 1979 in the area off northern Newfoundland

C.C.G.S. "Thomas Carleton" April 1979 in the Bay of Fundy.

The data includes simultaneous recordings of the following navaids:

"Narwhal"	Decca chains 7, 6, 9, 2 (each in its coverage area) recorded manually
	Loran-A 1H1, 1H2, 1H3, 1L3 (combinations of pairs of these) recorded manually
	Loran-C 9930XY, 9960WX recorded automatically
"Hudson"	Loran-A 1L2, 1L3 recorded manually
	Loran-C 7930WZ recorded automatically
"Thomas Carleton"	Decca chain 7 recorded manually
	Loran-C 9960WX recorded manually

The receivers used to record data were:

Decca Navigator MK12 (a different set on each cruise)
Mieco Model 209 Loran-A (different sets on "Narwhal" and "Hudson")
Internav Model 204 Loran-C (on "Thomas Carleton")
Austron Navigator 5000 (the same set on "Narwhal" and "Hudson")

Five data sets were formed from the collection and in each case the Decca/Loran-A/Loran-C 9930 bearings were converted using the program to Loran-C 9960W and X or Loran-C 7930 W and Z, resulting in deviations from the observed Loran-C. Table 1 summarizes the results of the test.

Table 1

Total Number	Type of Observations Converted	Loran-C Computed	Mean Deviation (μsec)
406	"Narwhal" Decca	9960 W 9960 X	0.45 0.45
85	"Narwhal" Loran-A	9960 W 9960 X	0.44 0.84
204	"Narwhal" 9930XY	9960 W 9960 X	0.28 0.36
176	"Hudson" Loran-A	7930 W 7930 Z	0.34 1.32
152	"Thomas Carleton" Decca	9960 W 9960 X	0.77 0.63

In each case the deviations usually showed a consistent positive or negative bias in the conversion, but occasionally scatter was evident as the deviations moved from a positive mean value to a negative mean value over a short period of time. Though no reason for this scatter has been found, the following factors should be considered:
(i) Decca and Loran-A bearings were recorded manually, and thus subject to human error. (The importance of this factor is reinforced by the fact that the smallest deviations were produced in the conversion of 9930XY to 9960WX, which were automatically recorded.)
(ii) Variable landpath in Decca signals, for which no compensation has been made, would lead to errors in the fix calculation and hence also in the computed Loran-C. (The Decca pattern corrections published by the Government of Canada were not applied throughout the test; however their application to selected points did improve the conversion. Though it has not been verified that this is true in general, a decision was made to use the corrections in the operation of the program.)
(iii) Each computed Loran-C TD requires two ASF calculations which are approximations using a somewhat crudely digitized coastline. The digitization is particularly crude in the Bay of Fundy area, and may contribute to the larger deviations produced by conversion of "Thomas Carleton" Decca.

Three in-house tests were also performed on the program:
(i) To check that the poor pattern geometry did not result in an erroneous fix a test was devised whereby positions were chosen in areas of differing geometry (near baselines, near baseline extensions, near the transmitters) and appropriate bearings were computed. These bearings, together with an approximate position obtained by offsetting the original position by 15 km, were input to the conversion program and the computed position retrieved. The Anticosti Decca chain was chosen as representative of all types of geometry and in each of 50 cases the computed position was within 0.01 minutes of the original position.
(ii) To check that likely hybrid pairs of bearings (i.e., pairs in which the chains differ - e.g., Decca 6 Green with Decca 7 Purple, or pairs in which the systems differ - e.g., Decca 7 Red with Loran-A 1H7) yield a fix, a test was devised whereby, for each of ten hybrid pairs, positions were chosen in the appropriate areas and bearings computed. These bearings, together with an approximate position obtained by offsetting the original position by 15 km, were input to the conversion program and the computed position retrieved. In each of 100 cases the computed position was within 0.01 minutes of the original position.
(iii) To check for gross errors in ASF calculations the ASF was calculated at 0.5 degree intervals over a grid 20 degrees north and south, and east and west of each station on the chains 9930, 9960 and 7930. No gross errors were detected. As an insurance against the occurrence of such an error during operation of the program checks were included which would cause termination of the conversion if an unreasonable ASF value were detected.

CONCLUSION

The computer program described above has been deemed sufficiently accurate to be made generally available. It is currently operational on two computer systems - a PDP 11/34 minicomputer and a CDC Cyber 170-6 - and could be easily implemented on other systems capable of handling FORTRAN IV and having sufficient memory (the CDC version requires approximately 140,000 computer words, while a rearranged PDP version requires approximately 50,000 words). Program execution time ranges from 20 to 40 seconds depending on the computer used and the type of conversion performed.

Meanwhile, possible ways to improve the accuracy of the program may be: (i) to obtain a more accurately digitized coastline for use in Loran-C ASF calculations; (ii) to obtain an accurate conductivity profile for the appropriate areas and incorporate it in the program (Brunavs' polynomials can accomodate conductivities from 0.00001 to 5.5 mho/ m); (iii) use the Loran-C calibration currently being carried out by the Canadian Hydrographic Service to obtain, if possible, pattern corrections for Loran-C similar to those available for Decca.

ACKNOWLEDGEMENTS

The subject of this paper is a result of work commissioned by the Canadian government Department of Fisheries and Oceans. R.M. (Mike) Eaton and Stephen Grant of the Navigation Group at the Bedford Institute of Oceanography played a vital role in the work. Also to be thanked are the masters and officers of the C.C.G.S. "Narwhal", C.S.S. "Hudson" and C.C.G.S. "Thomas Carleton" for their cooperation during data acquisition.

REFERENCES

(1) Bigelow, H.W. (1963): Electronic Surveying: Accuracy of Electronic Positioning Systems. Journal of the Surveying and Mapping Division, Proceedings of the American Society of Civil Engineers, October 1963. Reprinted in "Supplement to the Int. Hydrog. Review", Vol. 6, September 1965.

(2) Brunavs, P. (1977): Phase lags of 100kh Radiofrequency Ground Wave and Approximate Formulas for Computation. Report on contract work for the Canadian Hydrographic Service.

(3) Grant, S. (1979): Computing Geographic Coordinates from Combinations of Navigational Observations. Unpublished report.

LONARS: THIRTY FOOT GEODETIC POSITIONING FROM LORAN-C

John E. Boyd
The Johns Hopkins University
Applied Physics Laboratory
Laurel, Maryland 20810

ABSTRACT

The Loran Navigation Receiving System (LONARS) serves as the position reference for evaluation of submarine navigation equipment accuracy during submarine testing off the east coast of Florida. The program to develop this highly accurate Loran-C based system was completed by The Johns Hopkins University Applied Physics Laboratory in 1979. LONARS uses a minicomputer with programmed phase-locked loops and data editing to track as many as sixteen Loran-C signals. Computer peripherals provide real time display of program status and computed position and velocity as well as recording the time of arrival data for later, post mission processing. During system calibration conducted in May 1979, at-sea geodetic accuracy of better than thirty feet was demonstrated.

PURPOSE

A survey and comparative performance test of several commercially available radio navigation systems was conducted by the Applied Physics Laboratory in 1975. Fifty-foot accuracy, coverage to at least 60 nautical miles from shore, and ability to recover from a loss of signals while at sea were required of the system. The last requirement eliminated some CW systems from consideration due to the requirement to maintain a lane count from some point of initialization; the second eliminated some very accurate but line-of-sight systems. The study and field test failed to locate a radio navigation system that could meet these requirements in the test area (Reference 1).

DEVELOPMENT OF LONARS

Experience with Loran-C had convinced many that this system has the potential to provide positioning service with accuracy much greater than that usually observed (Reference 2). Under U. S. Air Force contract, the Laboratory designed and studied a Loran-C super receiver in 1972 (Reference 3), but no hardware was produced. This experience, together with the announced improvements in Loran-C coverage for the U. S. Coastal Confluence zone, prompted APL to propose the development of a highly accurate Loran-C based system for the submarine testing application. This proposal was approved by the Navy's Strategic Systems Project Office and the development was begun in early 1977. The system was to become known as the Loran Navigation Receiving System (LONARS).

The first phase of LONARS development was to assemble a prototype system that could be used to demonstrate that the accuracy goal of 50 feet was achievable. The first system comprised a Hewlett-Packard HP-1000 minicomputer system and a government furnished AN/BRN-5 Loran Sensor. Engineering Development Model 1 was then tested in the laboratory on live and simulated signals and in the Jacksonville, Florida area on a Laboratory research vessel. The results of this test indicated that the fifty-foot goal could be achieved by LONARS (Reference 4).

During the next phase, two additional units were assembled, and the computer program defining the essential characteristics of the LONARS receiver was substantially modified. Primarily because of the lack of availability of Navy AN/BRN-5s, a decision was made to design and build a replacement for use in LONARS. Four of these APL Loran Sensors were built and tested. The complete LONARS system was installed and initial calibration was performed in the fall of 1978. Additional calibration exercises were conducted in February and May of 1979 after some initial defects in the complex LONARS software were corrected.

LONARS DESCRIPTION

LONARS primary function is to provide an accurate record of the ship's positions at sea after the ship has returned to port. To support this post mission use of the data, a second LONARS is installed at a known, fixed location on shore. Any position errors indicated by this second set, referred to as a pattern monitor, are attributed to irregularities in the Loran-C signals, and the data from the shipboard LONARS are corrected by a corresponding amount. This process minimizes the effect of variations in the signal propagation speed due to natural causes as well as irregularities in the times of emission of the loran signals themselves. A secondary function of LONARS is to provide a real-time display of ship's position. The accuracy requirement for real time is not as stringent as for post mission and the accuracy performance is not as good due to the absence of pattern monitor corrections.

A block diagram of a LONARS set is shown in Figure 1. The computer used is an HP-2109B with 64K bytes of high speed memory. A dual channel direct memory access capability is used to receive data from the sensor and to transmit data to the magnetic tape recorder. Other equipment includes an HP-2648 graphics display terminal with dual cartridge tape drives, an HP-9866 thermal printer and a Kennedy Model 4344 cartridge tape unit. Each component has been installed in a special portable electronics box suitable for temporary installation aboard a submarine. A photograph of the system is shown in Figure 2.

The APL Loran Sensor (Reference 5) comprises an Austron 2082 tuned rf receiver modified to permit computer control of receiver gain, a Tektronics TM 500 series oscilloscope for display, an analog to digital converter, and a digital interface set for computer communications. The sensor uses a built-in 5 MHz crystal oscillator but will accept an external cesium beam standard or other external clock if desired. Programmable notch filters, used in the AN/BRN-5, were not designed into the APL Loran Sensor, but four manually adjustable notch filters are available on the Austron receiver. Built-in test circuitry supplies a variable amplitude 100 kHz test signal for calibration and checkout of the sensor.

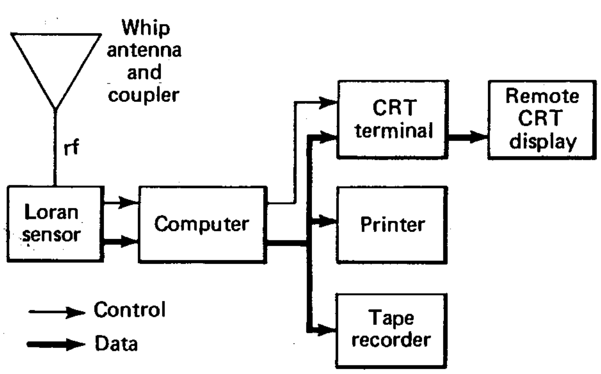

Fig. 1 Shipboard LONARS block diagram.

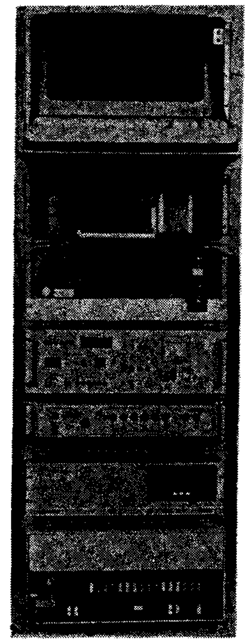

Fig. 2 LONARS shipboard set - from top, display terminal, paper take up device, printer, loran sensor and receiver, tape recorder, and computer.

To operate the system, the computer program is loaded from a tape cartridge in the terminal. After setting Greenwich mean time, the program is started and search mode commences. In the present configuration, GRI code 9930 is searched for a master (Carolina Beach, North Carolina) and then GRI code 7980 is searched for its master (Malone, Florida). When the second master is found the program enters settle/track mode. Upon entry, the signal track strobes for the two master stations and two secondary stations (Jupiter, Florida at 7980 and 9930) are somewhere on the pulse. The program proceeds to adjust the receiver gain for each signal, position each quadrature (zero crossing) strobe on a positive going zero crossing and to locate the standard track point on each pulse. Each Loran-C station's A and B phase code groups are considered to be separate signals and are tracked separately. A signal pair from a station is regarded as settled when both signals are gain adjusted, satisfactorily phase locked to the standard track point, and are giving the same time of arrival. When both Jupiter signals are settled, a time correction is computed and applied to synchronize LONARS time with coordinated universal time (UTC). This step is necessary to ensure that pattern monitor corrections will be accurately synchronized with the ship set data. Time must be entered at start-up to within one-half of the increment between times of coincidence of signals for a designated dual-rated station being tracked. For the current configuration, the Jupiter 7980 and 9930 times of coincidence are about 52 seconds apart. Time must therefore be entered to within 26 seconds of true Greenwich mean time.

When all four of the primary stations' signals are settled, a data-good indication is provided in the output status word and on the CRT display. The display (Figure 3) shows a representation of the nearby coastline, areas of at sea operations, and a cross hair indicating present ship's position. Displayed data include the measured time differences, UTC time, latitude, longitude, and speed north and east. A status word containing coded program information and a dead-reckoned position prediction are also shown. The screen is refreshed with new data about once per second, and time of arrival data are collected for recording at the same rate.

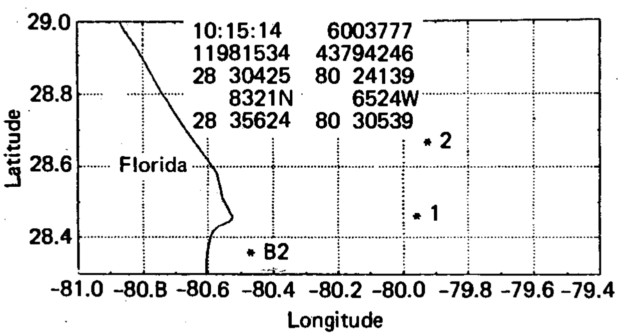

Fig. 3 LONARS CRT display - time differences are in nanoseconds, position in degrees and thousandths of minutes, and velocities in thousandths of knots.

As the LONARS program continues in settle/track mode, a background routine called nuisance search attempts to locate any other loran signals being received. If any are identified, they are placed in track, and data from the four primary stations are not taken when a cross-rate conflict occurs. If the located nuisance signal proves to be sufficiently weak it is dropped from track to allow room for stronger signals that could cause more serious cross-rate interference. LONARS can track up to 16 Loran signals, that is, eight station A-code/B-code pairs.

Search mode usually takes two to three minutes, while settle may last another eight to 15 minutes. It can take up to an hour for the nuisance track list to reach equilibrium; a typical list in the present area of operations includes six pairs during daylight and a full eight pairs at night.

CALIBRATION OPERATIONS SUMMARY

As mentioned above, calibration data were collected on several cruises which took place during three separate field tests. The data used in the final calibration analysis were drawn primarily from the final field test of 18 to 27 May 1979, with particular use of the 23 May data. During this test two LONARS shipboard sets were installed aboard a large Military Sealift Command ship, the 450-foot-long USNS Range Sentinel. The at-sea reference was provided by Cubic Corporation's Autotape DM-43, a three-range line-of-sight system with advertised accuracy of better than one meter. Four data collection runs were made on 23 and 24 May. Exceptionally good Autotape performance was obtained on 23 May, with consistent range measurements from all three responders observed out to longitude 80° 3'W. Three-range Autotape data were obtained several miles east of that point, but there is reason to reject these data as invalid. Data obtained during the November 1978 and February 1979 field tests were used for heading sensitivity tests and seasonal variability check, but they were not included in the signal propagation speed calibration because refinements to the LONARS real time computer programs had resulted in significant improvements to system accuracy by the May 1979 test and because sufficient data were obtained from that test alone to achieve the calibration.

Two LONARS shipboard sets (LONARS-SS) were installed side by side for the May 1979 phase of calibration. These sets, SS No. 2 and SS No. 3, were connected to a common antenna but were isolated from it and each other by very wide band, 10 dB attenuators. Each LONARS-SS had its own data recorder. The Autotape system included an internal clock, a controller and a separate data recorder. The antennas for LONARS and Autotape were installed side by side on the highest mast located amidship on the Range Sentinel, about 125 feet above sea level. The LONARS pattern monitor station, located ashore, was run continuously during all at-sea calibration runs. Each LONARS automatically synchronized to and subsequently computed coordinated universal time, after having initially been set to Greenwich mean time. This time synchronization is accurate to better than a millisecond in the output data, and ensured that both LONARS-SS and the LONARS pattern monitor were synchronized. The Autotape clock provided a digital read out which permitted synchronization of Autotape to LONARS within better than one second. Data collection proceeded at 1 sample per second.

As noted above, Autotape performance was exceptionally good during both of the 23 May runs. However, analysis of the Loran and Autotape data revealed that many of the Autotape measurements were in error by several tens of meters, particularly in range 2. This problem affected perhaps 10 percent of the data comparisons but had practically no effect on the calibration results since bad measurements were quite easily identified and eliminated.

There were three periods on 23 May during which the Autotape/LONARS differences were significantly larger than for the rest of the day. The first of these was a ramping error (maximum 60 feet) observed on the outbound run from the port to a distance of about eight miles. The second was a very large (several hundred feet) difference observed in the operating area, about 35 miles out. The third was a ramping error (maximum 55 feet) observed as three-range measurements were first regained on the inbound run. Each of these deviations appeared to affect longitude much more than latitude.

While it is impossible to say for certain whether these excursions were caused by LONARS or by the reference, they have been attributed to the reference for the following reasons:

a) No excursion was observed in the (stationary) LONARS pattern monitor.

b) The apparent time constant for each was long -- several tens of minutes. LONARS has no known means of varying this slowly, and the pattern monitor data proves that the variation was not in the Loran-C signals.

c) The excursions were nearly identical in the position differences generated from either of the two shipboard systems.

d) The first and third excursions were not repeated when the ship revisited the same geographic area on that day.

e) Examination of the excursions in Loran time difference coordinates reveals that the TDA and TDB errors are very highly correlated, pointing to a common cause. Such a commonality is extremely difficult to account for in the LONARS tracking routines since all signals are tracked independently. Furthermore, correlation cannot be attributed to the Loran-C service since TDA and TDB are formed from pairs of signals that are independent.

f) Possible physical explanations for such Autotape disturbances would be a surface reflection multipath for the first excursion and microwave ducting for the second and third. Most of the data from these latter excursions were in fact from locations beyond the physical line of sight.

The suspect data have been omitted from the plots in the following sections and have been excluded from the statistical summaries.

ANALYSIS SOFTWARE

Figure 4 depicts the data/analysis flow for the calibration analysis. After tape cleanup and reformatting (not shown), LONARS data were corrected with reference to pattern monitor data and compared to processed Autotape data. Programs used included:

NTPMC - Computes and applies LONARS pattern monitor correction, preparing a file of time differences ready to be processed by NTPOS.

NTPOS - Computes LONARS position fixes for desired times using input time differences. Interpolates input TD's if necessary.

NXMERINT - General purpose merge, interpolate, and subtract program. Time matches records from two files, interpolating if necessary, and computes differences as specified by the user.

NBSTAT - General purpose statistics program. Computes mean, standard deviation, and root-mean-square for blocks of specified size from an input file.

NBATAPE - Edits and corrects Autotape range measurements, supplying the correct lane, and computes a three range least-squares fix. Passes only those fixes for which the three measurements were consistent within two meters.

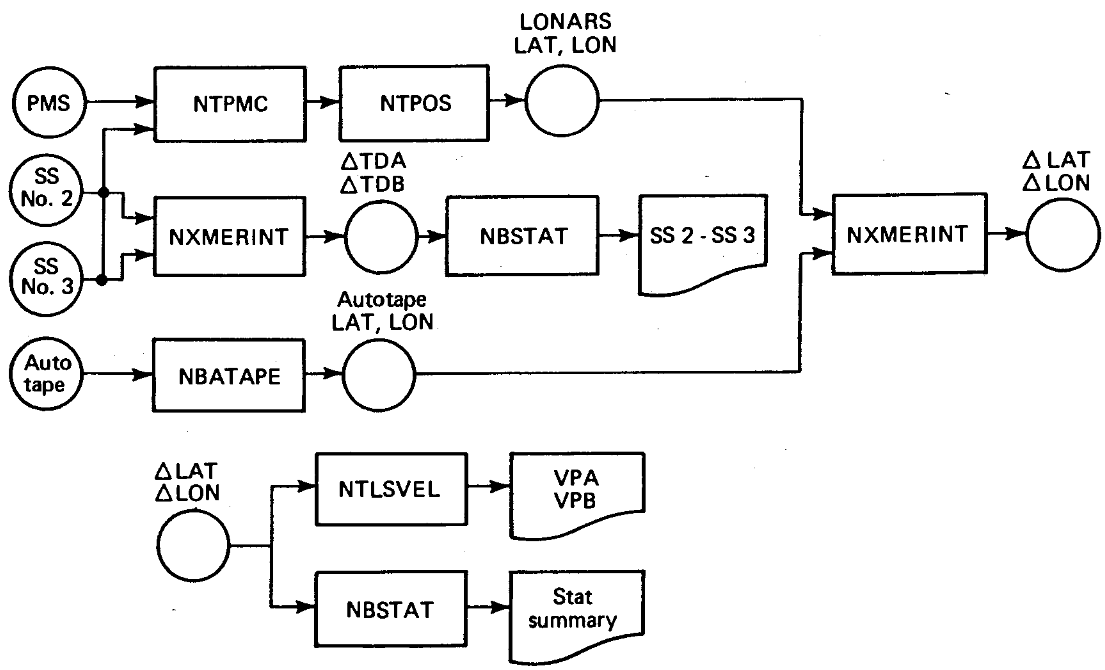

Fig. 4 LONARS calibration analysis flow.

NTLSVEL - Computes a least squares estimate of the best effective propagation velocities to be used in converting LONARS time differences to geodetic position. Best means giving the best agreement with the Autotape position.

CALIBRATION PARAMETERS

The primary purpose of the calibration was to determine empirically the values of the parameters to be used in the transformation of LONARS measured time differences to latitude and longitude. The goal was to make LONARS fixes agree with valid Autotape fixes over as wide an area as possible. Although a number of combinations of parameters could be selected, those used were the effective time difference propagation velocities, VPA_E and VPB_E, the effective emission delays, EDA_E and EDB_E, and two coordinate pairs assigned to be equivalent, thereby tying together the time difference and latitude/longtitude coordinate systems. This correspondence was made by matching the average measured pattern monitor station time differences to a location selected to minimize the mean Autotape-LONARS difference. The pattern monitor location so selected was 36 feet north and 38 feet west of the surveyed coordinates of the pattern monitor antenna. The calibration parameters are presented in Table 1.

Table 1

LONARS calibration parameters

	TDA	TDB
Loran GRI code	9930	7980
Stations:	Carolina Beach, NC	Malone, FL
	Jupiter, FL	Jupiter, FL
Effective propagation speed (VP_E) (m/μsec)	299.764	299.513
Effective emission delay (ED_E) (μsec)	13694.144	45199.707
Assigned PM coordinates	28° 25′ 2.76″ N	80° 36′ 25.18″ W

Programs NTPMC and NTPOS compute position using these parameters as follows:

1. Expected TDA and TDB for the pattern monitor are computed from the distance differences to station pairs (ΔR) as follows:

$$\begin{bmatrix} TDA_{REF} \\ TDB_{REF} \end{bmatrix} = \begin{bmatrix} \Delta R_A & O \\ O & \Delta R_B \end{bmatrix} \begin{bmatrix} 1/VPA_E \\ 1/VPB_E \end{bmatrix} + \begin{bmatrix} EDA_E \\ EDB_E \end{bmatrix}$$

2. Deviation of measured PM TDs from the expected values is then subtracted from the TDs measured on the shipboard LONARS.

3. Range differences are computed from the corrected TDs by

$$\begin{bmatrix} \Delta R_A \\ \Delta R_B \end{bmatrix} = \left[\begin{bmatrix} TDA \\ TDB \end{bmatrix} - \begin{bmatrix} EDA_E \\ EDB_E \end{bmatrix} \right] \begin{bmatrix} VPA_E \\ VPB_E \end{bmatrix}$$

4. The range differences are used to compute geodetic position.

Note that in this scheme the effective emission delays subtract out, and they have no effect on the range differences used to compute the fix for pattern monitor corrected data. EDA_E and EDB_E were selected to make the mean pattern monitor correction zero in order to reduce the errors of fixes computed from non-pattern monitor corrected data.

POST MISSION ACCURACY

Measured time differences from at-sea data were converted to latitude and longitude as described above for comparison to the at-sea reference, Autotape. Transformation parameter values used were those shown in Table 1. The processed loran data to Autotape differences were then plotted and analyzed.

Figures 5 and 6 depict the LONARS latitude correction (LAC) and longitude correction (LOC) in feet required to give agreement with the reference*. These plots show every third point of the data set, or roughly one comparison for every three good Autotape fixes. The data displayed were taken with LONARS-SS No. 2. They agree well with data from LONARS-SS No. 3 taken at the same time. The track of the survey ship during this exercise is plotted in Figure 7.

A statistical summary of the data shown in Figures 5 and 6 is presented in Table 2. Note that the mean error is nearly zero, both in this table and in corresponding plots, while at the LONARS pattern monitor and at the Navy wharfs a bias of about thirty feet is observed. It is believed that this phenomenon is due to a slight "grid warp" at the land/sea boundary. The effect is not at all large, but it

*For consistency, corrections are used throughout this report in place of errors. A correction is simply the negative of an error.

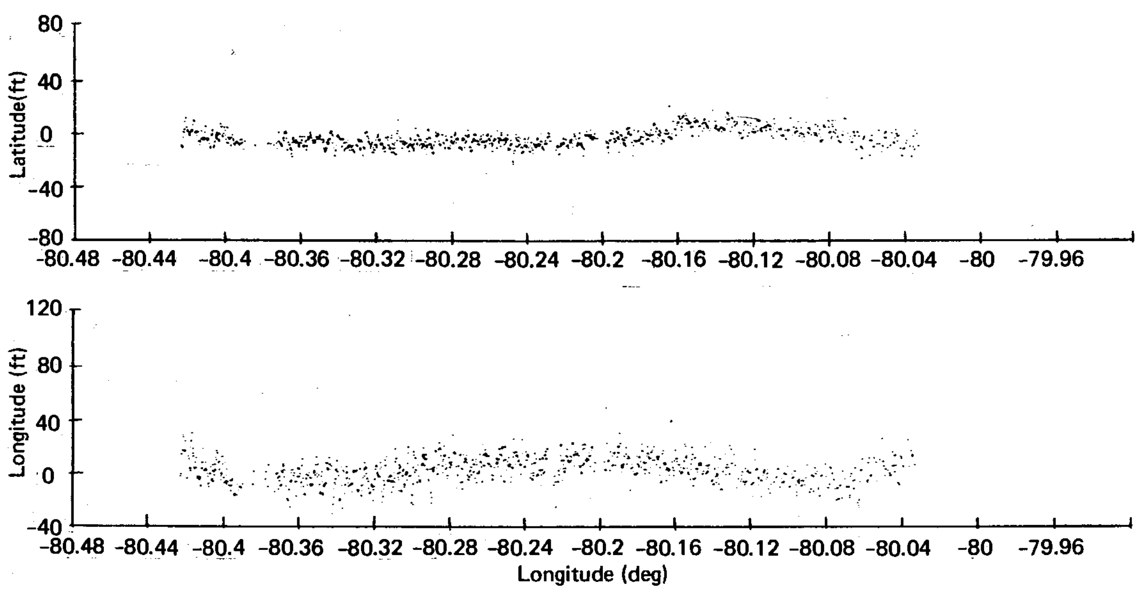

Fig. 5 Post mission LONARS correction data; 23 May 1979.

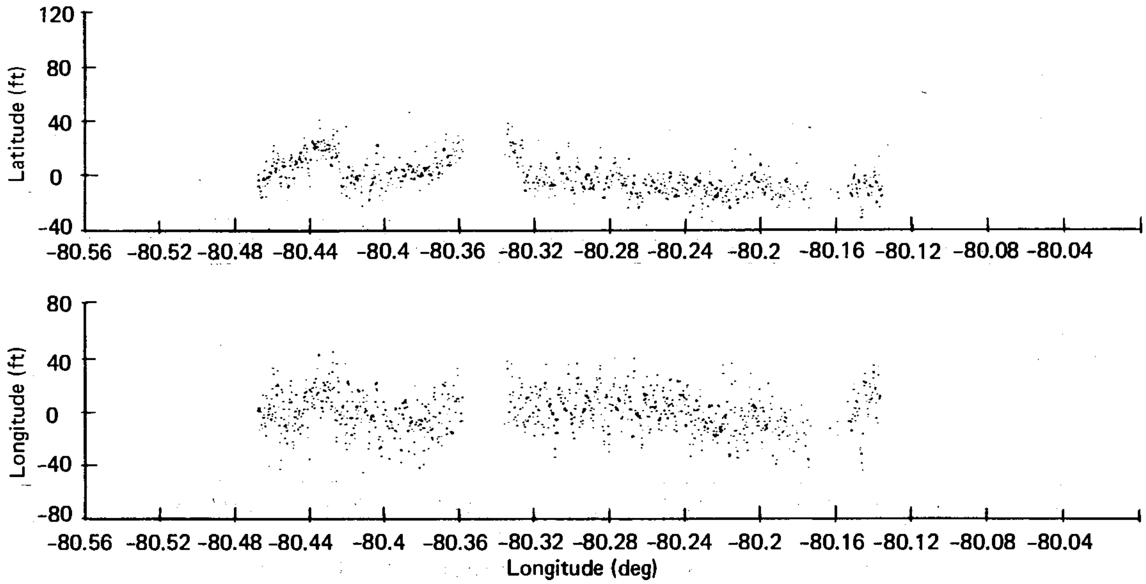

Fig. 6 Post mission LONARS correction data; 23 May 1979.

Table 2

At-sea post mission LONARS correction statistics

	Latitude (ft)	Longitude (ft)
Mean	-3	1
rms	10	13
rss of rms	16	

Based on 4848 comparisons to Autotape data taken at sea, 23 May 1979.

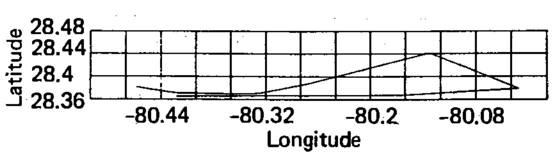

Fig. 7 USNS range sentinel track; 23 May 1979.

does cause a small bias in the in-port LONARS position using the coordinate conversion scheme described above. The distortion apparently disappears smoothly between the wharf and a point not more than 5.5 miles out, but poor Autotape geometry in this area prevented direct measurement of the changing LONARS error.

It was noted during data analysis that the LONARS Autotape difference approached the assumed Autotape accuracy of three to four feet. In fact, outlier data omitted from the plots and tables in this section were in all cases confirmed to be due to Autotape error. These facts suggest that some portion of the remaining LONARS/Autotape difference is Autotape error. Since the difference was well within the LONARS accuracy goal, however, no attempt was made to apportion the error between the two systems; the difference is attributed to LONARS in all statistical summaries and in the error model.

Figures 8 and 9 are included to give some indication of potential LONARS accuracy improvement by adding a smoother to the post mission computer program. Plotted are the means and rms values, respectively, of 20 point blocks of comparison data for this exercise. Some improvement is evident (note the difference in scales), but the results are not dramatic.

TWO SET AGREEMENT

A test was performed to evaluate the total LONARS receiver tracking noise by comparing the time difference outputs of two LONARS connected to the same antenna on a moving ship. Figure 10 depicts the difference between the time difference outputs of the two sets over a period of about 2.5 hours. The larger scatter in delta TDA at the beginning of the interval resulted from uncompensated cross-rate interference shortly after receiver start-up. After the nuisance stations have been located and placed in track the interference disappears. This effect is noticeable in TDA (9930) because of the slow relative motion between the 9930 stations in track and the 9960 stations not yet in track. The long

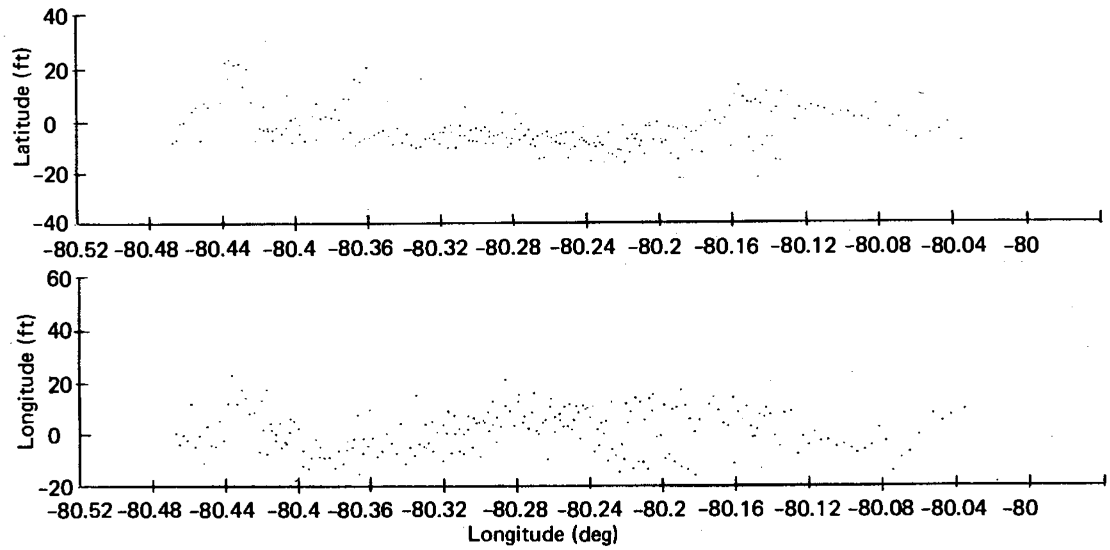

Fig. 8 Smoothed LONARS position corrections for 20-point blocks.

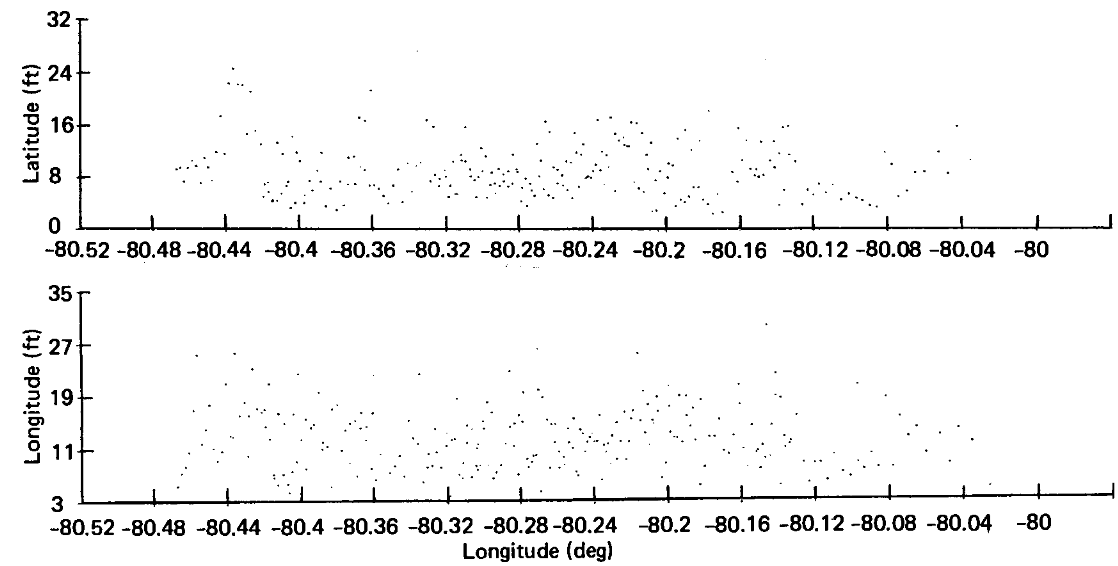

Fig. 9 RMS LONARS corrections for 20-point blocks.

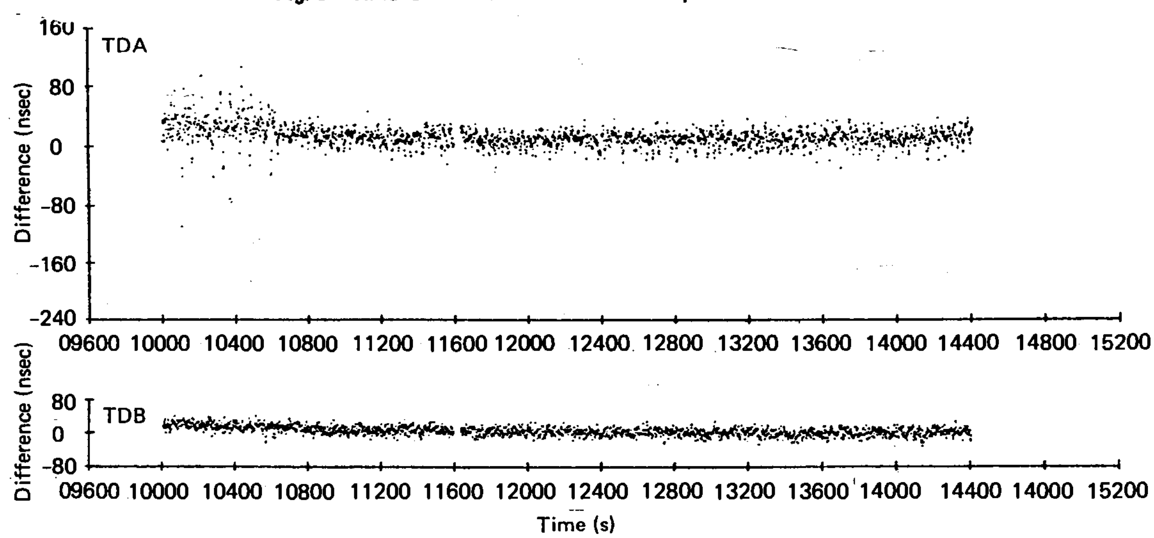

Fig. 10 Two set differences, LONARS 2 minus LONARS 1.

overlap of groups in these rates (about 3 seconds) guarantees that some of the data will be spoiled by the interfereing stations.

A shorter interval (9 minutes) of these data is shown in expanded scale in Figure 11. The 50 second gap is the result of momentary loss of the data-good indication in one or both sets, probably due to an automatic receiver gain adjustment.

Delta TDA is plotted against delta TDB in Figure 12 as a check on correlation. Since the time differences are derived from independently tracked stations, little or no correlation should appear in the TD outputs. None is apparent.

Table 3 contains a statistical summary of the data in Figures 10 and 11. Reducing the standard deviations by $\sqrt{2}$ gives 10 and 7 nanosecond estimates of the tracking noise of LONARS for TDA and TDB in this area.

LONARS ACCURACY IN TIME DIFFERENCE COORDINATES

This part of the analysis was performed to determine whether the errors in TDA and TDB were strongly correlated. Since TDA and TDB are determined independently in LONARS, such correlation could indicate the signals from Jupiter at 9930 and 7980 were correlated and were not

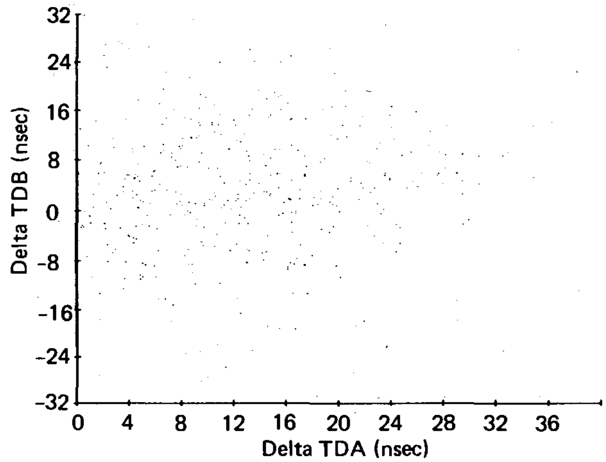

Fig. 12 Correlation of two set differences.

Table 3

Two set agreement statistics.

	Delta TDA (nanoseconds)	Delta TDB (nanoseconds)
Mean	+13	+4
STD deviation	14	10

Based on 8419 samples of data taken 23 May 1979 aboard USNS Range Sentinel.

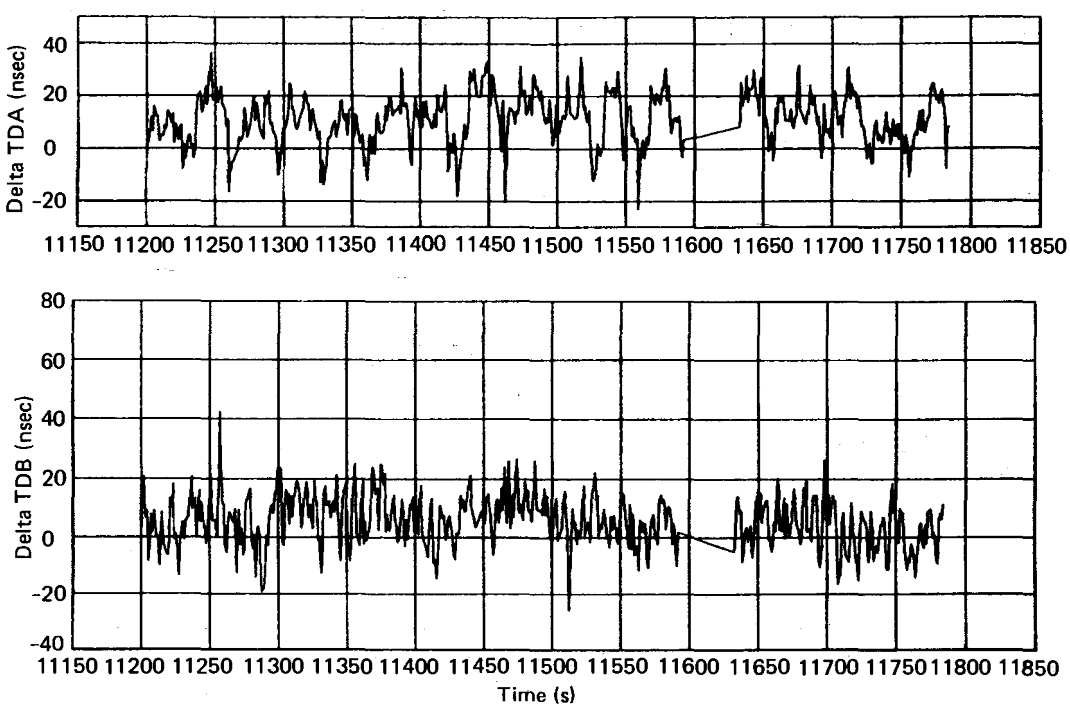

Fig. 11 Two set differences, expanded scale.

being corrected in the pattern monitor process (theoretically they should be substantially uncorrelated) or that a significant portion of the LONARS-Autotape difference was due to Autotape errors. No significant correlation was found after the Autotape data were edited.

Figure 13 depicts the Autotape-LONARS residuals, TDA correction and TDB correction, plotted on the same scale. Both scales are in nanoseconds. Note that there is no obvious linear relationship between the residuals. LONARS time difference corrections are plotted versus time in Figure 14.

EFFECT OF PATTERN MONITOR CORRECTION

To verify that pattern monitor corrections improve the LONARS data, a segment of dockside data covering approximately an hour was processed in several ways. These data, taken

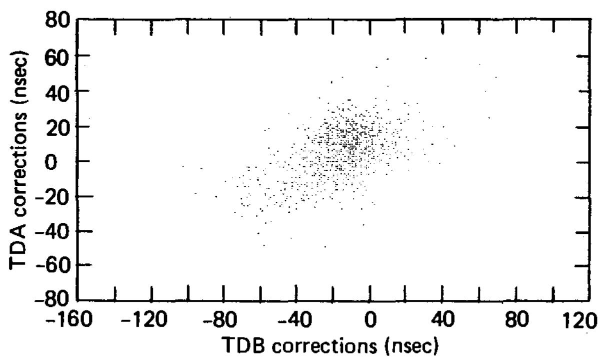

Fig. 13 Correlation of LONARS time difference corrections.

7 February 1979, had some residual cross rate interference contamination due to a deficiency (later corrected) in the real time LONARS program. Since cross rate interference usually affects only the A phase code or B phase code of a given Loran-C station in track, its presence can be detected by comparing A and B phase code arrival times and rejecting the data if the arrivals differ. The test threshold chosen in this test was about twice the standard deviation of the A-B arrival time difference for each station. A summary of the results is given in Table 4. In this table, qualified refers to the data editing just described. Note that very few of the data points were rejected, but that a significant drop

Table 4

Effect of pattern monitor correction

		Single set data		PM corrected data	
		Lat.	Lon.	Lat.	Lon.
All	N	3296		3296	
	RMS*	12	16	10	8
	RSS*	20		13	
Qualified	N	3122		3258	
	RMS*	10	14	7	6
	RSS*	17		9	

*In feet

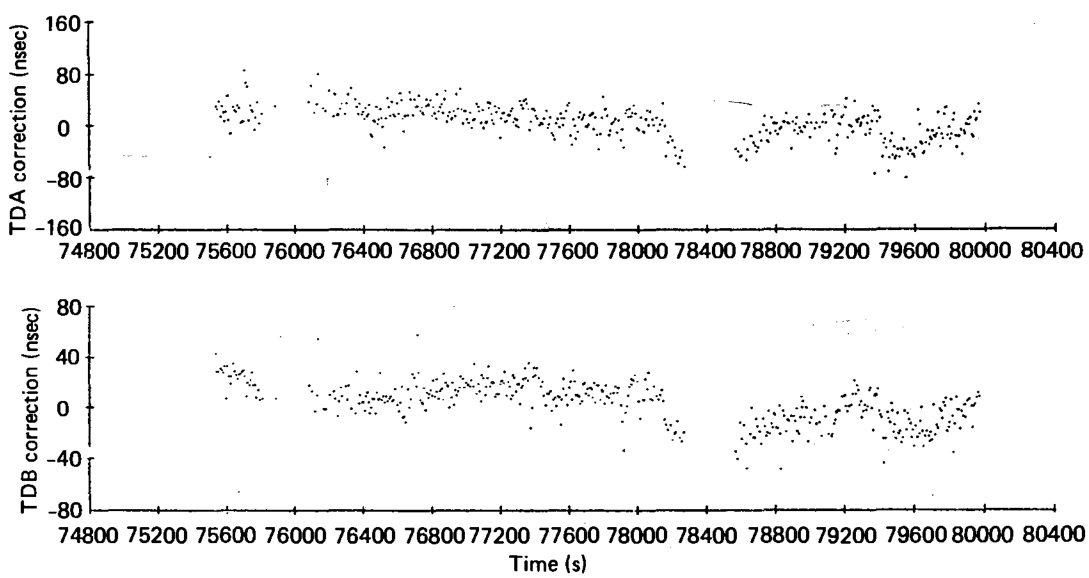

Fig. 14 Loran minus autotape in time difference coordinates.

Table 5

Estimated LONARS accuracy

	Real time		Post mission	
	Latitude	Longitude	Latitude	Longitude
Mean error	0	0	0	0
Uncertainty of mean	30	30	15	15
STD deviation	30	30	10	15
RSS	60		30	

All entries are in feet.

RSS is the root sum square of the uncertainty in the mean and the standard deviation for each axis.

in the scatter of the data resulted. The conclusion of this test was that pattern monitor corrections do indeed improve LONARS accuracy. Due to improvements in the LONARS computer program since these data were taken, the described technique of data editing is no longer as helpful; the present dockside accuracy resembles most closely the qualified, corrected block.

CONCLUSION

Based on the data taken during the calibration, LONARS accuracy is estimated to be 60 feet real time and 30 feet post mission in the Cape Canaveral operating areas, as shown in Table 5. The uncertainties in the mean shown in Table 5 reflect an allowance for error in the survey of Autotape responder sites, systematic Autotape error, and, for real time only, allowance for variation in the Loran-C signals themselves. The hardware, software and calibration technology used in LONARS can be used to derive highly accurate position and time from Loran-C in most areas where Loran-C signals are available.

REFERENCES

1. The Johns Hopkins University Applied Applied Physics Laboratory Technical Report, "PREDEM Test Results", POR-2040, L.G.Parsons, et al, 17 December 1975

2. Navigation, Vol. 21, No. 3, "How to Harvest the Full Potential of Loran-C", L.F.Fehlner and T.A.McCarty, Fall 1974

3. The Johns Hopkins University Applied Physics Laboratory Technical Memorandum, "Summary Report on USAF Super Receiver/Navigator Development", TG-1220, L.F.Fehlner, et al, June 1973

4. The Johns Hopkins University Applied Physics Laboratory Technical Report, "LONARS Phase I Development Report", POR-2670, J.E.Boyd, et al, April 1978

5. Wild Goose Association Eighth Annual Technical Symposium Proceedings, "The Design of the LONARS Sensor", J.A.Perschy, 17-19 October 1979

LONARS, AN EXAMPLE OF ROBUST REAL TIME FILTERING

T. W. Jerardi
The Johns Hopkins University
Applied Physics Laboratory
Laurel, Maryland 20810

ABSTRACT

The concepts and philosphy of ROBUST ESTIMATION (ROBUST is a technical statistical term. A procedure is ROBUST if it is not significantly affected by modest changes in the underlying assumptions.) are reviewed. In particular, the notion of sampling from contaminated distributions is addressed. It is shown that the Loran-C operating environment requires some type of ROBUST procedure.

As an example of ROBUST ESTIMATION, the LONARS tracking filter is described and simplified comparison to the more classic approaches is given. It is shown that ROBUST ESTIMATION is the basis for the superior performance demonstrated by LONARS.

LONARS, AN EXAMPLE OF ROBUST REAL TIME FILTERING

The LONARS system is a Loran-C based position reference system. The overall system is described in a companion paper by Mr. J. E. Boyd [2]. Most Loran-C receiving systems are labeled by the characteristic of its phase-lock process (e.g. linear, clipped linear, and hard limited). The appropriate label for the LONARS phase-lock process is "robust". The term robust refers to a statistical attribute of a process A process "which performs well under a variety of underlying conditions" [7] is called a robust process.

The basic function of a loran receiver is to produce the differences in times of arrival of several R. F. signals (Time Differences). From these data, one can then infer his position. Because the measurements made by the receiver are corrupted by noise the process becomes one of statistical estimation. It is from within the framework of statistical estimation theory that the design and analysis of loran signal processing schemes are conducted.

The operating environment of a Loran-C receiver is a logical starting point for any discussion of system performance. According to Feldman [4], "A prerequisite for the design of low frequency radio receivers is a model for the low frequency atmospheric radio noise that encompass the non-Gaussian nature of actual noise process and is sufficiently tractable to enable performance analysis and optimization of receiver design". The general characteristics of the Loran-C operating environment are well established [3, 4, 5].

It would seem that with a well established model the design and analysis should be straightforward (at least in principle). We should however observe Huber's caution: "The traditional approach to theoretical statistics was and is to optimize at an idealized model and then to rely on a continuity principle: what is optimal at the model should be almost optimal nearby. Unfortunately, this reliance on continuity is unfounded: the classical optimized procedures tend to be discontinuous." [7]. The solution to the design problem is to develop a robust procedure so that modest changes in the underlying noise distribution only produce modest changes in the estimated time differences.

The underlying noise amplitude distribution is indicated in Exhibit 1 (taken from [3] page 69, Figure 27). If the noise process were Gaussian the amplitude distribution would be a straight line[1] parallel to A in Exhibit 1. The The curve indicates there is a substantial portion of the distribution that follows the Gaussian law, while larger amplitudes tend not to follow the Gaussian law. Distribution of this type, Gaussian for small values and non-Gaussian for large values (high tails) are known as contaminated distributions [10]. The study of such contaminated distributions was the impetus for John Tukey's pioneering efforts in Robust Estimation Theory.

In order to fix our ideas concretely, an example is given in Exhibit 2. The plot is the amplitude and phase of 8 decoded Loran-C pulses (1 group) that have been contaminated with noise from the CCIR

1. The axes of the graph are Log and Log Rayleigh Probability, which is a form of Weibull Probability paper [8].

distribution (Exhibit 1). The signal to noise ratio (SNR) is 1, or 0 dB. Our attention is caught almost immediately by the two extreme values. A linear receiver would use all of these measurements with equal weight and the adverse impact of this is clear.

As Exhibit 2 indicates, the Loran-C signal format (8 pulses to a group) presents us with an almost ideal situation for applying some robust techniques to the measurements. If we view the 8 pulses as producing 8 independent samples of the amplitude and phase of the Loran-C signal for a fixed point in time, we can then process these 8 samples as a batch.

There are many robust procedures for handling batch data[2]. The LONARS system is based on the "trimmed mean" estimate as originally advocated by Tukey [10]. Exhibit 3 is a simplified flow chart for the LONARS procedure. The concept of trimming is straightforward, the data is ranked and some fixed fraction of the largest and smallest samples are discarded and the mean of the remaining samples is computed. LONARS allows for the selection of two trimming levels either 37½% or 25%. It should be observed that the 37½% trimmed mean for 8 samples corresponds to the median of the sample.

The process of computing a trimmed mean is highly nonlinear, and thus applying standard linear analysis tools would be inappropriate. There does exist an extremely valuable analysis tool for understanding robust estimators, the "influence curve" proposed by Hampel [6]. A finite sample version of Hampel's influences curve has been developed by J. W. Tukey [1, 9] and is sometimes called a sensitivity curve.

To obtain a sensitivity curve for some procedure and a sample size of n, we proceed as follows:

1. consider n-1 samples drawn from our basic population,

2. add to the above sample a variable, say x

3. for each x execute our procedure on the combined sample of size n,

4. plot n times the result of 3 versus x.

These curves give a vivid pictorial representation of the influence of extreme values on various procedures.

---

2. Reference 1 studies some 68 different procedures for location estimation.

Exhibit 4 gives the influences curves for the mean and the 37½% and 25% trimmed mean all for sample size of 8. A fundamental requirement for a procedure to be robust is that its influence curve be bounded.

The influence curve indicates the situation of extreme values, non-extreme conditions are handled by conventional techniques. Exhibit 5 gives the variance reductions for 3 procedures, mean (linear receiver), 25% trimmed mean and 37½% trimmed mean for normal noise. The relative efficiency compared to linear (which is optimal for normal noise) is also given.

As indicated earlier, the LONARS system has the capability of using either 37½% (median) or 25% trimming. Our experiences to date have not permitted us to detect any difference in performance between the two trimming levels under good conditions. As a consequence, the data presented by Boyd [2] is for the 37½% trimming, which is the defaulted (operational) arrangement. The 37½% trimming level is more conservative in that it allows for a higher level of contamination while the loss in normal noise efficiency is modest (good insurance policy with low premium).

Since most of robust estimation theory requires a substantial mathematical statistics background, I have included in Appendix A a characterization of the median which shows the parallels to least squares theory. It is hoped that the discussion in the Appendix will help those with limited statistical background appreciate the nature of this robust technique.

The performance of the LONARS system as given by Boyd clearly indicates the power of robust estimating.

REFERENCES

[1] Andrews, et al (1972). Robust Estimates of Location, Survey and Advances. Princeton University Press, Princeton, N.J.

[2] Boyd, John E. (1979). "LONARS: 30 Foot Geodetic Position from Loran-C", Presented at the 8th Annual WGA Convention, Williamsburg, VA

[3] CCIR (1964). Report 322, "World Distribution and Characteristics of Atmospheric Noise", International Telecommunications Union, Geneva, Switz.

[4] Feldman, D. A. (1972), "An Atmospheric Noise Model with Application to Low Frequency Navigation Systems", ScD Thesis, Massachusetts Institute of Technology

[5] Hall, H. M. (1966). "A New Model for 'Impulsive' Phenomena: Application to Atmospheric-Noise Communication Channels", SEL-66-052, Stanford University, Stanford, CA

[6] Hampel, F. R. (1974). "The Influence Curve and its Role in Robust Estimation", Journal of American Statistical Assoc. 69, pg 383-93

[7] Huber, P. J. (1977). Robust Statistical Procedures, SIAM, Philadelphia, PA

[8] Johnson, Norman L., Kotz, Samuel (1970). Distributions in Statistics, Continuous Univariate Distributions - 1, John Wiley, New York

[9] Mosteller, F., Tukey, J. (1977), Data Analysis and Regression, Addison-Wesley, Reading, MA

[10] Tukey, John W. (1960). "A Survey of Sampling from Contaminated Distributions" Contributions to Probability and Statistics, edited by I. Olkin et al Stanford University Press, Stanford, CA

EXHIBIT 2

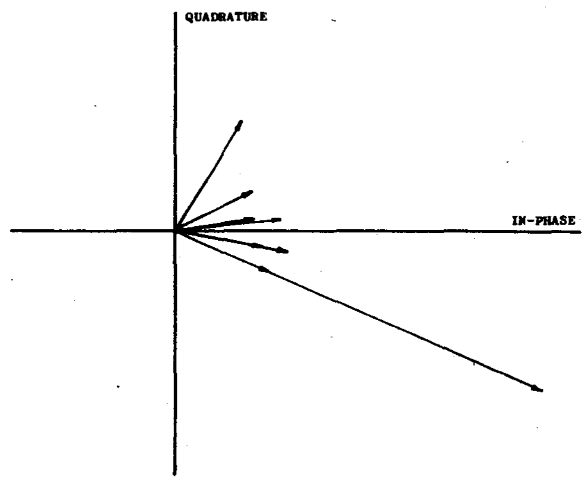

EXHIBIT 1

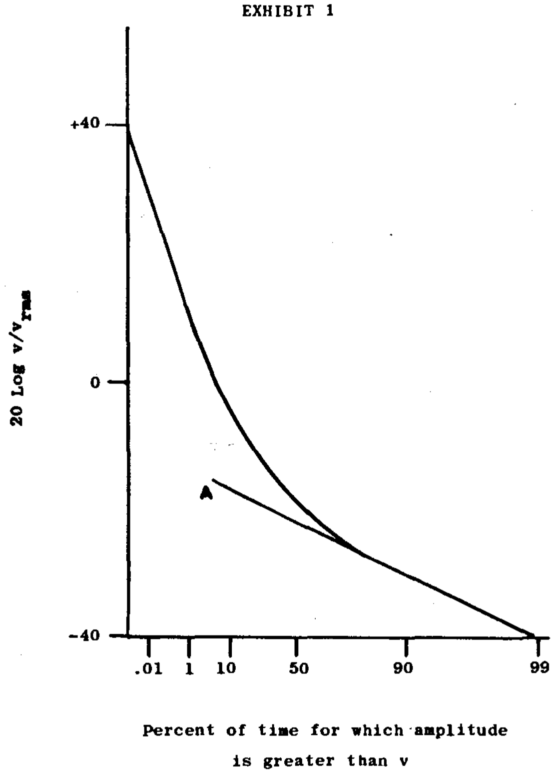

EXHIBIT 3

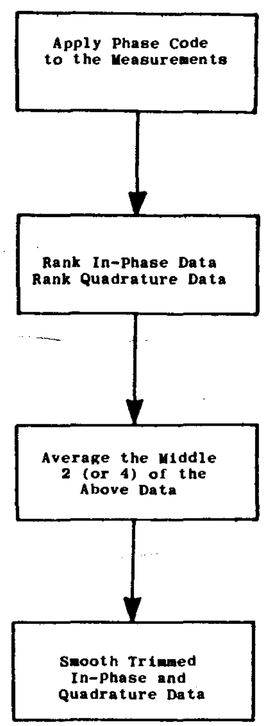

EXHIBIT 4

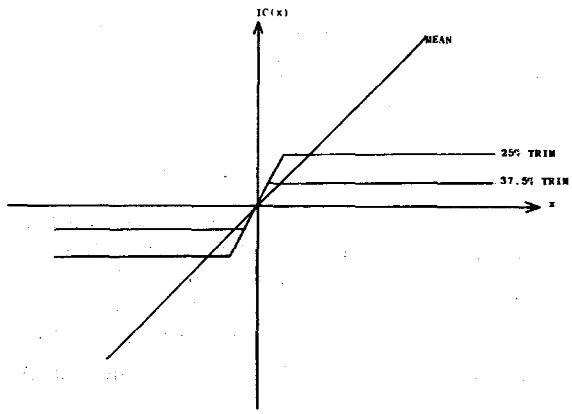

EXHIBIT 5

	Mean	25% Trimmed Mean	$37\frac{1}{2}$% Trimmed Mean
Variance Reduction	.125	.1477	.1682
Relative Efficiency	1.0000	.8463	.7432
	(0 dB)	(-.7 dB)	(-1.3 dB)

APPENDIX

WHY MEDIAN?

The data analyst is often confronted with the following problem: Given a batch of numeric data (observations), summarize this batch by a single number which is representative of a typical value. This summary value is known as an estimate of location.

An often used summary value is the arithmetic mean which is the average value of the observations. Another popular summary value is the median, which is a value for which half of the observations are larger and half smaller. How are these two notions related? Is there some common foundation for these concepts?

The answer to the second question is "yes" and in demonstrating this, some partial answers to the first question will appear. The common foundation is found in optimization theory. These two location estimates, the mean and the median, are the solutions to two quite similar optimization problems.

Let $x_1, x_2, \ldots, x_n$ be our batch and let x be the summary value we select. We then form

$$\epsilon_j = x_j - x \qquad (1)$$

which is known as the deviation, error, or residual of the j^{th} observation. We want our summary value to be such that the deviations are small. We propose to measure this smallness in two ways:

$$L_1(x) = \sum_{j=1}^{n} |\epsilon_j| \qquad (2)$$

$$L_2(x) = \sum_{j=1}^{n} \epsilon_j^2 \qquad (3)$$

These two formulas are known as loss of penalty functions. There are many other loss functions but these two are quite popular and have a certain intuitive appeal. We can now pose two optimization problems:

A. Choose x such that $L_1(x)$ is a minimum.

B. Choose x such that $L_2(x)$ is a minimum.

We will solve B first, since it is a straightforward application of calculus for finding a minimum of a function.

$$L_2(x) = \sum_{j=1}^{n} (x_j - x)^2 \qquad (4)$$

Now we need to find the derivative of L_2 with respect to x.

$$\frac{dL_2}{dx} = \frac{d}{dx}\sum_{j=1}^{n} (x_j - x)^2 \qquad (5)$$

$$= \sum_{j=1}^{n} \frac{d}{dx} (x_j - x)^2 \qquad (6)$$

$$= \sum_{j=1}^{n} 2\,(x_j - x)(-1) \qquad (7)$$

$$= -2\sum_{j=1}^{n} (x_j - x) \qquad (8)$$

Now to find an extremum we set

$$\frac{dL_2}{dx} = 0 \tag{9}$$

and solve, so:

$$0 = -2 \sum_{j=1}^{n} (x_j - x) \tag{10}$$

$$0 = \sum_{j=1}^{n} (x_j - x) \tag{11}$$

$$0 = \sum_{j=1}^{n} x_j - \sum_{j=1}^{n} x \tag{12}$$

$$0 = \sum_{j=1}^{n} x_j - nx \tag{13}$$

$$x = \frac{1}{n} \sum_{j=1}^{n} x_j \tag{14}$$

We thus see that the arithmetic mean is the solution to problem B. This estimate is sometimes called the minimum squared error or least squares.

In order to solve problem A we need some additional notation. Let $x_{(1)}, x_{(2)}, \ldots x_{(n)}$ be the data arranged in ascending order. So we have that

$$x_{(1)} \le \ldots \le x_{(n)} \tag{15}$$

Now our problem is to select x so that

$$L_1(x) = \sum_{j=1}^{n} |x_j - x| \tag{16}$$

is a minimum. We observe that

$$L_1(x) = \sum_{k=1}^{n} |x_{(k)} - x| \tag{17}$$

where we have simply reordered the terms of the summation. We will use this latter form of L_1 to solve the minimization problem. We must find a value of x where the rate of change of L_1 is zero. This value of x will minimize L_1 if lesser values of x have a negative rate of change of L_1 and greater values of x have a positive rate of change of L_1. Let

$$\Delta L_1 = L_1(x+\Delta x) - L_1(x). \tag{18}$$

With the aid of Exhibit A.1 we can readily compute ΔL. The observations in order are given across the top, and the value of x lies between $x_{(k)}$ and $x_{(k+1)}$. The values of $|x_{(j)} - x|$ are indicated by the horizontal line segments. Now the value of ΔL_1 can be seen to be

$$k\,\Delta x - (n-k)\,\Delta x \tag{19}$$

since there are k segments whose length increases by Δx while there are n-k segments whose length decreases by Δx. This is conveniently summarized by

$$\Delta L = \Delta x\,(l(x) - r(x)) \tag{20}$$

where

$r(x)$ = number of observations to the right of x (i.e. greater than x).

$l(x)$ = number of observations to the left of x (i.e. less than x)

So we have the rate of change of L_1 is

$$\frac{\Delta L_1}{\Delta x} = l(x) - r(x) \tag{21}$$

and this quantity is zero when

$$l(x) = r(x) \tag{22}$$

which is the defining characteristics of the median. Thus the median is the solution to problem A. The median is the minimum absolute deviation estimate of location.

EXHIBIT A.1

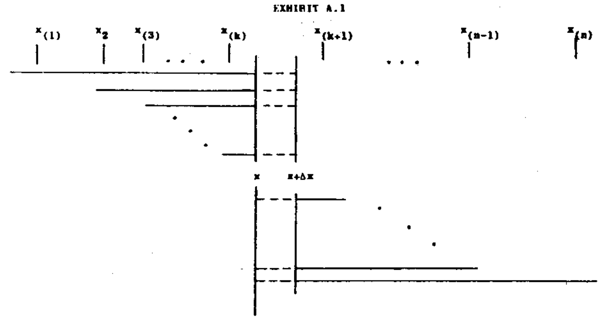

THE DESIGN OF THE LONARS SENSOR

by

James A. Perschy

The Johns Hopkins University Applied Physics Laboratory
Johns Hopkins Road
Laurel, Maryland 20810

INTRODUCTION

The purpose of this paper is to give the reader a brief overall description of the LONARS sensor. Critical modules are described in some detail. Performance parameters, such as gain and bandwidth, are included where pertinent to the overall performance of the sensor.

The paper first describes the entire sensor. The two major sections, the RF and the digital formatter, are then described separately. Next details of the RF attenuators, and the calibration circuit are given.

OVERALL DESCRIPTION

The Loran Sensor consists of two sections, the RF section and the format section. The RF section is shown in the upper left of Figure 1. The remainder of Figure 1 consists of the format section. The format section contains the analog-to-digital (A to D) Converter unit, the format logic unit, the calibration unit, and the front panel. The two signal inputs to the RF section are the Loran signal from the antenna, and the calibration signal from the calibration unit. Each signal inputs to an independent isolation transformer, T2. One signal input is selected by a solenoid activated coaxial switch. The selected signal is the input to 30 db programmable attenuator A. The programmable attenuator consists of independently switched 6 db and 24 db sections. The 6 db section gives an input to output voltage ratio of 2^{-1}; the 24 db section gives an input to output voltage ratio of 2^{-4}; and both attenuator sections give an input to output voltage ratio of 2^{-5}. The output of the 30 db programmable attenuator, A, is the input to the Austron type 2082 tuned RF receiver. The Austron receiver has a 35 KHz bandwidth centered around 100 KHz, and 4 tunable notch filters. The gain of the Austron receiver is set at 84 db giving an input to output voltage ratio of 2^{14}. Midway through the Austron receiver at a gain of approximately 42 db the signal is brought out through isolation transformer T1 and inputs to 30 db programmable attenuator, B. The output of programmable attenuator, B, is coupled back into the Austron receiver via the second isolation transformer, T1. The output of the Austron receiver inputs to 30 db programmable attenuator, C. The 30 db programmable attenuators, A, B, and C are identical. The output of attenuator, C is the output of the RF section.

The signal out of the RF section is the input to the A to D converter unit in the format section, Figure 1. The input of the A to D converter unit consists of an operational amplifier with a gain of 36 db. The operational amplifier has a low frequency RC rolloff at 20 KHz and at high frequency RC

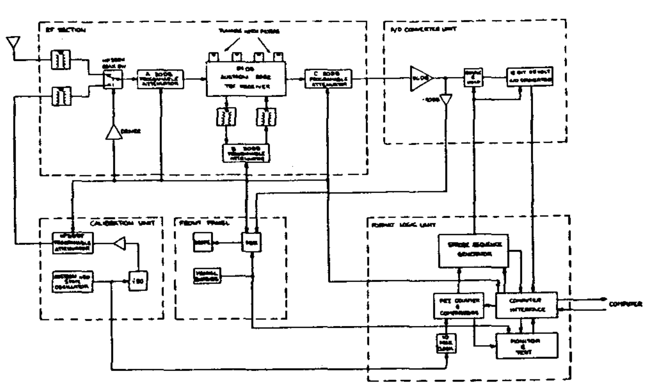

Fig. 1. Lonars Sensor Block Diagram

rolloff at 300 KHz. The output of the input amplifier drives an isolation amplifier which attenuates the signal 40 db and provides a monitor signal to the front panel. The output of the input amplifier also drives a Datel sample-and-hold module. The sample-and-hold module inputs to a Datel 12 bit analog-to-digital converter. The voltage conversion range is +5 volts to -5 volts. The converter treats all signals more positive than +5 volts as +5 volts, and all signals more negative than -5 volts as -5 volts. Analog signal processing ends at the analog-to-digital converter.

The digital output of the analog-to-digital converter inputs to the computer interface in the format logic unit, Figure 1. The computer interface stores the A-to-D converter sample for input to the computer. The computer interface also stores data from the computer pertaining to the operation of the Loran sensor. The strobe sequence generator in the format logic unit generates the appropriate sample strobe timing signals for search and track modes. The pulse repetition interval counter and comparators in the format logic unit maintains a measurement sequence clock and generates measurement sequence start commands. The monitor and test portion of the format logic unit facilitates closed loop testing through the computer of the Loran sensor. The 10 MHz clock portion of the format logic unit derives a 10 MHz clock from the 5 MHz oscillator in the calibration unit.

The calibration unit provides a signal to the RF section for measuring signal delay vs. gain through the RF section. The 5 MHz signal from the Austron model 1150 oscillator is divided by 50 to derive 100 KHz. The 100 KHz signal is inputted to a wide band solenoid activated HP355F programmable attenuator. The programmable attenuator provides a maximum attenuation of the signal of 120 db. The output of the programmable attenuator is the calibration mode input into the RF section. The front panel of the format section has an oscilloscope for monitoring the Loran signal. The front panel also has a display of the RF section attenuator settings, and switches for manually controlling the RF section attenuators and the calibration unit attenuator.

RF SECTION

The RF section photograph, Figure 2, shows the attenuator placements and cabling within the RF section of the Loran sensor. The antenna and calibrate signals input through separate isolation transformers to the HP 3331B coaxial switch. The output of the coaxial switch is the input to 30 db attenuator, A. The output of attenuator, A, is the antenna input to the Austron model 2082 tuned RF receiver. The output of the Austron receiver preamplifier inputs through isolation transformer T1 to 30 db attenuator B. The output of attenuator B is fed back into the Austron receiver via a second isolation transformer. The final output of the Austron receiver is the input of 30 db attenuator C. The output of attenuator C is the output of the RF section. The switch antenna and switch cal signals connect from the format section to the coaxial switch driver. Six attenuator control signals connect from the format logic portion of the sensor to the attenuators in the RF section. DC power is brought in from the back panel to the DC power distribution box in the RF section which filters the power and distributes the power to units in the RF section via shielded coaxial cable. The AC power cable feeds through the back panel to the DC power supply in the Austron receiver.

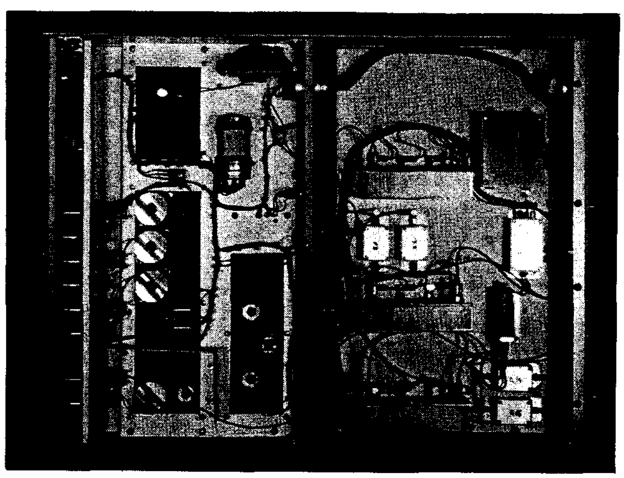

Fig. 2. RF Section

DIGITAL FORMATTER SECTION

Figure 3 is a photograph of the front panel of the digital formatter section of the LONARS sensor. The input monitor to the vertical amplifier of the oscilloscope consists of an array of switches through which signals may be summed. The signals available at the front panel for monitoring consist of the RF input to the A to D converter, the A to D converter strobe, the format logic pulse repetition interval counter interrupt to the computer, the pulse repetition interval interrupt clear from the computer, the RF data measurement direct memory access signal to the computer, the direct memory access clear signal from the computer, and the sync interval preset counter. Also available for monitoring on the oscilloscope are the +5, +15, -15, and +20 volt power supplies. All of the signals are isolated by resistors before being brought to the front panel. The oscilloscope trigger is selected by a second array of toggle switches. The signals available for triggering the oscilloscope are the sync interval preset counter, the pulse repetition interval interrupt, and the direct memory access interrupt. The non-operational red warning light next to the oscilloscope CRT, warns the operator that the manual RF attenuation mode or the manual calibration mode has been selected.

The receiver attenuator display consists of 6 green light emitting diodes located at the upper left of the front panel.

The sync interval selector consists of 5 binary coded decimal digit switches. Each switch connects to a decade of a binary coded decimal preset counter on the format logic board. The calibration section of the front panel consists of a toggle switch to select manual or computer control, a hexadecimal digiswitch to select the calibration attenuator setting under manual control, a toggle switch to select either the antenna or the calibration signal, and a toggle switch to gate the 100 KHz signal generator power on and off. The manual attenuator section of the front panel has a toggle switch to select either manual or computer control, and 2 octal digiswitches. One octal digiswitch selects the combinations of 6 db attenuators in the RF section. The other octal digiswitch selects the combinations of 24 db attenuators.

30 DB PROGRAMMABLE ATTENUATOR

The 30 db programmable attenuator diagram is shown in Figure 4. It consists of a 24 db attenuator section and a 6 db attenuator section isolated by voltage-follower amplifiers. The input impedance of the amplifier is 4 thousand ohms at 100 KHz. The output impedance is 20 ohms at 100 KHz. The switches in each attenuator section consist of 4 matched field effect transistors in one integrated circuit package. The on resistance of the transistors is 75 ohms. The off signal isolation of the field effect transistors is 80 db at 100 KHz and 500 ohms load resistance. The three voltage followers in the programmable attenuator are identical. Their function is to minimize phase shift in the attenuator due to impedance mismatches of the combinations of attenuator settings. The switches are shown in their zero attenuation position.

The picture of the 30 db attenuator, Figure 5, shows the circuit layout. The power inputs and power filters for +5, +15 and -15 volts are located at the bottom of the attenuator chassis. Above the power filters are the switch control

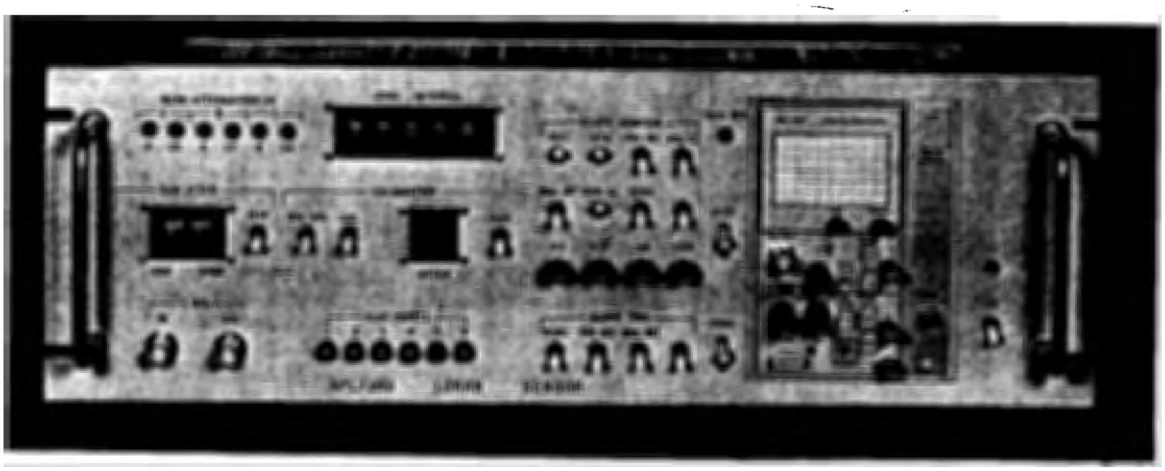

Fig. 3. Digital Formatter

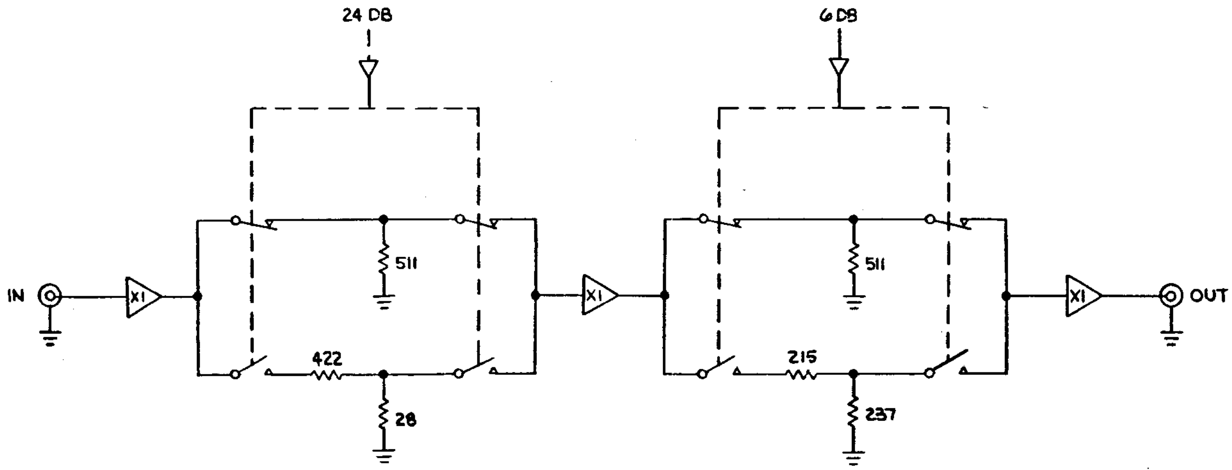

Fig. 4. Programmable Attenuator Circuit

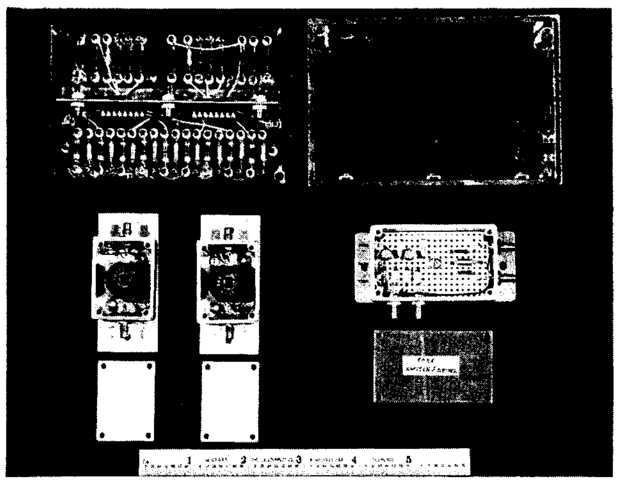

Fig. 5. Programmable Attenuator & RF Transformers

inputs for the 24 db and 6 db sections. Next, mounted on a bracket, are the signal switch integrated circuits and the voltage follower transistors. The signal input and output, and the attenuator resistors are located at the top of the chassis.

CALIBRATION UNIT

The calibration unit shown in Figure 6 consists of an Austron Model 1150 5-megahertz oscillator, a Hewlett-Packard model 355F 120 db programmable attenuator, and an electronic circuit board. The circuit board contains drivers for the solenoids in the programmable attenuator and circuitry to derive the 100 KHz calibration signal from the 5 MHz input.

Four solenoid drivers are required for the 4 sections in the 120 db maximum attenuator. The sections have attenuations of 10 db, 20 db, 30 db, and 60 db. The 100 KHz calibration circuit consists of a divide by 50 circuit and 100 KHz tuned amplifier. The 100 KHz gate signal controls power to the 100 KHz calibration circuit. To verify that the calibration signal is not feeding in to the antenna input of the RF section, measurements are made both with the calibration circuit powered and unpowered during the calibration of the Loran sensor. Also after Loran signal lockup the RF sensor is switched to calibration signal input and the sensor is tested for feedthru from the antenna input to the calibration input.

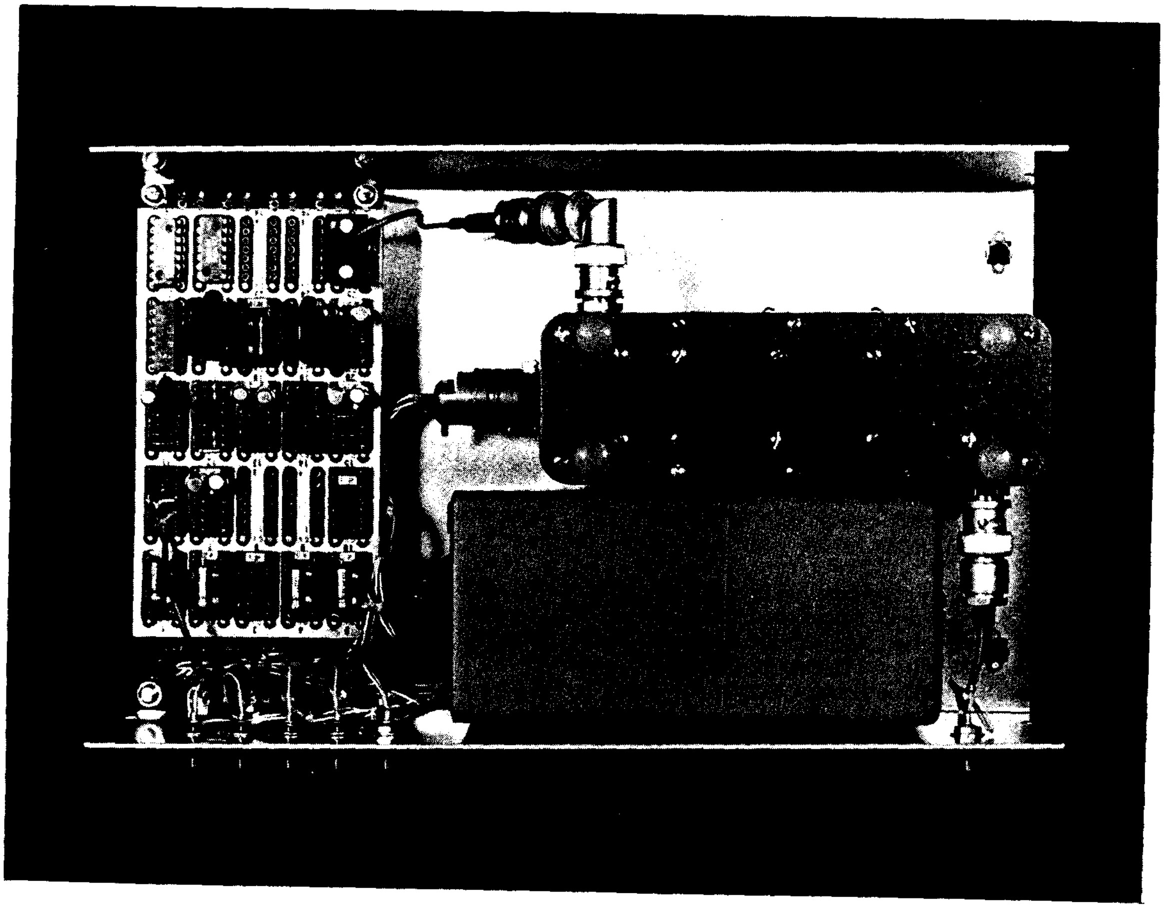

Fig. 6. Calibration Unit

REDUCTION OF INTERFERENCE TO LORAN-C

James P. Van Etten
ITT Avionics Division
390 Washington Avenue
Nutley, New Jersey 07110

ABSTRACT

The Loran-C multipulse transmissions have spectral lines at frequencies determined by the Group Repetition Interval (GRI) and the standard signal phase code pattern. Similarly, the receiver system receives all signals having spectral energy around spectral lines determined by the receiver strobe GRI and the strobe phase code pattern.

Whenever two loran chains with different GRI's have common spectral lines and the receiver strobe phase code pattern responds to these common spectral lines, there will be crossrate interference.

Previous studies have suggested (1) means to eliminate these interference effects by use of different transmitter phase code patterns and GRI selection and (2) methods to reduce the interference by selection of transmitter GRI's within a geographic area.

This paper suggests system means to "eliminate" crossrate interference through use of a unique family of GRI's and retention of the standard phase code pattern for the transmitted signals together with a different strobe phase code pattern in the receiver. Use of this proposal requires no system changes to the existing signal-in-space specification, but does require GRI assignment from a family of acceptable GRI's. This family of acceptable GRI's together with a defined receiver strobe phase code pattern insures that all Loran-C signals, as received, will be mutually orthogonal, thus "eliminating" crossrate interference on a worldwide basis.

This analysis also identifies the multiple frequencies throughout the 60-140 kilohertz band where stable carrier systems of relatively narrow bandwidth might be assigned or reassigned to "eliminate" synchronous CW interference.

INTRODUCTION

Captain W. F. Roland presented a paper[1] at this very technical symposium five years ago (1974) entitled "Loran-C Phase Code and Rate Manipulation for Reduced Cross Chain Interference". Captain Roland concluded that crossrate interference will not occur if the two rates have common prime factors and if one of the two chains has a balanced phase code.

Captain Roland's analysis was performed in the time domain with the aid of a diagram to determine the cross correlation of a crossrate signal with the receiver sampling system for the family of time-alignment possibilities.

Commanders Don Feldman, Paul Pakos and Cy Potts reported[2] upon a similar analysis at this technical symposium the following year (1975). This paper was entitled "On the Analysis and Minimization of Mutual Interference of Loran-C Chains". This analysis was accomplished in the frequency domain; they also concluded that crossrate interference can be practically eliminated by proper choice of phase code and GRI and stated it is possible to construct multi-chain systems in which each chain is essentially impervious to interference from its four nearest neighbors.

Clearly, the basis for a technical solution to crossrate interference had been suggested but selection of phase code and repetition rate to satisfy required criteria was assessed to be a serious matter and one that would identify with a high cost of implementation.

Consequently, these sound technical principles have not been applied; today I would like to extend the concepts presented in these two prior papers to define a systems approach to "eliminate" crossrate interference through use of a unique family of GRI's (all from the standard list of GRI's) and retention of the standard phase code pattern for the transmitted signal. The cost for reassigning GRI's is simply one of user notification and documentation. Receivers able to operate on all rates would require no modification. However, these receivers could be modified to utilize a balanced phase code (e.g., drop certain sampling strobes) and thereby eliminate crossrate interference.

Summary Of Proposed Concept

Master and secondary transmitters would continue to transmit standard Loran-C signals with standard phase code. GRI would be from a unique family of GRI's, all of which have been selected from the standard list of GRI's.

Receivers able to operate on all rates require no modification. However, it is proposed that receivers drop certain strobes such that a special balanced phase code tracking sequence is utilized for tracking (but not for search, etc.).

Figure 1 is a diagram, similar to that presented by Roland(1) which aids in assessing the interference effect of crossrate signals. The Group A and Group B receiver phase code pattern is entered at the top of the figure (in this example, the standard secondary phase code is shown), the Signal Phase Code Pattern (in this example, the Master Group A signal) is shown along the left side of the Group A and Group B elements of the diagram. The signal/receiver phase code correlations are shown in the diagonal matrix. The net crossrate correlation sum for this example is tabulated, assuming that there is one correlation of each signal and each strobe during a GRI crossrate period.

Notice that the net crossrate sum for Group B secondary strobe correlations with master Group A signals is zero because the Group B secondary code is balanced. Also, the net crossrate sum for the Group A secondary strobe correlations with the master Group A signals is + 4 because there is an excess of 4 positive strobes in the Group A secondary code and an excess of 1 positive signal in the Group A master signal (4 x 1 = 4).

Crossrate sum = number of excess strobes of one polarity X number of excess signals of one polarity.

Therefore, if the receiver phase code strobe pattern is balanced, the crossrate sum will be zero if all crossrate positions (every 1000 microseconds or submultiple thereof) are occupied.

Other considerations, such as rejection of delayed sky waves and minimization of crossrate period, also influence selection of the "optimum" balanced phase code.

Receiver Phase Code (for tracking)

Table I lists a number of "balanced" receiver strobe phase codes which might be utilized for tracking. The table also summarizes the pertinent characteristics associated with each phase code.

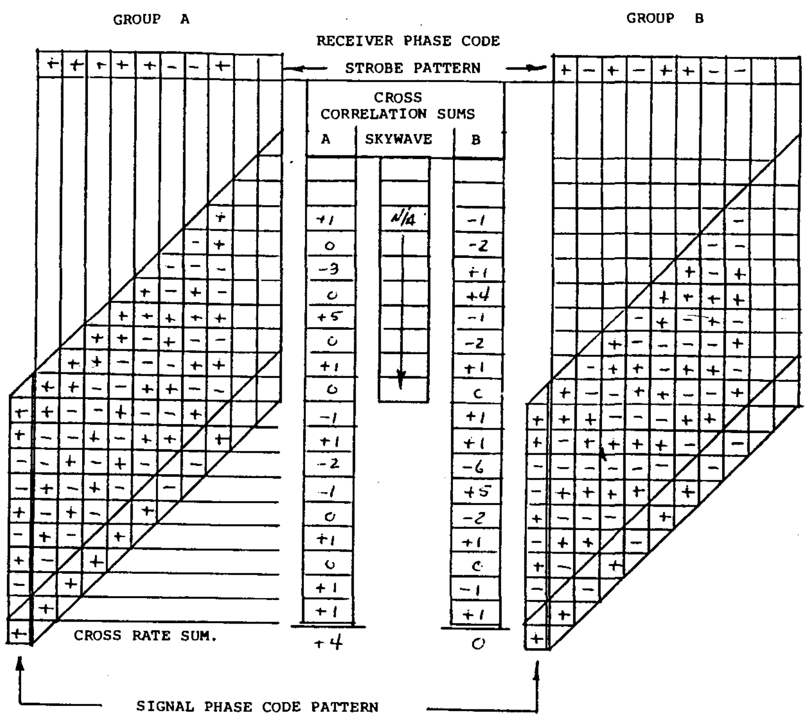

FIGURE 1 - CROSSRATE CORRELATIONS OF MASTER GROUP A SIGNALS AND SECONDARY PHASE CODE STROBES

TABLE I: "BALANCED" RECEIVER STROBE PHASE CODES: PERTINENT CHARACTERISTICS

Code I.D. No.	Signal	Receiver Strobe Phase Code	Phase Code Characteristics				Acceptable GRI's (3) Good/Fair
			Signals Sampled	Δ S/N DB	Delayed SW Protection (microsec.s)	PCF Zeros	
1.	Master	0+-00-+0 0 (1) 0--0+00+ 0	8	-3.0	4500	500N Hz	A,B/C
2.	Master	0+--+-+0 0 (1) 0--00++0 0	10	-2.0	3500	1000N Hz	B/C
3.	Master	++-00-0- + (1) +--00+0+ -	12	-1.25	3500	500N Hz	A,B/C
4.	Master	++--+-+- 0 (1) +---+-++ 0	16	-2.5	3500	1000N Hz	B/C
5.	Master	++--0-0- 0 (2) +--+0+0+ 0	12	-1.25	5500	500N Hz (4)	A/B
6.	Secondary	000++--0 (1) 000-++-0	8	-3.0	3500	500N Hz	A,B/C
7.	Secondary	000++--0 (1) 00+-++--	10	-2.0	2500	1000N Hz	B/C
8.	Secondary	00++0--0 (1) 00+-0+-0	8	-3.0	3500	500N Hz	A,B/C
9.	Secondary	00++0--0 (1) 00+-++--	10	-2.0	2500	1000N Hz	B/C
10.	Secondary	++-++--- (1) +-+-++--	16	-2.5	2500	1000N Hz	B/C
11.	Secondary	0+++00-+ (2) 0-+-00--	10	-2.0	6500	500N Hz (4)	A/B

NOTES:

	Maximum Crossover Period (3) (See table III) List A	List B	List C
(1) Crossrate Cancels over 1 GRI:	5 Sec	10 Sec	20 Sec
(2) Crossrate cancels over 2 GRI's:	10 Sec	20 Sec	40 Sec

(3) GRI's are identified as good if maximum crossover period <10 sec.
GRI's are identified as fair if maximum crossover period <20 sec.
GRI's are unacceptable if maximum crossover period >20 sec.

(4) PCF zeros at 0, 500 Hz, 1000 Hz, etc. for GRI's from List A.
PCF zeros at 0, 1000 Hz, etc. for GRI's from List B.
PCF zeros at 0, 2000 Hz, etc. for GRI's from List C.

Of particular significance is the reduction in S/N ratio resulting from sampling with each code versus sampling all 16 pulses, and the maximum sky wave delay for which full phase code sky wave cancellation is achieved. Other characteristics which will be discussed later are also tabulated.

The master and secondary receiver phase code tracking sequences that have been chosen, for illustration, are as follows:

No. 1	MASTER	0+-00-+0 0 0--0+00+ 0
No. 6	SECONDARY	000++--0 000-++-0

Since only half of the signals are tracked, there is a 3 dB reduction in signal/noise ratio. The master code protects against sky wave interference for sky waves delayed by up to approximately 4500 microseconds; the secondary code protects against sky wave interference for sky waves delayed by up to 3500 microseconds.

These master and secondary receiver phase code tracking sequences have a number of important characteristics. As noted, the signal weighting factors, a_i, are + 1, - 1 or 0 (e.g., for the secondary: $a_1 = a_2 = a_3 = a_8 = 0$; $a_4 = a_5 = +1$; $a_6 = a_7 = -1$; also, $a_9 = a_{10} = a_{11} = a_{16} = 0$; $a_{12} = a_{15} = -1$; $a_{13} = a_{14} = +1$). If we define this phase code time function as pcf (t), there is a corresponding phase code frequency function PCF (ω). PCF (ω) has a number of important characteristics depending upon the particular weighting value for a_i (e.g., + 1, - 1 or 0). These characteristics can be summarized as follows:

A. PCF (ω) has zeros at 0, 1000 Hz, 2000 Hz, etc. if sum of the a's in each group = 0.

$$\sum_{1}^{8} a_i = 0 \quad \text{and} \quad \sum_{9}^{16} a_i = 0$$

B. PCF (ω) has zeros at 0, 500 Hz, 1000 Hz, etc. if the sum of odd a's and the sum of the even a's in each group = 0.

(i.e., $a_1 + a_3 + a_5 + a_7 = a_2 + a_4 + a_6 + a_8 = 0$

and

$a_9 + a_{11} + a_{13} + a_{15} = a_{10} + a_{12} + a_{14} + a_{16} = 0$).

C. PCF (ω) has zeros at 0, 250, 500 Hz, etc. if

$$\left.\begin{array}{l}\text{sum of odd a's} = 0\\ \text{sum of even a's} = 0\end{array}\right\}\ \text{in each odd/even subgroup}$$

(i.e., $a_1 + a_5 = a_3 + a_7 = 0$, $a_2 + a_6 = a_4 + a_8 = 0$, etc.)

If C is satisfied, A and B are satisfied; if B is satisfied, A is satisfied.

The selected master and secondary receiver phase code tracking sequences satisfy B and C above. Therefore, PCF (ω), for codes No. 1 and 6, has zeros at 0, 500 Hz, etc.

Figure 2 is a diagram showing crossrate and delayed sky wave correlations of the master signal and the master phase code receiver strobes for the receiver code proposed. Crossrate sum is zero and sky wave protection is complete for sky wave delays up to 4500 (5000 - pulse width) microseconds.

Similarly, Figure 3 is a diagram showing crossrate and delayed sky wave correlations of the secondary signal and the secondary phase code receiver strobes for the receiver code proposed. Again, crossrate sum is zero and sky wave protection is provided for sky wave delays up to 3500 microseconds.

Transmitter GRI's

Because the selected receiver phase code tracking sequence PCF (ω) has zeros at 0, 500 Hz, 1000 Hz, etc. crossrate sums are zero when crossrate positions are occupied every 2000 microseconds or submultiple thereof (i.e., every 2000 microseconds, every 1000 microseconds, every 500 microseconds, etc.). Crossrate positions are occupied every 2000 microseconds (but not necessarily sequentially) when the maximum common factor in the GRI's is 2000 microseconds; similarly, crossrate positions are occupied every 1000 microseconds when the maximum common factor in the GRI's is 1000 microseconds.

We can identify a set of "orthogonal" group repetition rates such that each group repetition interval is a different prime number multiplied by 2000 microseconds, 1000 microseconds or 500 microseconds.

Table II is a table of pertinent prime numbers.

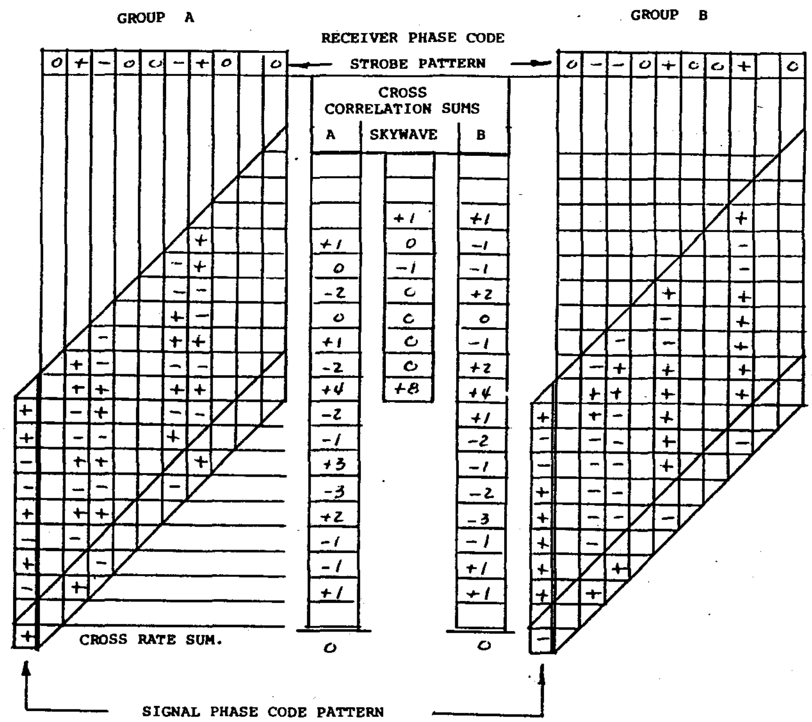

FIGURE 2 - CROSSRATE AND DELAYED SKYWAVE CORRELATION OF MASTER SIGNAL AND MASTER PHASE CODE RECEIVER STROBES

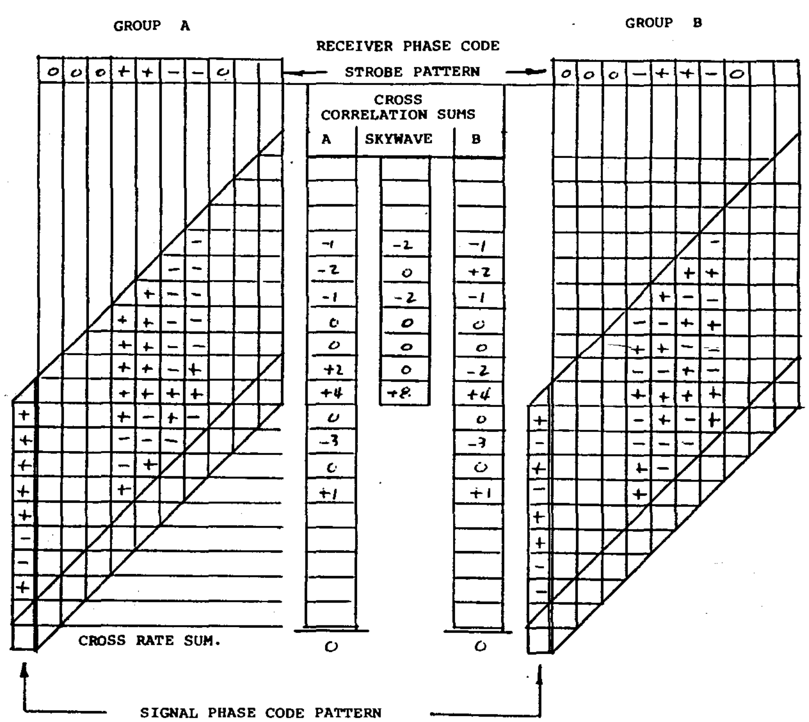

FIGURE 3 - CROSSRATE AND DELAYED SKYWAVE CORRELATIONS OF SECONDARY SIGNAL AND SECONDARY PHASE CODE RECEIVER STROBES

TABLE II

PRIME NUMBERS

2	37	83	149
3	41	89	151
5	43	97	157
7	47	101	163
11	53	103	167
13	59	107	173
17	61	113	179
19	67	127	181
23	71	131	193
29	73	137	197
31	79	139	199

Crossover period between two rates is as follows:

$$\text{Crossover Period} = \frac{(GRI)_1 \times (GRI)_2 \times 10^{-6}}{\text{Maximum Common Factor in GRI's}} \text{ seconds}$$

where GRI's are expressed in microseconds.

To "eliminate" crossrate interference, the crossover period should be short in comparison with the receiver time constant or averaging time. For Loran-C GRI's, the maximum crossover period will be less than 5 seconds if the common factor is greater than 2000 microseconds; the maximum crossover period will be less than 10 seconds, if the common factor is greater than 1000 microseconds; and the maximum crossover period will be less than 20 seconds, if the common factor is greater than 500 microseconds.

Table III is a listing of "orthogonal" rates with crossover periods less than 20 seconds; the 11 rates shown in List A and the 10 rates in List B are preferred because they have crossover periods less than 5 and 10 seconds respectively and are therefore short compared to typical marine receiver tracking loop time constants.

The USCG utilizes both "alternate" and "priority" dual-rate blanking.[3] It would appear that each of these techniques is compatible with this proposed receiver tracking strobe pattern. That is the balanced code of the receiver strobes will reject the unbalanced code of the crossrate signal whether blanked or not.

Reduction Of CW Interference

With phase code function (PCF) zeros at 500 N Hertz for receiver tracking, there are many presently assigned frequencies in the low frequency region which should no longer cause synchronous interference (with its inherent offset disturbance) to Loran-C. For example, NSS at 88 kHz (500 N Hertz, where N = 176) should not cause synchronous effects with the proposed Loran-C receiver tracking sequence regardless of assigned GRI because there is a PCF zero at 88 kHz. The majority of frequency assignments in the low frequency band (between 60 and 140 kHz) are at 350 Hertz intervals[4] (i.e., 60,000 + 350 N Hertz) whereas the PCF zeros are at 500 Hertz intervals (60,000 + 500 N Hertz). Present frequency assignments

TABLE III

"ORTHOGONAL" RATES WITH CROSSOVER PERIODS $<$ 20 SECONDS

BEST RATES LIST A: (crossover period $<$ 5 sec)	GOOD RATES LIST B: (crossover period $<$ 10 sec)	FAIR RATES LIST C: (crossover period $<$ 20 sec)
9800 (7^2 x 2000 µsec)	9700 (97 x 1000 µsec)	9950 (199 x 500 µsec)
		9850 (197 x 500 µsec)
9400 (47 x 2000 µsec)	8900 (89 x 1000 µsec)	9650 (193 x 500 µsec)
		9550 (191 x 500 µsec)
8600 (43 x 2000 µsec)	8300 (83 x 1000 µsec)	9050 (181 x 500 µsec)
		8950 (179 x 500 µsec)
8200 (41 x 2000 µsec)	7900 (79 x 1000 µsec)	8650 (173 x 500 µsec)
		8450 (13^2 x 500 µsec)
7400 (37 x 2000 µsec)	7300 (73 x 1000 µsec)	8350 (167 x 500 µsec)
		8150 (163 x 500 µsec)
6400 (2^5 x 2000 µsec)	7100 (71 x 1000 µsec)	7850 (157 x 500 µsec)
		7550 (151 x 500 µsec)
6200 (31 x 2000 µsec)	6700 (67 x 1000 µsec)	7450 (149 x 500 µsec)
		6950 (139 x 500 µsec)
5800 (29 x 2000 µsec)	6100 (61 x 1000 µsec)	6850 (137 x 500 µsec)
		6550 (131 x 500 µsec)
5400 (3^3 x 2000 µsec)	5900 (59 x 1000 µsec)	6350 (127 x 500 µsec)
		6050 (11^2 x 500 µsec)
5000 (5^2 x 2000 µsec)	5300 (53 x 1000 µsec)	5650 (113 x 500 µsec)
		5450 (109 x 500 µsec)
4600 (23 x 2000 µsec)		5350 (107 x 500 µsec)
		5150 (103 x 500 µsec)
		5050 (101 x 500 µsec)

which are nulled by the PCF zeros are shown in Table IV. Therefore, using this receiver phase code pattern will reduce interference from CW services at these frequency assignments.

TABLE IV

PRESENT LF FREQUENCY ASSIGNMENTS WHICH OCCUR AT ZEROS OF PCF FOR PROPOSED LORAN-C TRACKING FILTER

60 kHz	81.0	102	123
63.50	84.5	105.5	126.5
67.0	88.0	109.0	130.0
70.5	91.5	112.5	133.5
74.0	95.0	116.0	137.0
77.5	98.5	119.5	140.5

On the other hand, if a service at a different assigned frequency interferes with Loran-C it should only be necessary to shift its carrier a small amount to the nearest frequency which is an integer multiple of 500 Hz to reduce the synchronous interference to Loran-C. For instance, NPG at 114.95 kHz might be reassigned to 114.50 kHz or 115.00 kHz to reduce its synchronous interference effect.

Obviously, since other services operating within or near to the Loran-C frequency band have transmission bands which are wide compared to the PCF zeros at 500 N Hertz, there will continue to be non-synchronous interference from these services even after the carrier frequency has been reassigned. This is much less serious, however, since non-synchronous interference causes noise like perturbations whereas synchronous or near-synchronous interference can cause a position-offset type of disturbance that can be large and may go undectected.

SUMMARY

In summary, all Loran-C transmitter chains would be assigned GRI's from Table III with preference given to Lists A and B. List A contains GRI's with a common factor of 2000 microseconds; List B contains GRI's with a common factor of 1000 microseconds. The crossover period of GRI's from List A are less than 5 seconds and from List B less than 10 seconds. List C contains GRI's with crossover periods less than 20 seconds.

To avoid crossrate interference, users would utilize receiver strobe phase code sequences from Table I for the tracking function. Receivers would continue to employ normal practices of phase code selection for the search process. As previously noted, there are a number of possible receiver tracking phase code patterns; several are tabulated on Table I. The "best" code is a tradeoff between a number of factors:

1. The loss in S/N ratio compared with tracking all 16 pulses: Δ S/N in dB.
2. Delayed sky wave protection: protection to maximum delay is preferred; but protection from the effect of delayed sky waves to a delay of 3500 microseconds should be acceptable.
3. Phase Code Function (PCF) zeros at 0, 500 Hz, 1000 Hz are better than at only 0, 1000 Hz, etc. because it permits rate selection with more rapid crossover periods (i.e., GRI's from List A, Table III, are not suitable for codes 2, 4, 7, 9 and 10 because all signals would not be sampled by all strobes during a crossover period and full sampling is a prerequisite to cancellation).
4. Codes 1-4 and 6-10 cancel crossrate interference over one GRI period. Codes 5 and 11 cancel crossrate interference over two GRI periods. Therefore, crossrate cancellation periods for these two codes are twice as long and therefore less acceptable than the aforementioned codes. The GRI's on List C of Table III are unacceptable with codes 5 and 11 due to the extremely long crossover period. (PCF zeros are at 0, 500 Hz, 1000 Hz with GRI's from List A; 0, 1000 Hz, etc. with GRI's from List B; 0, 2000 Hz, etc. with GRI's from List C).
5. Codes 4 and 10 strobe all sixteen signals, but a reversed phase code polarity is utilized on the circled pulses.

On the basis of these tradeoff factors, master receiver tracking codes 1 or 3 are preferred; similarly secondary receiver tracking codes 6 or 8 are preferred.

On the basis of this analysis, it is suggested that all Loran-C GRI assignments be made from the family of acceptable GRI's tabulated on List A and List B of Table III. Also, it is suggested that receiver manufacturers select one of these pairs of balanced phase codes for the receiver tracking function to eliminate crossrate interference while retaining acceptable performance with respect to S/N environment, delayed sky waves and CW interference. Further it should be noted that if these steps are implemented, new means are available (involving small shifts in radio frequency assignments for other services) to reduce the effects of synchronous CW interference.

Finally, I would like to add a small word of caution: This proposal is based totally on analysis and has not been verified either by independent analytical effort or by experiment.

REFERENCES

1. "Loran-C Phase Code and Rate Manipulation for Reduced Cross Chain Interference" by W. F. Roland, WGA Technical Symposium, October, 1974.

2. "On the Analysis and Minimization of Mutual Interference of Loran-C Chains" by D. A. Feldman, P. E. Pakos and C. E. Potts, WGA Technical Symposium, October, 1975.

3. "Specification of the Loran-C Transmitted Signal" U.S. Coast Guard (G-WAN-2/73) dated 17 August 1979.

4. "International Frequency List", published at periodic intervals by l'Union Internationale des Tele'communications, Geneva, Switzerland.

LORAN-C PROPAGATION AND EQUIPMENT TIMING FLUCTUATIONS AND CONDUCTIVITY ESTIMATES OBSERVED IN THE GREAT LAKES REGION

John D. Illgen
Effects Technology, Inc.
5383 Hollister Avenue
Santa Barbara, California 93111

Tony Mason
Marinav Corporation
1140 Morrison Drive
Ottawa, Ontario Canada

Burt Gambill, Jr.
General Electric-TEMPO
816 State Street
Santa Barbara, California 93101

INTRODUCTION

A series of measurements have been completed at sites along radials from Loran-C transmitters through three different areas in the Great Lakes region. Coverage is provided by the newly configured Northeast Coast Loran-C chain. An Accufix transmitter provided Loran-C signals in the Northwestern area near Lake Superior. This paper includes a description of Loran-C propagation and equipment fluctuations observed. Data is presented from approximately 15 measurement sites. The analysis of timing fluctuations will focus on the following:

1. Minor changes in the TDs due to the passage of weather fronts over short and long propagation paths.

2. Magnification of timing fluctuations and local phase adjustments as distance increases from the control monitor.

3. Summary of RMS standard deviation and mean values (data represented for 24 hour period and 2 to 3 week periods).

4. Comparison with West Coast (USA) Loran-C and old East Coast (USA) timing fluctuations.

Additionally, the incremental time of arrival and time difference data obtained in the measurement program were used to obtain conductivity estimates. This portion of the analysis will focus on:

1. Comparison of conductivity values inferred from the data with original estimates from available conductivity maps.

2. Future data collection improvements.

EXPERIMENT CONFIGURATION

Figure 1 shows an outline of the Lakes, the measurement radials, paths to the secondaries for measurements along the radial from Master (Seneca) and initial estimates of the conductivity. The conductivity values were obtained from maps provided by the Telecommunication and Electronic Branch, Department of Transportation, Canada. While it is recognized that these conductivity maps are not for applications where high accuracy is required, they provide the best a priori estimates of expected conductivity variation in the area. Not shown in the figure is the fact that the area is relatively flat except near Caribou.

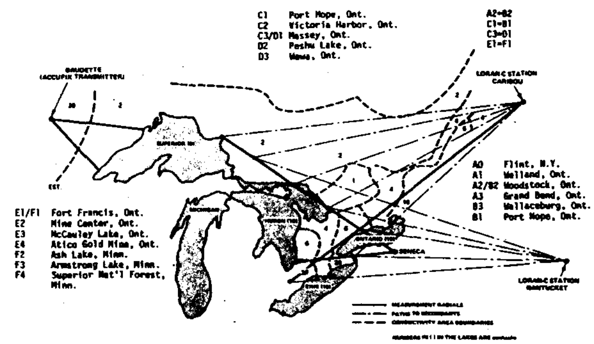

Figure 1. Great Lakes Measurement Area.

EQUIPMENT

Two vans were equipped with Loran-C receiving equipment. One van (mobile) was moved from site to site and the other van (fixed) was used for fixed site operation.

The mobile van contained an Internav M303 MK111 receiver (serial number 1303) interfaced with range-range (Model ρ-ρ3), and signal strength (Model SS4) accessories. Additionally, the M303 receiver was operating off the same cesium standard as a TOA calibrator (Loran-C simulator).

An Austron Model 5000 standard navigator was also in the mobile van. The Austron 5000 consists of antenna, RF amplifier, A/C converter, frequency standard, and clock which are all controlled by a mini-computer.

Two Internav LC-204 receivers were also housed in the mobile van. Both LC-204s and the M303 were operated off a single antenna. A spectrum analyzer and polaroid camera was used to obtain a measure of signal interference.

An MX1112 (Magnavox) NAVSAT receiver was used to obtain site locations. Typically 15 or more valid fixes were obtained. The latitude and longitude for each site (shown later) are the averages of the MX1112 fixes. Standard deviations of the fixes are about one-tenth nautical mile in both latitude and longitude.

The fixed site van contained an M303 MK111 receiver (serial number 1304) interfaced with range-range and signal strength accessories.

A U.S. Coast Guard portable simulator (Model GCF-W-541-A-S) was used to monitor Austron 5000 and M303 receiver operation.

Data from the M303s and Austron 5000 was recorded on tape cassette using a Texas Instrument Silent 733/ASR interfaced with each receiver. In all cases, the data samples are 100 second averages.

PARAMETERS MEASURED

Time Differences, Time of Arrival, signal-to-noise ratios, and signal strengths were measured.

Finally, some points about signal strength measurements:

1. The SS4 accessory to the Internav Loran-C receivers is designed to measure signal strength of a master and two secondaries.

2. The SS4 contains a time shared AGC loop. Attenuation within the loop is controlled to make the output amplitude equal to a standard value (the resulting attenuation in dB's is then a measure of signal strength).

3. Calibration of the SS4 is such that a reading of 60 dB corresponds to a field strength of about 60 dB above 1 microvolt/meter when using a 3-meter whip antenna.

This paper will only present results from the TD and TOA data. References 1 and 9 describe the signal strength and SNR data.

Time difference measurements were made using both receivers at the fixed and mobile monitor site.

TOA was measured using the TOA feature of the Austron 5000 and the range-range accessory of the M303 MK111. The procedure using the TOA equipment was as follows:

1. A site was occupied by the mobile monitor long enough to establish drift rates from the cesium standards and to obtain 15 or more NAVSAT fixes.

2. The TOA receivers maintained phase lock on the transmitter or interest while moving to the next site along the radial.

3. The TOA at the first site was subtracted from the TOA at the next site, accounting for cesium drift, and also secondary transmitter local phase adjustments if required.

This procedure produces a measure of the site to site change in TOA.

MEASUREMENT SITES AND PROCEDURES

Figure 1 illustrates the measurement sites for all radials (A through F). From 2 to 4 sites were occupied by the mobile monitor on each of 6 radials from a transmitter. The fixed monitor van stayed at one site on the radial while the mobile monitor traversed each radial.

A, C, and D were radials from the Seneca, N.Y. 9960 Master transmitter. B was a radial from the Caribou, Maine 9960 W secondary transmitter. E and F were radials from a low-power Accufix transmitter located at Pinewood, Ontario (9960 repetition rate was used).

The TOA and TD measurements were conducted in accordance with the original test plan summary shown in Table 1 (Reference 1). Table 1 shows the site itinerary, signals to be monitored at each site, and calculation and plots produced. In practice, very few deviations were made from the original plan.

Table 1. Test Plan Summary.

LOCATION	AUSTRON AND M303	ρ-ρ	PLOT	REMARKS
A2 (M) (Woodstock)	M,W,Y,C	M,C	MTOA,CTOA,CTD,WTD	Set MTOA at 10 ms. Set CTD at 70 ms.
Go to A0 (Near Seneca)	M,W,Y,C	M,C	MTOA,CTOA,CTD,WTD	Calc MPT(A0 to A2)=MTOA(A2)-MTOA(A0)=CTD(A0) - CTD(A2)
Go to A1 (Near Buffalo)	M,W,Y,C	M,C	MTOA,CTOA,CTD,WTD	Calc MPT(A0 to A1)=MTOA(A1) - MTOA(A0)=CTD(A0) - CTD(A2)
Go to A2 (Woodstock)	M,W,Y,C	M,C	MTOA,CTOA,CTD,WTD	Verify MPT(A0 to A2), Drift Rates, etc.
Go to A2 (Grand Bend)	M,W,Y,C	M,C	MTOA,CTOA,CTD,WTD	Calc MPT(A0 to A3)=MTOA(A3) - MTOA(A0)=CTD(A0) - CTD(A2)
Go to B3 (Wallaceburg)	M,W,Y,C	W,C	WTOA,CTOA,CTD-WTD,WTD	Set ρ-ρ WTOA = Austron WTOA
Go to B2 (Woodstock)	M,W,Y,C	W,C	WTOA,CTOA,CTD-WTD,WTD	Calc WPT(B2 to B3)=WTOA(A3 - WTOA(A2) =[CTD-WTD](B2) - [CTD-WTD](B3)
Go to B1 (Port Hope)	M,W,Y,C	W,C	WTOA,CTOA,CTD-WTD,WTD	Calc WPT(B1 to B3)
Move Fixed Monitor to B1(C1) (Port Hope)	M,W,Y,C	M,C	MTOA,CTOA,CTD,WTD	Set MTOA at 10 ms. Set CTD at 70 ms.
Go to C2 (Victoria Harbor)	M,W,Y,C	M,C	MTOA,CTOA,CTD,WTD	Calc MPT(C1 to C2)=MTOA(C2) - MTOA(C1)=CTD(C1) - CTD(C2)
Go to C3 (Massey)	M,W,Y,C	M,C	MTOA,CTOA,CTD,WTD	Calc MPT(C1 to C3)
Go to C1 (Port Hope)	M,W,Y,C	M,C	MTOA,CTOA,CTD,WTD	Verify Drifts, etc.
Move Fixed and Mobile to C3(D1) (Massey)	M,W,X,C	M,C	MTOA,CTOA,CTD,WTD	Verify MPT(C1 to C3)
Go to D2 (Pesha Lake)	M,W,X,C	M,C	MTOA,CTOA,CTD,WTD	Calc MPT(D1 to D2)
To go D3 (Wawa)	M,W,X,C	M,C	MTOA,CTOA,CTD,WTD	Calc MPT(D1 to D3)
Go to D1 (Massey)	M,W,X,C	M,C	MTOA,CTOA,CTD,WTD	Verify MPT(D1 to D3)
Go to E1	M,A, (accufix)	A,C	ATOA,CTOA,ATD,CTD	Set ATOA to 10 ms. Set CTD to 70 ms. ATOA in Accufix transmitter.
Go to E2	M,A,C	A,C	ATOA,CTOA,ATD,CTD	Calc MPT(E1 to E2)
Go to E3	M,A,C	A,C	ATOA,CTDA,ATD,CTD	Calc MPT(E2 to E3)
Go to E4	M,A,C	A,C	ATOA,CTOA,ATD,CTD	Calc MPT(E3 to E4)
Go to E1,F1	M,A,C	A,C	ATOA,CTOA,ATD,CTD	Verify MPT(E4 to E1)
Go to F2	M,A,C	A,C	ATOA,CTOA,ATD,CTD	Calc MPT(F1 to F2)
Go to F3	M,A,C	A,C	ATOA,CTOA,ATD,CTD	Calc MPT(F2 to F3)
Go to F4	M,A,C	A,C	ATOA,CTOA,ATO,CTD	Calc MPT(F3 to F4)
Go to F1	M,A,C	A,C	ATOA,CTOA,ATO,CTD	Verify MPT(F4 to F1)

The first column in Table 1 shows the position of the mobile monitor. The A refers to the radial between Loran-C station Seneca and measurement site Grand Bend (1 in Figure 1) and the 2 refers to the second site (Woodstock) extending along the radial from the transmitter also depicted in Figure 1. The M303 and Austron 5000 receivers were set up to monitor M (Seneca), W (Caribou), Y (Carolina Beach) or X (Nantucket), C (Calibrator), and A (Accufix transmitter) as presented in the second column of Table 1. As indicated in the table MTOA (Master Time of Arrival) and CTD (Calibrator Time Difference) were set. The mobile unit then proceeded to the site nearest the transmitter (A0 on Figure 1). The master propagation times (denoted as MPT in colume 5 of Table 1) from site A0 to A2 were determined. Then we obtain:

Incremental Master Propagation Time (A0 to A2)

= MTOA(A2)-MTOA(A0)*

= CTD(A0)-CTD(A2)* .

*These propagation times are then corrected for drift rates.

The mobile site was then moved to Buffalo (A1 in Table 1 and Figure 1) and a similar manipulation occurs as mentioned above except we now use A0 (Site nearest Seneca) and A1 (Buffalo). We then returned to A2 (Woodstock) to verify the Master Propagation Times, drift rates, etc. The final site along this radial is Grand Bend (A3 shown in Table 1 and Figure 1).

The description above applies to the other radials. Sites along radial B are designated as B1, B2, and B3 in Figure 1 for Caribou to Wallaceburg, and as C1, C2, C3 for radial C from Seneca to Massey. Figure 1 also shows D sites, ie, radial from Seneca extended to Wawa (sites D1 to D3) and the E and F radials from the Accufix Transmitter.

TIMING FLUCTUATIONS

This section includes a description of the magnitude and source of Loran-C timing fluctuations observed in the measurement area. These timing fluctuations are discussed in terms of propagation (effects of weather fronts and comments on the quality of the data for estimating conductivity) and equipment effects (transmitter and receiver). Data sources used in an attempt to isolate the fluctuations are described.

Chain Control

System accuracy starts with the mean and standard deviation of time difference errors. Standard deviation errors are a function of signal strength, external noise and internal receiver noise. Figure 2 shows typical RMS standard deviations obtained during the measurement period. The data sampling interval is 100 seconds. Additionally, the M303 and Austron 5000 data was edited in accordance with the edit functions (when TD1, TD2 and TD3 exceeds 1 μsec edit limit, 3σ and σ). The edit functions were suppressed for the D radial calculations due to the number of outliers caused by skywave contamination.

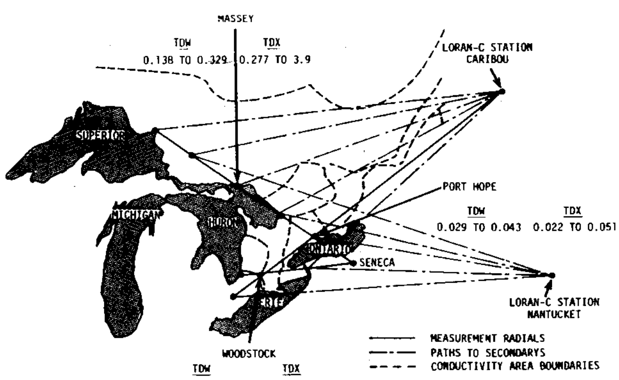

Figure 2. Typical Ranges of RMS Standard Deviations.

M303 TD measurements were conducted at Woodstock (A2) and Grand Bend (A3) simultaneously. Additionally, for the same time frame (days 287 to 289) it is interesting to compare TDW measured at the control site, Cape Elizabeth, Maine.* A standard deviation of 47 nanoseconds was observed at Woodstock (fixed site) for TDW. A larger standard deviation of 63 nanoseconds was observed at Grand Bend (mobile site). Now let's examine Figure 3(a) and (b). Figure 3 (a) (Woodstock) shows several short term (<15 minutes) and long term (>15 minutes) timing fluctuations. Several of these fluctuations have been chosen for comparison with Figure 3 (b). Timing fluctuations in Figure 3(b) (most distant site on radial A from Cape Elizabeth) are magnified considerably as compared to Figure 3(a) (representing a site closer to Cape Elizabeth). A similar trend occurs between TDW measured at Woodstock and Flint (measurement site closest to Cape Elizabeth control monitor). The TD timing fluctuations at Woodstock are about 50 to 100 ns larger than those measured at Flint. Figure 4 shows a segment of the Cape Elizabeth control plot. The center line on the grid is the Control System Time Difference (CSTD). The time difference representing Seneca-Caribou and its long term average are maintained at Cape Elizabeth and are held close as possible to a given reference value (or CSTD).

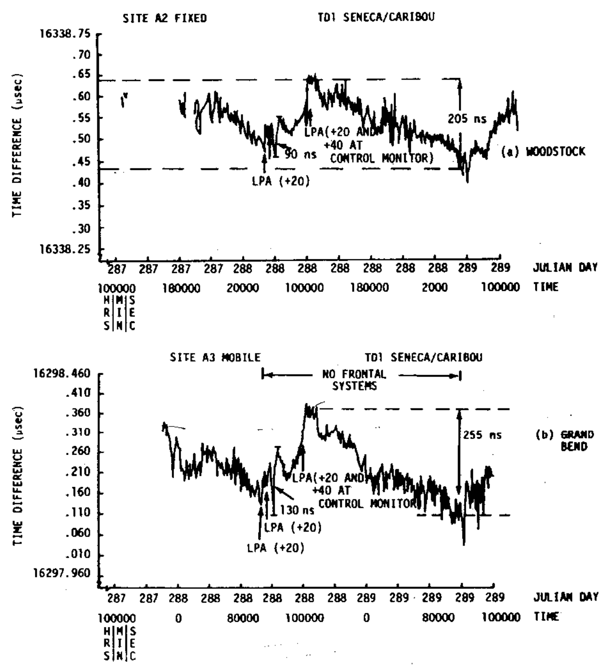

Figure 3. Comparison of TDW at Woodstock (a) and Grand Bend (b).

*Cape Elizabeth, Maine controls Loran-C Transmitter Station Caribou, and Sandy Hook, New Jersey controls Loran-C Transmitter Station Nantucket.

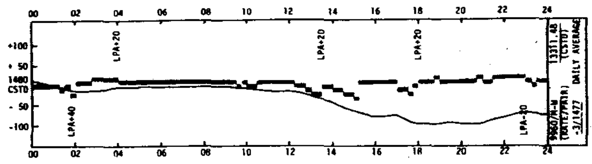

Figure 4. Control Plot for
Cape Elizabeth.

The result of such a policy as illustrated above and borne out in this data collection is that navigation signals in the vicinity of the control monitor are very stable as shown in Reference 2, while in a large portion of the coverage area the signals are more variable. The shortcoming of the current control policy can be demonstrated further. Figure 5 shows the grid of a hypothetical master-secondary pair. The relative spacing of time difference between the LOP's (Lines of Position) is constant. Consider a control monitor located at the position marked SAM (System Area Monitor or Control Monitor) and a User at R. Figure 5 is for normal condition with the TD's from 1 to 17. Now consider the effect of a decrease in propagation velocity over the entire coverage area. This situation is shown in Figure 6 where the TD at SAM has changed from 5 to 4 while the user's TD has increased from 13 to 14. SAM having detected a decrease in his TD inserts an LPA of 1 to bring his TD back on the numbers. The effect of this LPA is shown in Figure 7. SAM's TD has returned to 5 but the user's TD has further increased to 15. Thus, errors due to a change in propagation velocity are well corrected in the vicinity of SAM but magnified in the vicinity of the user.

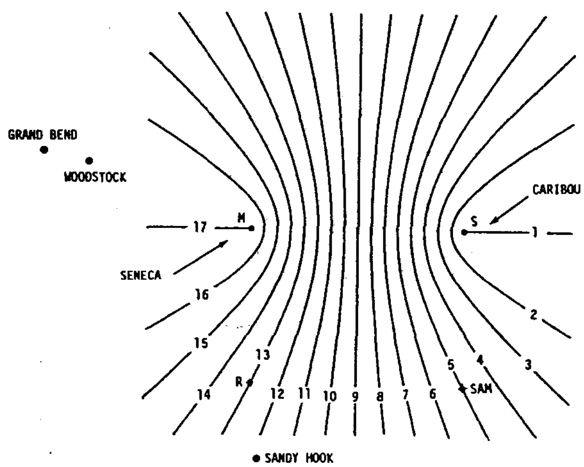

Figure 5. LOP's for a Hypothetical Grid with Constant TD Spacing Under "Normal Conditions".

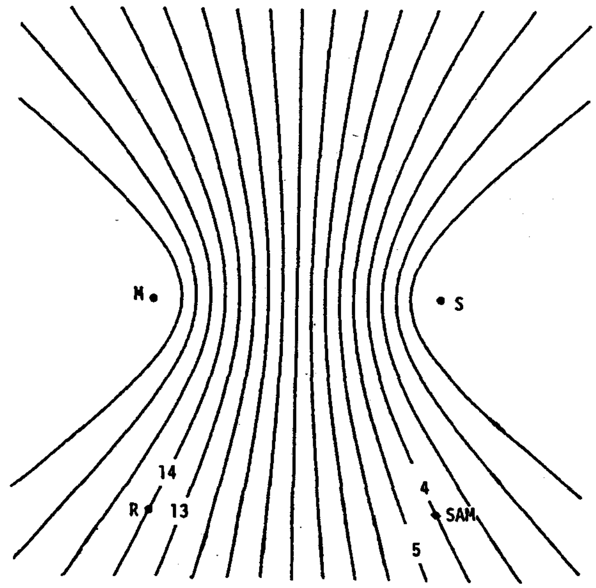

Figure 6. LOP's for a Hypothetical Grid with Constant TD Spacing Showing Decrease in Propagation Velocity.

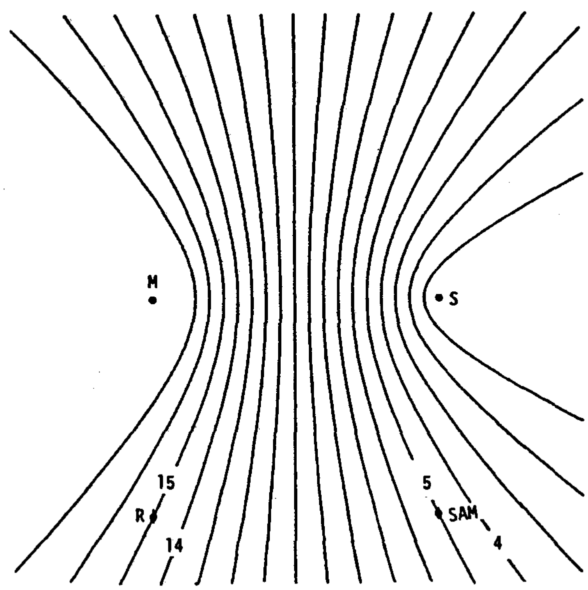

Figure 7. LPA Insert.

Changes in Figure 3 and data collected at Flint have magnified due to the current control policy. Figure 4 shows several instances where LPAs were inserted. These same fluctuations are indicated by the areas in Figure 3. However, Figure 3 shows the timing fluctuations magnified from Woodstock to Grand Bend. Continuous strip chart recordings which show a measure of TDW and TDX at Cape Elizabeth were observed to better define the location of the LPAs for identification on Figure 3. Several other examples have been found in the data (for example, sites A0 to A2).

Weather Front Observations

TD mean values do not exhibit changes of one-half to one microsecond even though 10 weather fronts passed over the paths. It has been stated that the passage of warm or cold fronts across a Loran-C propagation path induce large phase fluctuations (Reference 3). For example the Caribou (Loran-C Secondary Transmitter, W) to Woodstock (fixed site) propagation path is 670 nmi long. From October 2 to October 19, 1978, 10 frontal systems (as mentioned above) crossed the Caribou-Woodstock path. A mixture of cold (about 7) and warm (about 3) fronts passed either parallel or perpendicular to the path. No large (>75 to 100 or more ns) TD shifts attributed to the frontal systems could be observed in the data. TD shifts of about 50 to 100 ns occurred, but did not coincide with weather fronts.

The fixed site data (M303) collected at Port Hope showed stable conditions compared to both TDW and TDX measured at Woodstock. From day 295 to day 301 about 6 weather fronts passed over TDW and TDX. The RMS standard deviations were <50 ns for about 6 days and the mean values change from nearly 0 to 120 ns from one day to another. None of the frontal systems caused large (several hundred nanosecond) fluctuations. Lets follow 2 of the frontal systems. One large cold front was parallel along the entire Caribou-Port Hope propagation path on day 296 at about midnight. The front passed over the path on day 296 at about 0800 followed by another cold front (both were parallel to one another and separated by 100 miles). No significant (>50 ns) effects resulted from these cold fronts. Figure 8 illustrates the above as the cold front crossed TDX.

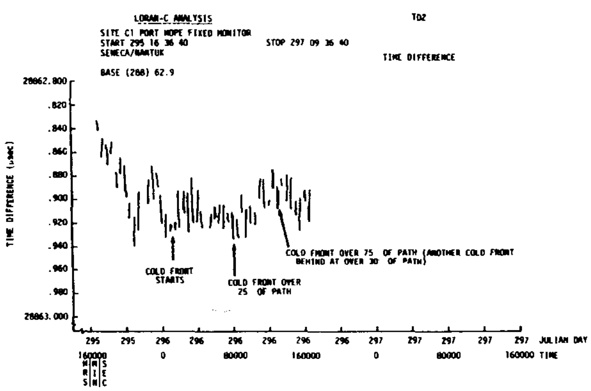

Figure 8. TDX Measured at Port Hope During Passage of Cold Front.

The RMS standard deviations at Massey (D-radial) are very large (.100 to 3.9 µsec). Although frontal systems passed over both TDX and TDW the most severe timing fluctuations occurred during time no frontal systems were present. TDs measured at the Loran-C system control sites (Cape Elizabeth, Maine, and Sandy Hook, New Jersey) show significant (standard deviation of about 60 ns, rms) TD fluctuations. Compensation for these fluctuations are not always made. Short term (10 to 20 minutes) fluctuation of about 100 to 200 nanoseconds have occurred at the controlled sites and compensation has not been made due to current control policy. However, due to the proximity of the measurement area with respect to the control site, and poor signal conditions, compensating for timing fluctuations at the control monitor would not have been of much value. The Loran-C system is probably providing signals in portions of the coastal waters (Atlantic Ocean) which are adequate (and where the necessary compensation for long term timing fluctuations are being made and impact the service area near the control monitors). The measurement sites on the D-radial are 300 to 400 nmi from the Master and about 700 to 900 nmi from Caribou, Nantucket, and Carolina Beach.

Measurement sites, Massey through Wawa, showed large (several hundred nanoseconds to several microseconds) standard deviations. Skywave contamination occurred at Peshu Lake and Wawa and may have influenced the data at Massey. Fortunately, TOAM along this radial was not severely affected and was used to deduce conductivity along this path.

WEST COAST LORAN-C EXPERIMENT

TD and TOA measurements have also been conducted over a large area in the Southern Triad of the West Coast, USA (Reference 2). One of the West Coast experiments was aimed at determining the stability of Loran-C signals. No Loran-C timing fluctuations could be attributed to larger atmospheric changes even though numerous cold and warm weather fronts (parallel and perpendicular to the propagation paths) passed over the various propagation paths. The timing fluctuations were typically below 35 ns (rms, standard deviation) each week for 12 weeks. Propagation fluctuations (rms, standard deviation) were below 20 nanoseconds and masked by receiver noise. Additionally, two receivers (LC204 and BRN-5) were colocated at Ft. Cronkhite (near San Francisco) monitoring TDX and TDY for ten continuous months. The propagation paths ranged between 50 nmi and about 475 nmi. The mean values over the entire 10 months (which included winter when the most severe fronts cross the paths) did not change more than 60 nanoseconds and rms standard deviations were <35 ns. The Ft. Cronkhite measurement site is only 100 miles north of the control monitor (located at Point Pinos, CA). This shows good control when the receiver (user) is near the monitor.

The West Coast results show a very stable (Southern Triad) Loran-C system which was not affected by frontal system passing over the propagation paths. Additionally, the results at Ft. Cronkhite show good control when the user is in the vicinity of the control monitor.

PREVIOUS EXPERIMENTS ON THE EAST COAST

The expectations, based on earlier East Coast data collections, that weather phenomena might change the groundwave phase by as much as .5 to 1 microsecond or more were not borne out in any of the data collected in the Great Lakes region and West Coast.

Diurnal fluctuations measured over a propagation path (573 nmi) between Carolina Beach and Dana have revealed one microsecond changes in the winter and .5 microsecond changes in the summer (Reference 4). The propagation paths in the Great Lakes experiment are as long as the Carolina Beach-Dana path (in both cases typically 550 to 650 nmi). There is a difference in conductivity of about a factor of 2 which should not have significant impact. These large timing fluctuations have been attributed to the passage of frontal systems. Attempts to explain the above changes in Loran-C TDs based on meteorological (ie, changes in temperature occurs the same time as the change in TD) explanations have been attempted by several researchers (References 3, 4, and 5). Even though the Loran-C data compares well with a specific weather parameter (temperature), the fact remains that diurnal TD timing fluctuations are about 4 to 5 times as great as can be explained by simple calculations using expected changes in the index of refraction.

Figure 9 and 10 (taken from Reference 6) show the idealized cold front in terms of N units (variation of the refractive index from unity). In the case of the cold front the variation in N would result in a prediction of a rapid change in the primary phase of 100 ns and a change of -60 ns for secondary phase. This yields a total phase lag increase of 40 ns. From Figure 10 it appears that warm fronts would not produce significant phase changes. It is estimated that shifts in TD's due entirely to atmospheric changes would not exceed 20 ns rms and are probably about 10 ns rms.

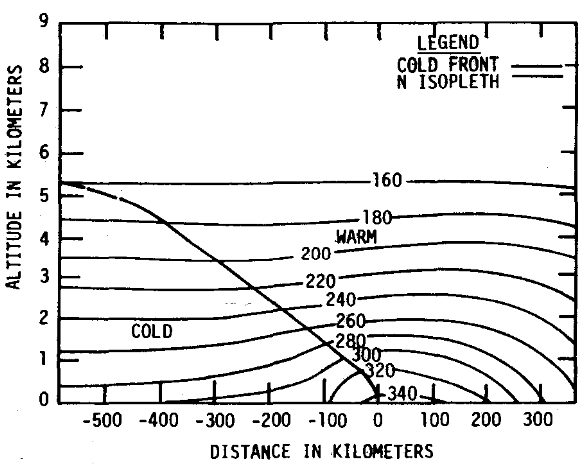

Figure 9. Idealized Cold Front in N Units (from Reference 6).

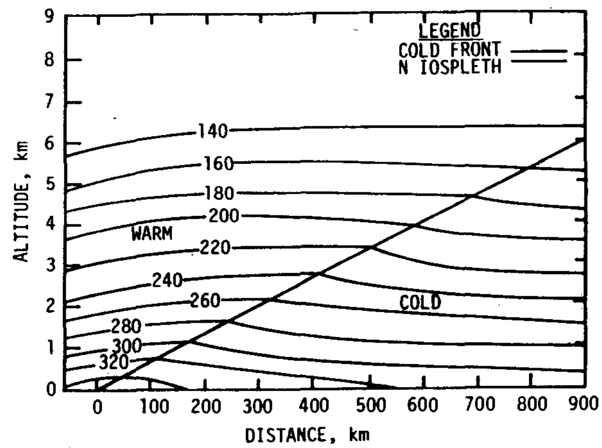

Figure 10. Idealized Warm Front in N Units (from Reference 6).

Results showing large deviations (.5 to 1 μsec) on the "old" East Coast chain could be due to the following:

1. Large propagation errors (.5 to 1 μsec) (refractive index changes) due to the passage of frontal systems. (Using standard propagation theory and results from the Great Lakes and West Coast data collection shows this to be unlikely.)

2. Large propagation errors resulting from a change in surface impedance (ie, frontal systems accompanied by a significant amount of precipitation would cause changes in surface impedance).*

3. Large errors due to older equipment (and system control) which have been interpreted as propagation errors.

4. Large errors due to receiver problems when collecting data.

5. Past experiments (Reference 4) report large TD fluctuations due to atmospheric effects (resulting from the passage of frontal systems) where the measurements were conducted at the transmitting stations may be suspect due to:

a. Local signal is from the near field; the distant signal pickup is from the far field.

b. There might be reradiation from the transmitting antenna into the receiving antenna.

c. There was a hugh signal imbalance, and the probability exists of extraneous pick affecting the phase accuracy.

*This does not explain the diurnal nature of the propagation fluctuations reported in previous experiments.

TIME OF ARRIVAL (TOA) DATA

The TOA taken at sites along 6 radials was used to compute the change in TOA, ΔTOA, between each adjacent pair of mobile measurement locations. The methods and results used in computing the ΔTOAs are presented below.

The mean TOA computed for each measurement site cannot directly be used to calculate ΔTOA's since the atomic clock at the transmitting station and the atomic clock in the receiver at the measurement site are not synchronized nor can perfect synchronization ever be achieved. Although the use of ΔTOAs eliminate a time offset between two clocks, compensation for the frequency offset must be performed. The frequency of atomic clocks is not absolutely stable and changes in a somewhat unpredictable manner. To compensate for the initial frequency offset and subsequent changes in frequency with time, a model of the atomic clock synchronization is needed. The model used is from Reference 10 and has the form

$$T_i(t) = \frac{1}{2} D_i \ (t-t_o)^2 + R_i(t_o) \ (T-t_0) + T_i(t_0) \tag{1}$$

where D_i is the fractional frequency drift per unit time, R_i the frequency offset and $t_i(t_o)$ is the time offset at time t_o. Since we are using ΔTOAs, the $T_i(t_o)$ will not be used. Thus we only need to know D_i and R_i. These quantities are estimated by fitting a least square line to the TOA data at each site. The slope of the line is then R_i for each site. Since they are usually not the same at each site, the difference between these values divided by (T_i-t_o) is an estimate of D_i between each pair of sites. Then using Equation 1 the mean TOA at the first site was calculated at the time when the mean TOA is defined at the second site. The difference of these numbers is the computed ΔTOA.

In some cases there were jumps in the TOA data for a particular site. This case was handled by using two least square fits, one for the data before the jump and the other for the data after the jump. The difference of the two straight line equations at the time of the jump was used as an estimate of the size of the jump. The first fit was used for ΔTOA calculations with the previous site while the second was used with the following site.

In some cases the first measurement site of a particular radial was repeated as the last measurement site. In these cases this return or closure of the measurement process allows one to estimate the error of the ΔTOA measurements and also to correct the computed ΔTOAs. The error is estimated by predicting the TOA for the last measurement (ie, the return to the first site) using all the previous data. This prediction is simply a repeated application of Equation 1 since the ΔTOA should be zero, and any difference in TOAs at the same site should be due to atomic clock synchronization errors. Unfortunately, this was not possible on all the radials which had closure because the receivers lost lock between measurement sites on the A radial (both receivers) and on radial E for the Austron 5000. On the D radial the closure error was 145 ns for the M303 and 200 ns for the Austron 5000 over a 6-day period. This compares somewhat poorly with the error level achieved during the propagation path measurements of the U.S. Coast Guard Loran-C Signal Analysis Project. For the E radial the closure error was 530 ns over an 8-day period for the M303. No closure error was available for the Austron 5000. On the F radial the closure errors were 313 ns for the M303 and 412 ns for the Austron 5000 over an 8-day period. It should be noted that there was a rather large frequency offset between the Austron's atomic clock and the Seneca transmitter's atomic clock. This offset should have been reduced by C-Field adjustments at the beginning of the measurement program. The particularly poor performance on the E radial may have been due to instability of the Accufix transmitting station.

For radials with closure, the ΔTOAs were further corrected by making the assumption that the error builds up uniformly in time over the measurement interval. Thus, a correction was computed for each ΔTOA proportional to the closure error and the time between the TOA measurements.

All the ΔTOA data is given in Reference 9. Additionally, the quantities t_o, $t = t - t_o$, R_i, D_i, and the mean TOA, $\overline{TOA}$, at each site are also given. Where possible, the closure-corrected ΔTOAs were included in Reference 9.

CONDUCTIVITY DEFINITION

The steps required to estimate conductivity from the measured time-of-arrival data are:

1. Compute the measured value of secondary phase correction between segments by subtracting the propagation time in air from the measured differential time of arrival.

2. Define conductivity segments boundaries along the propagation path.

3. Define a best estimate conductivity and a range of conductivity values for each segment.

4. Vary conductivity values in an iterative process, using Millington's technique to compute the secondary phase, and select conductivity values that minimize the RMS difference between measured and predicted secondary phase values.

In performing these steps above, the following limitations and conditions were observed in interpreting the results.

1. The measurements actually provide an estimate of effective conductivity for the entire segment between measurement sites.

2. The predicted solution for segments between measurement sites is coupled to the conductivity value assigned to segments outside the measurement area. The degree of coupling is influenced by the conductivity and position of the segment, ie,

a. Distant high conductivity segments have little influence on the results.

b. Low conductivity segments near the transmitter have maximum influence.

3. Assigned conductivity values for short segments have little influence on the results and thus values for short segments are not well defined.

4. When the number of measurements is less than the number of conductivity areas, the solution is not unique and judgement, based on limitations 1 through 3, must be used to select appropriate solutions.

SECONDARY PHASE AND CONDUCTIVITY RESULTS

The coverage and position location accuracy by Loran-C are determined by the signal amplitude and the predictability of the signal time of arrival in the area of interest. Both amplitude and signal propagation time (phase velocity) depend on the surface impedance along the propagation path between the coverage area and the transmitters. Figures 11 and 12 show the variation of signal attenuation (increased loss above inverse distance loss) and secondary phase (increased phase over primary phase variation in air) as a function of earth conductivity, where high conductivity corresponds to low surface impedance and vice versa. It can be seen from the figures that, in terms of measurable quantities, the phase variation is more sensitive to conductivity variations than amplitude. These phase and amplitude variations with conductivity drove the experiment design, where as described earlier, relative time of arrival measurements were made at points along a radial from a transmitter in the coverage area. The incremental changes in signal arrival time between sites measured along the radials have provided estimates of conductivity along the radial.

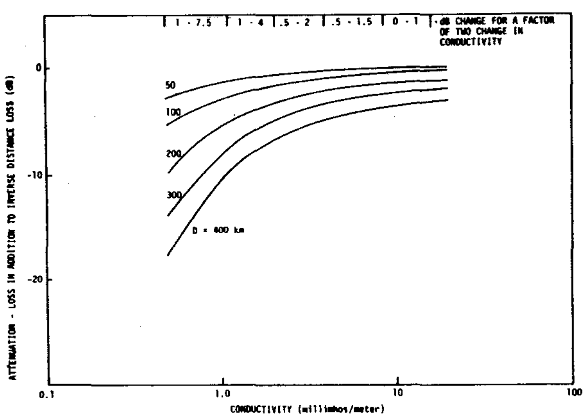

Figure 11. Attenuation Factor as a Function of Surface Conductivity and Distance.

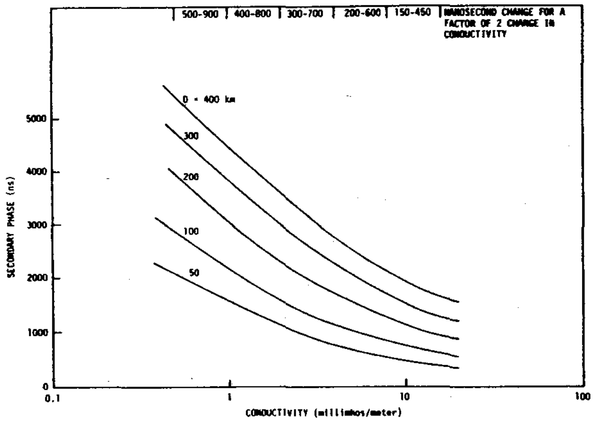

Figure 12. Secondary Phase Variation with Surface Conductivity and Distance.

In addition to time of arrival measurements, which received emphasis in both the experimental and analytical effort, time difference measurements were collected and a selected subset were analyzed to estimate conductivity values in areas not sampled by the time-of-arrival data.

Summary of Conductivity Results

The primary results are estimates of conductivity along the measurement radials. Figure 13 shows the measurement radials and their relationship to the Great Lakes and Loran-C transmitters. Also shown on the figure are boundaries of conductivity areas as defined by original conductivity maps (References 7 and 8) provided by the Canadian Ministry of Transportation. Numbers followed by a letter on the figure are the original estimates of conductivity from the conductivity maps. The letters are used to identify the areas in discussions in this section. Numbers in ☐ are estimates or ranges of conductivity obtained from processing the time-of-arrival data, where it has been assumed that the conductivity for the area is defined by the segment through the area. Numbers in ◇ are estimates of conductivity obtained by processing time difference data along the C radial.

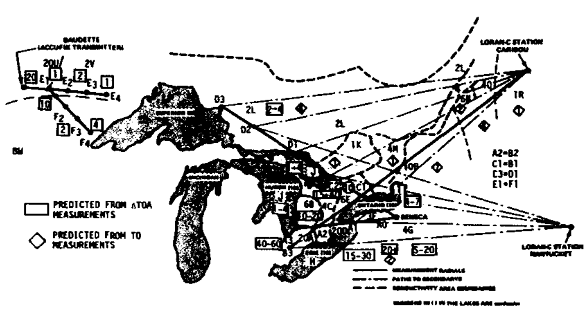

Figure 13. Measurement Radials and Conductivity Areas.

Note that estimated conductivities are shown for each measured segment for the E and F radials. This was done since the original boundary definition did not allow a reasonable match between measured and predicted phase increments.

Alternate presentations of the data are shown in Reference 9. Reference 9 shows plots of conductivity as a function of distance from the transmitter for radials A through D. The original conductivity values and values obtained by processing the data from the two receivers are shown. The range of measured values for the two receiver measurements are also included in Reference 9.

The revised conductivity estimates tend to be the same or slightly higher than the original values. A notable exception is the segment across the Georgian Bay (Lake Huron) where the effective conductivity estimate is lower than the original by a factor of 2 or more.

Accufix Transmitter Performance on Radials E and F

ATOA (Accufix transmitter) did provide reasonable data for determination of conductivity. However, there are segments of instability in the ATOA data.

We will now elaborate on the ATOA and ATD instabilities. The signals from Seneca were weak and skywave contamination is evident when examining the MTOA plots which show large (200 ns) deviations. The Master signal strength was so poor that the M303 at times generated a cycle jump command. This resulted in large deviations in the time difference data. The Accufix station went off the air on occasion. When the Accufix came back on-air the plots show ATD lowered by as much as .5 μsec. The Accufix transmitter on occasions jumped, followed by decreases in ATOA and ATD (200 ns occurred on day 326 at 1515 hours). This condition was later attributed to the generator at the Accufix transmitter site which was slightly overloaded by an electric heater. When the load was removed (day 327) ATOA was remarkably stable.

We have been unable to separate equipment and propagation induced fluctuations because the current configuration was primarily designed to obtain a measure of TOA, TD, and signal strengths along predetermined radials. These parameters have been used to determine conductivity over a wide area of the Great Lakes and to examine large (75 ns or greater) timing fluctuations in accordance with program objectives. As seen in previous paragraphs the data represents an excellent data base to evaluate chain control and future system configurations.

SUMMARY AND CONCLUSIONS

Timing Fluctuations

Loran-C timing fluctuations have been analyzed and results presented. These timing fluctuations are larger than those observed on the West Coast (USA) Loran-C chain (Southern Triad). The location of the system area monitor with respect to the Great Lakes area (and transmitters) and current control policy are the causes. With the addition of the Great Lakes chain improvements in the strengths and stabilities of signals are likely. The extent of these potential improvements have not been evaluated in this study.

The results of the analysis of Loran-C Timing Fluctuations in this effort are:

1. Weather fronts have not changed the groundwave phase 0.5 to 1 microsecond or more, as observed in previous experiments, and changes of 75 to 150 ns as observed could not be conclusively attributed to frontal systems.

2. With the current location of control monitors (or SAM's) in the Northeast chain timing fluctuations and local phase adjustments can be magnified in the Great Lakes region when compensation for timing fluctuations are made at the existing control sites.

3. TDW and TDX are stable and useful in the Eastern portion of the Great Lakes (Radials A, B, and C) but unstable in the Northwestern region (Radials D through F) as expected.

Conductivity Estimates

The incremental time of arrival and time difference data obtained in the measurement programs were useful in obtaining estimates of conductivity in parts of the measurement area. In general, where conductivity estimates are good, the conductivity values inferred from the measurements and analysis were somewhat higher (a factor of 2 to 4) than original estimates from available conductivity maps. One notable exception was a path segment across the Georgian Bay (Lake Huron) where the inferred conductivity value was significantly reduced below the original estimates.

In some cases, estimates of the conductivity values were difficult because of the sparse measurement sites and errors in closure in round trip measurements between widely separated sites.

Future experiments could be improved by obtaining a denser set of measurements to enhance the conductivity analysis. Additionally, the use of a TOA calibrator in conjunction with a receiver located near the transmitter would significantly improve TOA measurement accuracy.

ACKNOWLEDGEMENTS

The authors wish to thank Mr. George Yeaton (Canadian Hydrographic Office), Mr. Eric Schening (Canadian Coast Guard(, Mr. Brynn Davies, Mr. Ray Falkoner (Marinav Corp.), Mr. Pete Wilson (Marinav Corp.) for their valuable assistance and support. Additionally, we greatly appreciate the expert assistance provided by Dr. Larry Nelson (GE-TEMPO) who conducted the TOA data analysis. Appreciation is also extended to Ken Chapman and Bob Goddard (Internav) who assisted Marinav Corp. during the data collection.

REFERENCES

1. Illgen, J.D. and B. Gambill, Jr., Canadian Government Program for Loran-C Coverage in the Great Lakes Region: Analysis Plan, prepared by General Electric-TEMPO, for Marinav Corp., 10 October 1978.

2. Illgen, J.D. and D.A. Feldman, "Loran-C Signal Analysis Experiments, An Overview", September 21, 1978, to be published in the U.S. DOT and Wild Goose Proceedings.

3. Doherty, R.H. and J.R. Johler, "Analysis of Groundwave Temporal Variations in the Loran-C Radio Navigation System," Technical Memorandum 76-222, U.S. Department of Commerce, Office of Telecommunications, June 1976.

4. Frank, R.L. and D.L. McGrew, "Real Time Compensation of Loran-C/D Temporal Variations," Paper presented at Wild Goose Convention, October 2-4, 1974.

5. Doherty, R.H. and J.R. Johler, "Meteorological Influence of Loran-C Ground Wave Propagation," Paper presented at Second Annual Convention, Wild Goose Association, Washington, D.C., September 1973.

6. Bean, B.R. and E.J. Dutton, "Radio Meteorology," National Bureau of Standards, Monograph 02, March 1, 1966.

7. Provisional Ground Conductivity Map, Telecom Munitions and Electronics Branch, Department of Transport, Ohawa, Canada, Sheet 1 (Canada) and Sheet 2 (Ontario).

8. FCC Figure M3 - Estimated Effective Ground Conductivity in the United States.

9. Illgen, J.D., B. Gambill, Jr., and L.W. Nelson, "Loran-C Great Lakes Experiment: Coverage and Accuracy Determination," Vol. 1, March 26, 1979.

10. Blair, Byron E, NBS Monograph 140 - Time and Frequency: Theory and Fundamentals, National Bureau of Standards, U.S. Department of Commerce, May 1974.

A METEOROLOGICAL PREDICTION TECHNIQUE FOR

LORAN-C TEMPORAL VARIATIONS

BY

Robert H. Doherty, CRPL[1]
Lois W. Campbell, ASEC
Suren N. Samaddar, USCG
J. Ralph Johler, CRPL[1]

ABSTRACT

Temporal variations in the propagation time of the Loran-C pulses due to changes in the electrical boundary condition at the surface of the earth, or due to the atmospheric refractive index variations resulting from weather systems, interact with the propagation mechanism for the groundwave and result in degradation of the navigation accuracy for the navigator. Temporal propagation effects vary with geographic locations, climate, seasons, and perhaps on the long term correlation with the sun spot cycle. The magnitude of these effects approach the order of microseconds in anomalous geographic regions, degrading the quality of the navigation service that the transmitting system provides.

Extensive measurements and analysis programs have shown that temporal variations are greater during cold conditions than during warm conditions. Also, when the variations are greatest there is apparently correlation with the surface temperature and refractive index dry term.

The results of this theoretical study demonstrate how the temporal variations are correlated with the refractive index lapse rate. In the winter this lapse rate is functionally related to the surface refractive index dry term. In the summer the effect of the dry term and the wet term remain in an apparent delicate natural balance such that they tend to cancel thus reducing loran fluctuations and destroying the correlation with temperature variations. This theoretical study further demonstrates a technique where surface meterological measurements could be used to predict Loran-C temporal variations.

1. INTRODUCTION

Propagation errors occur in general because the Loran-C signal velocity varies with position. The signal is slowed down by the physical and electrical properties of the earth's air surface interface. These include the impedance or conductivity of the ground, the roughness or terrain variations of the surface, the refractive index of the atmosphere at the surface, and the lapse rate or (rate of change of refractive index with height above the surface).

Spatial (geophysical) variations, of the transmitted signals are primarily influenced by the inhomogeneities of the surface impedance and the variations in the terrain. Temporal (meterological) effects are produced by time changes in these spatial features, and are also influenced by the surface refractive index and the lapse rate of the refractive index of the earth's atmosphere, (which are known to change diurnally and with changing weather conditions).

The spatial propagation error dominates all other errors. However, it is time stable and its effects can be accommodated through grid calibration techniques. Methods involving time difference measurements have been used to warp the Loran-C hyperbolic grid lines to cancel out these fixed spatial dependent errors.

Temporal related propagation effects, although of smaller magnitude, create a more difficult problem for maintaining the most stable grid.

Theoretical studies as early as 1956, Reference (1), anticipated the existence of temporal changes in the phase of the Loran-C signal as a result of natural changes with time in the propagation mechanism of the ground wave. Fortunately the ground wave exhibits a remarkable stability with time. Without such stability, Loran-C precision navigation would not be possible. However, as the loran technical community strives for ever greater accuracy and precision, the small but measurable temporal variations in the ground wave propagation mechanism become more and more important. With a total allowable budget error in the order of 100 nanoseconds, temporal errors should be minimized to about 10 nanoseconds for the combination of propagation, transmitter, and receiver system errors to approach 100 nanoseconds.

2. OBJECTIVE

The primary objective of this propgram is to characterize temporal propagation variations in terms of secondary phase corrections as a function of distance for varying conditions related to meteorological changes. The variable parameters to be considered include the surface refractive index, the vertical lapse factor, and the electrical characteristics of the ground.

Although terrain effect is very important, its effect will not be considered here directly. Generally, irregularities in terrain increase the effective ground surface impedance, x. Therefore, to correctly interpret results presented here, the electrical characteristics of the ground mentioned above should be taken as the effective surface impedance which includes terrain effects.

3. ANALYSIS

3.1 Surface Index of Refraction (η_a)

The index of refraction of air at the surface of the ground grossly affects the primary wave propagation time and is usually designated by the constant value $\eta_a = 1.000338$. This is an average value given in reference (2) and it is certainly not a constant either geographically or temporally. Actually η_a may vary between 1.0002 and 1.0004 or, Reference (3), between 200 and 400 N-units where,

$$N = (\eta_a - 1)\ 10^6$$

Studies in reference (3) show that the secondary phase correction is substantially independent of the surface refractive index. However there is a strong correlation between the surface refractive index and the vertical lapse factor, α, and α strongly affects the secondary phase correction.

3.2 Vertical Lapse Factor (α)

Changes in surface temperature and indeed surface N-factor have been correlated strongly with the vertical lapse factor. Since the vertical lapse factor, which shall be designated as α, enters into the ground wave theory as a parameter, calculations of the ground wave parametric in α can be used to estimate the effects of climate and weather that are observed at the surface of the ground. Of course, if information on N-units aloft are available, these also can be used to deduce the α factor.

The temporal variations associated with weather changes at the surface of the ground have been clearly identified in a number of papers, References (4, 5, 6 and 7). Although strongly correlated with the surface value of index of refraction $\eta(h)$, $h = 0$, these variations can only be explained by the atmospheric vertical lapse variations in the index of refraction, $\eta(h)$, where h is the altitude above the surface.

For Loran-C, α may vary from less than 0.6 to 1.2 or greater and the atmosphere $\eta(h)$ is not necessarily exponential.

3.3 Secondary Phase Correction Calculations

The phase of a Loran-C ground wave signal is usually expressed as

$$\phi \quad \frac{\omega}{c}\eta_a d + \phi_c$$

where $\omega = 2\pi f$; (f being the signal freq Hz)

η_a = refractive index of air at ground level, $\eta_b = \eta(a+h)$, $h = 0$, $= \eta(a)$

c = velocity of light in vacuum

d = transmitter to receiver separation distance

ϕ_c = secondary phase correction, caused by finite impedance and refractive index discontinuities across the boundary along which the signal propagates.

Secondary phase correction can be expressed as:

$$\phi_c \cong (ak_1)^{1/3}\ \alpha^{\ 2/3}\tau_o \left(\frac{d}{a}\right) \qquad (1)$$

where

a = earth radius

k_1 = wave number = $\left(\frac{\omega}{c}\right)\eta_a$

$\tau_o \rightarrow$ is primarily influenced by surface impedance and is derived from the boundary condition at the surface of the ground as the zero'th root of a Riccati differential equation and at 100 kHz is typically ≈ 0.89.

$\alpha \rightarrow$ is associated with the lapse rate of the refractive index. The formula relating α to change of η with height is

$$\alpha = 1 + \frac{a}{\eta_a}\ \frac{d\eta_b}{db} \text{ where } b = a + h \qquad (2)$$

This equation has an alternate representation in terms of measurable atmospheric variables.

$$\alpha = 1 - \left(\frac{a}{h_b}\right)\left(1 - \frac{1}{\eta_a}\right)\left(1 - \frac{N_b}{N_a}\right) \qquad (3)$$

where $N_a = (\eta_a - 1)\ 10^6$

$N_b = (\eta_{h_b} - 1)\ 10^6$

h_b is altitude above the surface

The N-units can be written:

$$N = (\eta_a - 1)10^6 = \frac{77.6}{T}\left[P + \frac{4810e}{T}\right] \qquad (4)$$

together with the hydrostatic equation:

$$\frac{dP}{dh} + \frac{de}{dh} = -10g\rho \qquad (5)$$

where h is in meters

g = the gravitational constant, (cm sec^{-2})

ρ = density of air, (gm cm^{-3})

P = atmospheric pressure [millibars], (kg cm^{-1} sec $^{-2}$)

T = temperature [^{0}Kelvin],

e = partial peassure of water vapor [millibars], (kg cm^{-1} sec^{-2})

The 10 is necessary to make the equation dimensionally correct and dimensionally consistent with Equation 4.

Then,

$$\frac{dN}{dh} = -\left\{\frac{776 \times 1.268}{T} + \frac{77.6}{T^2}\left[P + \frac{962e}{T}\right]\frac{dT}{dh} + \frac{77.6}{T}\left[1 - \frac{4810}{T}\right]\frac{de}{dh}\right\} \quad (6)$$

and

$$\alpha = 1 + \frac{a}{\eta}\frac{d\eta}{dh}$$

where $\frac{a}{\eta} \sim a$ and $a = 6.378\ (10^6)$ meters. Reference 8.

α is evaluated at various temperatures using a unit height of 100 meters and $p = 1013.25$. Thus,

at -15°C $\quad \alpha = .756 - \left\{.0753 + .00277e\right\}\frac{dT}{dh} + .358\frac{de}{dh}$

at 0°C $\quad \alpha = .770 - \left\{.0673 + .00234e\right\}\frac{dT}{dh} + .301\frac{de}{dh}$

at 27°C $\quad \alpha = .791 - \left\{.0557 + .00176e\right\}\frac{dT}{dh} + .264\frac{de}{dh}$

at 35°C $\quad \alpha = .796 - \left\{.0529 + .00163e\right\}\frac{dT}{dh} + .251\frac{de}{dh}$

Also for homogeneous atmosphere* $\frac{de}{dh} = -\frac{mg}{RT}e$ (Reference 9)

at - 15°C $\frac{de}{dh} = -.0132e/100$ m

0°C $\frac{de}{dh} = -.0125e/100$ m

27°C $\frac{de}{dh} = -.0113e/100$ m

35°C $\frac{de}{dh} = -.0111e/100$ m

The temperature lapse rate would be expected to be between the adiabatic lapse rate of -.98°C/100 m and the dew point lapse rate of -.17°C/100 m. Reference (9) gives a derivation of the temperature lapse rate in a homogeneous atmosphere and indicates that for a mixing ratio of 10 mille which corresponds to 16 mb of vapor pressure the temperature lapse rate would be one-half the dry adiabatic value. Therefore, for purposes of evaulating α values, two average temperature lapse rates have been assumed that are: -.98°C/100 m and -.49°C/100 m.

Over land paths the diurnal temperature will vary considerably due to the solar heating and nocturnal cooling of the earth's surface. The extremes of the temperature variations are therefore assumed to reach from -4°C/100 m at noon to +4°C/100 m at midnight. These extremes represent a 8.16 or 4.08 multiplicative factor from the -.49 or -.98°C/100 m lapse rates. The water vapor lapse rate will change proportionally with the temperature lapse rate. Therefore the same multiplicative factors are applied to the $\frac{de}{dh}$ lapse rate as are applied to the $\frac{dT}{dh}$ lapse rate in an attempt to derive α values for winter and summer conditions from the formulas given in the previous section.

Meterological explanation of homogeneous atmosphere.

For Winter Conditions

Moderate Winter 0°C 50% humidity, e = 3mb, $\frac{de}{dh} = -.0375$ mb/100 m

	$\frac{dT}{dh}$		$\frac{de}{dh}$
Average Conditions	- .98°C/100 m	and	-.0375 mb/100 m
Homogeneous Atmosphere	- .49°C/100 m	and	-.0375 mb/100 m
Extreme for Noon	- 4°C/100 m	and	-.153 mb/100 m
	- 4°C/100 m	and	-.306 mb/100 m
Extreme for Midnight	+ 4°C/100 m	and	+.153 mb/100 m
	+ 4°C/100 m	and	+.306 mb/100 m

Extreme Winter - 15°C 50% Humidity e = 1 mb $\frac{de}{dh}$ = -.0132 mb/100 m

Average Conditions	-.98°C/100 m	and	-.0132 mb/100 m
	-.49°C/100 m	and	-.0132 mb/100 m
Extreme for Noon	- 4°C/100 m	and	-.0539 mb/100 m
	- 4°C/100 m	and	-.108 mb/100 m
Extreme for Midnight	+ 4°C/100 m	and	+.0539 mb/100 m
	+ 4°C/100 m	and	+.108 mb/100 m

For Summer Conditions

Moderate Summer 27°C 50% Humidity e = 17.5 mb $\frac{de}{dh} = -.198$ mb/100 m

Average Conditions	-.98°C/100 m	and	-.198 mb/100 m
	-.49°C/100 m	and	-.198 mb/100 m
Extreme for Noon	- 4°C/100 m	and	-.808 mb/100 m
	- 4°C/100 m	and	-1.62 mb/100 m
Extreme for Midnight	+ 4°C/100 m	and	+.808 mb/100 m
	+ 4°C/100 m	and	+ 1.62 mb/100 m

Extreme Summer 35°C High Humidity, e = 42 mb $\frac{de}{dh} = -.466$ mb/100 m

Average Conditions	-.98°C/100 m	and	-.466 mb/100 m
	-.49°C/100 m	and	-.466 mb/100 m

	$\frac{dT}{dh}$		$\frac{de}{dh}$
Extreme Noon	- 4°C/100 m	and	-1.90 mb/100 m
	- 4°C/100 m	and	-3.80 mb/100 m
Extreme Midnight	+ 4°C/100 m	and	+1.90 mb/100 m
	+ 4°C/100 m	and	+3.80 mb/100 m

TABLE 1

α Values Calculated for Various Conditions Listed Above

	$\frac{dT}{dh} = -.49$	$\frac{dT}{dh} = -.98$
Moderate Winter Conditions are T = 0°C		
Average	α = .795	α = .832
Extreme Noon	α = .975	α = 1.02
Extreme Midnight	α = .565	α = .519
Extreme Winter Conditions are T = -15°C		
Average	α = .790	α = .828
Extreme Noon	α = 1.03	α = 1.05
Extreme Midnight	α = .482	α = .463
Moderate Summer Conditions are T = 27°C		
Average	α = .781	α = .823
Extreme Noon	α = .709	α = .924
Extreme Midnight	α = .873	α = .658
Extreme Summer Conditions are T = 35°C		
Average	α = .738	α = .798
Extreme Noon	α = .328	α = .804
Extreme Midnight	α = 1.26	α = .787

The α values listed above can be interpreted as follows:

Winter conditions yield inverse correlation between propagation velocity and temperature as discussed extensively in Reference (5). That is, the lower the temperature the faster the signal travels or the smaller the phase delay for a given path. During summer conditions a negative term associated with $\frac{dT}{dh}$ and a positive term associated with $\frac{de}{dh}$ tend to cancel each other. During average or normal summer conditions these factors tend to offset keeping the alfa value between approximately .75 and .85. Also, under extreme summer conditions a correlation with temperature can average all the way from the winter time inverse correlation to a high temperature summer time direct correlation shown for + 35°C and $\frac{dT}{dh} = -.49$°C/100 m in Table 1.

Finally, these results suggest that Loran-C temporal variations both in the summer and in the winter should be directly predictable from surface measurements. The temperature and humidity lapse rates $\frac{dT}{dh}$ and $\frac{de}{dh}$ will be determined by the surface values of the temperature and humidity along with the history of their variations as observed and recorded in the immediate past. An experimental program to prove this should be initiated.

Another example derived from Reference (9) is shown in Figure 1. The information in Figure 1 and in Table 1 tends to show the same results. Figure 1 shows that when $\frac{de}{dh}$ in mb/100 m is equal to .4 x $\frac{dT}{dh}$ in °C/100 m the changes in the lapse rate $\frac{dN}{dh}$ will tend to cancel. For winter conditions where $\frac{de}{dh} = -.0132$ mb/100 m to -.0375 mb/100 m and $\frac{dT}{dh} = -.49$°C/100 m to -.98°C/100 m the condition for equilibrium is not met, whereas in the summer when $\frac{de}{dh} = -.198$ mb/100 m to -.466 mb/100 m and the $\frac{dT}{dh} = -.49$°C/100 m to -.98°C/100 m the condition for equilibrium is met and actually reversed.

All of this material then tends to support theoretical predictions of Loran-C temporal effects. It supports the observed large winter temporal variations and small summer temporal variations that have been consistently observed on the U.S. East Coast path between Dana, Indiana and Carolina Beach, N.C. An experiment utilizing Loran-C measurements and surface meteorological measurements over paths subject to extreme summer and winter conditions should establish this relationship through data analysis techniques.

4. ANALYTICAL RESULTS

4.1 Atmospheric Temporal Effects

Atmospheric temporal variations are correlated with surface refractive index and the vertical lapse rate of the surface refractive index. The phase temporal variations that are caused by changes in η_a, the surface refractive index, are caused by changes in the primary wave. The primary wave phase, ϕ, is,

$$\phi = \frac{\omega}{c}\eta_a d, \tag{6}$$

and the phase changes associated with the surface refractive index is simply

$$\Delta \eta_a \cdot d,$$

which quantity is in microseconds if d is in kilometers. Therefore, a change from

$$\eta_a = 1.0002 \text{ to } 1.0004,$$

(the maximum η_a variation) over a propagation path with a length of 1000 km would yield a phase change of 0.2 microseconds. Normally the change in average value ($\eta_a = 1.000338$) over a day or during a weather change would be only 40 N-units (N-units = $(\eta_a - 1)\,10^6$). Therefore, the maximum diurnal or weather change effect that would be attributed to changes in η_a for a 1000 km propagation path would be 0.04 microseconds, or 40 nanoseconds. This amount of variation may be nearly typical of the variations observed over a 1000 km propagation path during warm weather. However, in cold weather, the observed variations are typically an order of magnitude or more greater than this value, Reference (5). As a result the overall winter weather variations observed over an approximately 1000 km propagation path have been attributed to changes in the vertical lapse factor.

The theoretically calculated change in ϕ_c between the values of α from .65 to 1.2 is ∿1.5μs for seawater and ∿4.5μs for poor earth at a distance of 1600 km. It should be pointed out that the phase correction (radians) change $\Delta(\phi_c)$ is proportional to a $\Delta(\alpha^{\frac{2}{3}})$ and a Δd, where d is distance. Since $\Delta(\alpha^{\frac{2}{3}})$ is smaller than Δd the effect of $\Delta(\alpha^{\frac{2}{3}})$ on $\Delta(\phi_c)$ is more evident at greater distances. An expanded graph given in Figure 2 clearly illustrates the effects of α at short distances. This shows that $\Delta\phi_c$ is about 0.1μs at 200 km for a change in α from 0.65 to 1.0 over average ground.

The seasonal, diurnal and other temporal variations observed over the 1000 km propagation path between Dana, Indiana and Carolina Beach, Reference (5), can be explained by an α value of 1 ± .02 during the summer months and .70 ± .15 during the winter months. Although the secondary phase correction is least when the temperature is lowest (winter) and corresponding α is lowest, the variation in α is much greater in the winter than in the summer. For this reason, the temporal variations due to changes in the atmosphere are greatest during the winter months in regions which experience cold temperatures.

The signal tends to propagate with a greater average velocity in cold weather. Also, during cold weather, there appears to be a correlation between loran phase and temperature that does not exist during periods of warm temperatures. This phenomenon seems to be related to the water vapor content of the lower atmosphere. The N-units are given by equation (4). Although the first term (dry term) is larger than the wet term (second term), the change of N due to the water vapor alone, i.e., $\partial N/\partial e$ is larger than $\partial N/\partial T$ and $\partial N/\partial P$. For example, for a temperature of 15°C, a pressure of 1013 mb near ground level, and a relative humidity of 60% (i.e., e = 10 mb), one finds $N_{dry} \simeq 273$ units and $N_{wet} \simeq 45$ units. However, $\partial N/\partial e = 4.5/\text{mb}$, $\partial N/\partial T = -1.26/°\text{K}$ and $\partial N/\partial P = 0.27/\text{mb}$. Thus, as the temperature decreases far below the freezing temperature of water, the partial pressure of the water vapor drops significantly. Thus, it would seem that as long as the temperature is above the freezing point of water, the wet term of the refractive index would tend to keep the atmosphere homogeneous over the lower two or three kilometers of altitude. This region is considered to be the most important region for the determination of the α factor which in turn determines the precise value of the secondary phase correction (Reference 8). During the periods of cold temperatures, there is insufficient humidity to

FIGURE 1. ILLUSTRATING ΔN AS A FUNCTION OF Δe AND ΔT AT SELECT VALUES OF TEMPERATURE, T

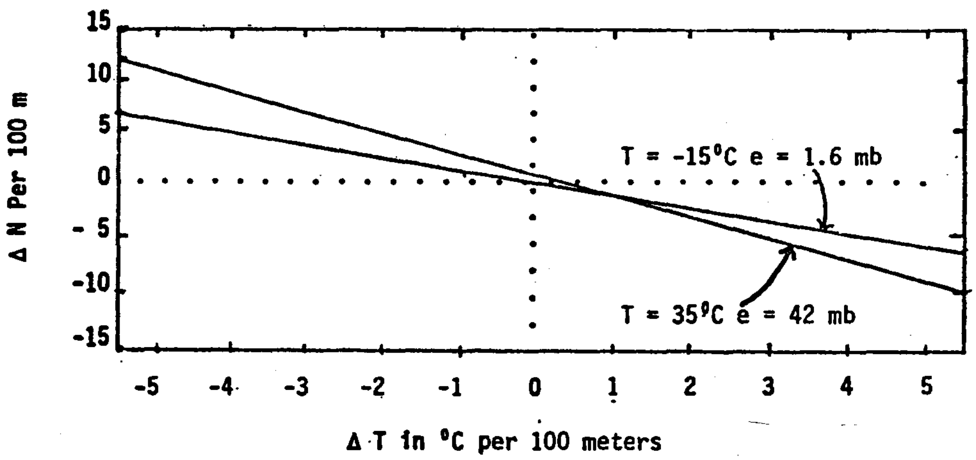

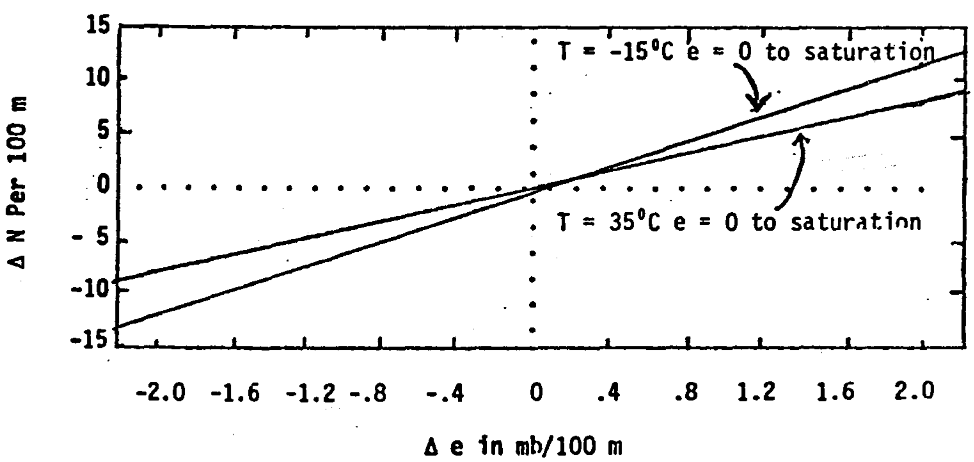

keep the atmosphere homogeneous and the average value of α assumes a value of $\alpha \sim .7$. Then, during extreme cold, the α value varies from $\alpha \sim .5$ to $\alpha \sim 1.0$.

4.2 Temporal Variation of Propagation Time Due to Ground Impedance Changes

Techniques for evaluating the ground impedance in the presence of ground horizons at various depths below the surface have been given, Reference (2). In general, the impedance, x, is a complex number,

$$x = |x| \exp (j \operatorname{Arg} x),$$

and can be constructed from varlues of ground conductivity, σ_1, σ_2, σ_3, ... , dielectric constant, ϵ_1, ϵ_2, ϵ_3, ... , and permeability, μ_1, μ_2, μ_3, ... , for the various ground horizons, provided the electromagnetic boundary conditions between such horizons are applied. Thus, the ground over which the electromagnetic wave propagates is in general nonhomogeneous, not only in the horizontal direction but also in the vertical direction.

The electrical ground conductivity or resistivity at the surface of the ground (i.e., the conductivity of the surface soil horizon) is not always the only important parameter in the determination of the ground surface impedance. The electromagnetic wave penetrates the ground to a considerable depth and in most overland situations one finds that the ground wave is strongly correlated in the space domain with subsurface horizons. Thus, the geologic age and characteristics of the basement

FIGURE 2. ϕ_c vs DISTANCE FOR VERTICAL LAPSE FACTOR (α) OF 1.0 AND 0.65, FOR GROUND IMPEDANCE $x = .033 \exp (j.77620)$

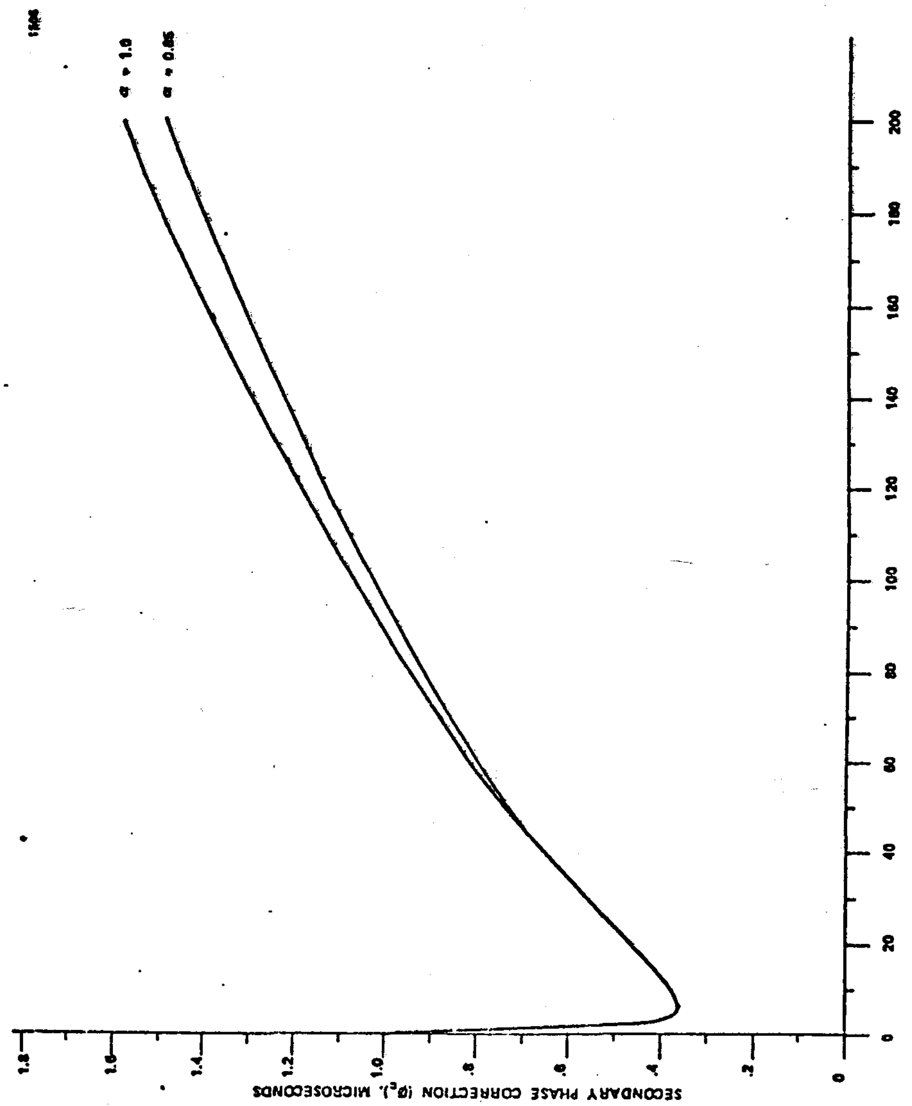

rock influences the surface impedance and hence the secondary phase correction.

The quantity, $|x|$, is normalized to the impedance of free space (= 377 Ohms), a universal constant of nature, and hence is actually dimensionless. One can express the effective ground impedance in terms of conductivity, σ, mhos/m and dielectric constant ε_2 (relative to ε_0 for free space, $\varepsilon = \varepsilon_2\varepsilon_0$). The permeability μ, is of little significance and hence, $\mu = \mu_0 = 4\pi\ (10^{-7})$ Henry m. For sea water, $\sigma = 5$ mhos/m. In the other extreme case, $|x| = .08$, and the corresponding conductivity $\sigma = .00076$. Effective surface conductivities of $\sigma = .0001$ have not, thus far, been observed in the natural ground of the earth at frequencies near 100 kHz. Conceptually it is difficult to visualize real conditions which would contribute to such low values in effective conductivity. In a real sense, the ground surface effective conductivity, as seen by the electromagnetic wave, is an aggregate of conductivities contributed by the various surface and subsurface horizons extending downward to an order of the skin depth for the wave. The contributing biases from subsurface rocks and soils is sufficient so as to maintain physical boundary conditions at the higher minimum values. Physically, it is highly improbable for contributing sources to permit such low values of effective conductivity. Accordingly, values of $\sigma = .0001$ can be considered nonphysical in so far as the propagation of radio waves which are influenced by the ground is concerned.

The impedance concept embraces all naturally occurring ground electrical properties which have been observed for Loran-C frequencies. Hence, this concept provides a compact generalization of physically realizable electrical properties. Here again and in this concept, effective conductivities like $\sigma = .0001$ are nonphysical and have no meaning for Loran-C. In fact, curves, when plotted parametric in σ, other parameters being constant, cross over as the value $\sigma = .0001$ is approached. Hence the secondary phase correction would decrease instead of increasing as a function of the corresponding impedance. To avoid this nonphysical domain of the complex impedance plane at Loran-C frequencies, it is necessary to move the phase angle of the impedance, Arg $x - \pi/4$, to the right in the complex impedance plane. This results, in effect, in a dielectric constant change. Plotted curves then represent physically realizable values of ground impedance at 100 kHz based upon Loran-C observations in the continental United States, Europe, the Mediterranean, and S.E. Asia. These values of impedance can be regarded as effective values over nonhomogeneous and irregular ground. Thus, in lieu of the use of the propagation simulation for nonhomogeneous and irregular ground, Reference (10), practical estimates of Loran-C secondary phase corrections can be obtained from experimental data or experience with the Loran-C system. The experimenter and navigator in the field can gain through experience the ability to estimate the ground impedance for any particular propagation path. Also, the physical realizability of a Loran-C observation can be ascertained immediately, especially when gross errors exist in the data. More subtle errors can also be detected with experience. Thus, proper interpretation of experimental data can present a frame work of theory within which all observations are subject to explanation. However, severely anomalous situations will require the integral equation/full wave for nonhomogeneous and irregular ground, Reference (10).

Consider first the nature of the ground in any particular locality as it changes with depth below the surface of the topmost layer of soil. A geoelectric section of the ground between the surface and some depth below (on the order of skin depth) the surface of the topmost soil horizon should be considered in a ground surface impedance estimate. Thus, the waves entering the ground are exponentially attenuated with depth, or distance through the material that comprises the ground, depending upon the conductivity, σ, or the resistivity, ρ. Although the ground is layered geologically, such layering does not necessarily represent an electrical boundary like much clearer air-ground boundary at the surface of the ground. But the ground does vary in electrical resistivity, ρ_i, dielectric constant, ε_i, and permeability, μ_i, $i = 1, 2, 3 \ldots$, with depth below the surface. Thus, the ground is anisotropic in the sense that the average resistivity, ρ_i, is different in a direction parallel to the surface as compared to the vertical direction below the surface. The basic quantity that can be used in the ground wave theory of propagation in the atmosphere above the surface of the ground is the ground impedance, x. This quantity represents a value of impedance reflected to the ground-air surface by all of the subsurface material of importance. With the aid of this impedance an electrical boundary condition for the ground wave can be established at the physically obvious air-ground interface. The problem is how to model the region below this interface. Experience has shown, Reference (2), that a three layer model is usually the best that can be accomplished in most land areas of the world. There is no theoretical limit concerning the number of layers or geoelectric horizons that can be used. The limit is the availability of geophysical data. Thus, in the three layer model one can use the top soil, the subsoil or hardpan (with water table) and the geologic structure.

This simplified model can be used to illustrate the effect of rainfall upon a desert propagation path between Searchlight, Nevada and Ft. Cronkhite, Calif. An examination of the geophysical data, Reference (2) indicates that under normal dry conditions that are found in the desert, the topmost soil horizon may exhibit great resistivity while the second horizon is saturated by the water table. The bedrock is often very high in resistivity. The topmost horizon comprising only a very few meters is subject to sudden changes during heavy rainfall. If this weather is extensive or covers a large portion of a propagation path, changes due to ground impedance may be observable.

Typical conditions along the propagation path over the desert in terms of a three horizon model is a 6 meter top horizon, $\sigma_1 = .0005$, below which is a water table horizon, $\sigma_2 = .01$, with a thickness of 10 meters. The bedrock can be assigned a conductivity, $\sigma_3 = .0005$. The corresponding value of surface impedance for desert values from Table 2 is:

$$x = 0.0325 \exp\left[j.7646\right]. \quad \text{(case A)}$$

An increase in the conductivity of the geologic structure to a value, $\sigma = .01$ would reflect a ground surface impedance of $x = .0332 \exp\ j1.023$ (case B). This is a highly inductive ground because the phase angle is considerably greater than $\pi/4 = .7854$. Suppose heavy rainfall causes the topmost horizon to reach a conductivity $\sigma = .01$. Then, from Table 2 calculated values we find:

$$x = .0236 \exp\left[j.7810\right] \quad \text{(case C)}$$

Using Arg $x - \pi/4 = -.0044$ radians (case C), $\phi_c \sim 4.20$ µs (microseconds) for a 1000 km propagation path. Also, $x = .033$ using Arg $x - \pi/4 = .238$ (case B) gives, $\phi_c = 5.00$ µs or a change of about 0.80 µs. This is a very great change and it is clearly physically possible but perhaps not probable under normal weather conditions.

The method for calculating x in the three or more horizon model is given in Reference (2). It is interesting to note that a path in the complex impedance plane which follows $|x| = .001$ and Arg $x - \pi/4 = 0$ (or slightly negative) up to a value of $|x| = .03$ and then moves to positive values Arg $x - \pi/4$ up to a value of $1.036 - .7854 = 0.151$ radians at $|x| = .08$ can be used to explain most Loran-C phenomenon in terms of secondary phase correction.

Table 3 gives values of t'_c, where

$$t'_c = \partial t_c/\partial d, \text{ ns/km}$$

parametric in the impedance magnitude, $|x|$, and the vertical lapse factor α. The corresponding values of ground effective conductivity, σ, are also given. These values are derived from calculated numerical values between 1000 and 1800 km.

It is of interest to note that a ± 18% change about $\alpha = .85$, between $\alpha = .70$ and $\alpha = 1.00$ produces a change in secondary phase correction derivative, $\Delta t'_c = .843$ ns/km. Also, a 36% change in the impedance $|x|$, between $|x| = .033$ and .045 produces a change in secondary phase correction derivative, $\Delta t'_c = .812$ ns/km. The corresponding change in the ground effective conductivity parameter, σ, is 47%. It thus appears that the impedance magnitude changes and the α-factor changes produce the same order of magnitude change in secondary phase correction whilst

TABLE 2

GROUND IMPEDANCE FOR THREE HORIZON MODEL

USING TYPICAL VALUES FOR DESERT REGION

CASE	σ_1	σ_2	σ_3	W_1	W_2	$\|x\|$	Arg x
B	.0005	.01	.01	6	10	.03320	1.0230
A	.0005	.01	.0005	6	10	.03254	.7646
	.0005	.01	.0036	6	10	.03312	.9221
	.002	.005	.00054	2	10	.0418	.4939
	.01	.01	.04	1	2	.0154	.9596
	.067	.067	.067	1.5	10	.00914	.7847
C	.01	.01	.01	1	2	.0236	.7810

σ_1 = Conductivity of top most horizon of soil

σ_2 = Conductivity of second soil horizon

σ_3 = Conductivity of bedrock

W_1 = Thickness, meters of top most horizon of soil

W_2 = Thickness, meters of second soil horizon

$W_3 = \infty$

TABLE 3

RATE OF CHANGE IN SECONDARY PHASE CORRECTION, t'_c, NANOSECONDS PER KILOMETER, FOR VARIOUS IMPEDANCE MAGNITUDES, $|x|$ AND VERTICAL LAPSE FACTORS, α.

$\|x\|$	α	t'_c, ns/km	σ	$\|x\|$	α	t'_c, ns/km
.033	.5	3.497	5	.001055	.85	2.233
	.55	3.675	.0557	.01		2.940
	.60	3.844	.0139	.02		3.701
	.65	4.011	.0051	.033		4.608
	.70	4.168	.0027	.045		5.420
	.75	4.320	.00076	.08		6.048
	.80	4.466				
	.85	4.608				
	.90	4.746				
	.95	4.880				
	1.00	5.011				

the conductivity must change about 11% more to produce an equivalent change. Thus, σ is less sensitive than $|x|$ and α in producing phase variations. In this we have assumed the variations are about average values $\alpha = .85$ and/or $|x| = .033$.

5. APPLICATION OF RESULTS

Monitoring and fine-timing adjustments of Loran-C Signals are performed by a System Area Monitor (SAM). The System Area Monitor has receiving equipment, usually located remotely, to continuously monitor the relative timing between master and secondary station transmissions. The SAM's normal function is to issue timing adjustments to the secondary station (Local Phase Adjustment, or LPA) to compensate for any frequency offset of the secondary station oscillator with respect to the master station oscillator, and includes propagation variations. These adjustments maintain the phase (cycle) time-difference at the assigned value (Controlling Standard Time Difference, CSTD).

The total adjustment thus contains both the oscillator drift and the temporal propagation variations along the path between the secondary stations and the SAM. This approach enhances the accuracy of a user navigating with Loran-C in the vicinity of SAM. However, because the Loran-C chains and SAM's are necessarily land-based; the typical user is quite far away, i.e. on the ocean or in harbors or estuaries. Thus the part of the timing adjustment which is attributable to temporal propagation variation over the transmitter-SAM path is not applicable over the transmitter to user path and its inclusion deteriorates the navigation accuracy of the user.

Therefore, if the temporal propagation variations at the SAM can be separated from the total timing variation, it would be possible to make adjustments which would compensate for oscillator drift alone.

6. VALIDATION OF RESULTS

In order to validate the results presented in this report, it is recommended that data be collected at a site (possibly a System Area Monitor) where knowledge of the electrical characteristics of the propagation path is fairly well understood and in a geographic location where extreme weather conditions are experienced (i.e. Northeast United States).

The secondary phase correction can be calculated when the ground impedance, x, (or conductivity and dielectric constant) of the propagation path and the vertical lapse factor of the refractive index, α, are known. If the electrical characteristics of the propagation path are known, then the vertical lapse factor becomes the most important parameter to be derived.

To determine α, knowledge of the temperature, atmospheric pressure and partial pressure of water vapor are needed both on the surface and at an altitude of ~ 2 km. Optimally, both the surface and altitude values should be measured. If only the surface values are available, it will be necessary to develop some typical vertical profiles for various climactic conditions. Also, the immediate history of the surface values of T and e may be used to determine appropriate lapse rates.

Using these measured (or derived) values of α along with continuous recordings of Loran measurements the experimenter can relate α with measured phase changes and validate the results presented in this report. Ideally all measurements should be made throughout the 24 hours of the day and throughout the four seasons of the year.

Figure 3 illustrates in an analytical block

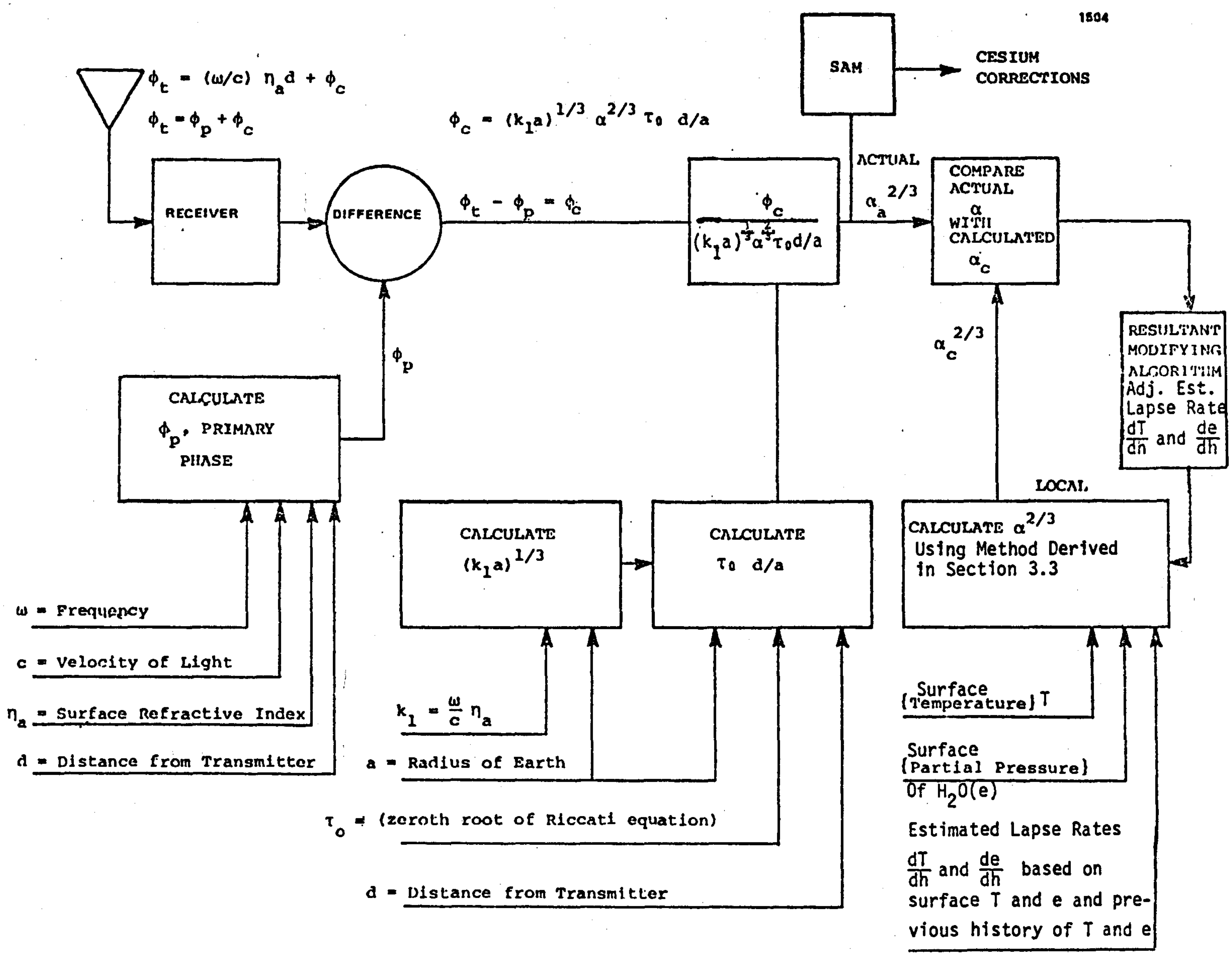

FIGURE 3
VALIDATION ANALYTICAL BLOCK DIAGRAM

diagram a receiver/processor system to compensate for secondary phase error due to meteorological effects such as temperature and pressure.

Although the block diagram shows propagation corrections being sent back to the SAM for cesium corrections, this system could very well be used to improve the fix of a moving platform.

To understand how this system operates, consider the familiar expression for the phase of a low frequency radio signal:

$$\phi = \frac{\omega}{c} \eta_a d + \phi_c$$

This expression has two components, ϕ_p (primary phase) and ϕ_c (secondary phase). ϕ_p is calculated from:

$$\phi_p = \frac{\omega}{c} \eta_a d$$

and ϕ_c is calculated from:

$$\phi_c = (k_1 a)^{1/3} \alpha^{2/3} \tau_o \frac{d}{a}$$

where α is developed from a meterological relationship given by Bremmer, H., 1949:

$$\alpha = 1 + a \times 10^{-6} \frac{dN}{dh}$$

$$\frac{dN}{dh} = -\left[\frac{776 \times 1.268}{T} + \frac{79}{T^2}\left\{p + \frac{9620e}{T}\right\}\frac{dT}{dh} + \frac{79}{T}\left(1 - \frac{4810}{T}\right)\frac{de}{dh}\right]$$

where e = partial pressure of water vapor (millibars)

T = Temperature (°Kelvin)

p = Total pressure in millibars

h = height in meters

The primary phase (ϕ_p) can be calculated in a straightforward way at a fixed SAM site, assuming distance (d) is known accurately. For a moving platform, distance becomes a dependent variable to be calculated, and updated, via the closed loops around the ϕ_p and ϕ_c processes.

It is interesting to note that at a SAM, e and T may not be known over the entire path. However, dT/dh and de/dh are the parameters of importance and they can be determined by the SAM, one point on the path. In a moving vessel, the navigator can acquire e and T not only along some segment of the propagation path, but also as a function of time. Implementation of this system (Figure 3) using these new data may improve his accuracy. The reader is directed to Section 4 for a more detailed explanation of the function of meterological effects upon Loran-C accuracy. It appears that predicted accuracies less than 50 feet may be realizable when processors sense ambient meterological conditions to fully reap the benefits of Loran-C.

7. CONCLUSIONS AND RECOMMENDATIONS

7.1 Conclusions

The most important parameter of concern in temporal variations is the atmospheric vertical lapse factor α. This factor can be related to the surface refractive index η_α, which directly affects the primary wave phase correction. Due to its correlation with the α factor, η_a affects the secondary phase correction only indirectly. Most observable temporal changes due to the atmosphere can be taken into account between values of α = 0.60 to 1.20.

The changes in secondary phase correction are proportional to $\Delta(\alpha^{\frac{2}{3}})$ and Δd (increments of two thirds power of alpha and distance). The effect of $\Delta^{\frac{2}{3}}$ increments is more pronounced at greater distances because of the linear increase with distance as a multiplicative factor. However, the variations in α are greater in the winter months than in the summer. Temporal variations in observations along a 1000 km path in the eastern U.S. can be explained by an α value of 1.0 ± .02 during the summer months and .70 ± .15 during the winter months.

The secondary phase correction is most sensitive to the electrical constants of the ground impedance, x. Values of the magnitude of the impedance range between $|x|$ = 0.001055 for sea water to $|x|$ = .08 for typical areas of the continental United States, Europe and parts of Asia. The latter value of impedance is inductive in nature and corresponds to a conductivity, σ = .00076 mhos/m with an accordingly adjusted value of dielectric constant. Temporal variations can also occur due to a change in the impedance of the ground due to precipitation. Although, as described in the example described in Section 4, a change of 0.8 μs is theoretically physically possible, it is not considered probable under normal weather conditions.

REFERENCES

1. Johler, J. R., Kellar, W. J., Walters, L. C., "Phase of the Low Radio Frequency Ground Wave," NBS Circular 573, 1956.
2. Johler, J. R., "Geophysical and Geological Data Base Evaluation for Loran-C Ground Wave Propagation Medium," CRPL$_i$ Report 78-9, 1978.
3. Johler, J. R., R. H. Doherty, "Temporal Effects of Natural Origin in Loran-C Ground Wave Propagation," CRPL$_i$ Report 79-1,5/1/79.
4. Samaddar, S. N., "The Theory of Loran-C Wave Propagation -- a Review," (U.S. Coast Guard, G-DOE-4, TP54, Washington, D.C. 20590; presented at 1978 Helsinki Conference of URSI; to be published).
5. Doherty, R. H. and J. R. Johler "Meteorological Infleunces on Loran-C Ground Wave Propagation," Journ. of Atm. and Terr. Phys. 37, 117 to 1124, 1979.
6. Dean, W. N., "Diurnal Variations in Loran-C Groundwave Propagation," (Magnavox Government and Industrial Electronics Co., Fort Wayne, Indiana), 1978.

7. Bean, B. R. and G. J. Dutton, Radio Meteorology, NBS Monograph 92, (Suptd. of Doc., U.S. Gov. Print. Off., Washington, D.C. 20402), 1966.

8. Samaddar, S. N., "Weather Effect on Loran-C Propagation," U.S. Coast Guard (to be published), 1979.

9. Craig, R. A., I. Katz, R. B. Montgomery and P. J. Rubenstein, "Meteorology of the Refractive Problem," Chap. 3 of Radiation Lab Series, Vol. 13, Propagation of Short Radio Waves, McGraw Hill, Edited by D. E. Kerr, 1951.

10. Johler, J. R., "Loran-C Ground Wave Secondary Phase Corrections Over Nonhomogeneous and Irregular Ground Using Transient Signal Propagation Techniques," CRPL; Report 78-12, (U.S. Coast Guard Contract DOT-CG-842923A, U.S. Coast Guard Headquarters, Washington, D.C. 20590; Prepared by: Colorado Research and Prediction Laboratory, Inc.) 1979.

PRELIMINARY STABILITY ANALYSIS OF THE ST. MARYS RIVER MINI-CHAIN

by

LT David L. Olsen
CWO Charles E. Isgett

Office of Research and Development
U.S. Coast Guard Headquarters
Washington, D.C. 20593

Temporal instabilities on the order of several hundred nanoseconds were measured over the mini-chain's service area between Fall 1977 and Spring 1978. These instabilities, if true, could render the mini-chain unusable for precision navigation on the St. Marys River. A careful recollection effort was deemed necessary to verify the chain's performance and to definitively judge its navigation capabilities. In addition, a methodology is desired for establishing the stability of Loran-C signals in the general harbor and harbor entrance environment. This methodology is being investigated using the mini-chain.

A one year in-depth study of the mini-chain's stability has begun. The major preparations involved the creation of three fixed monitor sites plus the improve- ment of equipment and staffing at the monitor-control station. Time differences are recorded around the clock at the three new sites and at several transmitter stations. Data collected between February and April this year demonstrated a worst case variation of approximately 200 nanoseconds. This period included not only environmental changes but also various refinements in the equipment. These data cannot be considered to be the final measure of the mini-chain's perfor- mance, but are nonetheless informative.

The time difference data is being analyzed by a rather simple model which separates variations into uniform propagation effects, local errors and control errors. The propagation component extracted from the preliminary data exhibits a high correlation with temperature, which can be attributed primarily to the vertical lapse rate of the index of refraction. The model bounds the physical effects which cannot be improved upon through equipment or procedural changes.

* * * * * * *

Biographical Sketch of LT Olsen

Lieutenant Olsen has been involved with the Loran-C navigation system since the start of his Coast Guard career in 1971. He spent his first tour of duty at the Coast Guard's Electronics Engineering Center in Wildwood, New Jersey, where he worked on the automation of Loran-C monitor and control equipment. Since 1975, Lt. Olsen has been assigned to the Office of Research and Development at Coast Guard Headquarters where he has been responsible for the development of Loran-C user equipment for precision navigation.

Lieutenant Olsen holds Bachelor and Master of Science degrees in Electrical Engineering from Iowa State University at Ames and the University of Illinois at Urbana. He is a member of the Wild Goose Association and the Institute of Navigation.

Biographical Sketch of CWO Isgett

Chief Warrant Officer Isgett is new in the field of Loran-C navigation systems. He has served as a project officer for the St. Marys River grid stability study since completing the Loran-C Engineering Course at the Coast Guard Academy in 1978. His project responsibilities have included site selection and equipment installation, plus writing programs to analyze the collected time difference measurements.

INTRODUCTION

Precise position determination with Loran-C depends on the existence of a stable, repeatable time difference (TD) grid. Grid stability analysis, together with the development of user equipment and TD surveying techniques, constitute the Coast Guard's three-pronged approach to harbor and harbor entrance (HHE) navigation. The Coast Guard's signal stability measurement program is presently concentrating on the St. Marys River mini-chain.

Data was first collected over the mini-chain's service area between fall 1977 and spring 1978 as input to the design and calibration of a grid prediction algorithm.[1] TD variations at several sites were unusually large, with an average of 300 nanoseconds and a maximum of 850 nanoseconds.[2] These instabilities, if true, could render the mini-chain unusable for precision navigation on the St. Marys River. Although reasonable care was taken in performing the measurements, the data remained suspect due to the equipment and methodology used. A careful recollection effort was deemed necessary to verify the chain's performance and to definitively judge its navigation capabilities.

PREPARATIONS

Preparations for a one year in-depth study of the mini-chain's stability were completed in early May 1979. The major tasks involved the creation of three fixed monitor sites plus the improvement of equipment and staffing at the System Area Monitor (SAM) station. Figure 1 shows the layout of the chain.

Fixed Monitor Sites

The new monitor sites are on the south end of the river at DeTour Village, mid-river at Dunbar Forest, and at Point Iroquois near the river's northern end. Each site has a 35-foot whip antenna with a groundplane and multicoupler. DeTour (Figure 2) and Dunbar are equipped with a Magnavox AN/BRN-5 receiver plus an Internav LC-204 receiver. Point Iroquois (Figure 3) has two LC-204 receivers.

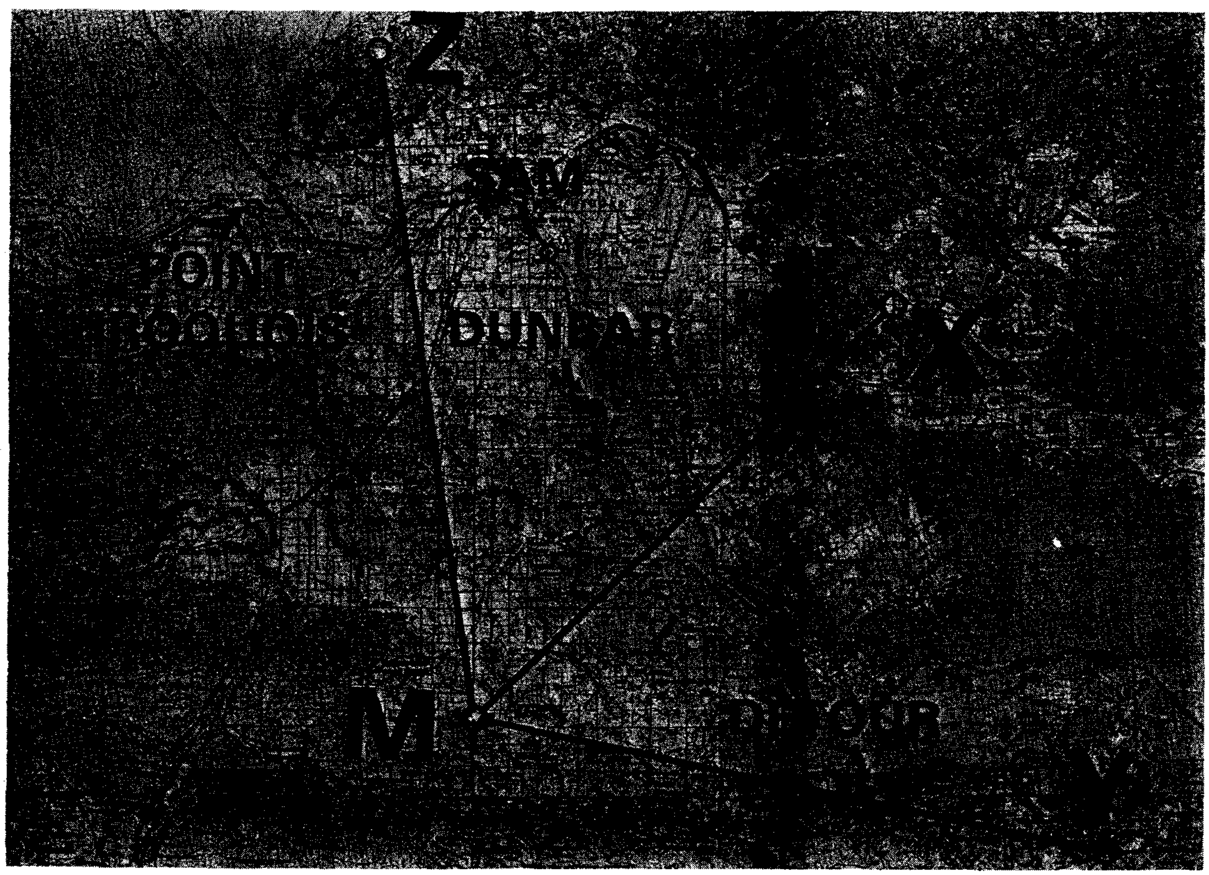

Figure 1. Layout of Mini-Chain with Reconfigured M-X

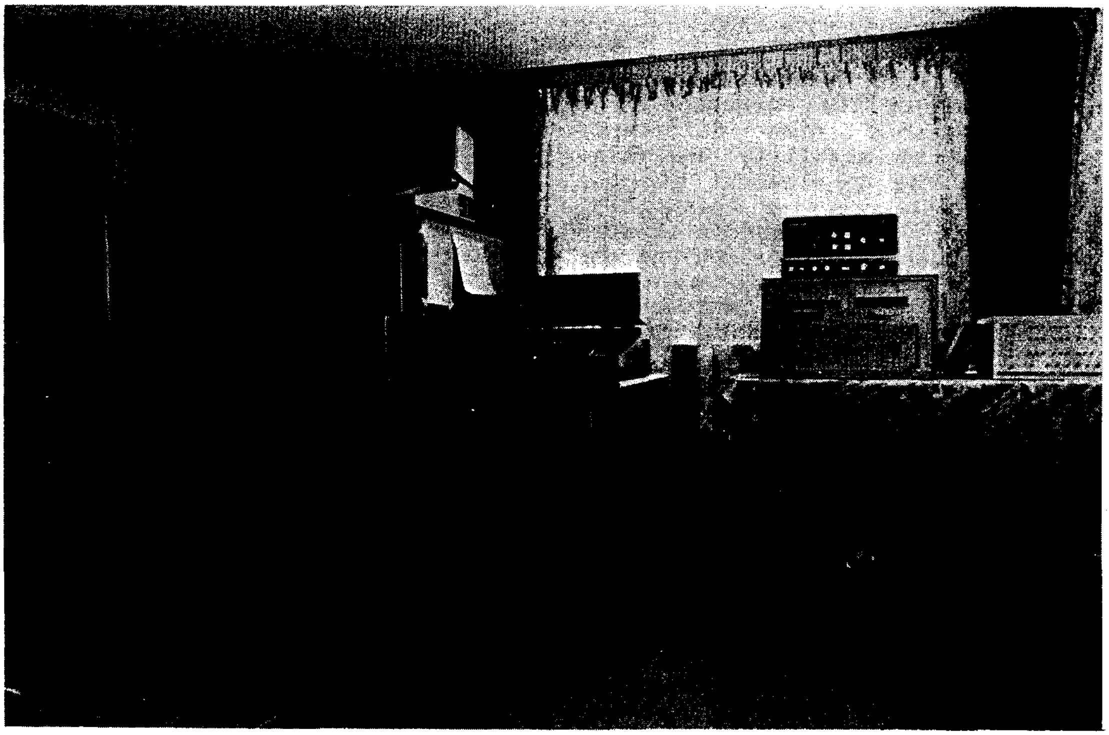

Figure 2. DeTour Village Monitor

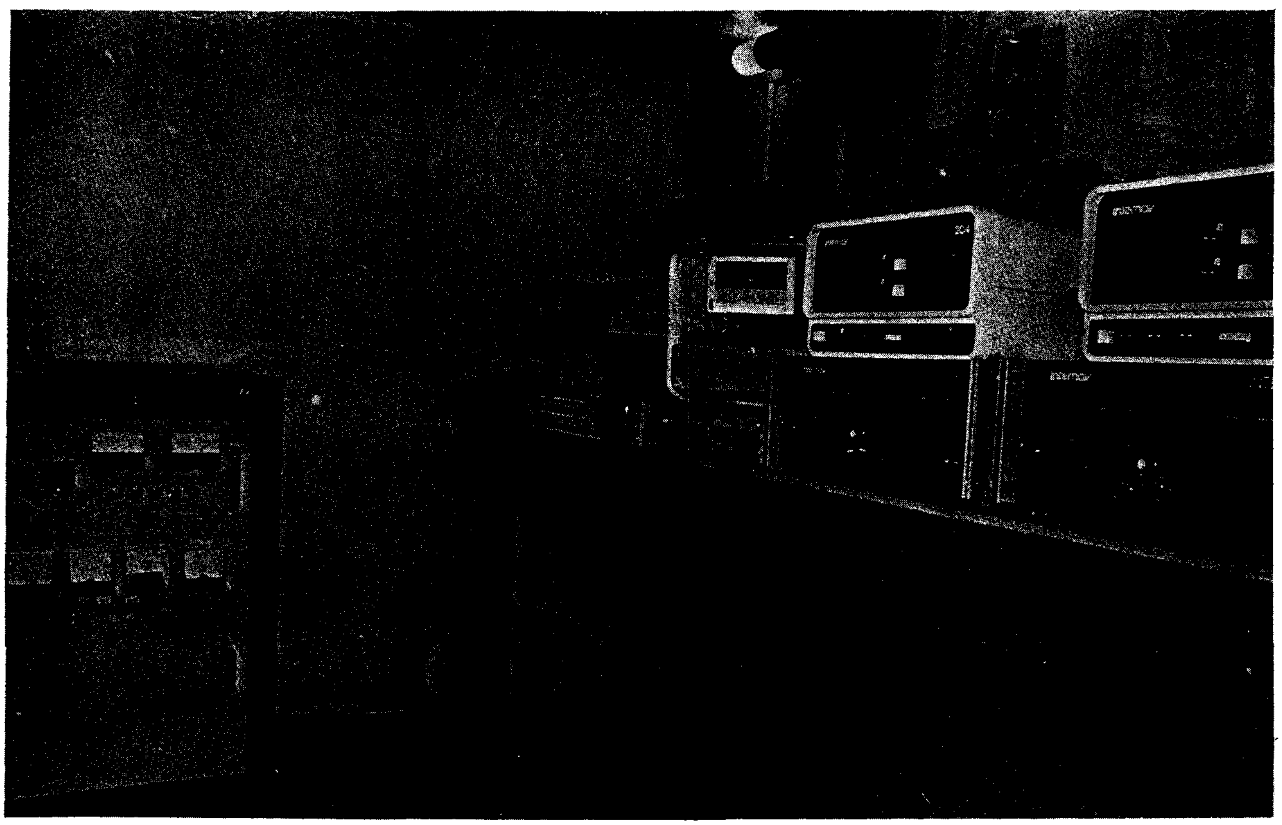

Figure 3. Point Iroquois Monitor

This setup enables each site to monitor all three baselines.

System Area Monitor

Figure 4 shows the SAM site, which has been converted to a Coast Guard standard suite. Control had previously been achieved using an Internav Model 303 monitor receiver, a short whip antenna, and an early prototype CALOC (Calculator Assisted Loran Controller) system. Since 4 May 1979, control has been performed using the 35-foot whip antenna and Austron 5000-CALOC system that is becoming standard equipment for long-baseline Loran-C chains. The mini-chain's group repetition interval was slowed from 4930 to 5930 to satisfy the Austron 5000's processing time requirements.

Chain Reconfiguration

The final step in preparation for the stability study was accomplished on 9 May 1979 when the Master and Xray station designations were interchanged. The switch was made to improve Master station availability. Prime power failures have been more frequent at the Gordon Lake, Canada site than at the Pickford, Michigan site. Power failures are significant since the transmitters have no emergency generators for backup. Also, repairs can be effected more quickly at the Pickford site due to the shorter travel times involved.

PRELIMINARY STABILITY ANALYSIS

The basic analysis relies upon one hour averages, termed the System Samples, collected at midday and midnight. The initial analysis period includes not only environmental changes, but also the above-mentioned refinements in the monitor and control equipment. The data cannot be considered the final measure of the mini-chain's performance, but are nonetheless informative. Figure 5 shows the midday TD fluctuations for one baseline at the three monitor sites. The worst case variation is approximately 180 nanoseconds.

Variations Model

The TD data has been analyzed by a rather simple yet elegant model:

$$\hat{Z} = \hat{A} \times \begin{bmatrix} \Delta TD \\ \hat{C} \end{bmatrix} + \hat{\varepsilon} \qquad (1)$$

where Z is the observation matrix containing the three TD records at each of the three monitor sites, A is

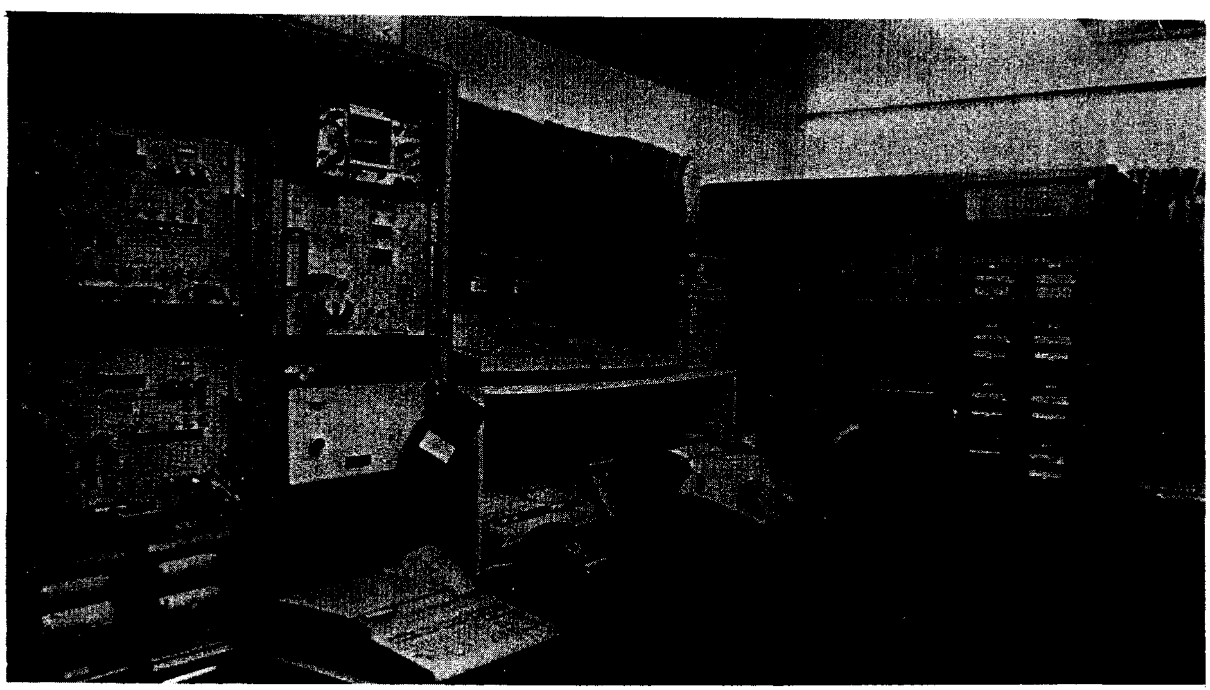

Figure 4. System Area Monitor

the transformation or geometry matrix describing the position of each site with respect to the baselines and the control station, ΔTD is a uniform change in propagation velocity, C is the common error matrix containing variations seen only by and corrected by the control station; and ε is the matrix containing local errors, unique to each site. The common variations are erroneous in the sense that no other site detected the changes that were compensated by the resulting transmitter timing adjustments. Any non-uniform propagation effects will be included in the local error terms. The least squares solution to the model is:

$$\begin{bmatrix} \Delta TD \\ \hat{C} \end{bmatrix} = \left[\hat{A}^T \hat{A}\right]^{-1} \hat{A}^T \hat{Z} \qquad (2)$$

Table 1 lists the common control errors extracted from the data for the periods before and after the chain reconfiguration and monitor station upgrade. Considerable improvement can be seen in the second set of numbers.

Figure 6 shows the uniform velocity of propagation effects extracted from the data, in units of nanoseconds per kilometer of baseline length. The propagation component is extracted as an estimate, based upon how each site would react to the postulated uniform propagation change. Such a change is expected to be primarily caused by temperature affecting the vertical

Table 1. Common Control Errors

	Nanoseconds (RMS)		
	C_x	C_y	C_z
22 Feb-8 May 1979	46	18	28
11 May-24 Sep 1979	7	7	6

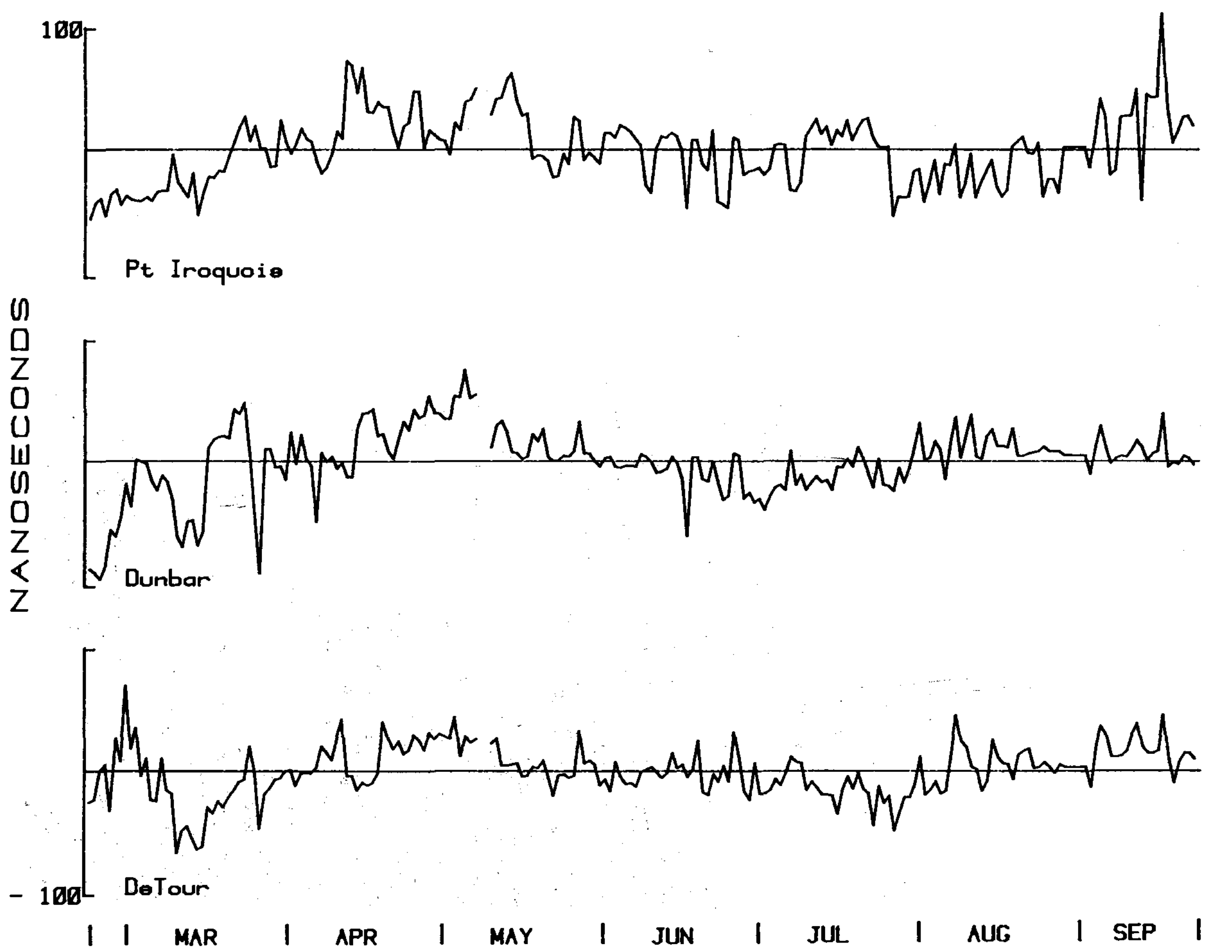

Figure 5. Master-Zulu Midday Time Difference Variations

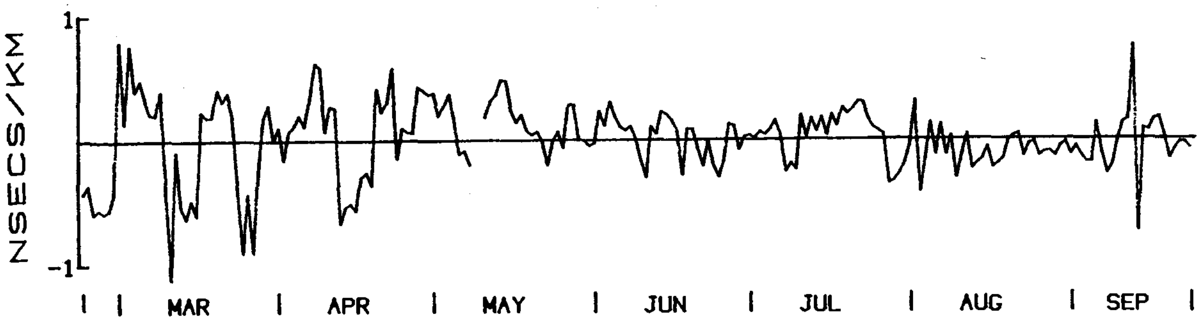

Figure 6. Uniform Propagation Velocity Changes

lapse rate of the index of refraction.[3,4]

The peak-to-peak propagation velocity change extracted from the data to date is approximately two nanoseconds per kilometer of baseline length. The corresponding time difference variations are obtained by multiplying the plotted values by the baseline lengths (54 to 62 km) and a proportionality constant for each site. The proportionality constant is zero for a site on the same hyperbolic TD line as the SAM and increases with distance from this line. Typical values are listed in Table 2.

Table 2. Typical Uniform Velocity Time Difference Changes (Nanoseconds)

	M-X	M-Y	M-Z
Gros Cap (North End)	40	−88	125
Six Mile Point (Near SAM)	−1	−2	9
DeTour Light (South End)	48	−95	132

The uniform propagation changes are interesting in that they represent a fundamental performance limit in the system. The significant point is that the information provides a bound on a physical effect which cannot be improved upon through equipment or procedural changes.

Figure 7 shows the mid-February to mid-April propagation velocity changes, superimposed with a plot of temperature recorded at the SAM. The correlation coefficient for these plots is approximately 0.7. This relatively high correlation confirms the expected temperature dependency. The correlation diminishes rapidly during late April and early May, after which there is negligible correlation with temperature. This diminishing correlation is expected, since the temperature dependency of the vertical lapse rate is predominantly a winter effect.[3,4]

Error Budget Analysis

Knowing the nature and source of the grid variations is interesting, but of no immediate value to the user. However, having determined the expected TD fluctuations, it is now possible to calculate the positioning errors that would result. Figure 8 is the plot of an error budget analysis

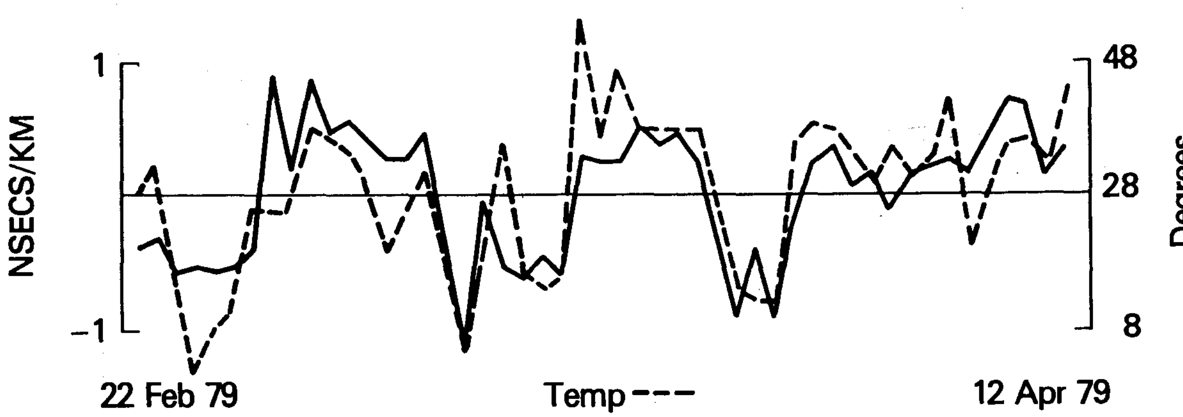

Figure 7. Winter Propagation Velocity Changes

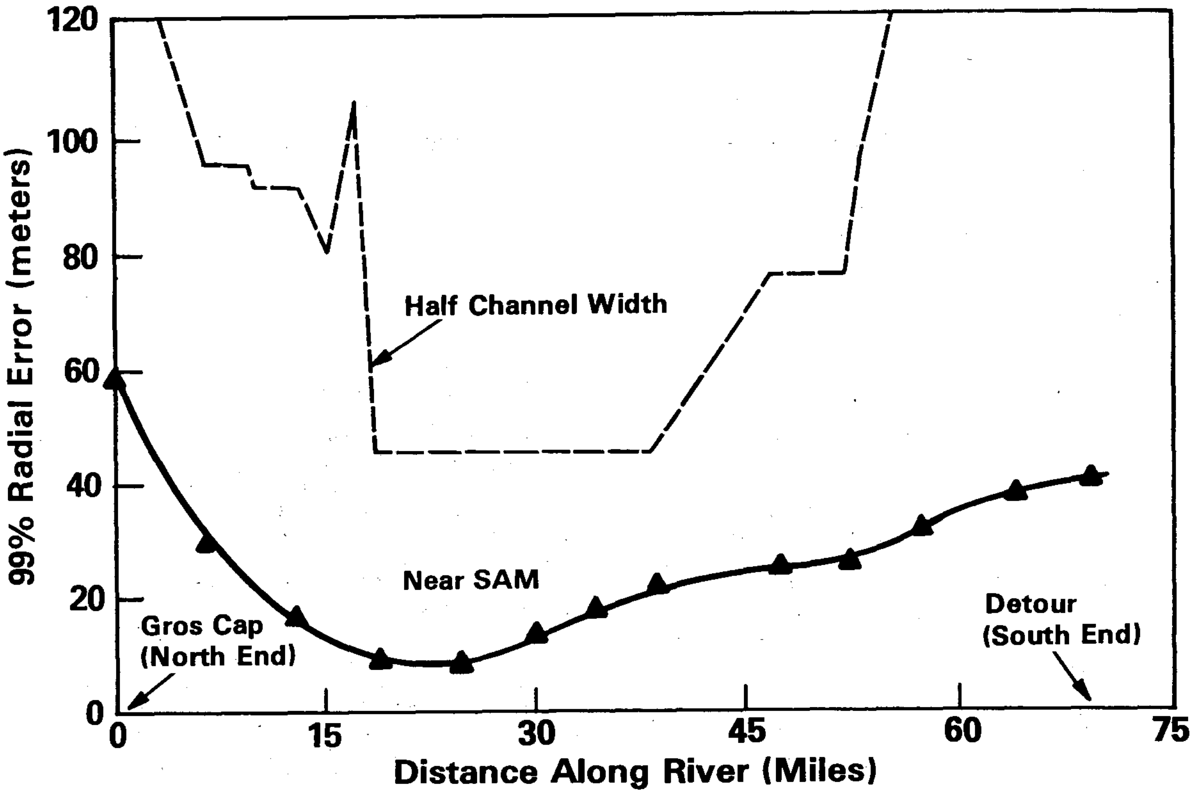

Figure 8. Error Budget Analysis

for a series of points along the St. Marys River. A user's time difference error has been allocated to three sources:

1. Uniform Propagation Velocity Changes. The maximum variation experienced to date (two nanoseconds per kilometer of baseline length) is used, recognizing that the river might be surveyed during one extreme and navigated during the opposite extreme. The narrower portions of the navigation channel are nearer the SAM and will experience the smallest variations, as can be seen from Table 2.

2. Control Errors. The "erroneous" control station adjustments are applied as normally distributed random numbers with a zero mean and a standard deviation equal to the smaller RMS values from Table 1.

3. Receiver Offsets. Assuming the use of a survey-quality receiver, 15 nanoseconds is allowed for the offset between a user's receiver and the calibration receiver which surveyed the river. The sign of the offset is allowed to vary randomly for each of the three TDs.

Radial error values are determined by computing a minimum variance three-TD "fix" according to an algorithm developed for our newest user equipment.[5] The 99 percent curve was determined by running a Monte Carlo simulation and plotting the resulting probability histogram. Also plotted is the half-width of the navigation channel. It can be seen that the 99 percent error is well within this half-channel distance for the entire river. This makes an interesting comparison, but the intent is not to imply that the half-channel width is an acceptable error in a radionavigation system. Allowances must also be made for navigation error and the half-width of the user's vessel (up to 16 meters).

HARBOR MONITOR PROGRAM

The Office of Research and Development is responsible for evaluating the effectiveness of the Loran-C system in providing the accuracy necessary to serve as a reliable, all-weather radio aid within the HHE environment. The desired technical approach is to extract the inherent accuracy of the system through improved understanding of the bounding physical elements. This understanding will be developed through analysis, model development, testing and verification.

The objective of the Harbor Monitor Program is to characterize the stability of the existing grid in the HHE areas of the United States. Quantification of the year-round temporal variations is required as input to an error budget analysis for each HHE area of interest.

Several sets of equipment have been developed previously for monitoring the operation of both the West Coast chain and the St. Marys River mini-chain. The Coast Guard Research and Development Center has constructed a prototype monitor system (Figure 9) consisting of hardware and software to allow remote dial-up access to the daily System Samples. These prototypes are presently deployed at the St. Marys River monitor sites.

Improved versions of the remote monitoring hardware will be installed in each harbor area studied. Up to ten sets will be installed during 1980. Two monitoring sites should be sufficient to characterize the grid stability in most regions. New York, San Francisco and Puget Sound are likely harbors for the first installations.

CONCLUSIONS

The St. Marys River stability analysis has begun its planned one-year effort. The preliminary results have established that the grid is reasonably stable, and that earlier reports showing much larger variations were apparently incorrect.

An analysis of the data has revealed a limiting physical effect in the form of changes in the velocity of propagation, uniform throughout the chain. These propagation changes have been as large as 130 nanoseconds at the ends of the river, but are much smaller near the control station.

An error budget analysis has projected three-TD fixes that are well within the half-width of the river's navigation channels. However, the addition of navigation error and the half-width of a typical vessel preclude making the implication that the mini-chain is capable of providing safe electronic-only navigation in every section of the St. Marys River at all times.

PROGNOSIS AND FUTURE EFFORTS

The data collected between now and next Spring should enable a definitive judgement to be made on the navigation capabilities of the St. Marys River mini-chain.

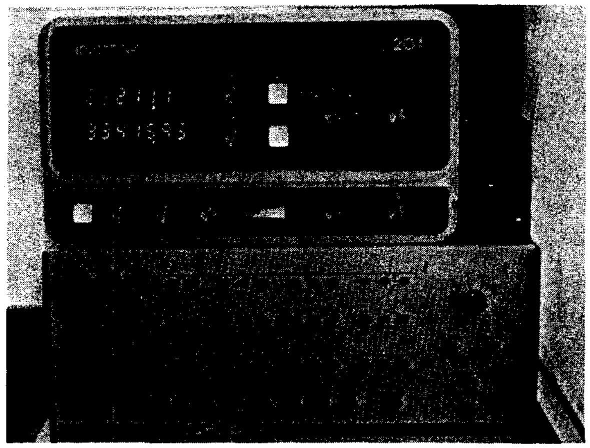

Figure 9. Harbor Monitor System

The geometry of the forthcoming Great Lakes Loran-C chain looks excellent in the St. Marys River area, and consideration is being given to supplementing this coverage with one mini-Loran-C station in lieu of an entire mini-chain. With this in mind, data collection has been started on the Dana-Seneca leg and will commence on transmissions from the new Baudette, Minnesota station when it comes on air.

REFERENCES

1. Warren, R.S., Gupta, R.R., and Healy, R.D., "Design and Calibration of a Grid Prediction Algorithm for the St. Marys River Loran-C Chain." The Analytic Sciences Corporation, Technical Information Memorandum TIM-1119-2, March 1978.

2. DePalma, L.M., and Gupta, R.R., "Seasonal Sensitivity Analysis of the St. Marys River Loran-C Time Difference Grid." The Analytic Sciences Corporation, Technical Information Memorandum TIM-1119-3, June 1978.

3. Doherty, R.H., and Johler, J.R., "Meteorological Influences on Loran-C Ground Wave Propagation." Journal of Atmospheric and Terrestrial Physics, Vol. 37, pp 1117-1124, 1975.

4. Campbell, L.W., Doherty, R.H., and Johler, J.R., "Loran-C System Dynamic Model: Temporal Propagation Variation Study." Final Report. Analytical Systems Engineering Corporation, Report No. ASECR 79-107, July 1979. To be published as U.S. Coast Guard Report No. CG-D-57-79.

5. Levy, L.J., and Schwab, V., "G Matrix Analysis for USCG Loran-C HHE Navigator Program," The Johns Hopkins University Applied Physics Laboratory, Memorandum S2R-79-008/ZT70S2R0, January 1979.

ECD VARIATIONS IN OVERLAND PROPAGATION

Walter N. Dean
Consultant
26619 Shorewood Rd.
Rancho Palos Verdes CA 90274

ABSTRACT

Analysis of Loran-C data taken in 1977-78, along with recent measurements made by the Coast Guard in 1979 reveals some interesting variations of ECD over a variety of land propagation paths. These indicate that the nature of the terrain, especially its vertical profile, appears the major factor to change ECD. An extremely high correlation with signal strength is also observed. The significance of these data to marine, air and terrestrial users is discussed.

INTRODUCTION

The U.S. West Coast Loran-C chain (9940) is unique in one major respect. Not only are its stations all situated in locations well away from the ocean, but the signals, to reach the ocean, must cross the most rugged terrain in the continental U.S. - the Cascade Range and the Sierra Nevada. This paper analyzes data taken over some of the land area, looking at what happens to the pulse shape as the Loran signal propagates over some of the paths. Most of the data analyzed were taken by the Coast Guard, flying an Austron 5000 in a C-130 in the summer of 1979. Also included are measurements made with an AN/BRN-5 on the ground in the winter of 1977-78. Figure 1 shows the locations of the stations and dots where data were collected. The shaded contours give a qualitative impression of the location and size of the mountain ranges.

ECD

The envelope of the Loran pulse has a slope which, for the first 60 microseconds, decreases monotonically.

In the "ideal" Loran pulse, the slope of the envelope has a certain slope coinciding with the zero crossing of the third cycle, and this defines zero ECD. If that value of slope occurs earlier, the ECD is called negative by that number of microseconds. The Coast Guard has gone to considerable trouble to build a Loran signal simulator at EECEN, Wildwood NJ which can produce pulses of ideal slope and variable ECD, so that receivers can be calibrated. Both the Austron 5000 and the BRN-5 used in these tests were checked there.

LCDR Bill Jones, USCG, reported last year to the WGA on ECD measurements made during 1977-78, including a large number on the west coast chain. He plotted the data points, fitted regression curves to them, and also showed a map identifying "suspected propagation anomaly areas". By looking closely at his figure 6, one can see that some of the points are as much as 4 microseconds away from the regression line. This paper will examine that phenomenon in more detail.

DATA ANALYSIS

Each of the data points used was an average of at least five minutes of readings. In the case of the aircraft readings, this obviously involves a position variation in the order of 15 miles. Since precision of location is not a factor in these measurements, an average position was estimated and used for data analysis.

Figure 2 shows variation of ECD with distance from the master station at Fallon, NV, and also includes a "theoretical" line of variation reported previously. Some of the points fit the curve rather poorly. Figure 3 plots field strength for the same set of points. Note that a number of points fall well below the "poor earth" curve. Most of these correspond to points of more negative ECD, as will be shown later.

Figure 4 shows ECD data for the W secondary at George WA. Again there is a wide spread of readings. One point nearly 900 miles has +2 ECD, another at 350 miles is zero.

Some additional insight is gained from figure 5 - points in the 300-400 mile range attenuated more, in the 800-900 mile range attenuated less than "normal".

The ECD data from the X secondary, Middletown CA, figure 6, is the most remarkable, with a shift of over 3 microseconds in only 200 miles in one case, and no shift at all in 450 miles in another.

Figure 7 shows the rapid attenuation associated with the ECD shift of the previous figure.

The Y secondary at Searchlight NV produces what appears, at first glance, to be a more "normal" ECD variation in figure 8. A closer look, however, reveals a nearly constant ECD out to 350 NM, another set nearly constant 350-500 NM, and two points at 650 NM with no change at all.

The field strength curve, figure 9 shows the expected - higher amplitude corresponding to small ECD shifts, lower amplitude corresponding to larger shifts.

In an attempt to make sense out of the ECD and field strength data, the readings were charted on maps of the area, to show where the different readings were obtained. The results were quite interesting. Figure 10 shows the M readings obtained in south-central California. The paths over the Sierras take their toll in ECD and amplitude, (0.1/72 near Fresno, 0.7/61 south of Mt. Whitney) but the signals recover ECD and strength crossing the Sacramento Valley. In Death Valley (lower right) the path from M is free of mountains, and ECD is virtually unchanged.

Figure 11 shows southern California and Y signal data. The ECD at Y was reduced by the Coast Guard from +2.5 to +1.6 because of cycle selection problems along the coast, and this figure shows why. The ECD is virtually unchanged by its propagation in this area, except one point (0.9/72) just as it crosses the Sierras.

In figure 12 the effects of the Sierra Nevada range on the Master signal can be seen. To the east of the range, ECD readings of 2.4 are obtained. To the west, 1.5 to 1.7 are seen, although figure 10 showed 2.4 farther north. However, directly south, along the range, the ECD drops below 1.0. This poses a bit of a problem for the Los Angeles area.

The signal from W (figure 13) 500 miles farther away than M but nearly the same direction, seems to be affected principally over the mountains. The slight difference in path may account for this.

The situation in northern California is even more disturbing. The Master signals, seen in figure 14, show a drop in ECD of over 2 microseconds just south of the Oregon border, where the signals cross Mt. Lassen and Shasta, but then recover completely farther north as the path avoids these peaks.

The signals from the X secondary behave in an even more startling manner, as seen in figure 15. Over the mountains of northern California, the ECD suddenly drops by as much as 3.7 microseconds, and without Mt. Shasta to blame it on.

The W signal from George WA also has problems, seen in figure 16. Going south from Oregon into California, the ECD suddenly drops by over 2 microseconds. A look at a larger map shows this coincides with the signal crossing the Cascade range. Farther south, the path is clearer, and the ECD recovers. The shadow of Mt. Shasta is also evident farther south.

The significance of these variations is illustrated in figure 17, which shows all four ECD's at six points in the area. Starting at the southernmost point, the ECD's are about as expected-about 2.5 for M and X, 1.2 for W and nearly 0 for Y. At the next point north, W has dropped to 0 while the others stay the same. A little farther north, M has suddenly dropped 2 microseconds, and Y has dropped about 1, but W has increased 0.5.

Thirty miles farther north, M has decreased more, W and Y have stayed the same, but X has decreased 1.5 microseconds while W decreased 0.5 and X decreased 1 microsecond. Sixty miles farther north, M and W are back to 2.4, Y has increased by 2 microseconds, but X is still negative.

With the ECD behaving like this, it would not be at all surprising if Loran receivers had occasional cycle selection problems.

CONCLUSIONS

It seems safe to say that something about rugged mountainous terrain produces a marked decrease in ECD, even at relatively short distances. It is also apparent from the data that non-rugged terrain appears to have practically no effect on ECD. In fact, a signal whose ECD has been sharply decreased by passage over rugged terrain appears frequently to "recover" in propagating over a subsequent valley. In fact, by selecting data shown here, one could conclude that the decrease (1) is, or (2) is not a localized effect.

The most important conclusion to be drawn is that designers of Loran receivers, especially if they are intended for overland use, need to be aware of the propagation problems of which this paper is only a sample. One potentially important observation is the correlation between decreases in ECD and decreases in field strength. This could provide ammunition to the theoretical analyst and to the receiver designer in attacking the problem.

FIG. 1 - WEST COAST LORAN

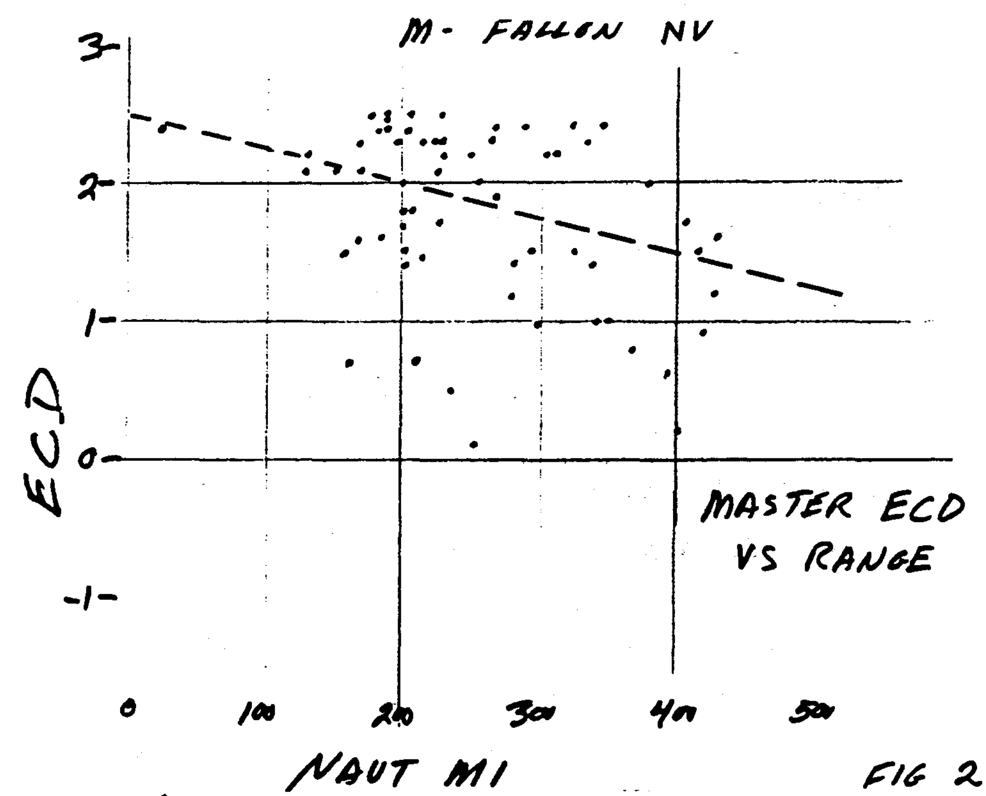
M- FALLON NV
3
2
1
0
-1
ECD
MASTER ECD
VS RANGE
0
100
200
300
400
500
NAUT MI

FIG 2

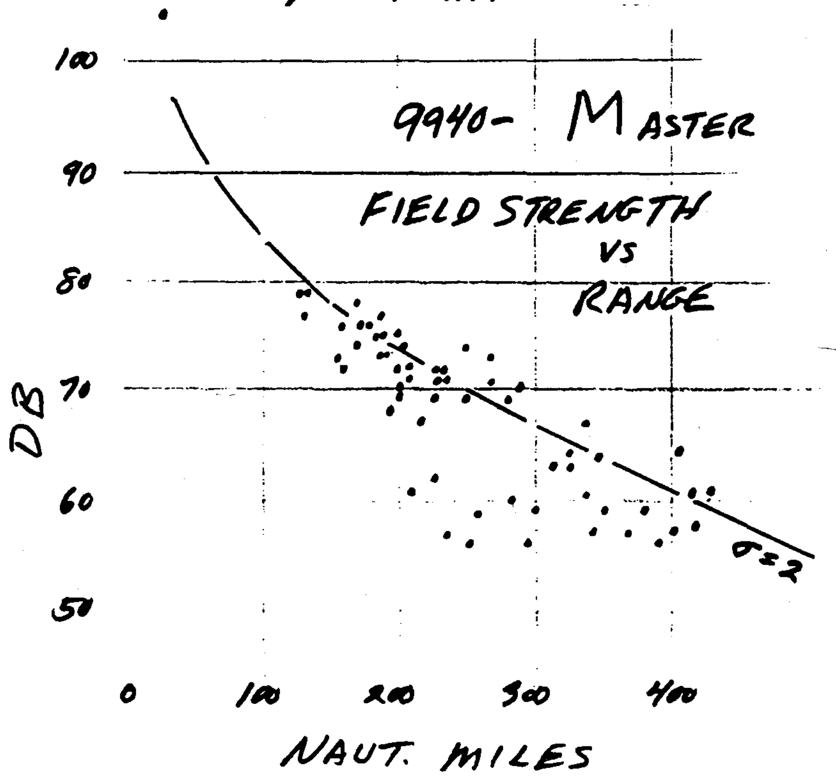
100
90
80
70
60
50
DB
9940- MASTER
FIELD STRENGTH
VS
RANGE
σ=2
0
100
200
300
400
NAUT. MILES

FIG 3

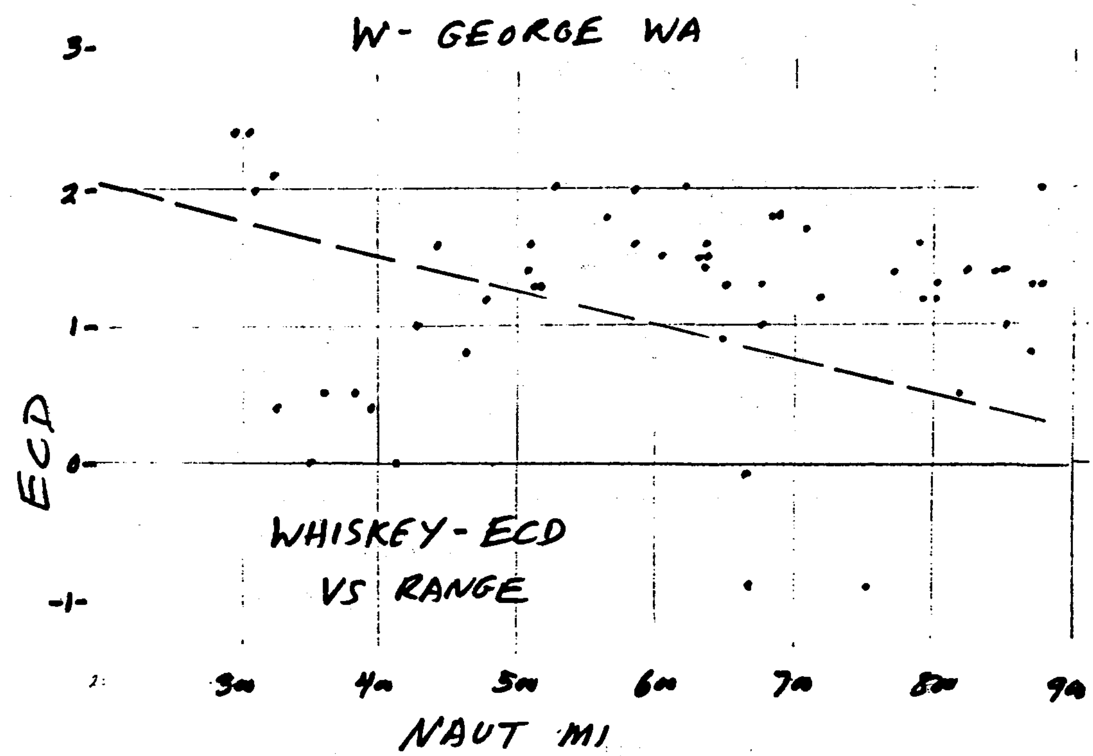
W- GEORGE WA
3-
2-
1-
0-
-1-
ECD
WHISKEY-ECD
VS RANGE
300
400
500
600
700
800
900
NAUT MI
FIG 4

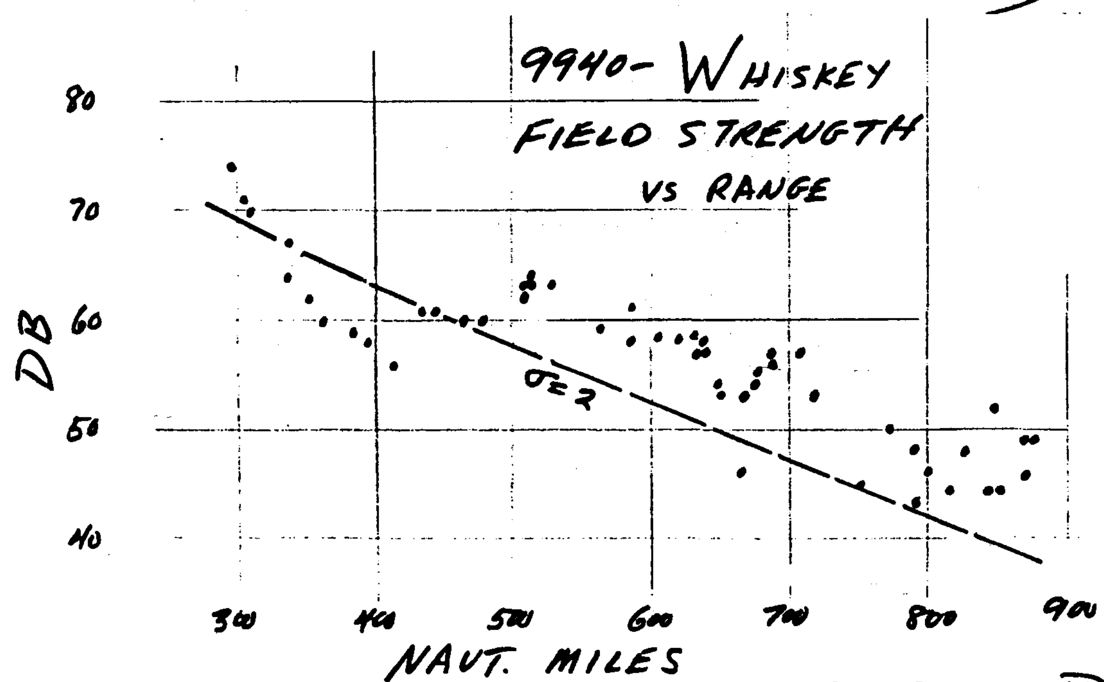
9940- WHISKEY
FIELD STRENGTH
VS RANGE
80
70
60
50
40
DB
σ=2
300
400
500
600
700
800
900
NAUT. MILES
FIG 5

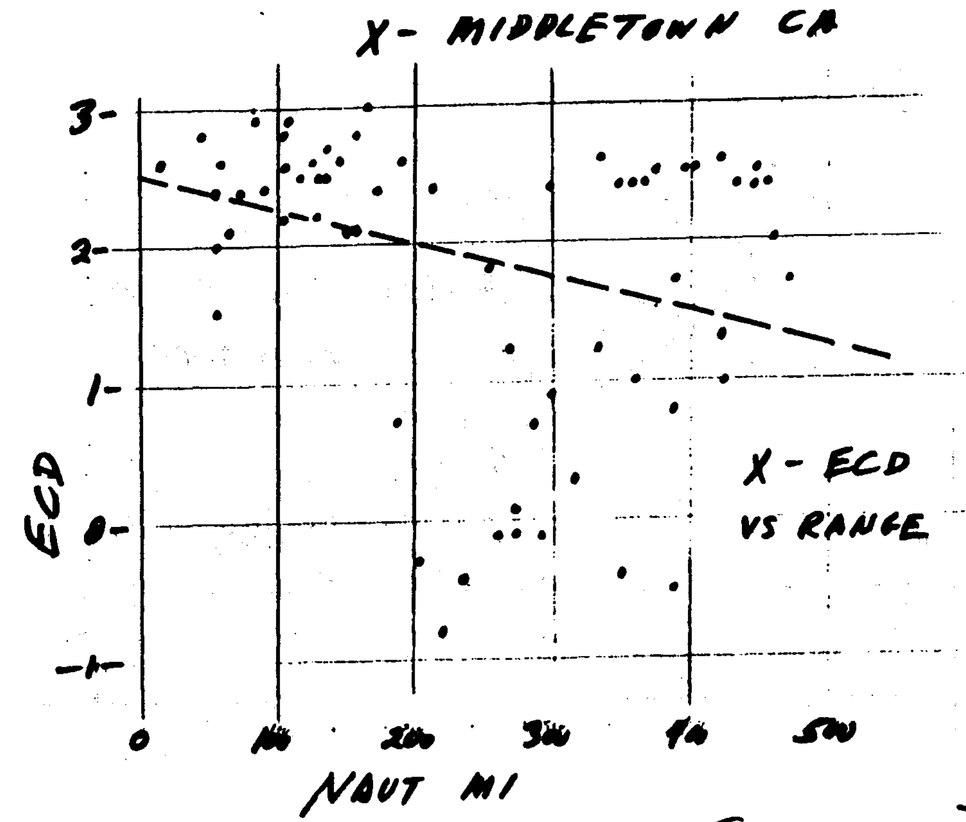
X- MIDDLETOWN CA
3-
2-
1-
ECD
0-
-1-
0
100
200
300
400
500
NAUT MI
X - ECD
VS RANGE

FIG 6

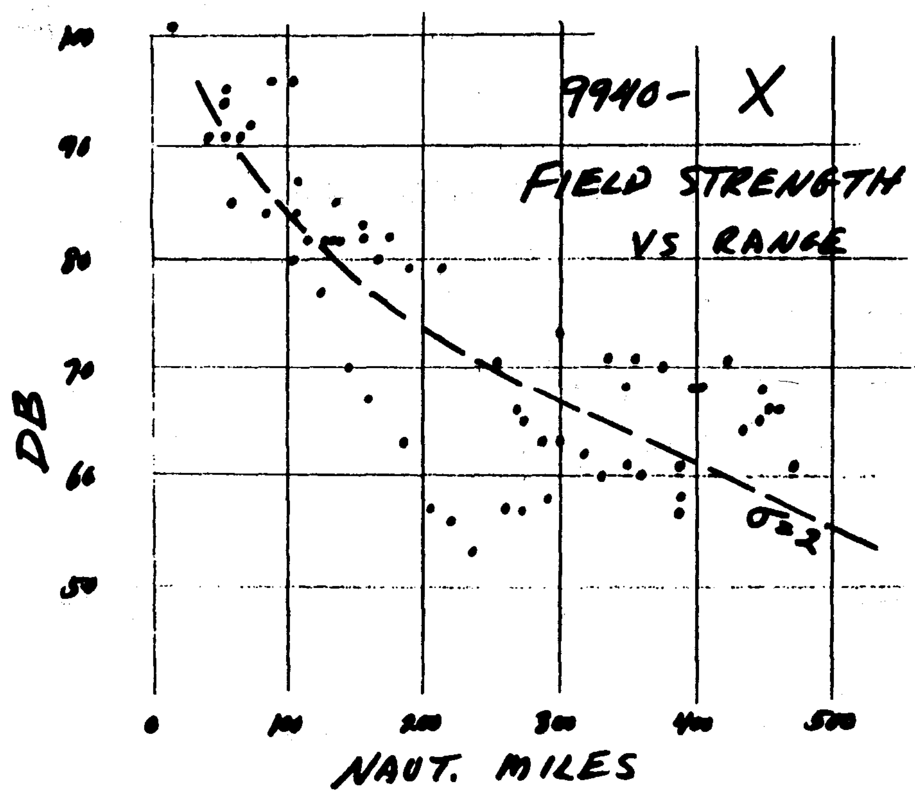
100
90
80
70
60
50
DB
9940- X
FIELD STRENGTH
VS RANGE
σ=2
0
100
200
300
400
500
NAUT. MILES

FIG 7

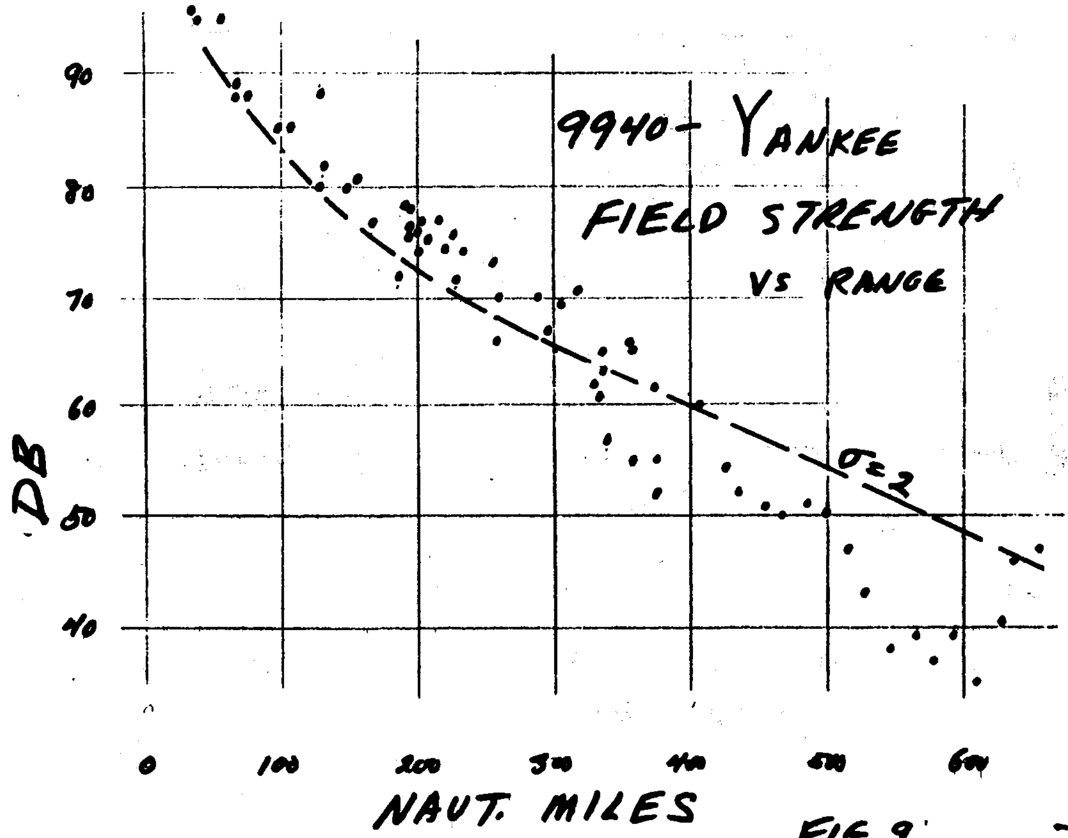
9940 - YANKEE
FIELD STRENGTH
VS RANGE
σ = 2
DB
90
80
70
60
50
40
0
100
200
300
400
500
600
NAUT. MILES

FIG 9

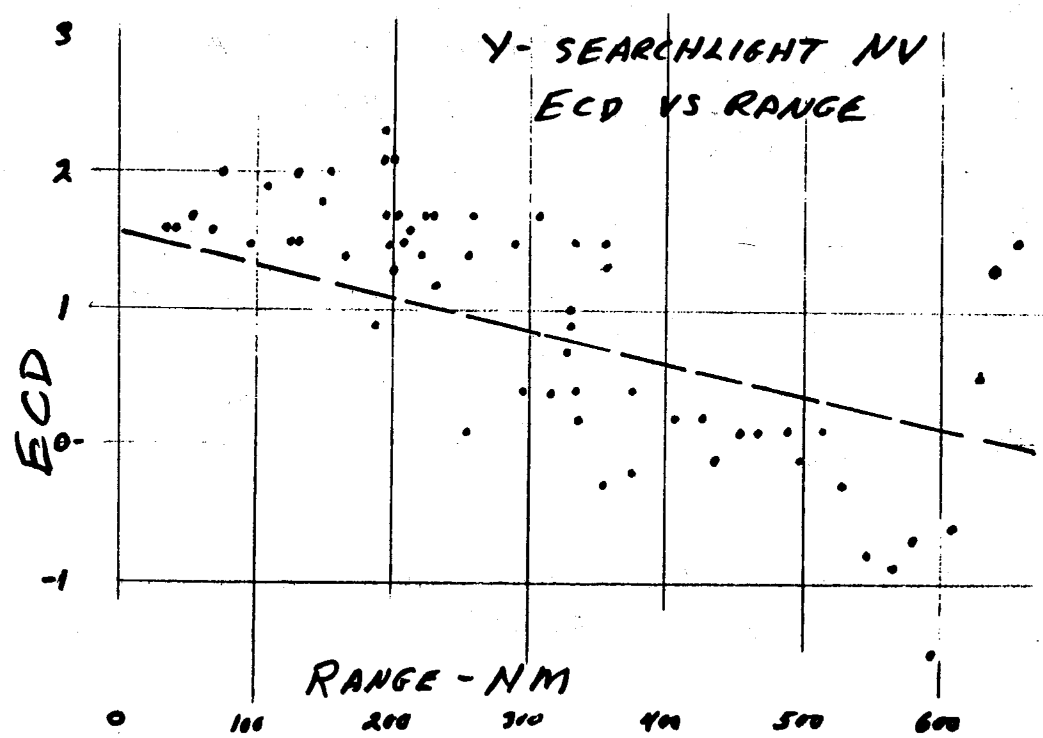
Y - SEARCHLIGHT NV
ECD VS RANGE
ECD
3
2
1
0
-1
RANGE - NM
0
100
200
300
400
500
600

FIG 8

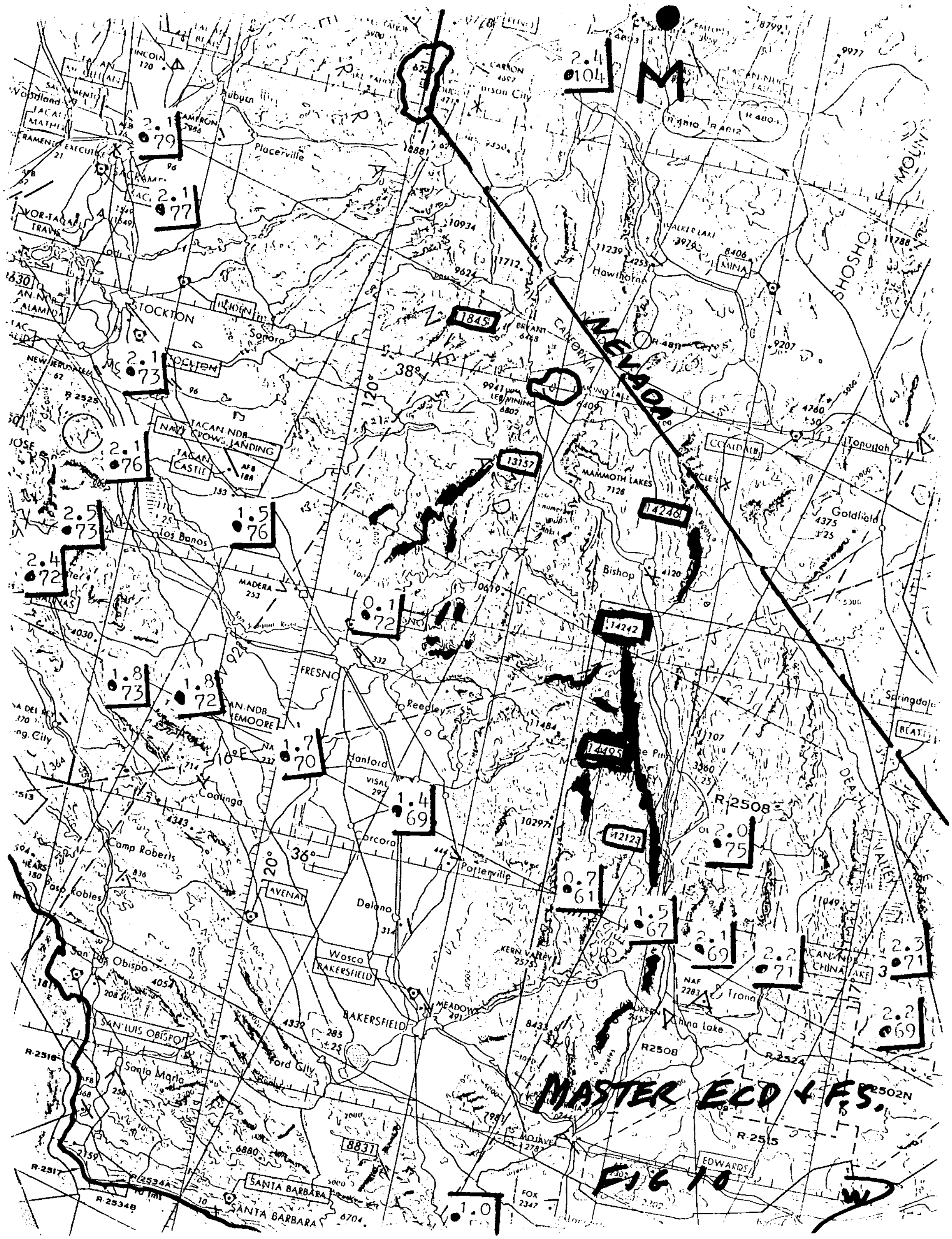

MASTER ECD + F.S.
FIG 10
NEVADA
CALIFORNIA
STOCKTON
FRESNO
BAKERSFIELD
Bishop
Mammoth Lakes
Hawthorne
Goldfield
Placerville
Sonora
Los Banos
Reedley
Hanford
Coalinga
Porterville
Delano
Wosco
China Lake
Trona
Mojave
Paso Robles
San Luis Obispo
Santa Maria
Santa Barbara
Camp Roberts
Tonopah
Springdale

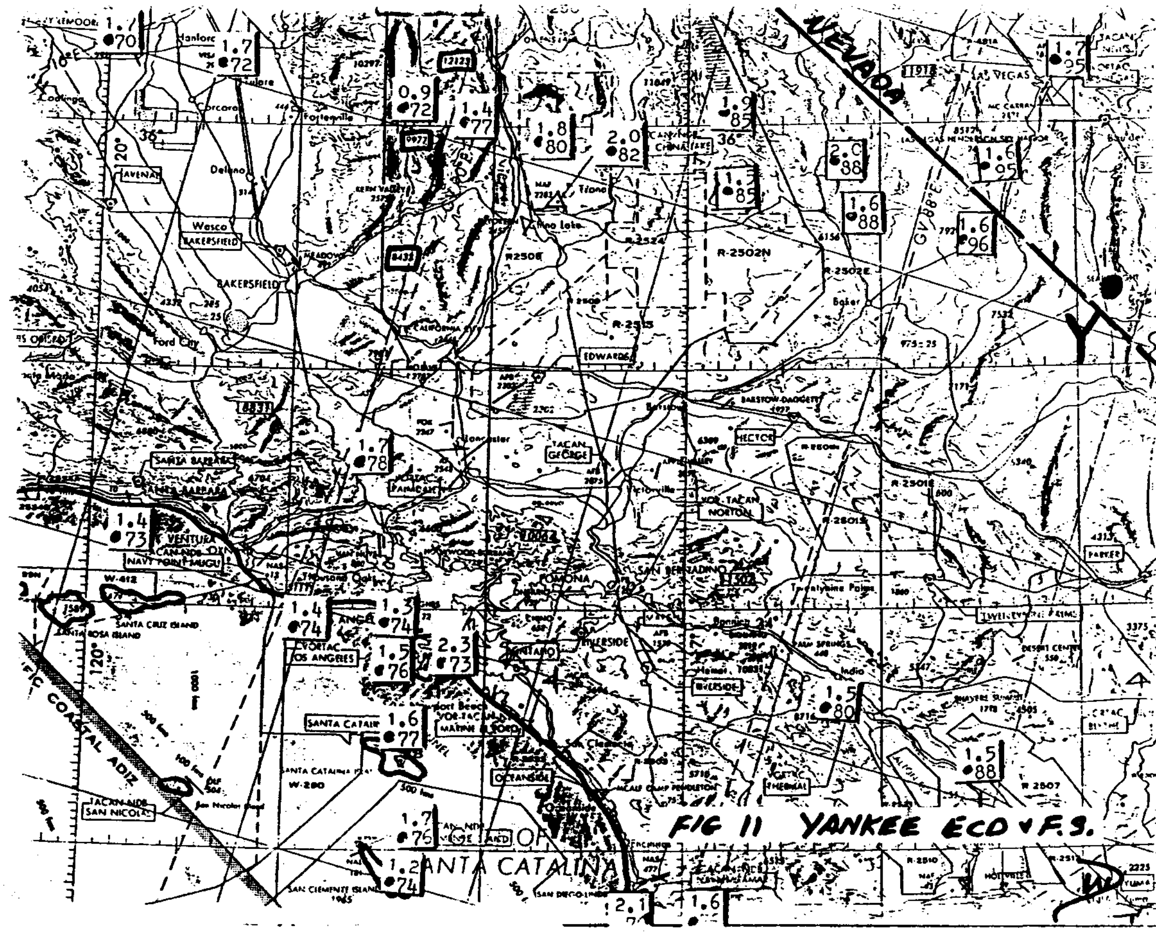
NEVADA
LAS VEGAS
BAKERSFIELD
Wasco
Delano
SANTA BARBARA
VENTURA
NAVY POINT MUGU
SANTA CRUZ ISLAND
SANTA ROSA ISLAND
POMONA
SAN BERNARDINO
EDWARDS
HECTOR
R-2508
R-2502N
R-2502E
SANTA CATALINA
SAN NICOLAS
PACIFIC COASTAL ADIZ
FIG 11 YANKEE ECD + F.S.


NEVADA
LAS VEGAS
BAKERSFIELD
Wasco
Delano
300 NM
M
SANTA BARBARA
SANTA CRUZ ISLAND
SANTA ROSA ISLAND
POMONA
SAN BERNARDINO
EDWARDS
HECTOR
R-2508
R-2502N
R-2502E
SANTA CATALINA
SAN NICOLAS
PACIFIC COASTAL ADIZ
FIG 12 - MASTER ECD + F.S.


W
800 N.M.
FIG. 13 - WHISKEY ECD & F.S.
PACIFIC COASTAL ADIZ
LOS ANGELES
SANTA CATALINA
EDWARDS
BAKERSFIELD
SAN NICOLAS
TWENTYNINE PALMS
BLYTHE
PARKER
NORTON
OCEANSIDE

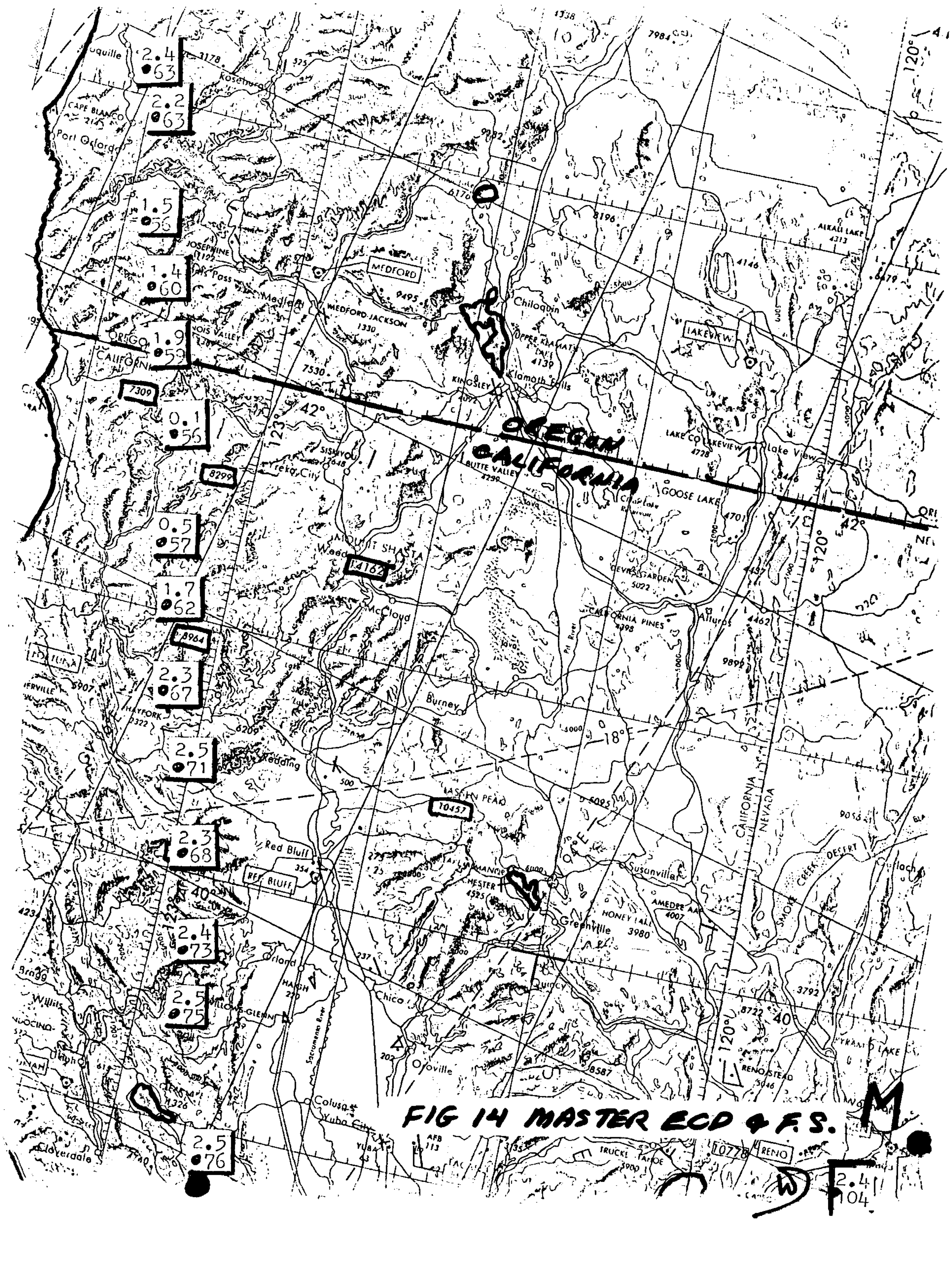

OREGON
CALIFORNIA
MEDFORD
Medford
Chiloquin
Klamath Falls
LAKEVIEW
Lake View
GOOSE LAKE
Yreka City
MOUNT SHASTA
Weed
McCloud
Burney
Redding
Red Bluff
Susanville
Greenville
Quincy
Chico
Oroville
Orland
Willows-Glenn
Colusa
Yuba City
Willits
Cloverdale
Port Orford
CAPE BLANCO
CALIFORNIA
NEVADA
RENO
FIG 14 MASTER ECD & F.S.

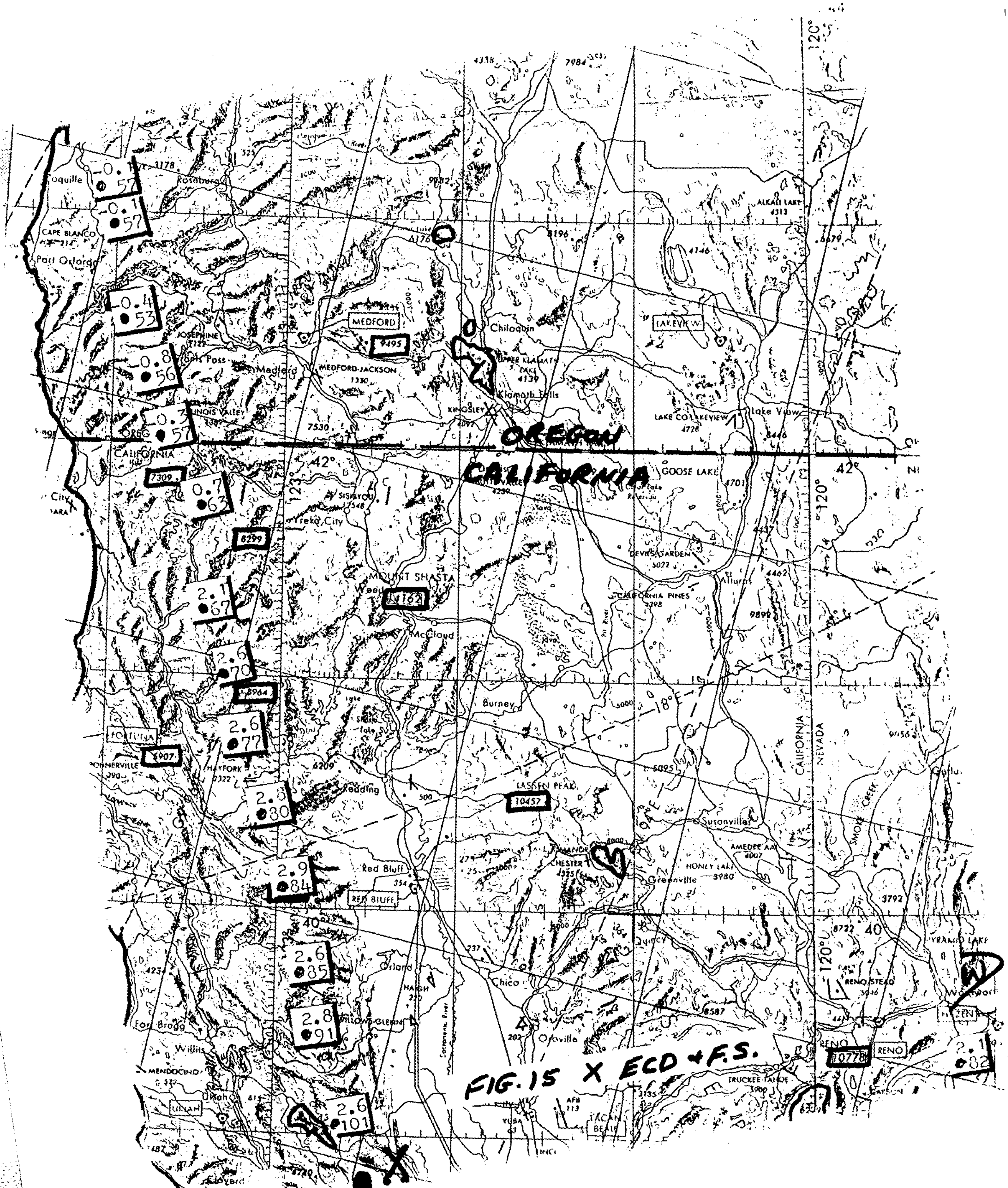

FIG. 15 X ECD + F.S.

FIG. 16 W EOD + F.S.

FIG.17 ECD COMPARISON

THE CONVENTION SCENE

WGA PRESIDENT, BAHAR UTTAM, OPENS THE AWARD CEREMONIES

CONVENTION CHAIRMAN AND BANQUET TOASTMASTER, LLOYD HIGGINBOTHAM

BANQUET GUEST SPEAKER: DAVID WILTSHIRE, PRESIDENT OF THE NATIONAL MARINE ELECTRONICS ASSOCIATION

THE OUTSTANDING SERVICE AWARD IS PRESENTED TO LLOYD HIGGINBOTHAM BY BAHAR UTTAM

LOREN BRUNNER RECEIVES
THE MEDAL OF MERIT

CAPT. WILLIAM MOHIN RECEIVES
THE PRESIDENTS AWARD

MRS. RAYMOND BAETSEN ACCEPTS AN HONORARY MEMBERSHIP FOR HER HUSBAND, DECEASED

JIM VAN ETTEN RECEIVES
THE BEST PAPER AWARD

FELLOW HONKERS BILL WALKER, BAHAR UTTAM AND DAVE WILTSHIRE ENJOY REFRESHMENTS ON THE PATIO

"WHAT'S A HONKER?"

DAVE OLSEN: "RAY, EXPLAIN THE FUNDAMENTALS OF LORAN-C TO THE YOUNG GOSLING"

DON FELDMAN DESCRIBES THE OPERATION OF **PILOT**, WHICH GAVE ALL OF THE *NAVIGATORS* AT THE CONVENTION A CHANCE TO DEMONSTRATE THEIR SKILL

CAPT. BILL ROLAND, CO-CHAIRMAN OF THE CONVENTION

WE COULD HAVE DANCED ALL NIGHT

REGISTERED ATTENDANCE

WILD GOOSE ASSOCIATION 8TH ANNUAL TECHNICAL SYMPOSIUM

17 - 19 OCTOBER 1979

WILLIAMSBURG, VIRGINIA

Paul Abramson
DOT/TSC
Kendall Square
Cambridge, MA 01778

Ray Abraczinskas
LEAR SIEGLER, INC.
4141 Eastern Avenue, SE
Grand Rapids, MI 49508

Rich Adams
SYSTEMS CONTROL, INC.
2326 South Congress
West Palm Beach, FL 33406

Walter J. Ambrose
SPERRY GYROSCOPE
25 Dumbarton Drive
Huntington, NY 11743

Bernard Ambroseno
EPSCO MARINE
411 Providence Highway
Westwood, MA 02090

Everett Anderson
USCG
Avery Point
Groton, CT 06340

Carl S. Andren
NAVIGATION SYSTEMS, INC.
8841 Monard Drive
Silver Springs, MD 20910

John J. Anthony
USCG
2100 2nd Street, SW
Washington, DC 20593

Glen E. Baer
JHU/APL
Johns Hopkins Road
Laurel, MD 20810

Eric Bick
EFFECTS TECHNOLOGY, INC.
5383 Hollister Avenue
Santa Barbara, CA 93111

Steve Bigelow
MEGAPULSE
8 Preston Court
Bedford, MA 01730

Daniel Blitz
SANDERS ASSOCIATES, INC.
Daniel Webster Highway
Nashua, NH 03061

John Boyd
JHU/APL
Johns Hopkins Road
Laurel, MD 21045

Barry Breen
GOULD, INC.
2908 Cullen Street
Fort Worth, TX 76107

Robert D. Bronson
MORROW ELECTRONICS, INC.
4740 Ridge Drive, NE
Salem, OR 97303

Keith R. Bruhl
COMMAR, INC.
3110 Faber Drive
Falls Church, VA 22044

Loren E. Brunner
USCG (RET)
154 Old Norwich Road
Quaker Hill, CT 06375

E. W. Buebel, Jr.
LSA SCIENTIFIC CORP.
109 Beaver Court
Cockeysville, MD 21030

John M. Beukers
BEUKERS LABS, INC.
8 Old Wood Road
Stony Brook, NY 11790

David A. Carter
DOT/NHTSA (NTF-13)
400 7th Street, SW
Washington, DC 20590

Lois W. Campbell
ANALYTICAL SYSTEMS ENG. CORP.
5 Old Concord Road
Burlington, MA 01803

Frederick J. Chambers
TELEDYNE SYSTEMS CO.
6712 Randiwood Lane
West Hills, CA 91307

A. L. Comstock
TELEDYNE HASTINGS — RAYDIST
P. O. Box 1275
Hampton, VA 23661

Bruce A. Conway, Capt.
USAF
ESD/OL AF (DET AF00)
Eglin AFB, FL 32542

Alan Cook
COLORADO RESEARCH & PREDICTION
1898 South Flatiron Court
Boulder, CO 80301

J. F. Culbertson, Capt.
USCG
15781 Exeter Street
Westminster, CA 92683

John M. Currie
INTERNAV
Bedford, MA 01730

Harold Dahl
DAHL LORAN SERVICE
46 North Water Street
New Bedford, MA 02740

Peter H. Dana
AUSTRON NAVIGATION
8330 Burnet Road #138
Austin, TX 78758

Walter N. Dean
VERDES ENGINEERING CO.
26619 Shorewood Road
Rancho Palos Verdes, CA 90274

John D. Dobbs
LEAR SIEGLER, INC.
4141 Eastern Avenue, SE
Grand Rapids, MI 49508

Jim Doherty
USCG – Box 50
FPO, NY 09510

Robert H. Doherty
COLORADO RESEARCH & PREDICTION
1898 South Flatiron Court
Boulder, CO 80301

Bob Dugan
USCG
CGR & DC
Groton, CT 06340

Charles R. Edwards
JHU/APL
Johns Hopkins Road
Laurel, MD 20810

Henry H. Elliott
JHU/APL
Johns Hopkins Road
Laurel, MD 20810

Robert Erikson
FAA/NAFEC
Bldg. 301 ANA-120 Tilton Road
Atlantic City, NJ 08405

Leo Fehlner
JHU/APL
118 Quaint Acres Drive
Silver Spring, MD 20904

Don Feldman
USCG
400 7th Street, SW
Washington, DC 20590

W. M. Flanders, Capt.
USCG – TSC
Kendall Square
Cambridge, MA 01810

Bruce Francis
AUSTRON NAVIGATION, INC.
8330 Burnet Road #138
Austin, TX 78758

Robert L. Frank
16500 North Park Drive – Suite 720
Southfield, MI 48075

Ronald H. Frazier
USCG
2100 2nd Street, SW
Washington, DC 20593

Ronald J. Fredricks
LEAR SIEGLER, INC.
4141 Eastern Avenue, SE
Grand Rapids, MI 49508

David Freese
USCG – EECEN
RD 1 Box 316
Cape May Court House, NJ 08210

T. Fujino
KODEN ELECTRONICS CO., LTD.
Z-10-45 Kami-Osaki, Shinagaua
Tokyo, JAPAN 141

Burt Gambill
GENERAL ELECTRIC CO.
816 State Street
Santa Barbara, CA 93110

Thomas J. Gilmartin
USCG – EECN
Wildwood, NJ 08204

Robert B. Goddard
INTERNAV CORP.
65 Wiggins Avenue
Bedford, MA 01730

Dennis J. Granato
DMAHTC
Navigation Department
Washington, DC 20315

George T. Gunther
USCG — EECEN
Wildwood, NJ 08206

R. R. Gupta
THE ANALYTIC SCIENCES CORP.
6 Jacob Way
Reading, MA 01867

Gerald A. Gutman
NAV-COM, INC.
2 Hicks Street
North Lindenhurst, NY 11757

John E. Hanna, Jr.
DEFENSE MAPPING CENTER
6500 Brookes Lane
Washington, DC 20315

William H. Haynes, Cdr.
USCG — Activities Europe Box 50
London, ENGLAND
FPO NY 09510

L. D. Higginbotham
SPERRY
4 Townsend Road
Acton, MA 01720

William H. Hilbun, III
HUGHES AIRCRAFT CO.
7614 Appaloosa Trail
Orange, CA 92669

Joseph L. Howard
MITRE CORP.
P. O. Box 208
Bedford, MA 01810

John Illgen
EFFECTS TECHNOLOGY, INC.
5383 Hollister Avenue
Santa Barbara, CA 93101

Charles E. Isgett
USCG
2100 2nd Street, SW
Washington, DC 20590

Tom Jerardi
APL/JHU
Johns Hopkins Road
Laurel, MD 20810

J. Ralph Johler
COLORADO RESEARCH & PREDICTION
1898 South Flatiron Court
Boulder, CO 80301

William E. Jones
USCG
COMDT USCG (G-FEE-4)
Washington, DC 20590

Vern Johnson
ITT AVIONICS
500 Washington Avenue
Nutley, NJ 07110

William J. Judge
AMECOM DIVISION
5115 Calvert Road
College Park, MD 20740

James D. Kelly
THE ANALYTIC SCIENCES CORP.
6 Jacob Way
Reading, MA 01867

Thomas R. Klaus
MOTOROLA
1301 East Algonquin Road
Schaumburg, IL 60196

Walter W. Kohl, Capt.
USCG
4313 Southwood Drive
Alexandria, VA 22309

William Leeseman
SPERRY GYROSCOPE
Marcys Road Station
Great Neck, NY 11020

James P. Lewicki
USCG
USCG R&D, Avery Point
Groton, CT 06340

Jack Ligon
USCG
5078 Coleridge Drive
Fairfax, VA 22032

James A. Lovell
AILTECH DIVISION OF EATON CORP.
16 Narcissus Drive
Syosset, NY 11791

Reuben E. Maine
SPERRY MARINE SYSTEMS
770 Chapel Hill Road
Charlottesville, VA 22901

A. William Marchal
ONI
P. O. Box 23504
New Orleans, LA 70183

Carl S. Mathews
MARITIME ADMINISTRATION
7114 Murray Lane
Annandale, VA 22003

Michael Marchand, Capt.
USAF
ESD/OL-AF (DET AFOC)
Eglin AFB, FL 32542

Thomas A. McCarty
JHU/APL
Johns Hopkins Road
Laurel, MD 20310

Frank W. McDermott
ITT AVIONICS DIVISION
1701 L Street, NW
Washington, DC 20030

Edward L. McGann
MEGAPULSE, INC.
8 Preston Court
Bedford, MA 01730

C. D. McGillem
PURDUE UNIVERSITY
West Lafayette, IN 47907

James Michalik
MOTOROLA, INC.
1301 East Algonquin Road
Schaumburg, IL 60196

B. C. Mills
USCG
COMDT USCG (G-WAN/TP-14)
Washington, DC 20590

Adam W. Mink
DMAAC
5475 Alnwick Drive
St. Louis, MO 63129

William B. Mohin
DOT
400 7th Street, SW
Washington, DC 20590

Paul Monette
USCG
P. O. Box 3-5000
Juneau, AK 99802

F. W. Mooney
USCG
Governors Island
New York, NY 10004

James C. Murdock
NY DEPT. OF MOTOR VEHICLES
Swan Street Building
Albany, NY 12228

Tom Nolan
MITAGS
5700 Hammonds Ferry Road
Linthicum Heights, MD 21090

William F. O'Halloran
JAYCOR
300 Unicorn Park Drive
Woburn, MA 01801

David L. Olsen, Lt.
USCG HQD
Washington, DC 20590

C. J. Pannell
SPERRY CORP.
9 Gates Avenue
Bethpage, NY 11803

Jacob Parness
MITRE CORP.
1820 Dolly Madison Boulevard
McLean, VA 22101

Garry Perchik
ITT AVIONICS
500 Washington Avenue
Nutley, NJ 07110

James A. Perschy
JHU/APL
Johns Hopkins Road
Laurel, MD 20810

Dexter Phibbs, II
P. O. Box 1275
TELEDYNE HASTINGS — RAYDIST
Hampton, VA 23661

David Pietraszewski
USCG R&D CENTER
Avery Point
Groton, CT 06340

Stephen P. Plusch
USCG
COMDT (G-EEE-4)
Washington, DC 20590

William Polhemus
POLHEMUS ASSOCIATES
Box E
Cambridge, VT 05444

C. E. Potts
USCG
630 Sansome Street
San Francisco, CA 94126

Frederick H. Raab
PNSI
240 Staniford Road
Burlington, VT 05401

William F. Rice
ITT
54 Middlesex Turnpike
Bedford, MA 01730

V. R. Robillard
USCG
1313 Tampa Drive
Honolulu, HI 96819

Mortimer Rogoff
4201 Cathedral Avenue, NW
Washington, DC 20016

Ronald G. Roll
JHU/APL
Johns Hopkins Road
Laurel, MD 20810

William F. Roland
USCG
7506 Rolling Road
Springfield, VA 22153

Allen E. Rolland, Cdr.
USCG
USCG R&D CENTER
Groton, CT 06340

Stephen Roth
MORROW ELECTRONICS, INC.
4740 Ridge Drive, NE
Salem, OR 97303

Garry Running
DOT (CANADA)
Place De Ville
Ottawa, Ontario, CANADA

Surendra N. Samaddar
USCG
G-DST-1/TP54
Washington, DC 20509

Karl R. Schroeder
USCG
661 Bay Green Drive
Arnold, MD 21012

Edward H. Schober
ESO-AIRE
216 Passaic Avenue
Fairfield, NJ 07006

W. Schorr
USCG
4528 Arendale Square
Alexandria, VA 22309

Andrew Sedlock
USCG
12400 Sarah Lane
Bowie, MD 20715

H. T. Sherman, Cdr.
USCG
13 Lemonwood Place
Pittsburg, CA 94565

Gordon W. Shillito
USCG EELEN
Wildwood, NJ 08260

D. H. Shumaker
USAF (ESD/OSND)
32 Forge Village Road
Westford, MA 01886

Frank Skestone
LEAR SIEGLER, INC.
4534 North Lindbergh Boulevard
Bridgeton, MO 63044

Morton F. Spears
SPEARS ASSOCIATION, INC.
249 Vanderbilt Avenue
Norwood, MA 02062

Harry C. Strunz
MITRE CORP.
1820 Dolly Madison Boulevard
McLean, VA 22101

Thaddeus E. Swiecki, Capt.
AMERICAN AIRLINES PILOT
602 Buffalo Drive
Arlington, TX 76013

Dalton Szelle
SPERRY
5 Marseille Drive
Locust Valley, NY 11560

Brian Terry
NORDCO LTD.
Box 8833
St. John's, Newfoundland, CANADA

Herbert H. Thompson
US DRUG ENFORCEMENT AGENCY
4214 University Drive
Fairfax, VA 22030

Frank Tiernan
AMECOM — LITTON
College Park, MD 20740

Jimmie L. Toms
AUSTRON NAVIGATION, INC.
1800 Old Meadow Road
McLean, VA 22102

Aylmer R. Trivers
USCG
17 Green Valley Lakes
East Lyme, CT 06333

Bahar Uttam
JAYCOR
300 Unicorn Park Drive
Woburn, MA 01801

Jim VanEtten
ITT AVIONICS
390 Washington Avenue
Nutley, NJ

R. A. Vanina
INTERNATIONAL NAVIGATION CORP.
65 Wiggins Avenue
Bedford, MA 01730

William G. Walker, Cdr.
USCG
8809 Kenilworth Drive
Springfield, VA 22151

Joseph G. Wall, Jr.
JHU/APL
Johns Hopkins Road
Laurel, MD 20810

Ronald S. Warren
THE ANALYTIC SCIENCES CORP.
6 Jacob Way
Reading, MA 01867

Billy J. Watkins
WATKINS ASSOCIATES
P. O. Box 205 — N. Dayton Station
Dayton, OH 45404

John Wells
NASA — LANGLEY RESEARCH CENTER
MS 490
Hampton, VA 23662

Don A. Williams
CUBIC WESTERN DATA
9233 Balboa Avenue
San Diego, CA 92123

David D. Wiltshire
TEXAS ELECTRONICS CO.
Box 1407
Port Arthur, TX 77640

Peter M. Winkler
EMORY UNIVERSITY
Math Department
Atlanta, GA 30322